



TECHNICAL REPORT 0-6783-1
TXDOT PROJECT NUMBER 0-6783

Use of Carbon Fiber Reinforced Polymer (CFRP) with CFRP Anchors for Shear-Strengthening and Design Recommendations/Quality Control Procedures for CFRP Anchors

James O. Jirsa
Wassim M. Ghannoum
Chang Hyuk Kim
Wei Sun
William A. Shekarchi
Nawaf K. Alotaibi
Douglas K. Pudleiner
Jinying Zhu
Shukui Liu
Helen Wang

December 2015; Published March 2017

<http://library.ctr.utexas.edu/ctr-publications/0-6783-1.pdf>



Technical Report Documentation Page

1. Report No. FHWA/TX-16/0-6783-1		2. Government Accession No.		3. Recipient's Catalog No.	
4. Title and Subtitle Use of Carbon Fiber Reinforced Polymer (CFRP) with CFRP Anchors for Shear-Strengthening and Design Recommendations/Quality Control Procedures for CFRP Anchors			5. Report Date December 2015; Published March 2017		
			6. Performing Organization Code		
7. Author(s) James O. Jirsa, Wassim M. Ghannoum, Chang Hyuk Kim, Wei Sun, William A. Shekarchi, Nawaf K. Alotaibi, Douglas K. Pudleiner, Jinying Zhu, Shukui Liu, Helen Wang			8. Performing Organization Report No. 0-6783-1		
9. Performing Organization Name and Address Center for Transportation Research The University of Texas at Austin 1616 Guadalupe St., Suite 4.202 Austin, TX 78701			10. Work Unit No. (TRAI5)		
			11. Contract or Grant No. 0-6783		
12. Sponsoring Agency Name and Address Texas Department of Transportation Research and Technology Implementation Office P.O. Box 5080 Austin, TX 78763-5080			13. Type of Report and Period Covered Technical Report September 2012–December 2015		
			14. Sponsoring Agency Code		
15. Supplementary Notes Project performed in cooperation with the Texas Department of Transportation and the Federal Highway Administration.					
16. Abstract The objective of the study was to demonstrate the feasibility of using bi-directional layouts of CFRP for shear strengthening of bridge girders. In a previous project (0-6306), it was demonstrated that uni-directional CFRP strips and CFRP anchors improved the shear strength of reinforced concrete elements. Because the data on the bi-directional layout of CFRP was limited, additional work carried out to understand the behavior and design of CFRP strips and anchors for bridge elements subjected to large shear forces. The tests indicated that bi-directional CFRP layouts did not consistently improve the shear capacity but the loads at first shear cracking increased (20 to 40 % over the loads for uni-directional layouts of T-beams and less than 10% for pile cap girders), which improved serviceability by reducing crack widths and improving the stiffness of the members. Anchor installation is critical to shear strengthening so quality control procedures are needed to make sure that material used and installation procedures meet design requirements.					
17. Key Words CFRP, Carbon Fiber Reinforced Polymers, Shear, Strengthening, Uni-directional and Bi-directional Layouts, Anchors, Beams, Girders, Quality Control			18. Distribution Statement No restrictions. This document is available to the public through the National Technical Information Service, Springfield, Virginia 22161; www.ntis.gov.		
19. Security Classif. (of report) Unclassified	20. Security Classif. (of this page) Unclassified	21. No. of pages 288		22. Price	



**THE UNIVERSITY OF TEXAS AT AUSTIN
CENTER FOR TRANSPORTATION RESEARCH**

Use of Carbon Fiber Reinforced Polymer (CFRP) with CFRP Anchors for Shear-Strengthening and Design Recommendations/Quality Control Procedures for CFRP Anchors

James O. Jirsa
Wassim M. Ghannoum
Chang Hyuk Kim
Wei Sun
William A. Shekarchi
Nawaf K. Alotaibi
Douglas K. Pudleiner
Jinying Zhu
Shukui Liu
Helen Wang

CTR Technical Report:	0-6783-1
Report Date:	December 2015; Published March 2017
Project:	0-6783
Project Title:	Bi-Directional Application of Carbon Fiber Reinforced Polymer (CFRP) with CFRP Anchors for Shear-Strengthening and Design Recommendations/Quality Control Procedures for CFRP Anchors
Sponsoring Agency:	Texas Department of Transportation
Performing Agency:	Center for Transportation Research at The University of Texas at Austin

Project performed in cooperation with the Texas Department of Transportation and the Federal Highway Administration.

Center for Transportation Research
The University of Texas at Austin
1616 Guadalupe St, Suite 4.202
Austin, TX 78701

<http://ctr.utexas.edu/>

Disclaimers

Author's Disclaimer: The contents of this report reflect the views of the authors, who are responsible for the facts and the accuracy of the data presented herein. The contents do not necessarily reflect the official view or policies of the Federal Highway Administration or the Texas Department of Transportation (TxDOT). This report does not constitute a standard, specification, or regulation.

Patent Disclaimer: There was no invention or discovery conceived or first actually reduced to practice in the course of or under this contract, including any art, method, process, machine manufacture, design or composition of matter, or any new useful improvement thereof, or any variety of plant, which is or may be patentable under the patent laws of the United States of America or any foreign country.

Notice: The United States Government and the State of Texas do not endorse products or manufacturers. If trade or manufacturers' names appear herein, it is solely because they are considered essential to the object of this report.

Engineering Disclaimer

NOT INTENDED FOR CONSTRUCTION, BIDDING, OR PERMIT PURPOSES.

Project Engineer: James O. Jirsa
Professional Engineer License State and Number: Texas No. 31360
P. E. Designation: Research Supervisor

Acknowledgments

This project was funded by the Texas Department of Transportation (TxDOT) under Project No. 0-6783. The support of the project manager, Darrin Jensen, and project panel members Bernie Carrasco, Leon Flournoy, Nicholas Horiszny, Yi Qiu, Lianxiang Du, and Kwangsuk Suh is greatly appreciated.

TABLE OF CONTENTS

Chapter 1. Introduction	1
1.1 BACKGROUND.....	1
1.2 OBJECTIVES	1
1.3 WORK PLAN	1
1.4 ORGANIZATION OF FINAL REPORT	4
Chapter 2. Panel Tests	7
2.1 OVERVIEW.....	7
2.2 EXPERIMENTAL PROGRAM.....	7
2.2.1 Design Considerations.....	7
2.2.2 Design Considerations.....	7
2.3 TEST RESULTS	11
2.3.1 Overview of the Test Results	11
2.3.2 Behavior of Typical Panel Test	12
2.3.3 Effect of CFRP Strip Inclination	12
2.3.4 Effect of CFRP Layout.....	13
2.3.5 Effect of Amount of Steel Reinforcement.....	14
2.3.6 Load Contribution of CFRP Strips and Steel Reinforcement.....	14
2.3.7 Effects of Concrete Strength	15
2.3.8 Effects of the Amount of CFRP Material	15
2.3.9 Effects of Anchorage Layouts	16
2.4 CONCLUSIONS	16
Chapter 3. T-Beam Tests	19
3.1 OVERVIEW.....	19
3.2 OBJECTIVES	19
3.3 EXPERIMENTAL PROGRAM.....	19
3.3.1 Test Matrix	19
3.3.2 Steel Reinforcement	24
3.3.3 Concrete.....	26
3.3.4 Carbon Fiber Reinforced Polymer (CFRP) Application	26
3.3.5 Test Setup	28
3.3.6 Instrumentation.....	30
3.4 TEST RESULTS OF 24-IN. DEEP T-BEAMS	33
3.4.1 Results of Beams with a 14-In. Web and A/D of 1.5	33
3.4.2 Results of Beams with a 14-In. Web and A/D of 3	36
3.4.3 Results of Beams with 8-In. Web and A/D of 3	39
3.4.4 Strain Variations in Transverse Reinforcement.....	43
3.4.5 Steel-CFRP Interaction in Uni-Directional Layout versus Bi-Directional Layout.....	44
3.4.6 Analysis of Contributions of Concrete, Steel, and CFRP to Shear Strength.....	45

3.4.7 Observations on Cracking Behavior.....	48
3.5 TEST RESULTS OF 48-IN. DEEP T-BEAMS	50
3.5.1 Test 48-3-14-1 (Control)	50
3.5.2 Test 48-3-14-2 (Uni-Directional / 10-in. Strips)	52
3.5.3 Test 48-3-14-3 (Uni-Directional / 5-in. Strips)	55
3.5.4 Test 48-3-14-4 (Bi-Directional / Wide Spacing).....	57
3.5.5 Test 48-3-14-5 (Bi-Directional / 10-in. Strips).....	59
3.5.6 Test 48-3-14-6 (Bi-Directional / 5-in. Strip)	61
3.5.7 Test 48-3-14-7 (10-in. Stirrups Spacing / Uni-Directional)	63
3.5.8 Test 48-3-14-8 (Uni-Directional / Double Layers).....	65
3.5.9 Test 48-3-14-9 (Bi-Directional / Double Horizontal).....	66
3.5.10 Test 48-3-14-10 (10-in. Stirrup Spacing / Bi-Directional).....	68
3.6 SUMMARY OF TEST RESULTS OF 48-IN. DEEP T-BEAMS	70
3.7 ANALYSIS OF TEST RESULTS	70
3.7.1 Control vs. Uni-Directional	70
3.7.2 Uni-Directional vs. Bi-Directional	73
3.8 CONCLUSIONS	80
Chapter 4. I-Beam Tests	83
4.1 OVERVIEW AND OBJECTIVE.....	83
4.2 EXPERIMENTAL PROGRAM.....	83
4.2.1 Test Specimen	83
4.2.2 Test Variables.....	85
4.2.3 Test Setup	86
4.3 TEST RESULTS	89
4.3.1 Overview of the Test Results	89
4.3.2 Effect of CFRP Layout.....	93
4.4 CONCLUSIONS	96
4.5 SUMMARY COMMENTS.....	96
Chapter 5. Pile Cap Girder Tests.....	97
5.1 OVERVIEW AND OBJECTIVE.....	97
5.2 EXPERIMENTAL PROGRAM.....	97
5.2.1 Test Specimens.....	97
5.2.2 Test Variables.....	100
5.2.3 Test Setup	106
5.3 TEST RESULTS	110
5.3.1 Overview of the Test Results	110
5.3.2 Single Curvature Results	111
5.3.3 Double Curvature Results.....	113
5.3.4 Effects of CFRP.....	116
5.4 CONCLUSIONS	121
5.5 SUMMARY COMMENTS.....	122

Chapter 6. Small-Scale Beam Tests	123
6.1 OVERVIEW AND OBJECTIVE.....	123
6.2 EXPERIMENTAL PROGRAM.....	123
6.2.1 Overview of Experimental Program.....	123
6.2.2 Typical Specimen Preparation and Strengthening.....	125
6.2.3 Test Matrix Details	130
6.2.4 Data Collection and Processing.....	149
6.2.5 Material Properties of CFRP and GFRP.....	155
6.3 TEST RESULTS	156
6.3.1 Series 1	156
6.3.2 Series 2	175
6.3.3 Series 3	180
6.3.4 Series 4	182
Chapter 7. Evaluation of Non-Destructive Test Procedures	193
7.1 OBJECTIVE.....	193
7.2 DETECTION OF ARTIFICIALLY INSTALLED DEFECTS.....	193
7.2.1 CFRP Strip Installation and Defect Detection.....	193
7.2.2 CFRP Anchor Installation and Defect Detection	196
7.3 LOADING INDUCED DEBONDING DETECTION.....	201
7.3.1 Sounding Tests	202
7.3.2 Ultrasonic Tests.....	205
7.4 IN-SITU DEBONDING MONITORING	207
7.4.1 Standard Beam Debonding Monitoring.....	207
7.4.2 Monitoring T-Beam Debonding	210
7.5 FINDINGS AND RECOMMENDATIONS	213
Chapter 8. Design and Detailing Recommendations for CFRP Anchors.....	215
8.1 DESIGN APPROACH	215
8.2 DESIGN GUIDELINES.....	216
8.2.1 Notations and Definitions.....	216
8.2.2 Sizing CFRP Anchors.....	217
8.2.3 Anchor Hole Details.....	219
8.2.4 Anchor Patch Geometry	220
8.3 DESIGN EXAMPLE	220
Chapter 9. Design and Detailing Recommendations for CFRP Shear Strengthening.....	223
9.1 OBJECTIVE.....	223
9.2 MATERIAL INTERACTION	223
9.2.1 Concrete Contribution	223
9.2.2 Transverse Reinforcement Contribution	226
9.3 SHEAR DESIGN EQUATIONS	231
9.3.1 Strength Reduction Factors	231

9.3.2 Proposed Shear Strengthening Design Guidelines	231
9.4 EVALUATION OF THE DESIGN EQUATIONS.....	234
9.4.1 Concrete Contribution Comparison.....	235
9.4.2 Shear Capacity.....	235
9.5 DETAILING REQUIREMENTS FOR CFRP LAYOUTS.....	236
9.5.1 Spacing Requirements.....	237
9.5.2 Use of Bi-directional CFRP Layouts.....	237
9.5.3 Strip Orientation.....	238
9.5.4 Anchor Requirements.....	238
Chapter 10. Quality Control of FRP Design, Installation, and Materials.....	239
10.1 OVERVIEW.....	239
10.2 TEST SPECIMEN AND PROCEDURE	239
10.2.1 Test Boundaries.....	242
10.2.2 Concrete Specimen Details	242
10.2.3 Concrete Specimen Preparation	243
10.2.4 FRP Installation.....	243
10.2.5 Testing.....	244
10.3 INTERPRETATION OF RESULTS.....	246
10.4 APPLICATIONS.....	246
10.4.1 Material and Design Qualification	246
10.4.2 Pre-qualifying an Installer for Anchored FRP Systems	246
10.4.3 Evaluating Field Material and Installation Quality	247
References	249
Appendix A: Design Example using the Proposed Design Guidelines.....	253

LIST OF FIGURES

Figure 2-1: Panel test concept	8
Figure 2-2: Test setup.....	8
Figure 2-3: View of test specimens	9
Figure 2-4: Details of steel reinforced panels.....	9
Figure 2-5: Formation of first cracking	10
Figure 2-6: Horizontal strain contours for typical panel (B5-45-2-5).....	12
Figure 2-7: Load-strain responses of panels with uni-directional CFRP layouts.....	13
Figure 2-8: Load-strain responses of panels with bi-directional CFRP layouts.....	13
Figure 2-9: Load-strain responses of panels with uni- and bi-directional CFRP layouts (30°, 60°).....	14
Figure 2-10: Load-strain responses of panels with different steel ratios.....	14
Figure 2-11: Load-strain responses of panels with various reinforcements.....	15
Figure 2-12: Load comparisons of specimens with differing concrete strengths and bi- directional CFRP layouts.....	15
Figure 2-13: Load versus average horizontal strains of panels reinforced with CFRP strips or sheets.....	16
Figure 2-14: Load versus average horizontal strains for panels with intermediate CFRP anchors	16
Figure 3-1: Test notations for T-beams	20
Figure 3-2: CFRP layouts used in 24-in. T-beams, $a/d = 3$	21
Figure 3-3: CFRP layouts used in 48-in. T-beams, $a/d = 3$	22
Figure 3-4: Transverse reinforcement for 24-in. T-beams	24
Figure 3-5: Cross-section of 14-in. web beam	24
Figure 3-6: Cross-section of 8-in. web beam	25
Figure 3-7: Steel cage of 48-in. T-beams, 27'8" beam (top), 40' beam (bottom).....	25
Figure 3-8: Cross-section of 48-in. deep T-beams	26
Figure 3-9: Different configurations used for vertical CFRP strips	26
Figure 3-10: Middle anchors for horizontal strips in bi-directional, top (before), bottom (after).....	27
Figure 3-11: Middle anchor detail (left), CFRP anchor (right).....	27
Figure 3-12: Amount of CFRP material for single and double layers of strips.....	28
Figure 3-13: Test setup for 24-in. T-beams.....	28
Figure 3-14: Test setup for 48-in. deep T-beams	30
Figure 3-15: Strain gages locations for 24-in. deep T-beams.....	31
Figure 3-16: Strain gages locations for 48-in. T-beams	32
Figure 3-17: Optical measurement system used in the testing program.....	33
Figure 3-18: 24-1.5-14-1 (left), 24-1.5-14-2 (right) [$a/d=1.5$, $b=14$ -in].....	34
Figure 3-19: Normalized shear vs. displacement for beams with a/d of 1.5	35
Figure 3-20: 24-in. deep beams with $a/d=3$, $b=14$ -in., and different amount of CFRP.....	36
Figure 3-21: Cracking behavior of bi-directionally strengthened specimens.....	36

Figure 3-22: Normalized shear versus displacement for 14-in. web with a/d of 3.....	38
Figure 3-23: Shear contributions for 14-in. web with a/d of 3	39
Figure 3-24: Cracking of 24-3-8-1	40
Figure 3-25: Cracking of 24-3-8-2	40
Figure 3-26: Concrete crushing behind anchors (24-3-8-2).....	40
Figure 3-27: Cracking of 24-3-8-3	41
Figure 3-28: Flange-web crack interface (24-3-8-3).....	41
Figure 3-29: Cracking of 24-3-8-4	41
Figure 3-30: Normalized shear versus displacement for 8-in. web beams with a/d of 3.....	42
Figure 3-31: Shear contributions of 8-in. web with a/d of 3	43
Figure 3-32: Strains in stirrups at different loading stages of 24-3-8 (Uni) and 24-3-14-1 (Bi-S).....	44
Figure 3-33: Strain variations in steel and CFRP, 24-3-8-2 (left), 24-3-8-3 (right).....	45
Figure 3-34: Shear contributions of 14-in. web beams with a/d of 3	46
Figure 3-35: Shear contributions of 8-in. web beams with a/d of 3	47
Figure 3-36: Steel contribution to shear capacity for 8-in. web beams.....	48
Figure 3-37: Cracking pattern of 8-in. web beams.....	49
Figure 3-38: Cracking pattern of 14-in. web beams.....	50
Figure 3-39: Cracking of 48-3-14-1	51
Figure 3-40: Crack width measurement of 48-3-14-1	51
Figure 3-41: Shear response of test 48-3-14-1 (control)	52
Figure 3-42: Test 48-3-14-2, cracking (top), failure (bottom).....	53
Figure 3-43: Shear response of test 48-3-14-2 (uni-10")	54
Figure 3-44: Principal strain profiles of test 48-3-14-2.....	54
Figure 3-45: Failure of 48-3-14-1 (top), cracking of 48-3-14-2 (bottom), under equivalent load.....	55
Figure 3-46: Shear response of test 48-3-14-3	56
Figure 3-47: Debonding of strips in 48-3-14-3	56
Figure 3-48: Cracking pattern of 48-3-14-3	57
Figure 3-49: Shear response test 48-3-14-4.....	58
Figure 3-50: Test 48-3-14-4 before (top) and after (bottom) failure	58
Figure 3-51 Shear response of test 48-3-14-5	59
Figure 3-52 Cracking and failure of 48-3-14-5	60
Figure 3-53 Shear contribution of steel stirrups and CFRP strip of test 48-3-14-5.....	60
Figure 3-54: Shear response of test 48-3-14-6	61
Figure 3-55: Cracking pattern and failure of test 48-3-14-6.....	62
Figure 3-56: Shear response of test 48-3-14-7	63
Figure 3-57: Principal strain profile of test 48-3-14-7 at major events [east side].....	64
Figure 3-58: Test 48-3-14-7 before (top) and after (bottom) failure [west side].....	64
Figure 3-59: Shear response of test 48-3-14-8	65
Figure 3-60: Failure of test 48-3-14-8	66

Figure 3-61: Shear response of test 48-3-14-9	67
Figure 3-62: Principal tensile profile of test 48-3-14-9 at major events.....	67
Figure 3-63: Test 48-3-14-9 before failure (top) and after failure (bottom).....	68
Figure 3-64: Shear response of test 48-3-14-10	69
Figure 3-65: Failure of test 48-3-14-10	69
Figure 3-66: Comparison of shear response of test 48-3-14-1 (control) and 48-3-14-2 (uni 10").....	71
Figure 3-67: Principal tensile strain of 48-3-14-1 (control-left) and 48-3-14-2 (uni- directional-right).....	72
Figure 3-68: Shear contributions of control test (top) and uni-directional test (bottom)	73
Figure 3-69: Shear versus shear deformations of control, uni-directional, and bi- directional tests.....	74
Figure 3-70: Failure of bi-directional test 48-3-14-6.....	74
Figure 3-71: Failure of uni-directional test 48-3-14-2, west side (top) and east side (bottom).....	75
Figure 3-72: Transverse steel contribution to the shear strength of control, uni-directional, and bi-directional tests.....	76
Figure 3-73: Crack width at mid-depth of control, uni-directional and bi-directional tests.....	77
Figure 3-74: Principal tensile strain profile for uni-directional test (left) and bi-directional test (right)	78
Figure 3-75: Shear contributions of control, uni-directional, and bi-directional tests.....	79
Figure 4-1: Honeycomb repair	83
Figure 4-2: Tendon profile	84
Figure 4-3: CFRP strengthening.....	84
Figure 4-4: CFRP anchor installation for uni- and bi-directional CFRP layout.....	85
Figure 4-5: CFRP area comparison	86
Figure 4-6: Test setup.....	88
Figure 4-7: View of test setup showing load cells and hydraulic ram.....	89
Figure 4-8: Anchorage failure of the tendons.....	90
Figure 4-9: Strengthening of the cut end.....	90
Figure 4-10: Appearance of test span after shear failure.....	91
Figure 4-11: Appearance of test span after bond failure	92
Figure 4-12: Shear strain calculation.....	93
Figure 4-13: Shear strain response of I-beams with different CFRP layouts.....	94
Figure 4-14: Principal tensile strain contours for an applied shear of 377-kips.....	95
Figure 4-15: Principal tensile strain contours for an applied shear of 416-kips.....	95
Figure 4-16: Shear contribution of CFRP, steel, and concrete (Uni-18R and Bi-18).....	96
Figure 5-1: Shear crack in pile cap girder	97
Figure 5-2: Longitudinal reinforcement	98
Figure 5-3: Transverse reinforcement	99
Figure 5-4: Experimental test matrix.....	100
Figure 5-5: Test nomenclature.....	101

Figure 5-6: Various CFRP strip layouts	103
Figure 5-7: CFRP anchor details	104
Figure 5-8: CFRP surface area comparison.....	106
Figure 5-9: Single curvature test setup and statics	107
Figure 5-10: Reaction in the test region (2-1000 kip load cells)	107
Figure 5-11: Applied load	107
Figure 5-12: Double curvature test setup and statics.....	108
Figure 5-13: Small applied load	108
Figure 5-14: Large reaction	109
Figure 5-15: Small reaction	110
Figure 5-16: Normalized shear contributions at cracking and ultimate shear capacity.....	111
Figure 5-17: Single curvature shear load-displacement curves.....	112
Figure 5-18: S-C-VA-HN crack pattern prior to CFRP installation.....	113
Figure 5-19: Bond and shear cracks	114
Figure 5-20: D-U-VA-HA flexural stiffness reduction	114
Figure 5-21: Double curvature shear load-displacement curves	115
Figure 5-22: D-U-VA-HA premature horizontal strip fracture	116
Figure 5-23: Double curvature mid-height crack width comparison.....	117
Figure 5-24: Single curvature anchored uni-directional.....	118
Figure 5-25: Double curvature uni-directional layouts, uncracked and cracked comparison	119
Figure 5-26: Double curvature fully wrapped and anchored uni-directional layouts, cracked sections.....	119
Figure 5-27: CFRP anchor post-failure	120
Figure 5-28: Double curvature fully wrapped uni- and bi-directional layouts, uncracked sections	120
Figure 5-29: Double curvature anchored uni- and bi-directional layouts.....	121
Figure 6-1: Anchor layouts.....	123
Figure 6-2: Beam specimen before CFRP installation (Series 1 to 3).....	124
Figure 6-3: Large beam specimens before CFRP installation	124
Figure 6-4: CFRP system loading in a three point load beam test	125
Figure 6-5: CFRP system loading in a concrete beam with inclined cracking.....	125
Figure 6-6: Specimen preparation before CFRP installation.....	127
Figure 6-7: Typical prepared specimen.....	127
Figure 6-8: CFRP anchors and CFRP strips (Huaco, 2009).....	128
Figure 6-9: Mixing the epoxy components (Huaco, 2009)	128
Figure 6-10: Saturating holes and surfaces (Hauco, 2010)	128
Figure 6-11: Applying CFRP strips.....	129
Figure 6-12: Fanning the anchor	129
Figure 6-13: Specimens with CFRP installed.....	130
Figure 6-14: Detailed drawings of concrete specimen	131
Figure 6-15: Detailed drawings of specimen with CFRP.....	132

Figure 6-16: Shear/tension failure mode in small beams	132
Figure 6-17: Concrete beam shear failure (Huaco, 2009)	133
Figure 6-18: Equivalent anchor area and anchor material ratio	134
Figure 6-19: Layout of unbonded specimens	135
Figure 6-20: Specimen nomenclature.....	136
Figure 6-21: Description of specimen nomenclature for Series 2	140
Figure 6-22: Test parameters for Series 3 beams	142
Figure 6-23: Description of specimen nomenclature for Series 3	143
Figure 6-24: Detailed drawings of concrete specimen	144
Figure 6-25: Detailed drawings of concrete specimen	145
Figure 6-26: Beam specimen failure	145
Figure 6-27: Typical steel reinforcing cage used in the larger specimens of Series 4	146
Figure 6-28: Diagram of forces and reinforcing bar layout.....	146
Figure 6-29: Specimen nomenclature.....	148
Figure 6-30: Test setup.....	149
Figure 6-31: Types of targets	150
Figure 6-32: Setup of the optical measurement system.....	151
Figure 6-33: Statics of beam specimen	153
Figure 6-34: Beam equilibrium (Sun, 2014)	153
Figure 6-35: Load deflection plots for total and net deflection at midspan.....	154
Figure 6-36: Contour plot of strain in the x direction.....	155
Figure 6-37 Targets used to find average strain and max strain.....	155
Figure 6-38 Loading and test setup for series 1-3	157
Figure 6-39 Typical load deflection plots for strip and anchor failure modes (Sun 2014)	157
Figure 6-40 Counter plot of strain ϵ_x in the x-direction (longitudinal direction) at various loading stages (Sun 2014)	158
Figure 6-41 Concrete beam shear failure (Huaco, 2010)	158
Figure 6-42 Delamination between CFRP strip and anchor.....	159
Figure 6-43 Area and targets selected for strain measurements.....	161
Figure 6-44 P_{ult} / P_{exp} vs. failure modes.....	164
Figure 6-45 Comparison of mean and maximum values of ϵ_{sx} 98% ult for different strip widths	165
Figure 6-46 Strain comparison between mean and maximum ϵ_{sx} 98% ult for different strip widths tests sustaining strip fracture and with an anchor material ratio of 1.41	166
Figure 6-47: Strain comparison between mean and maximum ϵ_{sx} 95% exp for directly comparable tests with 5-in. strips and different anchor-material ratio	168
Figure 6-48: Typical load versus deflection responses for tests with different bond condition and AMR=1.41 (1 in. = 25.4 mm, 1 kips = 4.45kN).....	170
Figure 6-49: Concrete-CFRP bond stress versus slip relations based on the optical measurement data	171
Figure 6-50: Load transfer from CFRP strip to CFRP anchor and concrete	172

Figure 6-51: Load vs. deflection of nominally identical test specimens	174
Figure 6-52: Anchor pullout.....	175
Figure 6-53: CFRP strip fracture.....	176
Figure 6-54: GFRP pullout, sectional view.....	176
Figure 6-55: Specimens with GFRP anchors exposed	177
Figure 6-56: Load versus strain for 5-in. bonded specimens	178
Figure 6-57: Load versus strain for 3-in. bonded specimens	179
Figure 6-58: Location of strain gauges.....	180
Figure 6-59: Loading diagram.....	182
Figure 6-60: Test setup.....	183
Figure 6-61: Typical load-deflection response for a test in Series 4	183
Figure 6-62: Concrete specimen failure leading to anchor pullout	185
Figure 6-63: Placement of strain gauges in Series 4	187
Figure 6-64: Strains for a 10-in. wide strip with one anchor.....	188
Figure 6-65: Strains for a 10-in. wide strip with two anchors.....	188
Figure 6-66: Comparison of failure stress versus normalized strip area parameter	189
Figure 6-67: Comparison of failure stress for tests from Series 1 and 4	190
Figure 6-68: Bond stress between CFRP anchor and strip at ultimate load	191
Figure 7-1: Artificial defect fabrication	193
Figure 7-2: Specimen with artificial defects after CFRP installation.....	194
Figure 7-3: Sounding method test setup.....	194
Figure 7-4: Time domain signals.....	195
Figure 7-5: Wavelet of signals	196
Figure 7-6: Schematic of the CFRP and anchor defects.....	197
Figure 7-7: Concrete slab before installation of CFRP strips and anchors.....	198
Figure 7-8: Concrete slab after installation of CFRP strips and anchors	198
Figure 7-9: Anchor defect detection using the sounding method.....	199
Figure 7-10: Time domain signals for anchor #1 and anchor #2.....	200
Figure 7-11: Frequency domain signals for anchor #1 and anchor #2	201
Figure 7-12: Frequency variation of signals obtained from anchor #1 and anchor #2.....	201
Figure 7-13: Load induced debonding detection using the sounding method.....	202
Figure 7-14: Time domain signals from measuring points.....	203
Figure 7-15: Frequency domain signals from measuring points	204
Figure 7-16: Changes in resonance frequencies along the length of the beam.....	205
Figure 7-17: Load induced debonding detection using the ultrasonic method.....	206
Figure 7-18: Time domain signals from the ultrasonic method	206
Figure 7-19: Normalized signal amplitude for ultrasonic method.....	207
Figure 7-20: Sensor arrangement on beam.....	207
Figure 7-21: Signals of sensor #9.....	208
Figure 7-22: Signals of sensor #2.....	208
Figure 7-23: Wave propagation.....	209

Figure 7-24: Debonding process of the beam.....	209
Figure 7-25: Evaluation of debonding length.....	210
Figure 7-26: T-beam PZT sensor arrangement.....	210
Figure 7-27: Cross-section of T-beam.....	211
Figure 7-28: Time domain signals for the T-beam prior to loading.....	211
Figure 7-29: Normalized time domain signals for the T-beam prior to loading.....	212
Figure 7-30: Changes in the normalized peak amplitude due to the applied load.....	212
Figure 7-31: Shear crack formation at sensors #6 and #7	213
Figure 8-1: Plan view of anchor system; left: anchor prior to adding patches, right: patches over anchor	215
Figure 8-2: Isometric view of anchor system	215
Figure 8-3: Anchor fan details.....	218
Figure 8-4: Anchor hole details.....	219
Figure 8-5: Example layout.....	222
Figure 9-1: Comparison of the shear area definition	224
Figure 9-2: Correlation between the concrete shear stress coefficient and the transverse reinforcement.....	225
Figure 9-3: Clamping force perpendicular to the shear crack	225
Figure 9-4: Flexural-shear crack	227
Figure 9-5: Evaluation of theta using the full and simplified MCFT (Bentz et al., 2006)	228
Figure 9-6: Experimental shear crack angle for S-U-VN-HN.....	229
Figure 9-7: Comparison of shear crack angles	229
Figure 9-8: Minimum and average CFRP strains across the critical shear crack at failure.....	230
Figure 9-9: CFRP variables used for shear strength calculations (ACI Committee 440, 2008).....	234
Figure 9-10: Comparison of the detailed and simple concrete contributions.....	235
Figure 9-11: Comparison of the experimental-to-predicted shear capacity	236
Figure 9-12: Detailing for a bi-directional CFRP layout.....	237
Figure 10-1: Isometric view of specimen.....	239
Figure 10-2: Test specimen details.....	240
Figure 10-3: FRP detailed layout, right side shows patch layout.....	241
Figure 10-4: Test setup.....	241
Figure 10-5: Formwork modifications	243
Figure 10-6: Self-reacting test setup.....	244
Figure 10-7: Boundary conditions.....	245
Figure 10-8: Commercial modulus of rupture test setup.....	245
Figure A-1: Cross-section of the T-beam example	253
Figure A-2: Designed uni-directional layout using the detailed concrete contribution.....	255
Figure A-3: Designed bi-directional layout using the detailed concrete contribution.....	256
Figure A-4: Vertical boundary anchor	259
Figure A-5: Horizontal boundary anchor	259
Figure A-6: Horizontal intermediate anchor	260

Figure A-7: Designed uni-directional layout using the simple concrete contribution.....	261
Figure A-8: Designed bi-directional layout using the simple concrete contribution.....	262
Figure A-9: Vertical boundary anchor	266
Figure A-10: Horizontal boundary anchor	266
Figure A-11: Horizontal intermediate anchor	267

LIST OF TABLES

Table 1-1: Organization of final report	5
Table 2-1: Test specimen variables	10
Table 2-2: Test result summary	11
Table 3-1: Test matrix for T-beams.....	20
Table 3-2: Summary of 14-in. wide web beams with a/d of 1.5 (deep beams)	35
Table 3-3: Summary of 14-in. wide web beams with a/d of 3	37
Table 3-4: Summary of 24-in. deep beams with 8-in. wide web beams and a/d of 3.....	42
Table 3-5: Shear contributions of 14-in. web beams with a/d of 3.....	46
Table 3-6: Shear contributions of 8-in. web beams with a/d of 3.....	47
Table 3-7: Test results of 48-in. deep T-beam series	70
Table 4-1: Concrete strength	84
Table 4-2: I-beam test matrix	85
Table 4-3: Summary of the test results.....	90
Table 5-4: Nomenclature description	101
Table 5-5: Single curvature test summary.....	113
Table 5-6: Double curvature test summary	116
Table 5-7: Single curvature shear contributions.....	118
Table 5-8: Double curvature shear contributions	121
Table 6-1: Details for anchor fans.....	137
Table 6-2: Test details	138
Table 6-3: Test details	141
Table 6-4: Test details	143
Table 6-5: Test variables for Series 4.....	148
Table 6-6: Fiber material properties.....	156
Table 6-7: Epoxy material properties	156
Table 6-8: Summary of experimental results for Series 1	162
Table 6-9: Experimental results for effect of strip width on strip fracture	164
Table 6-10: Results for tests sustained strip fracture and with an anchor material ratio of 1.41 for different strip widths.....	166
Table 6-11: Experimental results for effect of anchor-material ratio on strip fracture.....	167
Table 6-12: Results for strip fracture tests with 5-in. strips	168
Table 6-13: Results for anchor rupture tests with 5-in. strips and different anchor-material ratios	169
Table 6-14: Experimental results for effect of concrete strength on strip fracture.....	171
Table 6-15: Experimental results for effect of concrete strength on anchor rupture.....	172
Table 6-16: Experimental results for effect of fan geometry on strip fracture	173
Table 6-17: Summary of experimental results for Series 2	177
Table 6-18: Summary of experimental results for series 3.....	181
Table 6-19: Effects of anchorage type.....	181

Table 6-20: Summary of experimental results for Series 4	186
Table 6-21: Effect of strip width	186
Table 9-1: Proposed shear strengthening design equations.....	232
Table 9-2: Variable notation.....	233

Chapter 1. Introduction

1.1 BACKGROUND

The Texas highway system is handling larger volumes of traffic and heavier loads than were expected when many bridges were designed. Some truck traffic may need to be rerouted to avoid overloading bridges of questionable strength. CFRP strengthening to repair damage in critical locations or to remedy insufficient capacity for permitted overloads provides a valuable addition to structural preservation and life extension techniques.

The objective of the study is to demonstrate the feasibility of using bi-directional CFRP layouts for shear strengthening of large bridge beams and girders. This project is an outgrowth of project 0-6306 in which it was demonstrated that uni-directional CFRP strips and CFRP anchors could be used to improve the shear strength of reinforced concrete elements. The prime objective of that study was to evaluate the role of CFRP anchors. The tests showed that without anchors, the CFRP strips debonded and there was no significant improvement in the shear capacity. With CFRP anchors, it was possible to achieve a 40-50% increase in shear capacity. Tests of four 54-in. deep I-beams with both uni-directional and bi-directional CFRP strips indicated that the use of bi-directional strips led to improved shear behavior. Because data on bi-directional layouts of CFRP was limited, additional work was needed to understand the behavior of the CFRP in strengthening members subjected to large shear forces.

The previous study indicated that the quality of CFRP installation is a key element of the strengthening technique. There is a need for quality control procedures to make sure that the materials are used properly and the installation meets the design requirements. Currently there are no well-established quality control procedures available for CFRP anchors.

1.2 OBJECTIVES

The objectives of the research included the following items:

- Identify parameters that influence the shear strength provided by the bi-directional application of CFRP strips with CFRP anchors.
- Determine the extent that bridge elements benefit from bi-directional CFRP shear layouts and CFRP anchors.
- Provide design guidelines for shear strengthening using bi-directional application of CFRP strips with CFRP anchors.
- Provide engineers with design guidelines for CFRP anchors (e.g. embedment depth, spacing, and configuration pattern).
- Provide installation procedures for CFRP anchors for quality assurance.
- Determine design details that will enable the anchor to fully develop the strength of the CFRP strip.
- Develop in-situ anchor testing methodology using NDT procedures for quality control of installation.

1.3 WORK PLAN

To accomplish the objectives outlined above, three main tasks were carried out:

1. Study of bi-directional CFRP applications for shear strengthening of various bridge elements
2. Development of anchor design and quality control procedures
3. Provide design guidelines for implementation of CFRP materials and detailing requirements for improving the shear performance of bridge elements.

Task 1: Bi-Directional CFRP Applications

The following tasks were conducted to address the research objectives related to bi-directional applications of CFRP.

Task 1a: Panel Tests

Small-scale panels were tested to study the parameters that influence the shear strength provided by bi-directional CFRP. Panel tests were easy to conduct and enabled investigation of a wide range of parameters in a cost-effective manner. Results from these tests will guide the full-scale bridge-section tests that are necessary to develop the required design guidelines.

Key parameters investigated:

- Amount of CFRP
- CFRP inclination
- Amount of steel reinforcement
- Concrete strength
- Anchorage

Task 1b: T-Beam Tests

Test on T-beams strengthened with bi-directional CFRP were tested to study the effects of key parameters identified in the panel test program under realistic boundary conditions representative of rectangular sections. Several T-beams with overall heights of 24-in. and 48-in. that were tested in project 0-6306 with uni-directional CFRP applications were repeated to determine if bi-directional CFRP layouts were more efficient.

Key parameters investigated:

- Shear-span-to-depth ratio (a/d ratio)
- Amount of steel shear reinforcement
- Amount of bi-directional CFRP
- Concrete strength
- Beam web width

Task 1c: I-Beam Tests

Initially, an extensive program of full-scale prestressed I-beams was proposed. However, the Project Panel decided that I-beam tests were not a high priority. Although the intent was to procure beams from producers providing prestressed beams to TxDOT, that avenue did not materialize and it was possible to only obtain one beam, which was delivered to the laboratory. The tests conducted on that beam, a TX46 section, did not provide as much data as desired but corroborated the earlier findings that indicated a significant improvement in the cracking performance of the beams and control of crack widths.

Task 1d: Pile Cap Girder Tests

The initial intent of this task was the use of CFRP materials to strengthen full-scale prestressed U-beams. The Project Panel determined that observed cracking in pile cap girders was a more significant issue and suggested that Task 1d be focused on such beams. The program was modified accordingly. Since pile cap girders are usually large sections with wide webs, the test specimens were designed to use the largest possible cross-sections (32-in. x 32-in.) that could be tested in the laboratory. The Project Panel also recommended that both completely wrapped sections, as well as U-wraps with anchors be used since cap girders may have other beams resting on them and it will be impossible to completely wrap the entire shear span of the cap girder.

The following test matrix was derived to address the issues raised by the Project Panel:

- Effects of loading conditions
- Efficiency of retrofitting uncracked and cracked sections
- Placing CFRP anchors in known tension regions
- Efficiency of CFRP anchors relative to fully wrapped systems
- Effectiveness of fully wrapped and anchored uni- and bi-directional layouts

Task 1e: Design guidelines for bi-directional CFRP shear strengthening

Using the test result from the tasks above and data from project 0-6306, design guidelines for application of uni- and/or bi-directional CFRP strips with CFRP anchors for shear strengthening of various bridge elements were developed. The guidelines extend the procedures developed in project 0-6306 for sections with fairly narrow webs to sections with wide webs. The interaction between the concrete, steel, and CFRP materials carrying shear was shown to be important and that interaction is expected to be even more critical in narrow web members.

Task 2: Anchor Design and Quality Control Procedures

The focus of Task 2 was to address the following goals:

- Provide engineers with design guidelines for CFRP anchors (e.g., embedment depth, spacing, and configuration pattern).
- Determine minimum material properties that will enable the anchor to fully develop the strength of the CFRP material.
- Evaluate in-situ anchor testing methodology for quality control of installation.

The following sub-tasks were carried out to accomplish the stated objectives related to anchor design and quality control procedures.

Task 2a: Procedures for quality control of CFRP anchor installation

The objective of this task was to develop a simple test that could be used to qualify a particular CFRP material and/or a CFRP anchor installation. Based on the tests from Project 0-6306, work continued on the use of a standard 3-point-load beam test (commonly used to determine modulus of rupture for concrete pavements). Benefits of using the standard beam tests are: 1) they are widely used in structural engineering laboratories so most laboratories have the necessary equipment to conduct the tests; 2) the beams are (6"x6"x24") making them easily maneuverable by two workers without the need for lifting equipment; and 3) given the first two benefits, the cost of conducting such tests is reasonable.

The intent of this phase of the project was to:

- Optimize the test setup and beam design by varying details to achieve the most reliable and convenient design. Variables included: amount of CFRP, CFRP materials, and concrete strength.
- Evaluate the results obtained from the tests to determine the number of tests that need to be conducted to obtain a representative sample. Workmanship is the primary reason for variability in the data because there are a number of steps involved in the installation of CFRP strips and anchors and at each point in the process, small differences in workmanship may influence the performance. Information on variability is needed to set values for accepting or rejecting an installation or material.

Task 2b: Tests to optimize anchor design

Using the beam setup from Task 2a, the design and detailing of anchors were studied. Variables investigated:

- Area of CFRP in anchor
- Ratio of strength of CFRP anchor to strength of CFRP strip
- Depth of anchor into concrete substrate
- Size of anchor hole
- Radius of chamfer around the hole
- Anchor fan geometry
- Concrete strength

CFRP anchor design specifications and detailing requirements were developed. The specifications will allow designers to determine all anchor-hole dimensions, the amount of material to use in a given CFRP anchor, and anchor fan geometry, given the area of the CFRP sheet to be developed and concrete strength. This task was closely coordinated with Task 2a.

Task 2c: Evaluation of in situ non-destructive techniques for determining quality of CFRP sheet and anchor installations

To ensure proper transfer of forces between CFRP sheets and anchors, nondestructive testing (NDT) was evaluated as an in-situ method for quality control of CFRP installations. Ultrasonic methods were used to evaluate the quality of bond between CFRP sheets and anchors, CFRP sheets and concrete, and to detect voids in anchor holes.

The study included two steps as described below.

- **Step 1** - Perform ultrasonic tests on standard beams to determine the best test NDT procedure and parameters to quantify voids in anchor installation and to detect delamination between CFRP sheets/anchor and sheets/concrete.
- **Step 2** - Perform NDT measurements on T-beam tests.

Task 3: Final Report and Project Summary Report

The final report includes experimental results and analyses of the data that were used to develop the design recommendations for CFRP shear strengthening including the design of CFRP anchors. Detailing requirements for both strips and anchors have been developed. Guidelines for installation of CFRP strips and anchors are presented and accompanied by guidelines for quality assurance of anchor installations.

1.4 ORGANIZATION OF FINAL REPORT

Table 1-1 provides a guide to the reader for the organization of the final report indicating the location of various tasks vis-à-vis the chapters in the report.

Table 1-1: Organization of final report

Tasks	Topic	Chapter	Topic
Task 1: Bi-Directional CFRP Applications		1	Introduction
Task 1a	Panel Tests	2	Panel Tests
Task 1b	T-Beam Tests	3	T-Beam Test
Task 1c	Prestressed I-Beam Tests	4	I-Beam Tests
Task 1d	Pile Cap Girder Tests	5	Pile Cap Girder Tests
Task 1e	Design guidelines for bi-directional CFRP shear strengthening	9	Design and Detailing Recommendations for CFRP Shear Reinforcement
Task 2: Anchor Design and Quality Control Procedures			
Task 2a	Procedures for quality control of CFRP anchor installation	6	Small-Scale Beam Tests
		10	Recommendations for Quality Assurance Tests
Task 2b	Tests to optimize anchor design	6	Small-Scale Beam Tests
		8	Design and Detailing Recommendations for CFRP Anchors
Task 2c	Evaluation of in-situ non-destructive techniques for determining quality of CFRP sheet and anchor installations	7	Evaluation of Non-Destructive Test Procedures
Task 3: Final Report and Project Summary Report			

Chapter 2. Panel Tests

2.1 OVERVIEW

Because the data on the bi-directional layout of CFRP was limited in Project 0-6306, additional work was needed to understand the behavior of the CFRP in strengthening thin webs subjected to large shear forces. The observed shear strength increases in I-beams tested in project 0-6306 raised the following fundamental questions: 1) how did the thin anchored CFRP sheets that have no compression strength increase the compression capacity of a strut, and 2) why uni-directional CFRP layouts did not perform, as well as bi-directional layouts.

2.2 EXPERIMENTAL PROGRAM

2.2.1 Design Considerations

Small-scale panel tests were the starting point to investigate the parameters that influence the shear strength provided by bi-directional CFRP. Panel tests are relatively cheap and permit investigation of a number of parameters in a cost-effective manner. Results from these tests helped guide the large-scale tests that are needed to develop the design guidelines.

The panels were tested under compressive forces applied over a restricted area (Figure 2-1). Such loading generated a bottle-shaped compressive strut between loading and reaction points. The panels loaded in this fashion are intended to imitate the compression struts that form in the webs of I-beams as illustrated in Figure 2-1. The panels were 3-ft. by 3-ft. square and 6-in. thick. The test setup is shown in Figure 2-2.

2.2.2 Design Considerations

Several panels strengthened with CFRP strips are shown in Figure 2-3. Figure 2-3(a) shows uni-directional strips that are oriented at different angles to the vertical crack that forms through the panel. Figure 2-3(b) shows bi-directional arrangements so that comparisons can be made between the two cases. Another variable was the amount of steel reinforcement provided. Different amounts of CFRP strips and steel bars were used to verify effect of reinforcements. For the tests with intermediate anchors, the faces were fully wrapped (no strips) and the horizontal CFRP sheets were overlapped on the vertical sides of the panel. The details of panels with one or two layers of steel reinforcement are shown in Figure 2-4. The confining plates (shown in Figure 2-5) were installed before loading to prevent concrete crushing failure at the load and reaction plates. The side plates were clamped to the panel with three bolts that were tightened to provide confinement of highly-stressed concrete under the loading plates.

In addition, two concrete strengths were targeted in this study, normal strength of 5 ksi and high strength of 11 ksi to evaluate the effects of concrete strength on CFRP behavior. Table 2-1 shows a listing of the 23 specimens tested. The specimen notation is summarized below Table 2-1.

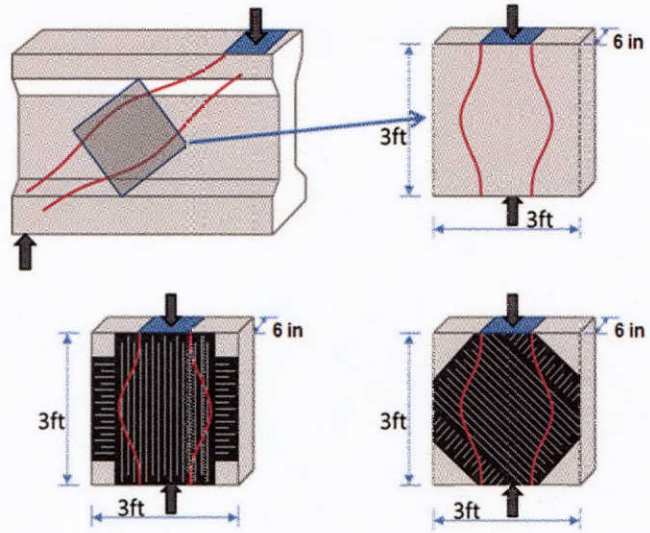


Figure 2-1: Panel test concept

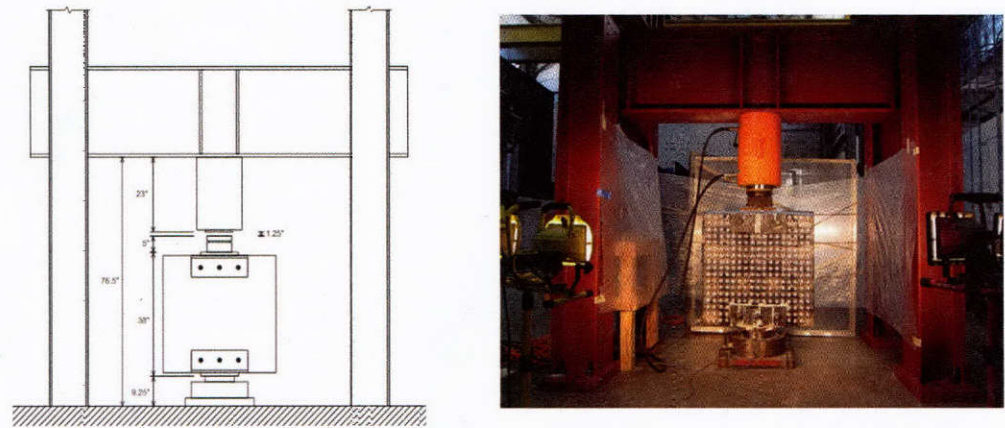
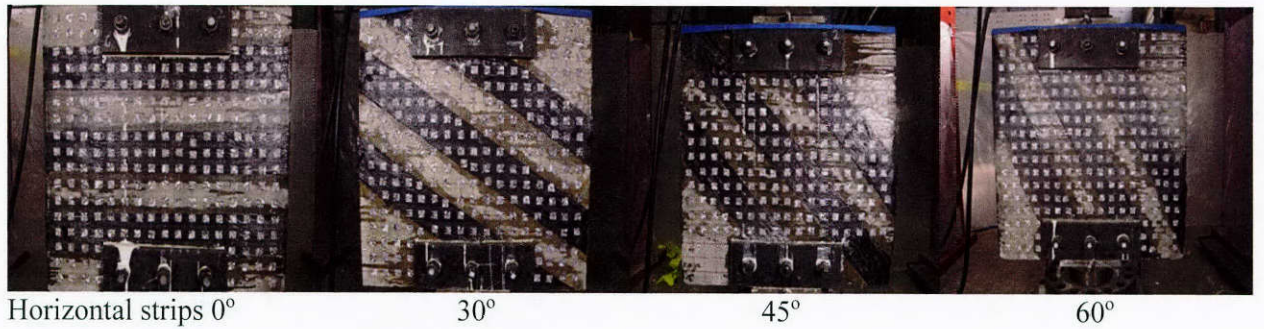
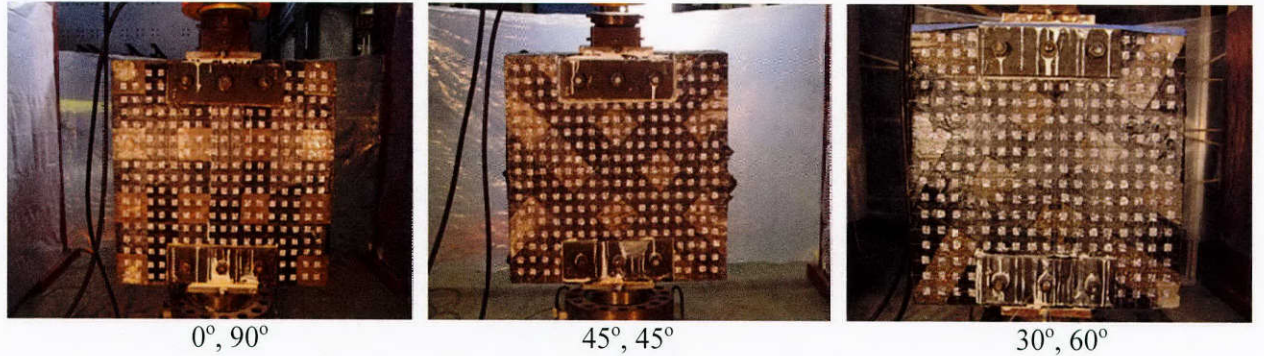


Figure 2-2: Test setup



a) Uni-directional CFRP sheet layouts and angles



b) Bi-directional CFRP sheet layouts and angles

Figure 2-3: View of test specimens

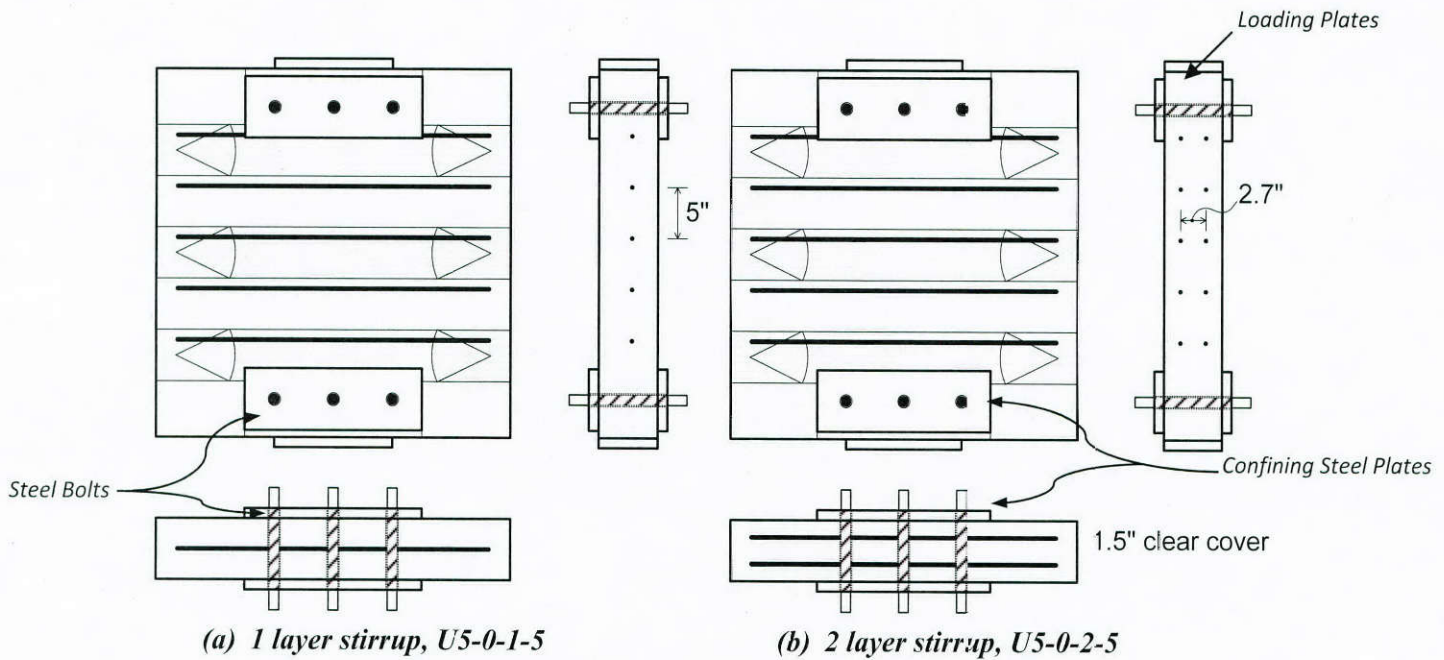
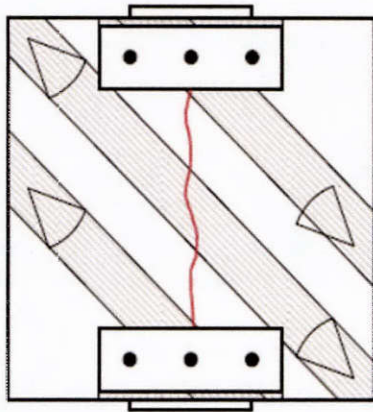
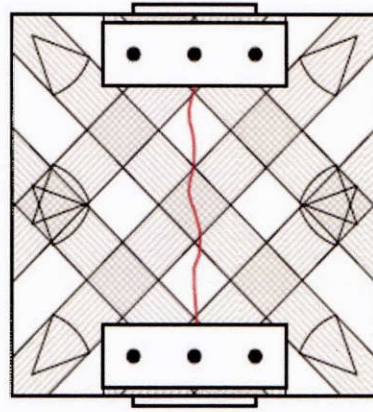


Figure 2-4: Details of steel reinforced panels



Uni-directional strips



Bi-directional strips

Figure 2-5: Formation of first cracking

Table 2-1: Test specimen variables

Concrete strength	Steel Reinforcement	CFRP layout	CFRP strip inclination	Notation
Normal strength	None	Non-reinforced	n/a	C0-0-0-5
		Uni-direction	0°	U5-0-0-5
			30°	U5-30-0-5
			45°	U5-45-0-5
			60°	U5-60-0-5
		Bi-direction	0°, 90°	B5-0-0-5
			45°	B5-45-0-5
			30°, 60°	B5-60-0-5
		Fully wrapped In both directions	0°, 90°	B36-0-0-5-0an
			0°, 90°	B36-0-0-5-4an
	0°, 90°		B36-0-0-5-6an	
	Rebar mat	Non-reinforced	n/a	C0-0-2-5
		Uni-direction	0°	U5-0-1-5
			0°	U5-0-2-5
30°			U5-30-2-5	
45°			U5-45-2-5	
60°			U5-60-2-5	
Bi-direction		45°	B5-45-2-5	
		30°, 60°	B5-60-2-5	
High strength	None	Non-reinforced	n/a	C0-0-0-11
		Bi-direction	0°, 90°	B5-0-0-11
			45°	B5-45-0-11
			30°, 60°	B5-60-0-11

Notation: First group of letter: U and B--Uni- and Bi-directional layouts, and CFRP strip width in inch; Second group: Angle of CFRP layout; Third group: Number of reinforcing bar layers; Fourth group: Nominal concrete strength in ksi; Fifth group: Number of intermediate anchors

2.3 TEST RESULTS

2.3.1 Overview of the Test Results

A total of 23 panels were tested. Table 2-2 shows a summary of test results of all the panels. A typical specimen failure was triggered by crushing of the compressive strut between the loading and reaction bearing plates, which led to large horizontal deformations and vertical cracking along panel centerline. Test results are evaluated in terms of the load capacity and the deformation of the panels in the horizontal direction (splitting strains). Panel tests are categorized in six different groups to evaluate the effects of CFRP strengthening with respect to 1) inclination of CFRP from principle crack in uni-directional CFRP layouts, 2) inclination of CFRP from principle crack in bi-directional CFRP layouts 3) effect of CFRP layout, 4) effect of amount of reinforcing materials, 5) load contribution of CFRP strips and steel reinforcement, 6) effect of concrete strength. Cracking loads generally occurred in a narrow range close to that of the control panel. The only tests that showed consistently higher cracking loads were the fully wrapped panels (B36) because the added CFRP material provided more restraint to lateral deformations and delayed the formation of the vertical crack. It should be noted that determining first cracking was difficult when much of the concrete surface was covered with a CFRP strips or sheets and the only indication was a change in the stiffness of the specimen.

Table 2-2: Test result summary

Specimen	Cracking load (kips)	Maximum load (kips)	Increment from control specimen	
			kips	%
C0-0-0-5	220	364	0	0
U5-0-0-5	201	486	122	34
U5-30-0-5	198	472	108	30
U5-45-0-5	202	448	84	23
U5-60-0-5	204	474	110	30
B5-0-0-5	232	475	111	31
B5-45-0-5	210	431	67	18
B5-60-0-5	227	462	98	27
B36-0-0-5-0an	289	540	176	48
B36-0-0-5-4an	290	572	208	57
B36-0-0-5-6an	284	563	199	55
C0-0-2-5	269	590	0	0
U5-0-1-5	274	635	45	8
U5-0-2-5	275	650	60	10
U5-30-2-5	265	588	-2	0
U5-45-2-5	292	626	36	6
U5-60-2-5	263	566	-24	-4
B5-45-2-5	309	656	66	11
B5-60-2-5	310	629	39	7
C0-0-0-11	298	617	0	0
B5-0-0-11	328	595	-22	-4
B5-45-0-11	381	749	132	21
B5-60-0-11	405	733	116	19

2.3.2 Behavior of Typical Panel Test

Figure 2-6 represents typical behavior of a panel that was reinforced with two layers of bars and strengthened with a 5-in. wide bi-directional CFRP layout with 45-degree angle. The panel failed by concrete crushing between the CFRP strips. All of the strain plots represent horizontal strains averaged over the height of the panel at the centerline.

Figure 2-6(b) shows the strain contour before cracking (250 kips). Average horizontal strain was 0.0002 at this load level. In Figure 2-6(c), tension zone can be clearly seen after the cracking load. The tensile strain outlines the formation of a compressive strut. Strains were higher at the unreinforced concrete surface between CFRP strips (Figure 2-6(d)) and development of a well-defined compressive strut is evident in the figure. The strain contour in Figure 2-6(e) was taken before the maximum applied load on the panel. At that load level, the average horizontal strain measured across a gage length of 8" over the height of the panel was 0.003.

CFRP strengthened panels had similar strain distributions and progressions during tests. However, the locations of the widest cracks varied according to CFRP strip layout.

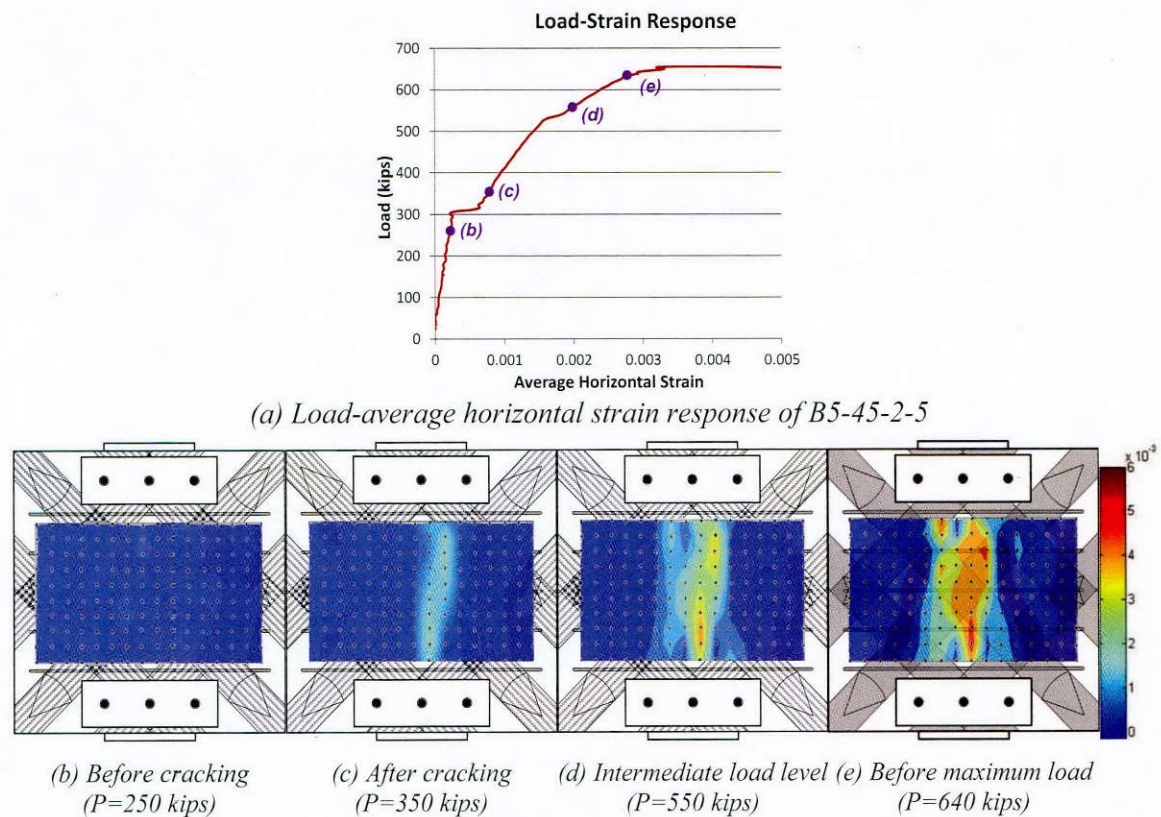


Figure 2-6: Horizontal strain contours for typical panel (B5-45-2-5)

2.3.3 Effect of CFRP Strip Inclination

As can be seen in Figure 2-7 the cracking loads of the uni-directional CFRP reinforced panels were similar to each other but post-cracking stiffness was different. The average strains in the strips with lower inclination from horizontal were smaller at all load levels. The maximum strength of the uni-directionally reinforced panels tended to decrease as the inclination of the strips to the crack decreased.

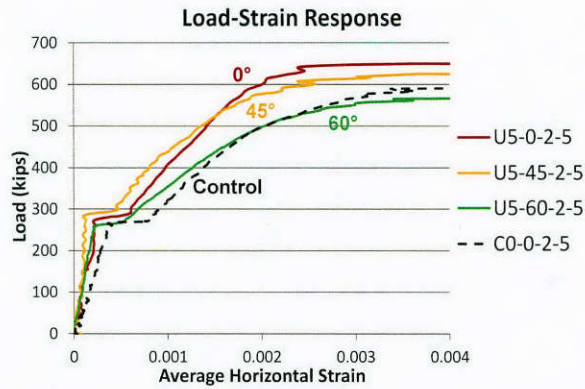


Figure 2-7: Load-strain responses of panels with uni-directional CFRP layouts

The effect of the bi-directional CFRP strip inclination layout is shown in Figure 2-8. Vertical CFRP strips were ineffective in contributing to the panel strength (Kim, 2014). Therefore, U-0-2-5 was considered to represent a bi-directional CFRP layout with horizontal and vertical strips. The cracking loads increased in the case of the two inclined bi-directional layouts. Micro-cracks did not immediately lead to wider cracks. The bi-directional CFRP strip layout resulted in all panels reaching similar maximum load capacity regardless of the strip inclination. A relatively small variation in the average horizontal strain at the same loads can be observed with the bi-directional CFRP layouts.

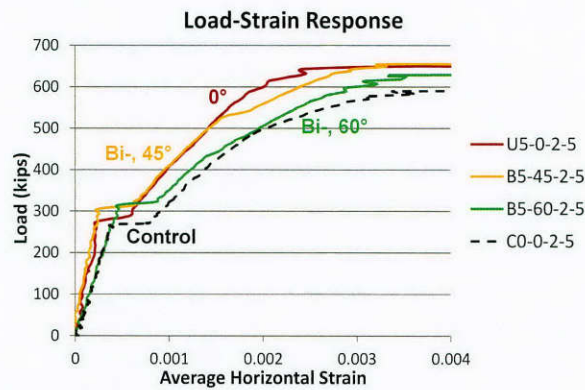


Figure 2-8: Load-strain responses of panels with bi-directional CFRP layouts

2.3.4 Effect of CFRP Layout

In Figure 2-9, load versus average horizontal strains are plotted for specimens U5-30-2-5 and B5-60-2-5. As can be seen in the figure, cracking and peak loads were higher with the bi-directional CFRP layout. Also, the average strain in the panel with the bi-directional layout was considerably smaller than in the panel with the uni-directional layout at the same load level.

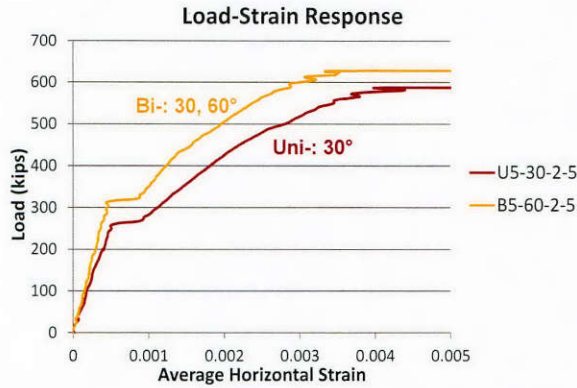


Figure 2-9: Load-strain responses of panels with uni- and bi-directional CFRP layouts (30°, 60°)

2.3.5 Effect of Amount of Steel Reinforcement

Figure 2-10 shows the load-strain responses of the three panels with different amounts of steel reinforcement. All the panels were reinforced with the same CFRP strip layout. The panels with steel reinforcement were considerably stiffer compared to U5-0-0-5. Large strains were observed in the panel that was only reinforced with CFRP strips. However, in the case of the rebar reinforced panels, lower levels of splitting strain were recorded. The CFRP strips allowed the panels to reach similar peak load level since the CFRP continued to restrain lateral expansion after the reinforcement yielded.

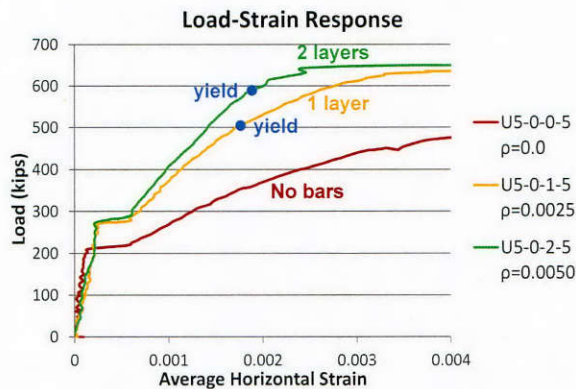


Figure 2-10: Load-strain responses of panels with different steel ratios

2.3.6 Load Contribution of CFRP Strips and Steel Reinforcement

In Figure 2-11, load-strain curves are plotted for panels with and without steel reinforcement. It should be noted that the steel reinforcement increases the capacity of the panel and that the CFRP contribution is smaller when steel reinforcement and CFRP are used together. As can be seen in this figure, the cracking load increased about 23 % when bars were added. However, different load increases were observed in the panels with different combinations of materials. The specimen with both CFRP strips and bars had the largest load increase and the lowest average horizontal strain at the same load levels. The force that could be contributed by the CFRP strips and the bars was the same. However, the load contribution of the steel reinforced panel to the panel strength was considerably greater than the CFRP contribution to the strengthened panel.

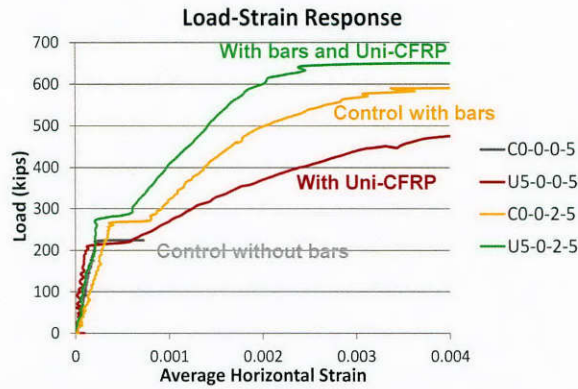


Figure 2-11: Load-strain responses of panels with various reinforcements

2.3.7 Effects of Concrete Strength

Figure 2-12 compares strengthened panels with different concrete strength and bi-directional CFRP layouts. The increase in concrete strength from 5 to 11 ksi resulted in an increase in cracking load of 36 % and in maximum load of 146 % of the high strength control panel. The increases in cracking load using bi-directional CFRP strips were highly correlated with tensile strength of the concrete. Using the $\sqrt{f'_c}$ as an indicator of the concrete strength, the tensile strength of the 11 ksi concrete would be about 48% higher than the 5 ksi concrete.

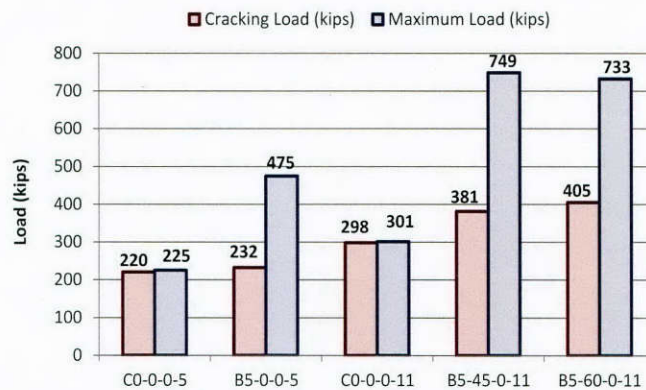


Figure 2-12: Load comparisons of specimens with differing concrete strengths and bi-directional CFRP layouts

2.3.8 Effects of the Amount of CFRP Material

Specimens B5-0-0-5 and B36-0-0-5 were compared to evaluate the effects of the CFRP material amount on panel performance. Figure 2-13 shows the load-strain responses of these panels. The cracking load of B36-0-0-5 was 32 % higher than that of the control panel, while the cracking load of B5-0-0-5 was only 5 % higher than that of the control specimen. A 250 kip increase in maximum load was obtained with the use of CFRP strips. However, a maximum load increase of only 315 kips was achieved when the amount of CFRP material was doubled in the fully wrapped application. The incremental strength gain obtained by doubling the amount of CFRP in the fully wrapped specimen was therefore only 65 kips from what was achieved in the strip-reinforced specimen. As observed in the I-girder tests (Kim et al., 2012), the strength increase in the panels was not proportional to the increase in the amount of CFRP used.

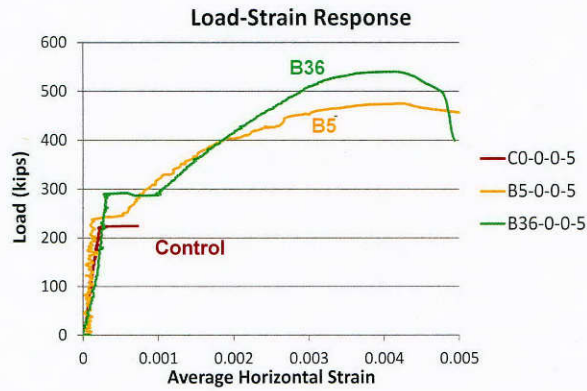


Figure 2-13: Load versus average horizontal strains of panels reinforced with CFRP strips or sheets

2.3.9 Effects of Anchorage Layouts

Figure 2-14 shows the load-strain responses of the fully wrapped panels with different intermediate CFRP anchor arrangements. The overall panel behavior was similar regardless of the number or presence of intermediate anchors. However, the additional anchors allowed the horizontal fibers to reach higher strains without significant loss of capacity beyond the maximum load. The anchors reduced the length over which the strains across the cracked regions of the panel could develop. As a result, the reduced length between the intermediate anchors resulted in higher strains being developed and higher post-peak loads being maintained.

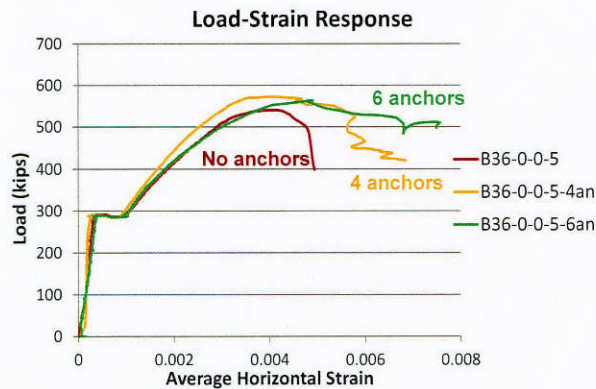


Figure 2-14: Load versus average horizontal strains for panels with intermediate CFRP anchors

2.4 CONCLUSIONS

Uni-directional CFRP layouts

- The uni-directional CFRP layouts did not significantly change the panel cracking load from that of the control test regardless of the angle of inclination.
- Increasing the angle (0° ~ 90°) between the CFRP fibers and the vertical splitting crack in the compressive strut led to increased maximum loads and decreased critical crack widths in the uni-directionally reinforced panels.

Bi-directional CFRP layouts

- Bi-directional CFRP layouts resulted in significant increases in the maximum loads of panels.
- Nearly identical cracking and maximum loads were observed in the orthogonal bi-directional CFRP layouts regardless of the CFRP angles.
- Bi-directional CFRP applications improved cracking performance of concrete members with higher strength concrete. Increases in cracking loads of about 36% were achieved in panels with high-strength concrete but only 5% in panels with regular-strength concrete.
- These findings can explain the significant increase in cracking load observed when strengthening bridge girders with high-strength concrete using bi-directional CFRP (Kim et al., 2012).
- The percentage increases in panel strengths were similar regardless of the concrete strength.
- Panel strength increases were not proportional to the amount of CFRP used. Doubling the amount of CFRP did not double the strength contribution of the CFRP.

Bi-directional vs. uni-directional CFRP layouts

- Higher cracking and maximum strength gains were obtained with bi-directional CFRP layouts than that of uni-directional CFRP applications.
- The bi-directional CFRP layouts controlled cracking better than uni-directional CFRP layouts. Strains perpendicular to the vertical splitting cracks of the bi-directionally strengthened CFRP layouts were lower compared to strains of the uni-directionally strengthened panels at all load levels.
- Effective shear crack control in concrete members and an increase in cracking load can be obtained with bi-directional CFRP applications compared with uni-directional CFRP layouts.

Effect of steel reinforcement

- Steel reinforcement was more effective in controlling the average horizontal strains in the cracked region than CFRP strips. There was better bond between the steel reinforcement and the concrete. This bond deteriorated less rapidly than did the debonding of the CFRP strips.
- Steel reinforcement in the panel reduced the contribution of the CFRP strips. Even though the tensile capacity of the steel reinforcement was the same as that of the uni-directional CFRP strips, the difference in bond properties between steel and CFRP limited the tensile force that could be developed in the CFRP.
- The addition of CFRP strips resulted in higher stiffness of the panels. The addition of CFRP strips to members with high transverse steel ratios is not likely to be very effective in improving the shear strength of the members.

Effect of intermediate CFRP anchors

- The introduction of intermediate CFRP anchors allowed the CFRP sheets to achieve more uniform strain distributions and better crack control. Such intermediate anchors may be useful for controlling shear cracks in concrete members and maintaining, or even increasing the concrete shear strength at cracking.

Chapter 3. T-Beam Tests

3.1 OVERVIEW

Extensive research has been devoted in the last decade to evaluate the use of externally bonded CFRP material in strengthening RC members in shear. Laboratory tests have demonstrated the value of strengthening with CFRP (Triantafillou, 1998; Khalifa et al., 1999; Adhikary et al., 2004; Zhang and Hsu, 2005; Pellegrino and Modena, 2006). However, the majority of these studies mainly focused on small scale, rectangular cross-sections with no or little transverse reinforcement, which are not representative of actual in-service members (Bousselham and Chaallal, 2006). A significant increase in shear strength was observed when externally bonded CFRP material is fully wrapped around the RC beams. Yet, when CFRP laminates were U-wrapped or side-bonded, debonding between CFRP laminates and concrete surface prevented the full utilization of the tensile capacity of CFRP material (Khalifa and Nanni, 2000; Chen and Teng, 2003; Zhang and Hsu, 2005).

The use of CFRP systems consisting of uni-directional CFRP strips anchored with CFRP anchors for shear strengthening of RC beams can result in a significant shear strength gain. The application of bi-directional CFRP laminates with CFRP anchorage provided a shear strength gain up to 40%. For this reason, the performance of the bi-directional application of CFRP laminates with CFRP anchors needs to be investigated to understand the shear mechanism that caused this difference between uni-directional and bi-directional applications of CFRP.

3.2 OBJECTIVES

Design recommendations for shear strengthening with FRP material that currently exist in design guides have different shortcomings. Most of these design recommendations were developed based on small-sized test specimens that may not represent the practical size of the members in Texas bridges. Recommendations were based on experimental test data that include some test specimens with no shear reinforcement, which may not be representative of practical members. Furthermore, the current recommendations do not include guidelines for anchored FRP systems and are limited to applications such as side bonded, U-wrap, and fully-wrapped systems.

The objectives of this task were to 1) evaluate the feasibility of using bi-directional CFRP laminates with CFRP anchors in shear strengthening of full-scale reinforced concrete beams with different shear reinforcement ratios, and 2) determine the difference between the uni-directional and bi-directional applications of CFRP in shear strengthening of reinforced concrete beams.

3.3 EXPERIMENTAL PROGRAM

3.3.1 Test Matrix

The experimental program for this task consisted of a total of 18 tests. Eight tests were performed on 24-in. deep T-sections while the other ten tests were performed on 48-in. deep T-sections. The full-scale reinforced concrete T-beams were designed to allow for direct comparison with previous experimental testing conducted in TxDOT project No. 0-6306.

A T-section was selected to reflect a typical bridge where the beam is part of a monolithic bridge deck. In this case, complete wrapping of the cross-section is not feasible. Using a U-wrap around the web of the cross-section is more suitable. However, in such a case, the failure mode of the U-wrap approach is likely to involve premature debonding. Therefore, CFRP anchors were provided to prevent this type of failure (Orton et al., 2008; Orton et al., 2009; Kim et al., 2011).

In the 24-in. deep T-beams tests, two tests were performed on a beam with a 14-in. wide web and a span-to-depth ratio (a/d) of 1.5. Two tests were conducted on a beam with a 14-in. wide

web and an a/d of 3. No control or uni-directional tests were included in the test matrix because these tests were previously carried out as part of TxDOT Project 0-6306. After the tests with 14-in. webs were completed, four tests were carried out on beams with 8-in. webs, to more closely reflect the range of web thicknesses of I-beams. Ten 48-in. deep T-beams with 14-in. webs constituted the remainder of the tests.

The 24-in. deep T-beam specimens and four of the 48-in. deep T-beam specimens were designed so that two different regions were tested on each beam. The final six 48-in. deep T-beam specimens were designed with three test regions in each beam. Table 3-1 shows the test matrix.

Table 3-1: Test matrix for T-beams

Depth	Shear span-to-depth ratio	Web Width	Stirrups Spacing (in.)	CFRP Application	No. of CFRP Layers		Concrete strength f'_c at 28 days	Test Notation (See Fig. 3.1)
					Vertical	Horizontal		
24	1.5	14	4	Bi-directional	Single	Single	3200	24-1.5-14-1
	1.5	14	4	Bi-directional	Double	Double		24-1.5-14-2
	3	14	10	Bi-directional	Single	Single	3200	24-3-14-1
	3	14	10	Bi-directional	Double	Double		24-3-14-2
	3	8	10	None	-	-	2500	24-3-8-1
	3	8	10	Uni-directional	Single	-		24-3-8-2
	3	8	10	Bi-directional	Single	Single	3400	24-3-8-3
	3	8	10	Bi-directional	Double	Double		24-3-8-4
48	3	14	18	None	-	-	2900	48-3-14-1
	3	14	18	Uni-directional	Single	-		48-3-14-2
	3	14	18	Uni-directional	Single	-	5400	48-3-14-3
	3	14	18	Bi-directional	Single	Single		48-3-14-4
	3	14	18	Bi-directional	Single	Single	4530	48-3-14-5
	3	14	18	Bi-directional	Single	Single		48-3-14-6
	3	14	10	Uni-directional	Single	-	48-3-14-7	
	3	14	18	Uni-directional	Double	-	4570	48-3-14-8
	3	14	18	Bi-directional	Single	Double		48-3-14-9
	3	14	10	Bi-directional	Single	Single		48-3-14-10

A simple notation system was established to designate each test. Each test label consists of four identifiers. Figure 3-1 illustrates the notation system used. Key parameters of each test are shown in Table 3-1.

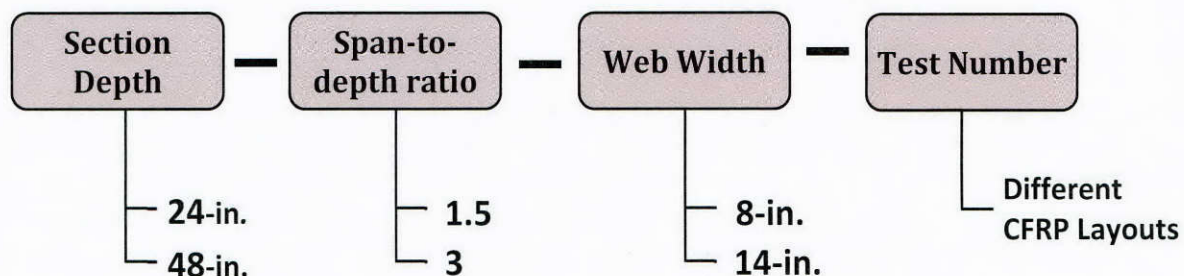


Figure 3-1: Test notations for T-beams

CFRP strips were applied on the web of the specimen vertically and horizontally to form uni- or bi-directional configuration. CFRP anchors were installed to provide anchorage for CFRP strips.

For 24-in. deep beams with an a/d of 3, the layout of CFRP strips is shown in Figure 3.2. The 5-in. wide vertical strips were spaced at 10-in. on center. The 5-in. wide horizontal strips were spaced at 10-in. on center. Both vertical and horizontal CFRP strips were anchored. Vertical strips were anchored with CFRP anchors at the ends only, whereas horizontal CFRP strips were anchored with middle-anchors as well as end-anchors.

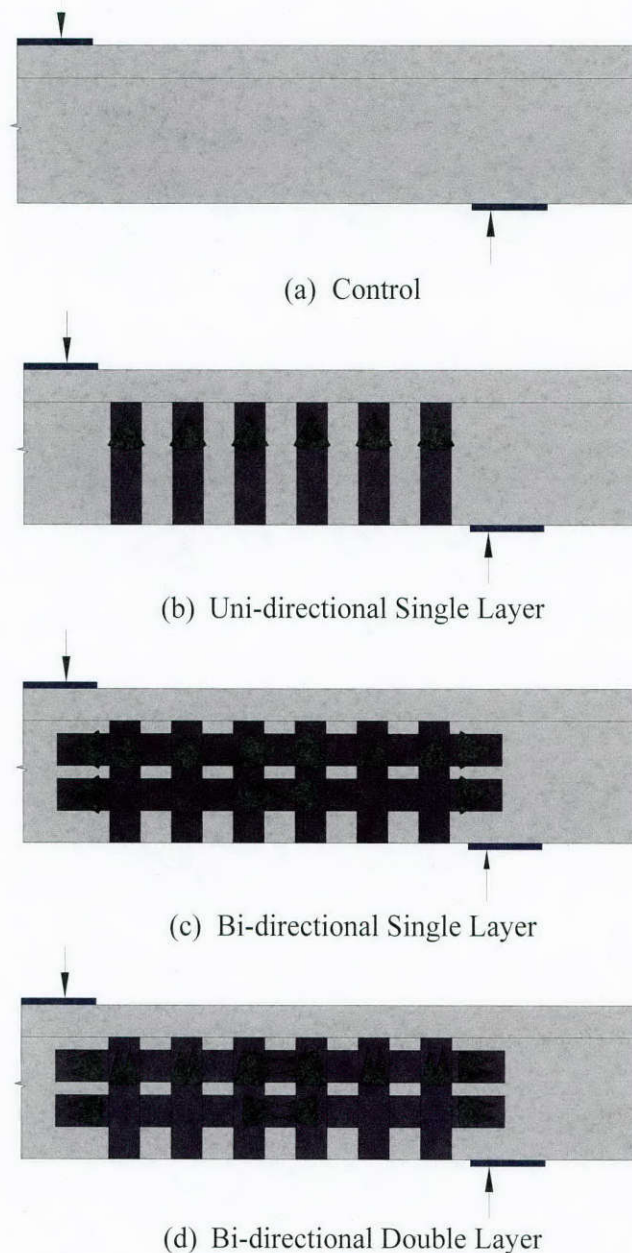


Figure 3-2: CFRP layouts used in 24-in. T-beams, $a/d = 3$

For the 24-in. deep T-beams with a/d of 1.5, the spacing of the vertical and horizontal CFRP strips was the same as shown for the beams with a/d of 3.

Figure 3-3 shows the CFRP layouts of the 48-in. deep T-beams series.

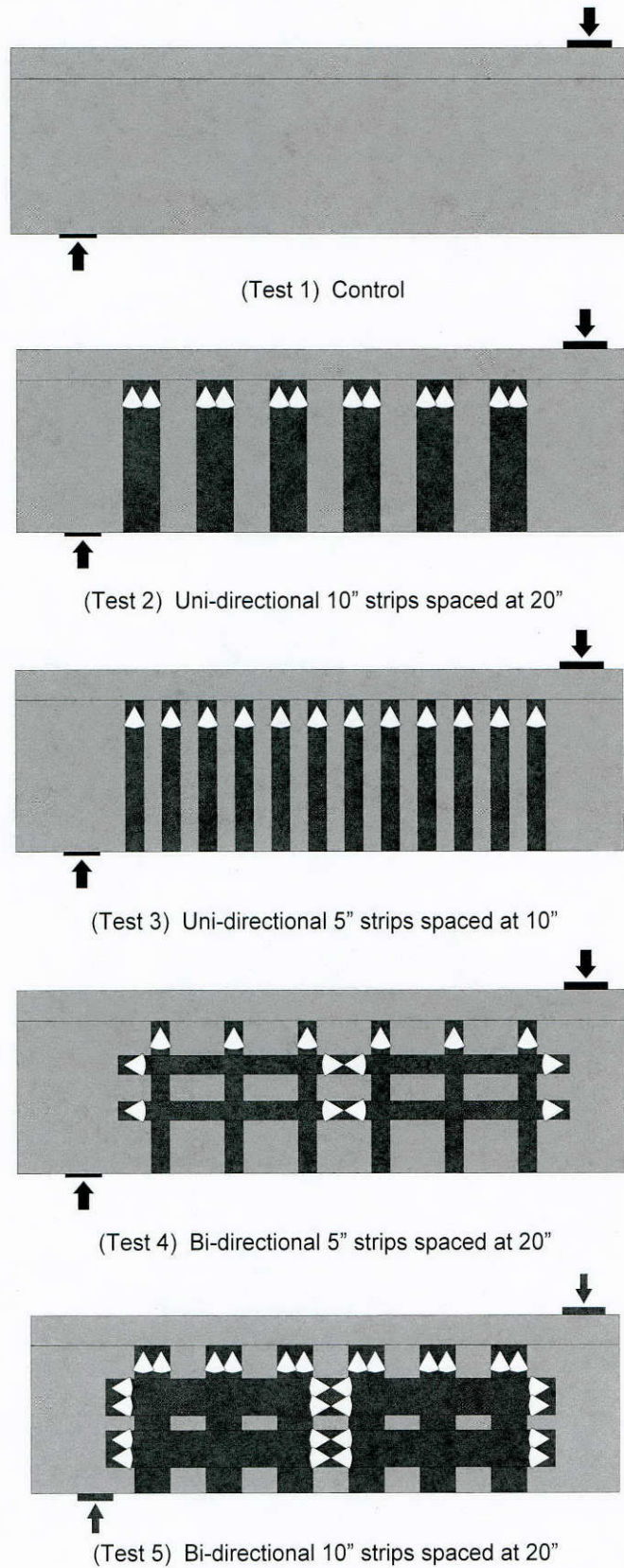
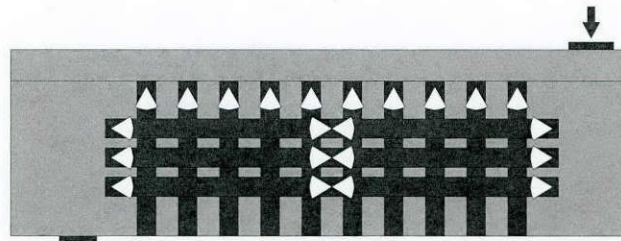
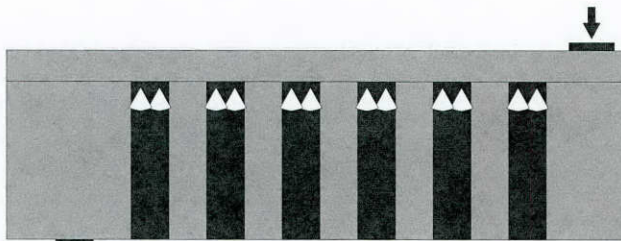


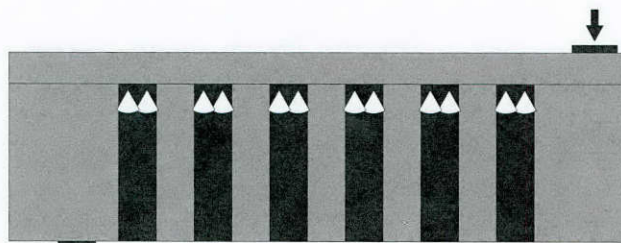
Figure 3-3: CFRP layouts used in 48-in. T-beams, $a/d = 3$



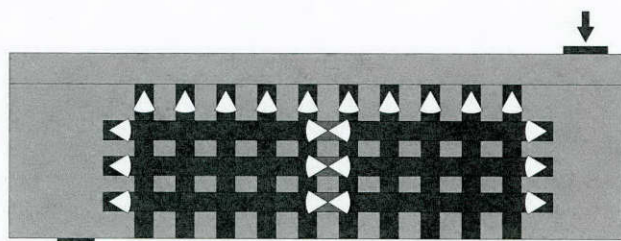
(Test 6) Bi-directional 5" strips spaced at 11"



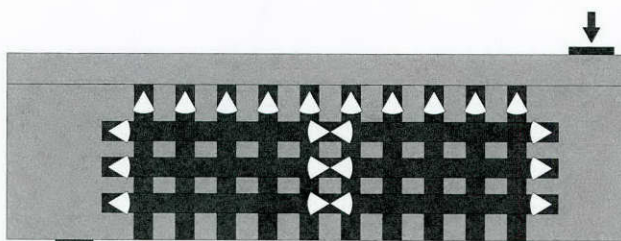
(Test 7) Uni-directional 10" strips spaced at 20" - 10" stirrup spacing



(Test 8) Uni-directional 10" strips spaced at 20" - Double layer



(Test 9) Bi-directional 5" strips



(Test 10) Bi-directional 5" strips - 10" stirrup spacing

Figure 3-3: CFRP layouts used in 48-in. T-beams, $a/d = 3$ (cont.)

3.3.2 Steel Reinforcement

The amount of internal transverse shear reinforcement affects the shear resistance of RC members. Furthermore, numerous in-service RC beams were found to be deficient in shear due to insufficient shear reinforcement (Khalifa and Nanni, 2000). The maximum allowable spacing for transverse reinforcement based on current code provisions (AASHTO, 2014 and ACI-318-11) was used in the test program. Figure 3-4 shows the transverse reinforcement spacing for the 24-in. deep T-beams.

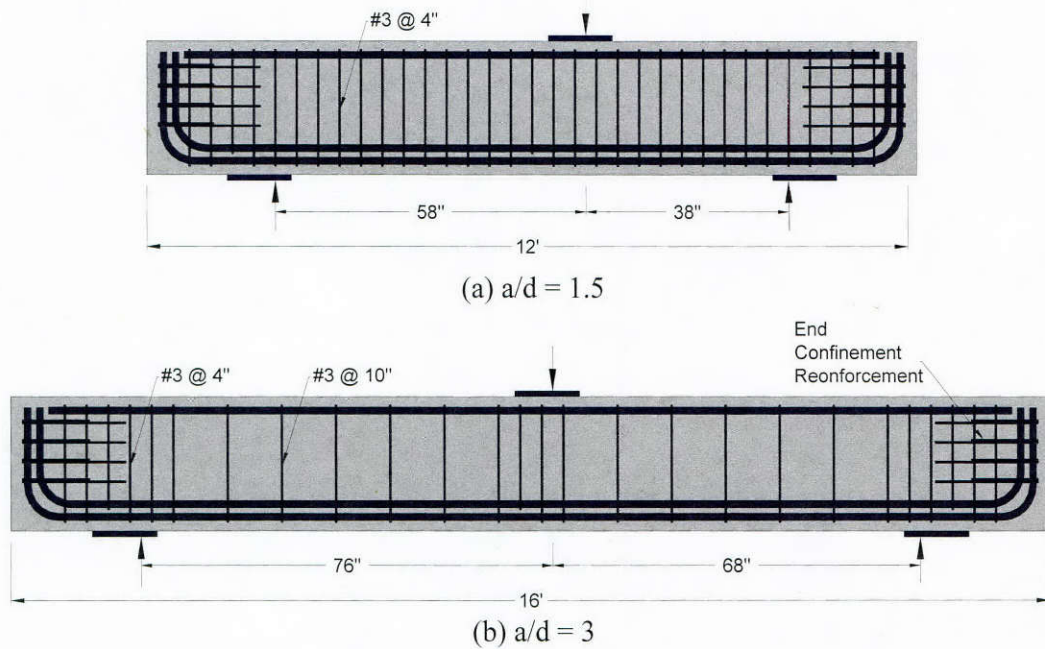


Figure 3-4: Transverse reinforcement for 24-in. T-beams

The cross-sections of 14-in. web specimen and 8-in. web specimen for the 24-in. deep T-section series are presented in Figure 3-5 and Figure 3-6.

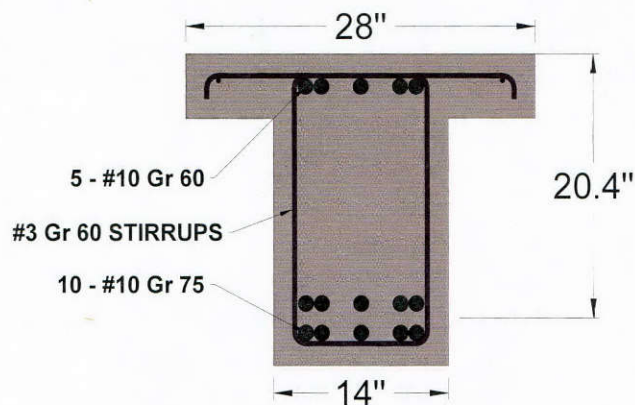


Figure 3-5: Cross-section of 14-in. web beam

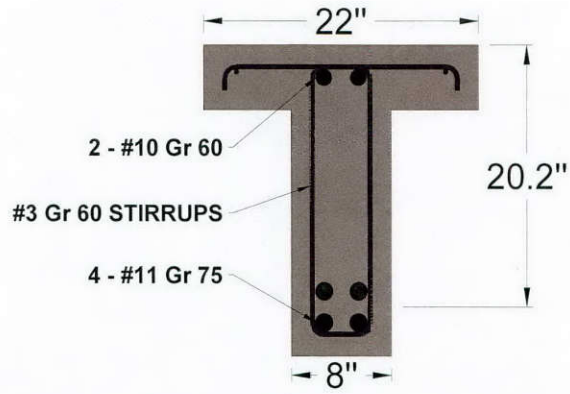


Figure 3-6: Cross-section of 8-in. web beam

For the 48-in. deep T-beams series, all beams were constructed with 14-in. wide webs. Figure 3-7 shows the reinforcement details for 48-in. deep T-beams. The cross-section of the 48-in. deep T-beams is shown in Figure 3-8.

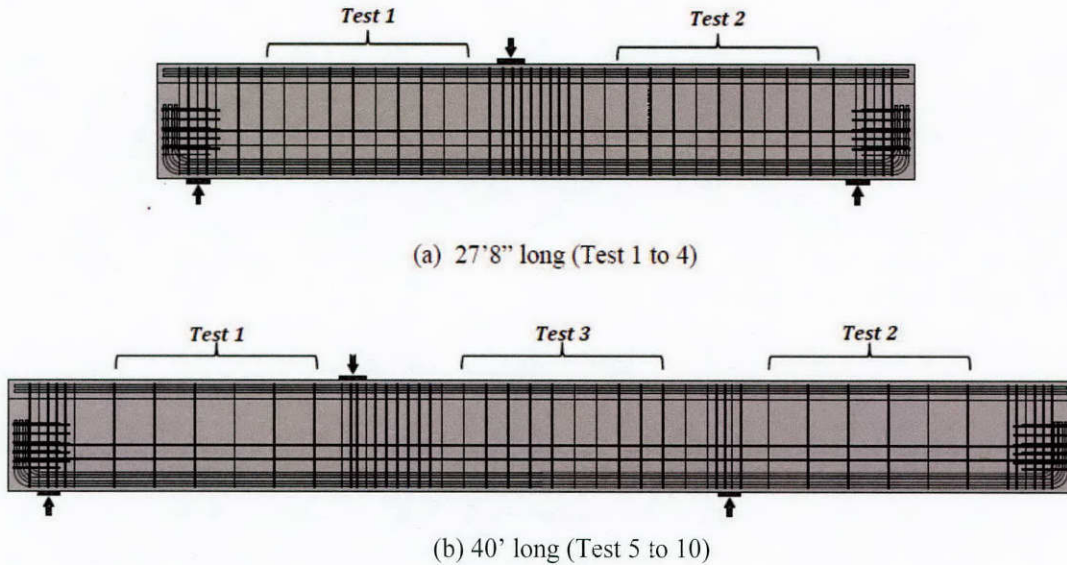


Figure 3-7: Steel cage of 48-in. T-beams, 27'8'' beam (top), 40' beam (bottom)

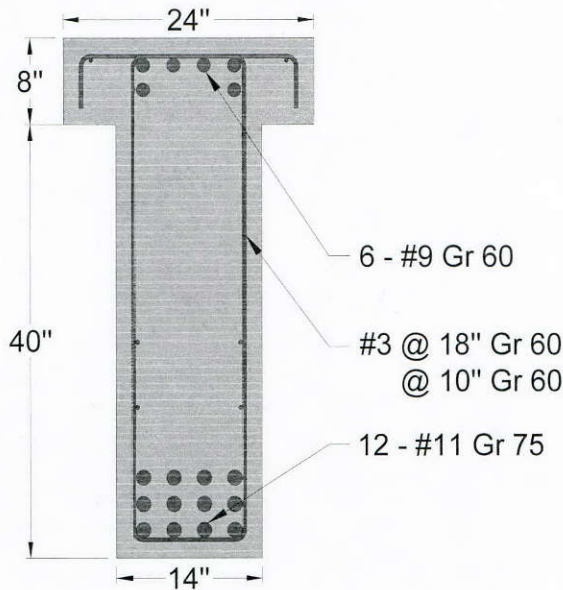


Figure 3-8: Cross-section of 48-in. deep T-beams

3.3.3 Concrete

Concrete with a relatively low 28-day compressive strength was used. Concrete compressive strengths of all beams tested are reported in Table 3-1. A low strength concrete was expected to reduce the concrete contribution to the total shear resistance and contributions from internal transverse reinforcement and external CFRP reinforcement were expected to be a larger percentage of the shear capacity.

3.3.4 Carbon Fiber Reinforced Polymer (CFRP) Application

For the application of bi-directional CFRP in the first test specimen, the vertical strips consisted of a single strip that was cut and installed. The end of the strip was attached at the top of the web on one side and then extended under the soffit to the other top side of the web. The installation of a single strip around the web of the beam was found to make the application process more difficult. Consequently, for the remaining specimens, two strips were spliced over the soffit of the web. Figure 3-9 illustrates the two methods used in applying vertical CFRP strips. The splicing of vertical strips considerably eased the installation process of bi-directional CFRP application. There were no problems with strips with splices reaching fracture.

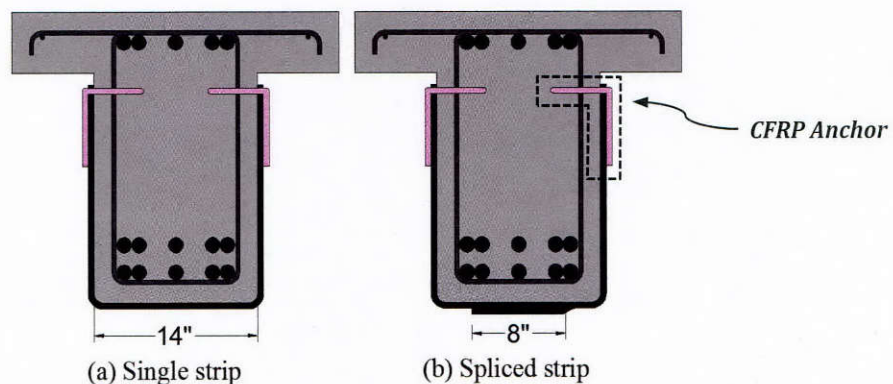


Figure 3-9: Different configurations used for vertical CFRP strips

To develop the full tensile capacity of the horizontal strips, CFRP end-anchors were used. However, for specimens with a shear span-to-depth ratio of three, these horizontal strips were long enough so end-anchors alone may not allow them to reach their full tensile capacity or to control cracking. Therefore, an additional middle-anchor was installed to reduce the anchorage distance of the horizontal strips, as shown in Figure 3-10.

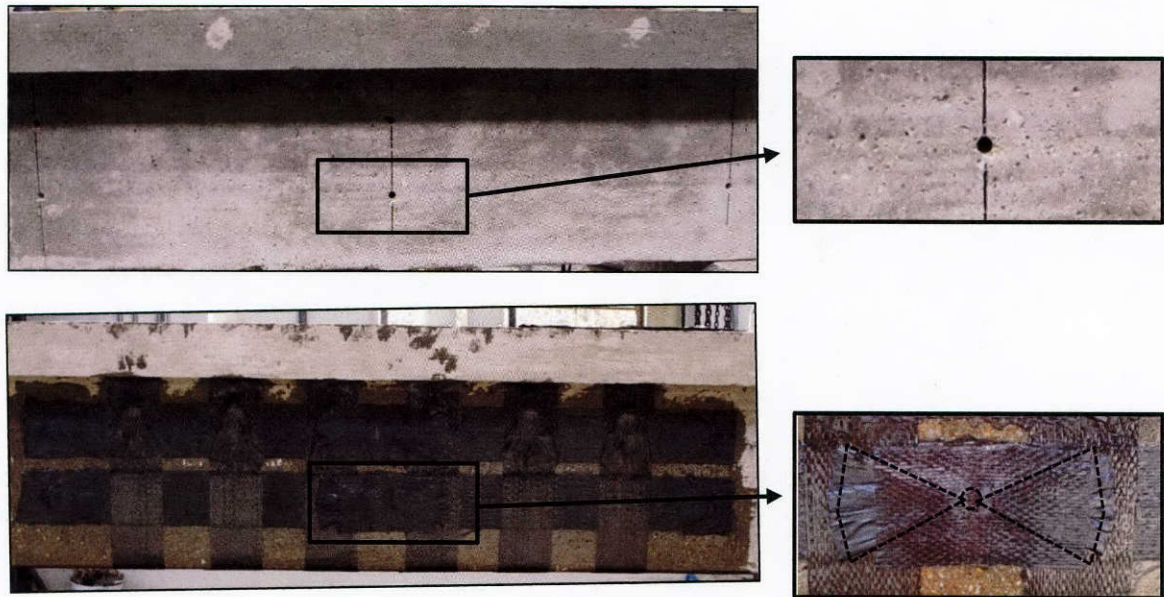


Figure 3-10: Middle anchors for horizontal strips in bi-directional, top (before), bottom (after)

The middle-anchor consisted of single anchor with a cross-sectional area greater than the end-anchor. In this study, CFRP anchors with 1/2-in. diameter were used as end-anchors; while CFRP anchors with 5/8-in. diameter were used as middle-anchors. The fan portion of the middle-anchor was split in two parts and fanned out in two opposite directions, as shown in Figure 3-11. A typical CFRP anchor used in this experimental program is also shown in Figure 3-11.

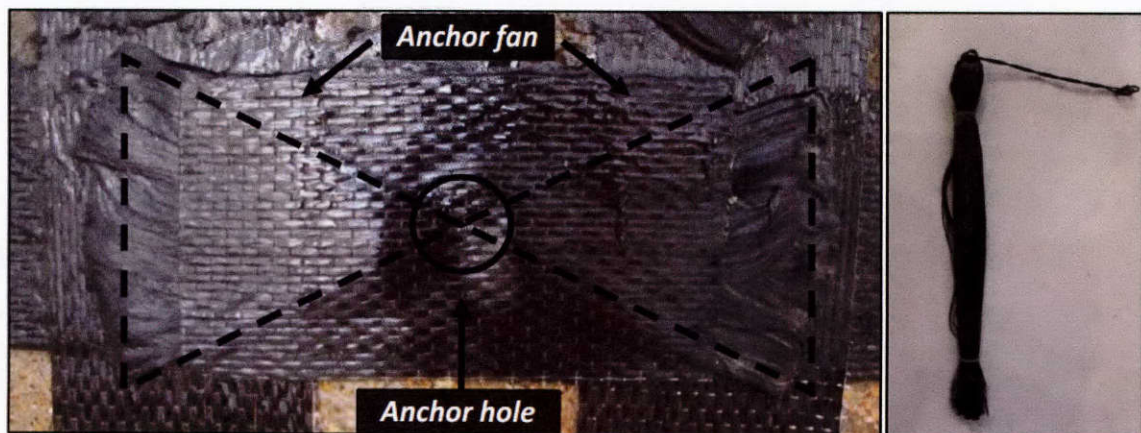


Figure 3-11: Middle anchor detail (left), CFRP anchor (right)

An anchor with a total cross-sectional area equaling at least twice the area of the CFRP strip was recommended (Orton et al., 2008) to develop the full tensile capacity of that CFRP strip.

The force developed in a strip should generate fracture of the strip rather than anchor failure. Design and detailing provisions for anchors are included in chapter 8 of this report.

For the case where the area of the CFRP strip was doubled, two anchors were installed instead of a single anchor in order to satisfy the cross-sectional area requirement (Figure 3-12). It was reported that multiple anchors provide better force transfer than a few large anchors (Orton et al., 2008). A detailed description of bi-directional application of CFRP strips with CFRP anchors in shear strengthening applications is discussed in Alotaibi, 2014.

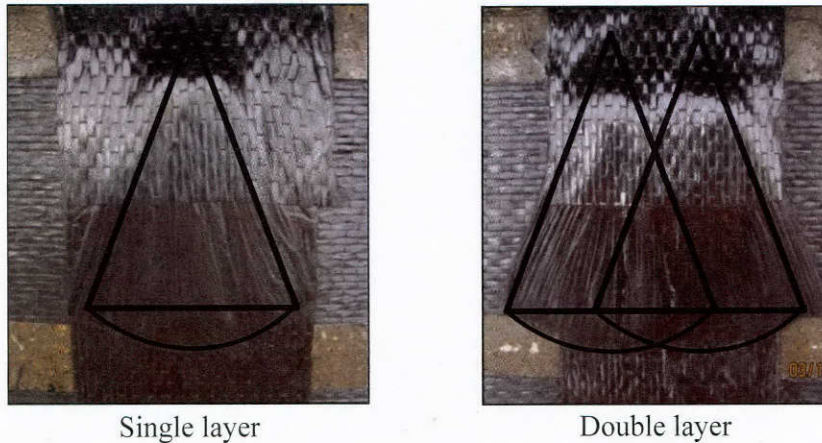


Figure 3-12: Amount of CFRP material for single and double layers of strips

3.3.5 Test Setup

A three-point loading system was used to test all specimens in the 24-in. series (Figure 3-13). For the test setup shown, the load was applied between the two reactions resulting in a larger shear force in the shorter span (test span) and a smaller shear force in the longer span, which was however still large enough to risk shear failure in the longer span. Therefore, to perform two tests from each specimen with the given test setup, pre-stressed external clamps were used to increase the shear capacity of the longer region. When the second span was tested, the first span was clamped so that it would support the shear force from the second test.

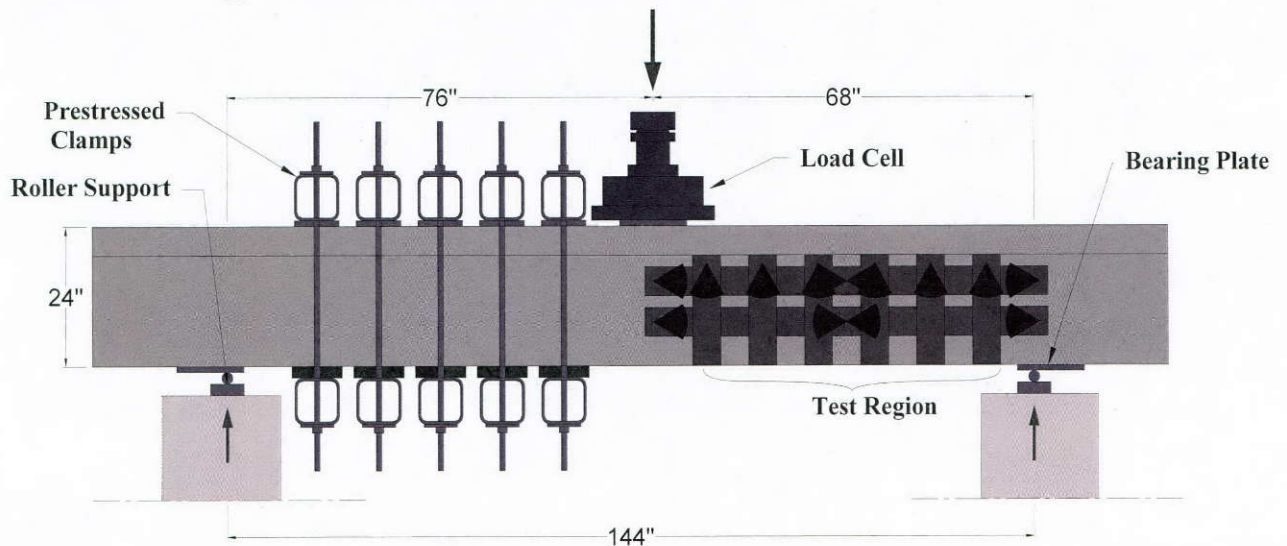


Figure 3-13: Test setup for 24-in. T-beams

The loading configuration of the 48-in. deep T-beams is shown in Figure 3-14(A). For the test setup shown, a loading frame with a 2,000 k hydraulic ram was used to apply load to the beams being tested. All specimens were simply supported by two identical reactions comprised of a 3-in. thick bearing pad that rested on a 4-in. thick loading plate, which transformed the reaction to two 1,000k load cells as shown in Figure 3-14(B). To perform two tests from each specimen with the test setup, pre-stressed external clamps were used to increase the shear capacity of that region as described above for the 24-in. T-beams. Also, due to the possible explosive failure of the test span, loading had to be stopped before failure occurred to allow testing the second span (Figure 3-14[C]).

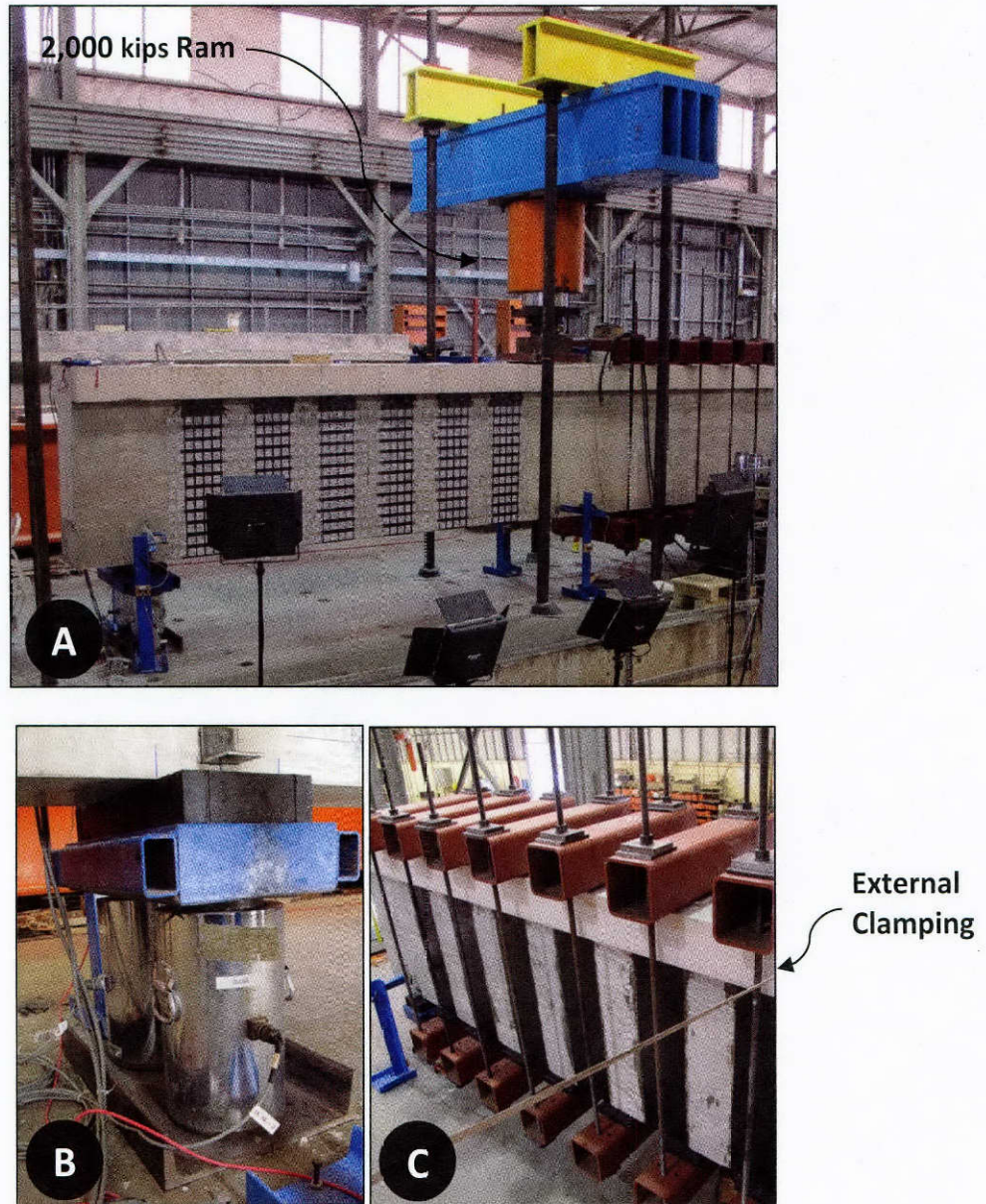
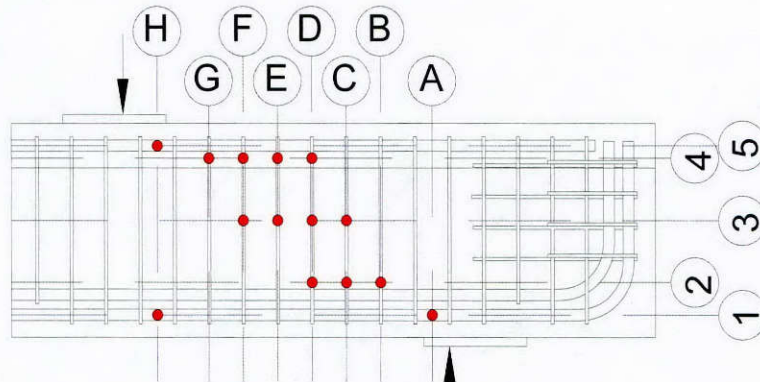


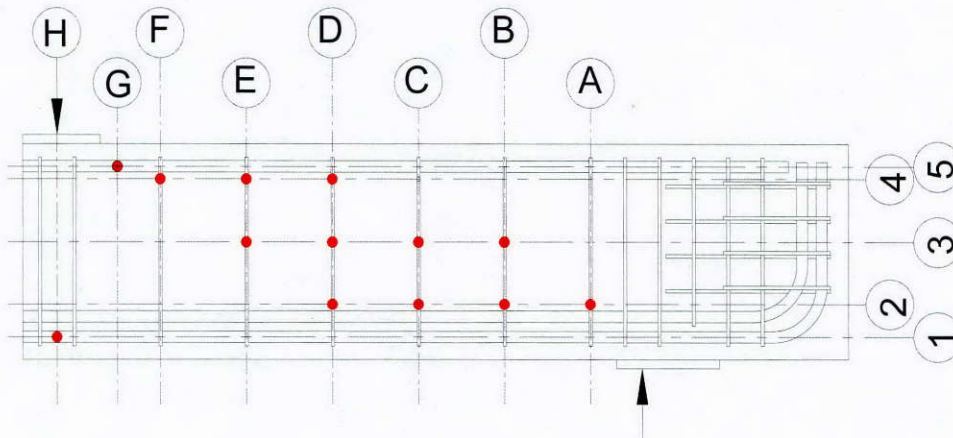
Figure 3-14: Test setup for 48-in. deep T-beams

3.3.6 Instrumentation

Strain gages were used to monitor strains in the transverse and longitudinal steel reinforcement. Most of the strain gages were placed on transverse reinforcement to determine the force carried by the steel stirrups. To monitor strains in the longitudinal reinforcement, additional strain gages were placed on the longitudinal bars to monitor maximum strains at peak moment locations. Strain gage locations in the 24-in. deep beams are shown in Figure 3-15. Strain gages were applied primarily to stirrups on one face of the web, with a few additional strain gages placed on the other face. For the 48-in. deep series, strain gage locations for specimens with stirrups at 18-in. and 10-in. spacing are shown in Figure 3-16.

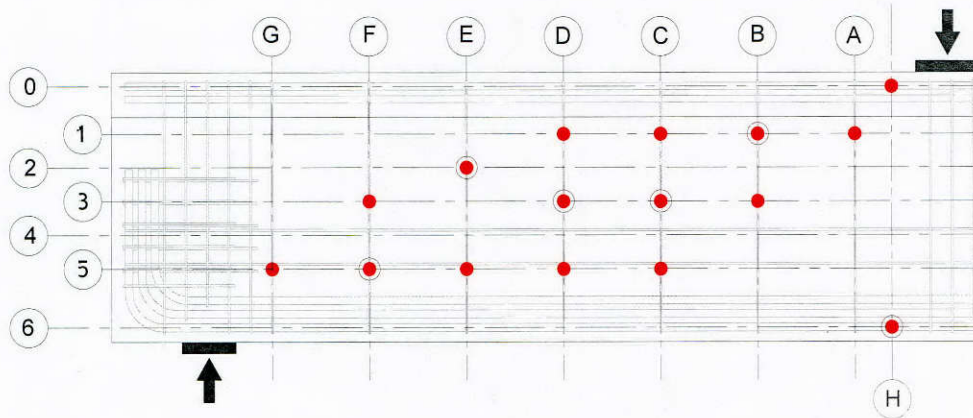


(a) a/d of 1.5, stirrups spaced at 4-in.

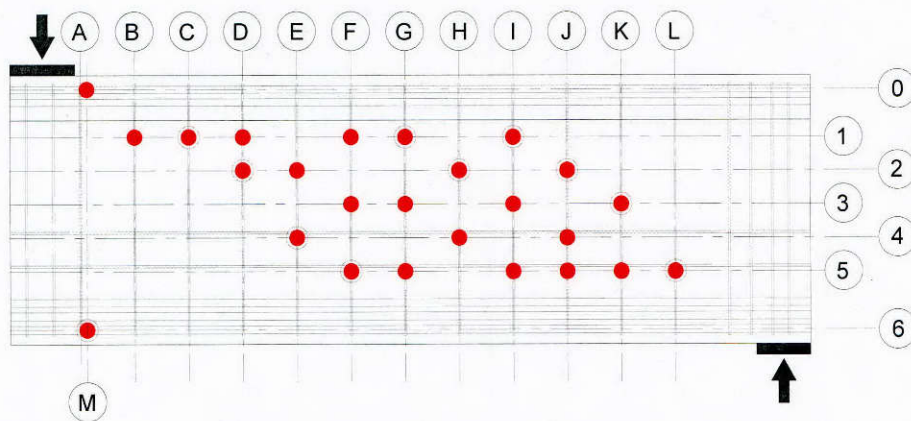


(b) a/d of 3, stirrups spaced at 10-in.

Figure 3-15: Strain gages locations for 24-in. deep T-beams



(a) Stirrups spaced at 18-in.



(b) Stirrups spaced at 10-in

Figure 3-16: Strain gages locations for 48-in. T-beams

An optical measurement system was used to monitor deformations of the targets on the test specimens. The measured changes in deformation between selected targets were used to determine average strains in the CFRP strips and the concrete. A detailed description of the optical measurement system in the current testing program is included in Chapter 6 (6.2.4.1). Figure 3-17 illustrates the optical measurement system used to monitor the T-beam specimens.

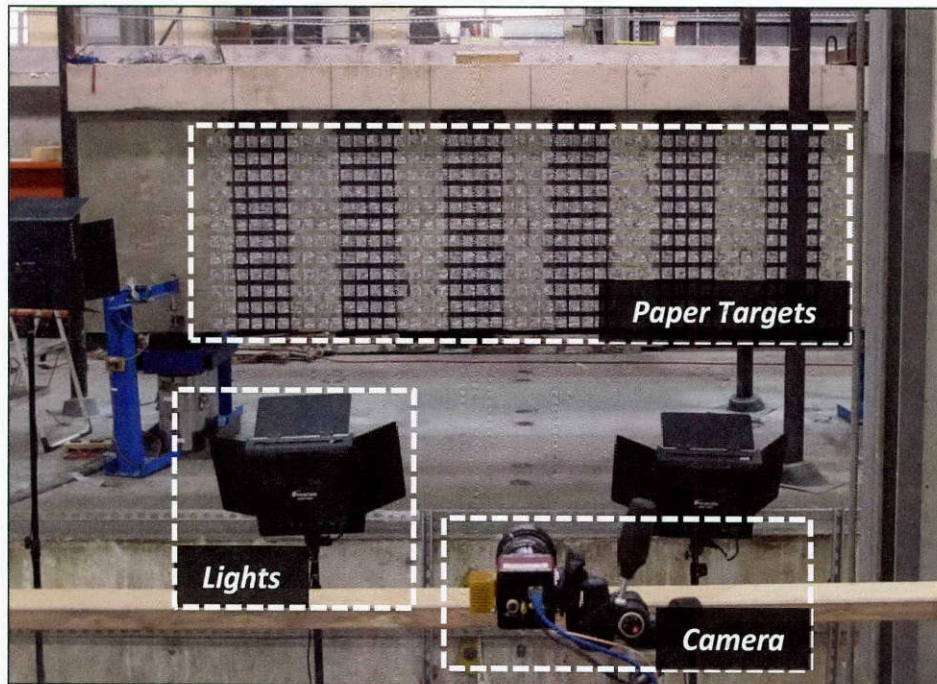


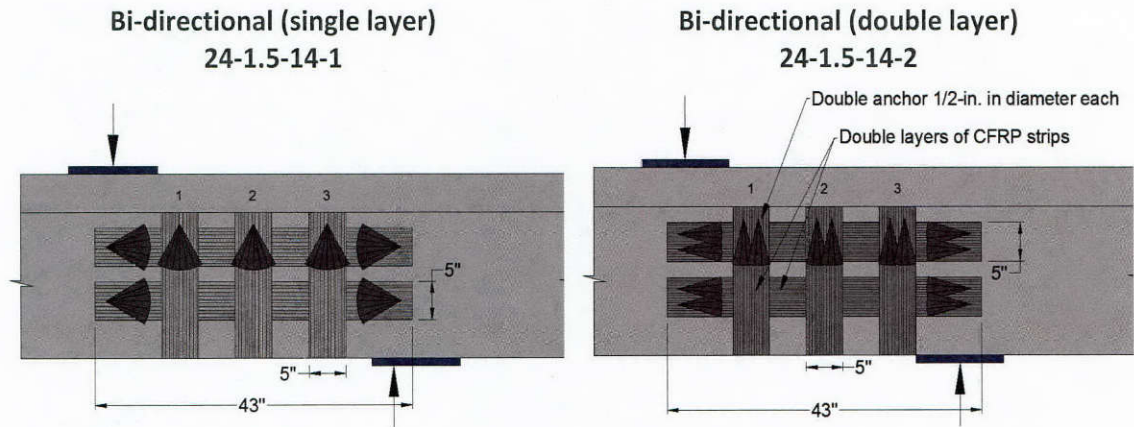
Figure 3-17: Optical measurement system used in the testing program

3.4 TEST RESULTS OF 24-IN. DEEP T-BEAMS

This section presents results obtained from the eight tests conducted on 24-in. deep T-beams. These results are divided into three groups based on 1) web width of 14-in. or 8-in., 2) shear span to depth ratio of 1.5, and 3) shear span-to-depth ratio of 3.

3.4.1 Results of Beams with a 14-In. Web and A/D of 1.5

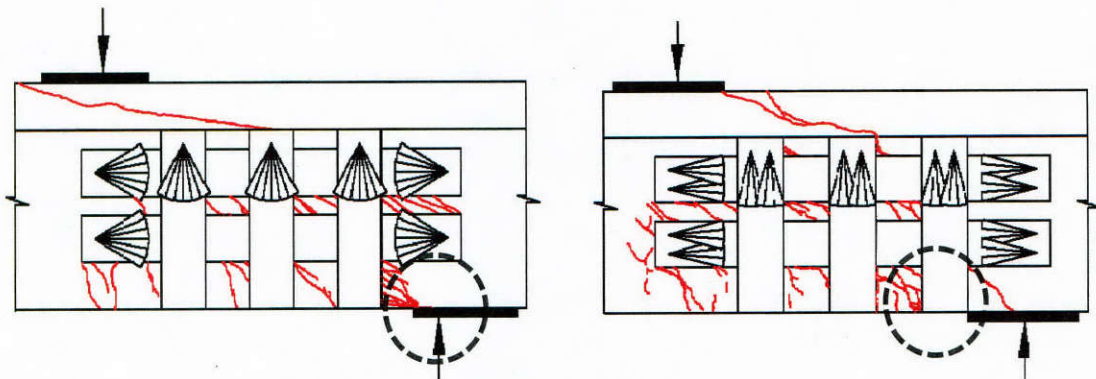
Specimens with $a/d \leq 2$ are classified as deep beams. The shear failure mechanism of a deep beam is usually controlled by the crushing of the concrete strut that forms between the point load and the support. In both tests, shear cracks initiated in the web of the specimen after reaching an applied shear of approximately 83 kips. As the applied load increased, additional shear cracks continued to form between the point load and the reaction. The failure was a combination of concrete crushing at the face of the node next to the support and the crushing of concrete strut that formed between the point of applied load and the support as shown in Figure 3-18(b).



(a) CFRP Layout



(b) Concrete Crushing Failure



(c) Cracking Pattern

Figure 3-18: 24-1.5-14-1 (left), 24-1.5-14-2 (right) [$a/d=1.5$, $b=14$ -in]

The maximum strain recorded in vertical CFRP strips was 0.007 in vertical strip #2, while the maximum strain recorded in the horizontal CFRP strip was 0.004 in the upper strip. All the stirrups within the test region yielded except the one closest to the point load (G4). The control specimen and the uni-directional specimens were tested in TxDOT project 0-6306 and allowed for a direct comparison with the specimens tested in this experimental program (24-1.5-14-1 and 24-1.5-14-2). The test results are summarized in Table 3-2.

Table 3-2: Summary of 14-in. wide web beams with a/d of 1.5 (deep beams)

Test Name	CFRP Layout	Shear Capacity V_{max} (kips)	Concrete strength f_c' (psi)	Maximum Normalized Shear $\frac{V_{max}}{f_c' \cdot b_w \cdot d}$	Ratio of $\frac{V_{strengthened}}{V_{control}}$	Displacement (in.)
24-1.5-3*	Control	233	3300	0.246	-	0.27
24-1.5-4*	Uni	264	3300	0.279	1.3	0.48
24-1.5-14-1	Bi-S	259	3200	0.284	1.5	0.31
24-1.5-14-2	Bi-D	255	3200	0.280	1.4	0.36

* Tested in TxDOT Project 0-6306

The forces were directly transferred from the load point to the closest reaction. As a result, the shear failure mechanism is dominated by crushing of the concrete strut and at the face of the node. Therefore, test results were normalized with respect to the compressive strength of the concrete. Normalized shear strength versus displacement curves for the beams with a/d of 1.5 are shown in Figure 3-19.

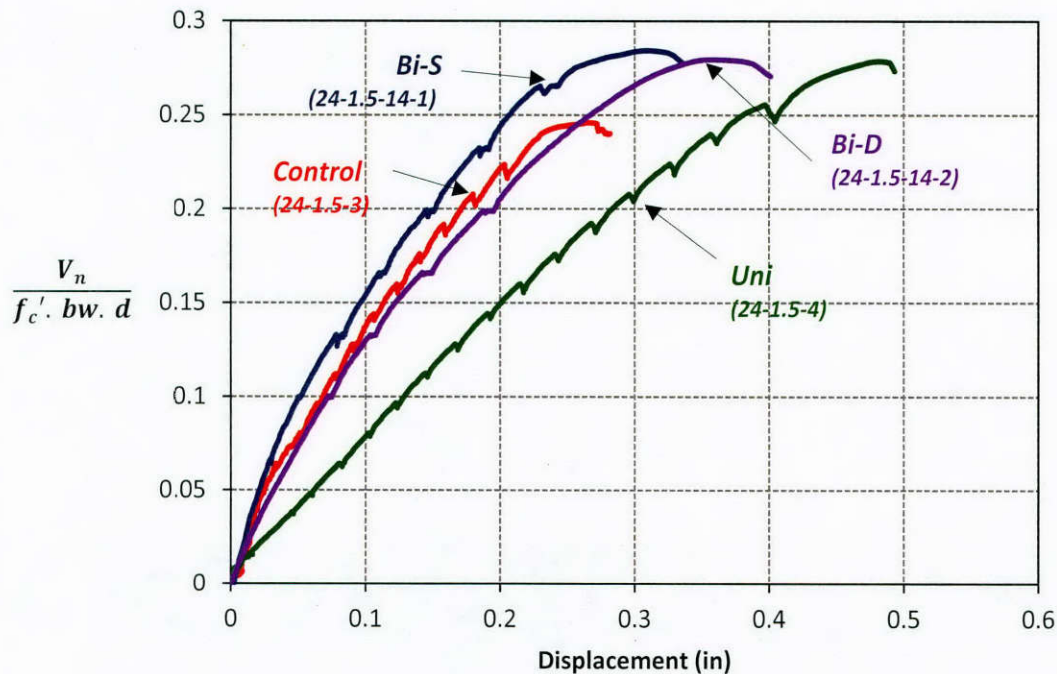


Figure 3-19: Normalized shear vs. displacement for beams with a/d of 1.5

The initial stiffness of all test specimens is almost identical except for specimen 24-1.5-4, which was initially tested as control specimen 24-1.5-3. The cracked specimen was then strengthened and retested as 24-1.5-4. The CFRP strengthening system had a negligible effect on the stiffness of the reinforced concrete members. All strengthened specimens had higher strength and reached greater displacement than the control specimen.

The control specimen peak strength was $14\sqrt{f_c'} \cdot b_w \cdot d$ (in psi units), which is above the upper limit on shear capacities in most codes. Since the mode of failure was controlled by the concrete, the CFRP strips had a minor influence on the behavior of the beam.

3.4.2 Results of Beams with a 14-In. Web and A/D of 3

Two tests were conducted with identical details except for the amount of CFRP material used. The CFRP layouts and the cracking patterns for both tests in this series are presented in Figure 3-20.

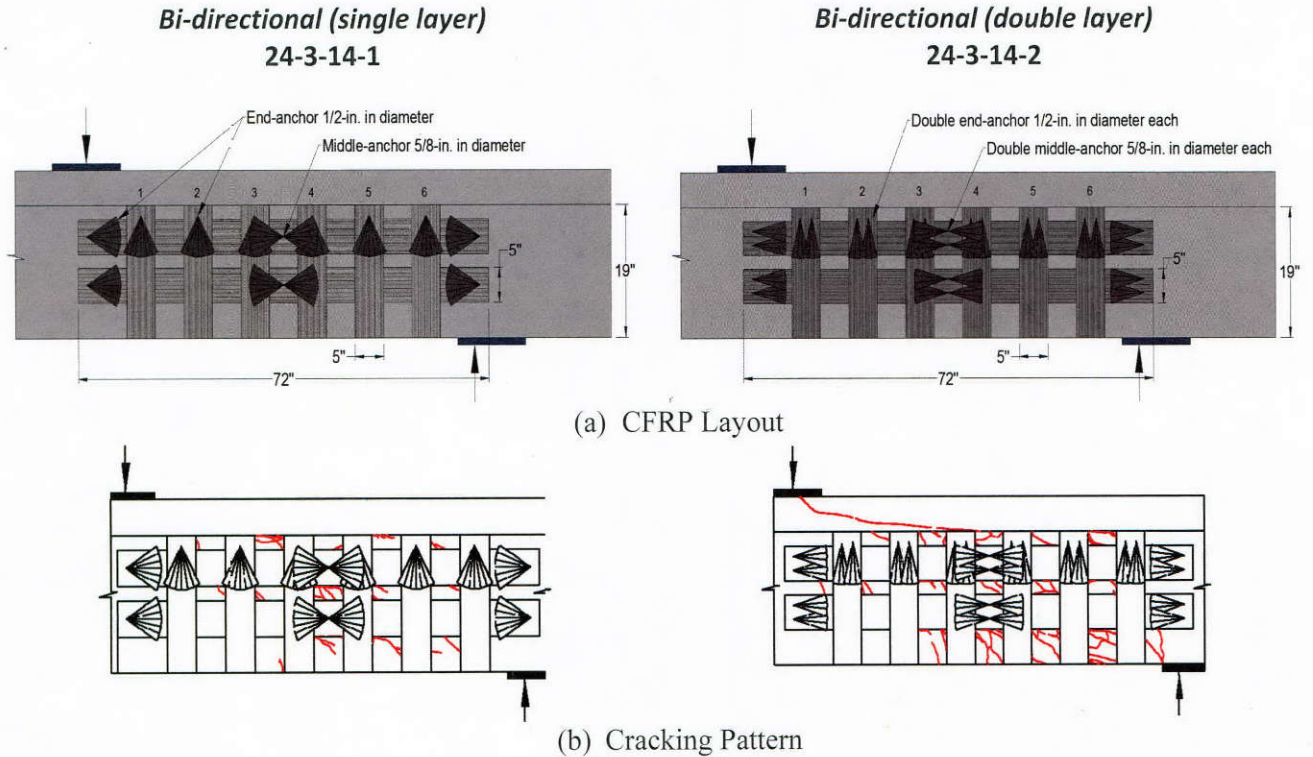


Figure 3-20: 24-in. deep beams with $a/d=3$, $b=14$ -in., and different amount of CFRP

Shear cracking initiated in the web of the beam after reaching an applied load of approximately 150 kips. As the applied load increased, additional cracks developed that could be observed between the CFRP strips. The failure was initiated by large cracks at the web-flange interface (Figure 3-21).

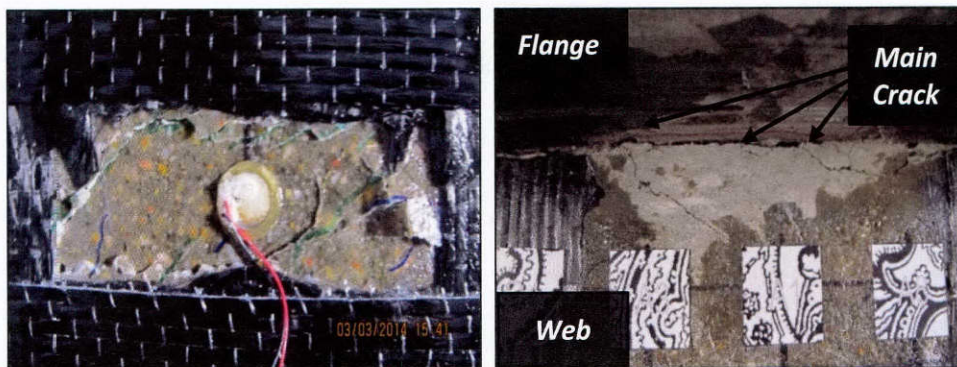


Figure 3-21: Cracking behavior of bi-directionally strengthened specimens

The major crack at the web-flange interface led to a failure in the web directly behind the CFRP anchor. The maximum strain recorded in vertical CFRP strips was 0.006 in strip 2 and the maximum strain recorded in the horizontal CFRP strips was 0.0015 in the lower strip

These two tests were designed to be directly compared with two tests performed under TxDOT Project 0-6306 (control and uni-directional). Results of four tests were normalized by the square root of the compressive strength of concrete $\sqrt{f_c'}$ because the shear failure mechanism was controlled by the tensile strength of concrete. The normalized shear capacities of specimens in the second category are presented in Table 3-3.

Table 3-3: Summary of 14-in. wide web beams with a/d of 3

Test Name	CFRP Layout	Shear Capacity V_{max} (kips)	Concrete strength f_c' (psi)	Maximum Normalized Shear $\frac{V_{max}}{\sqrt{f_c'} \cdot b_w \cdot d}$ (psi)	Ratio of $\frac{V_{strengthened}}{V_{control}}$	Beam Displacement at load point (in.)
24-3-2*	Control	105	3600	6.1	0	0.47
24-3-8*	Uni	151	3600	8.8	1.44	0.54
24-3-14-1	Bi-S	156	3200	9.7	1.59	0.46
24-3-14-2	Bi-D	167	3200	10.4	1.70	0.59

* Tested in TxDOT Project 0-6306

It is important to mention that specimen 24-3-8 tested in TxDOT Project 0-6306 failed due to the combination of CFRP strip rupture and CFRP anchor fracture. Strip rupture means that the full capacity of the strengthening system was utilized. However, neither CFRP strip rupture nor CFRP anchor fracture was observed in any of the specimens strengthened bi-directionally. Since the capacity of the strengthening system was not developed, the shear capacity of the beam was limited by other failure modes. The normalized shear strength versus beam displacement for the control and the strengthened specimens of this category is presented in Figure 3-22. Reduction in the initial stiffness of 24-3-2 and 24-3-8 was due to the fact that both of these tests were conducted as the second test on a beam. For instance, test 24-3-8 was conducted after test 24-3-7, which means that some minimal cracking was introduced to span 24-3-8 while testing 24-3-7.

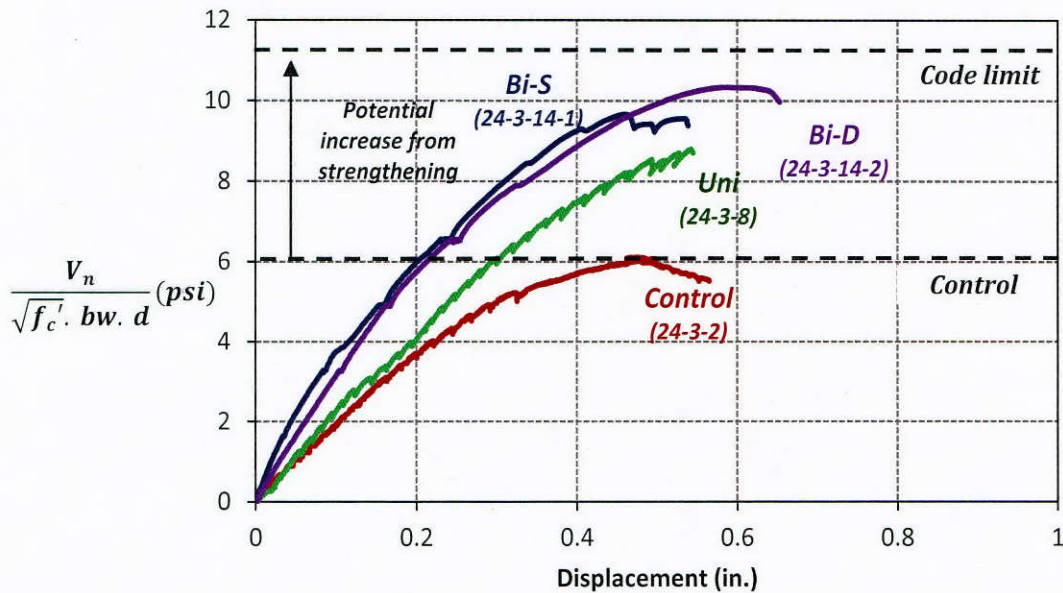


Figure 3-22: Normalized shear versus displacement for 14-in. web with a/d of 3

A substantial shear strength gain was observed in the bi-directionally strengthened specimens in comparison to the control specimen: a 60% increase in 24-3-14-1 and 70 % in 24-3-14-2. Specimen 24-3-2 had a somewhat low shear capacity of $6.1 \sqrt{f_c'} \cdot b_w \cdot d$ (psi). Test 24-3-14-2 had a shear capacity of $10.4 \sqrt{f_c'} \cdot b_w \cdot d$ (psi units) that is slightly less than the sum of the concrete shear contribution limit ($3.5 \sqrt{f_c'} \cdot b_w \cdot d$) and steel shear contribution limit ($8 \sqrt{f_c'} \cdot b_w \cdot d$) given in code provisions. The shear strength was increased slightly when double layers of CFRP strips were applied bi-directionally. The results also indicate that the CFRP shear strengthening system had a marginal effect on the peak deformation of the beams.

The contributions of the different materials to the shear capacity of the 24-in. deep T-beams with 14-in. webs and a/d of three are plotted in Figure 3-23. The steel contributions remained constant for all the specimens. However, as more CFRP was added the concrete contribution tended to decrease. Steel and CFRP contributions were determined from measured strains of the elements crossing the critical crack and the concrete contribution was determined by subtracting the steel and CFRP contributions from measured shear capacity.

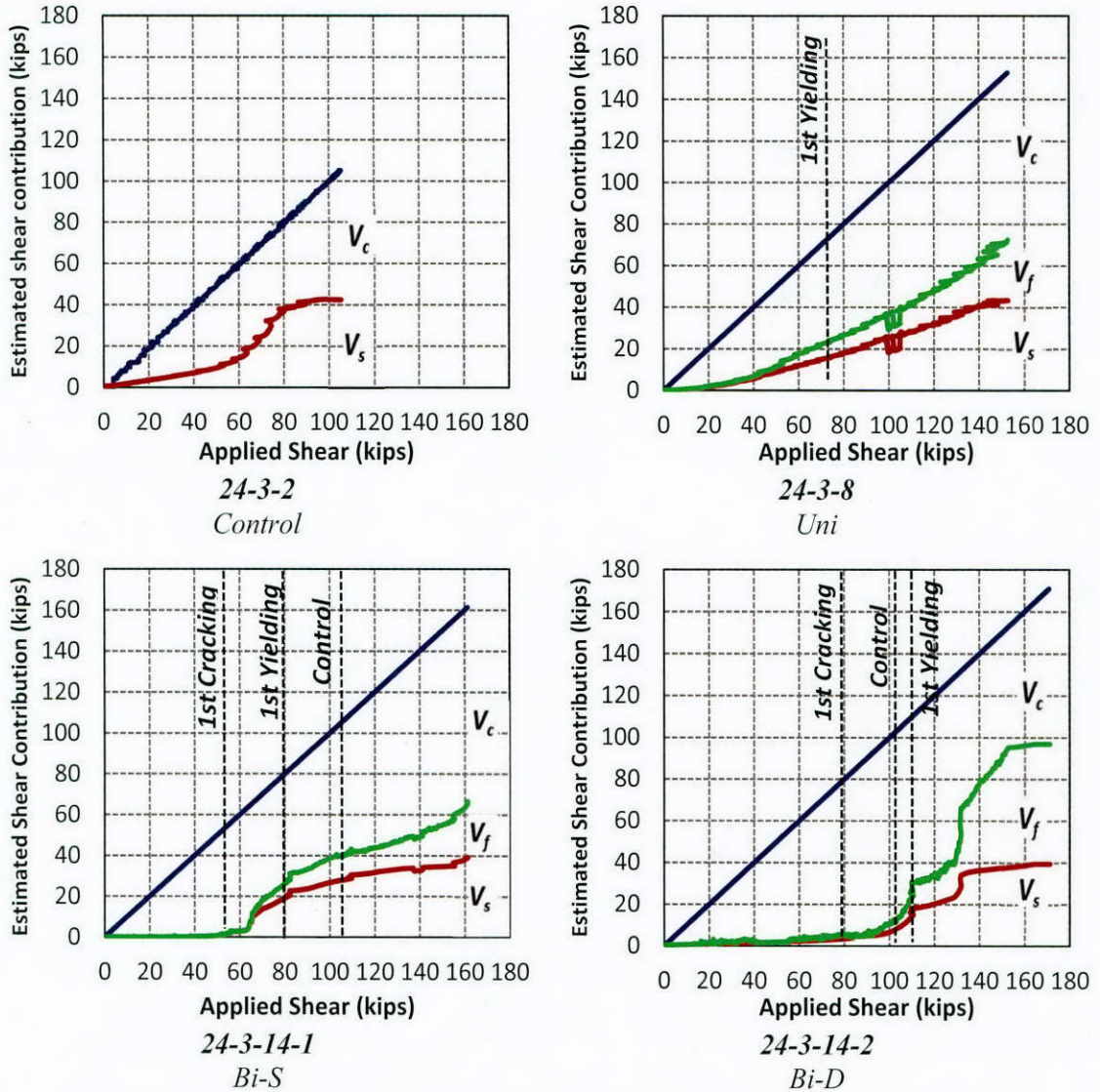


Figure 3-23: Shear contributions for 14-in. web with a/d of 3

3.4.3 Results of Beams with 8-In. Web and A/D of 3

Four tests were conducted on specimens with an 8-in. web width. All the tests in this series were performed with an a/d of three. The behavior of specimens strengthened with single and double layers of bi-directional CFRP was compared to the control specimen and to the specimen with a uni-directional application of CFRP.

In the control test (No CFRP), shear failure occurred at 76 kips. As the load increased, a principal crack started to form at an angle of 35° and propagated simultaneously toward the support and the flange (Figure 3-24).

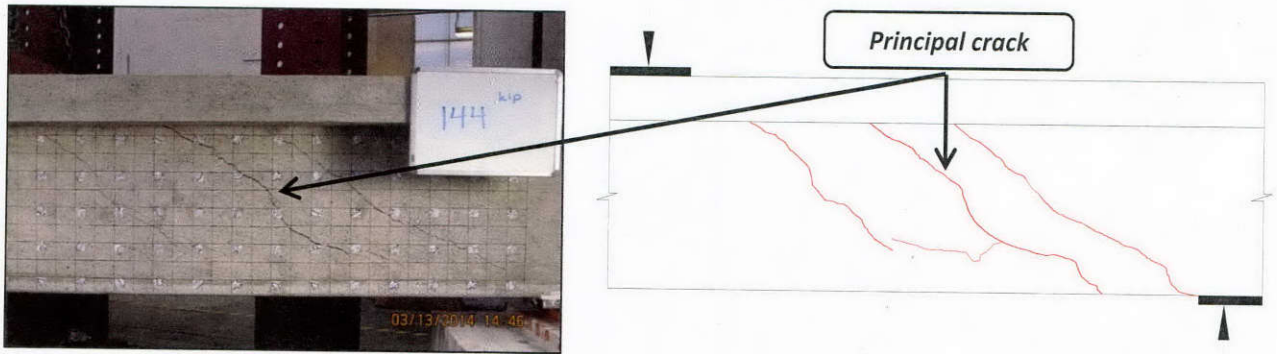


Figure 3-24: Cracking of 24-3-8-1

In test 24-3-8-2, uni-directional CFRP strips and CFRP anchors were installed as illustrated in Figure 3-25. Shear failure occurred at 99 kips.

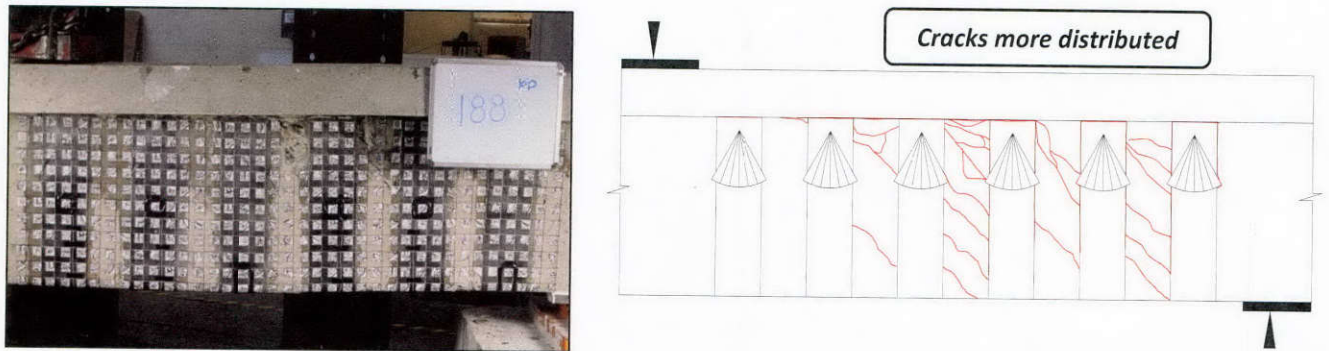


Figure 3-25: Cracking of 24-3-8-2

The principal crack formed at an angle of 44-deg. and propagated simultaneously toward the support and the flange, resulting in the web crushing failure (Figure 3-26).



Figure 3-26: Concrete crushing behind anchors (24-3-8-2)

In test 24-3-8-3, one layer of CFRP strips and CFRP anchors were installed in both directions as can be seen in Figure 3-27.

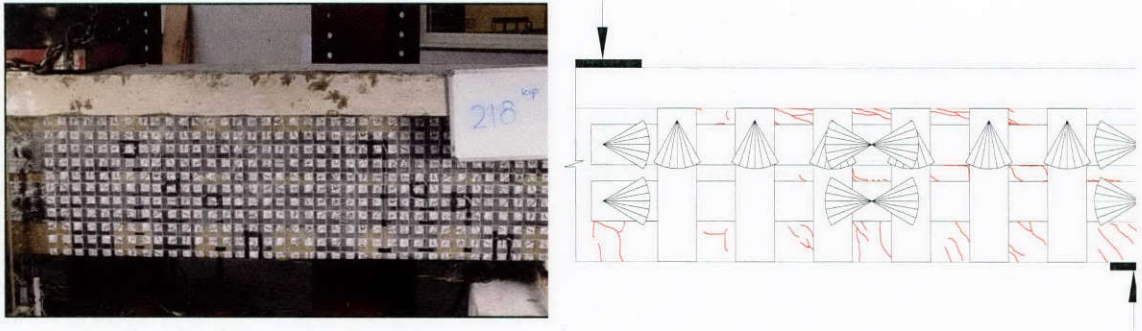


Figure 3-27: Cracking of 24-3-8-3

Shear failure occurred at 115 kips (applied load of 218 kips). This resulted in a principal crack that crossed the web-flange interface. No CFRP strip rupture or anchor rupture was observed. However, minor cracks around CFRP strips and the crack at the web-flange interface led to a failure of the web directly behind the CFRP anchor (Figure 3-28).



Figure 3-28: Flange-web crack interface (24-3-8-3)

In test 24-3-8-4, two layers of CFRP strips and two CFRP anchors per strip width were installed in both directions as shown in Figure 3-29.

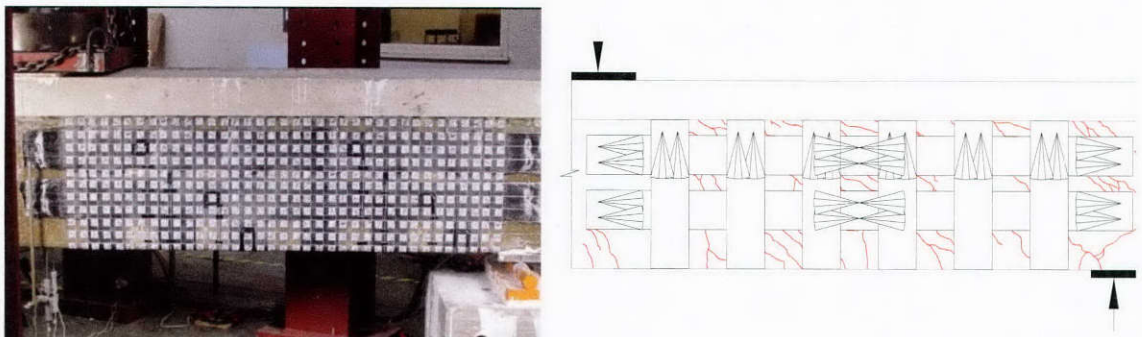


Figure 3-29: Cracking of 24-3-8-4

As the load increased, shear cracks propagated toward the web-flange interface. Shear failure occurred at 118 kips (applied load of 223 kips).

Test results were normalized by the tensile strength of concrete $\sqrt{f_c'}$. The normalized shear capacities of test specimens are summarized in Table 3-4.

Table 3-4: Summary of 24-in. deep beams with 8-in. wide web beams and a/d of 3

Test Name	CFRP Layout	Shear Capacity V_{max} (kips)	Concrete strength f_c' (psi)	Maximum Normalized Shear $\frac{V_{max}}{\sqrt{f_c'} \cdot b_w \cdot d}$ (psi)	Ratio of $\frac{V_{strengthened}}{V_{control}}$	Beam Displacement at peak capacity (in.)
24-3-8-1	Control	76	2500	9.4	0	0.49
24-3-8-2	Uni	99	2500	12.2	1.3	0.64
24-3-8-3	Bi-S	115	3400	12.3	1.31	0.60
24-3-8-4	Bi-D	118	3400	12.6	1.35	0.60

The control and the uni-directionally strengthened specimens failed in diagonal tension. The failure of the bi-directionally strengthened specimens was due to the failure of the concrete in the web behind the CFRP anchor. The normalized shear strength versus the displacement under the point load for the control and the strengthened specimens is presented in Figure 3-30.

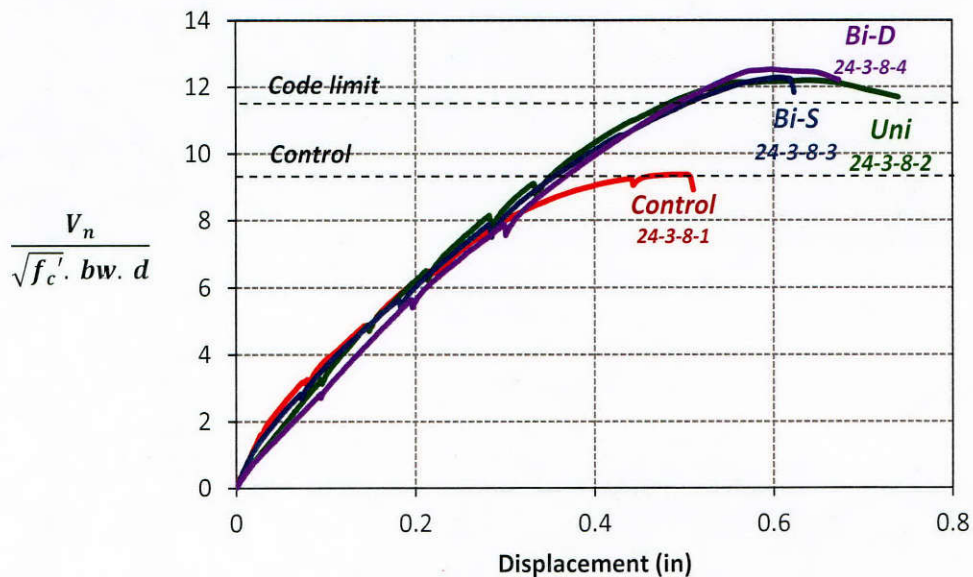


Figure 3-30: Normalized shear versus displacement for 8-in. web beams with a/d of 3

The strengthened specimens had higher strength than the control test. The control and strengthened specimens showed similar initial stiffness. The bi-directionally strengthened specimens did not exhibit a higher strength than the uni-directionally strengthened specimen, as in the tests with 14-in. webs. The maximum shear strength gain in the beams with 8-in. webs was 35%, as observed in 24-3-8-4. The lower strength gain of specimens with 8-in. webs in comparison with the beams with 14-in. webs may be attributed to the high shear strength ($9.4\sqrt{f_c'} \cdot b_w \cdot d$) of the control test (24-3-8-1). This means that the narrow web was carrying a shear of about 80% of the upper limit ($11.5\sqrt{f_c'} \cdot b_w \cdot d$) of ACI-318. All strengthened specimens failed just above the ACI limit. Figure 3-31 shows the shear contribution of each component for the beams with 8-in. webs.

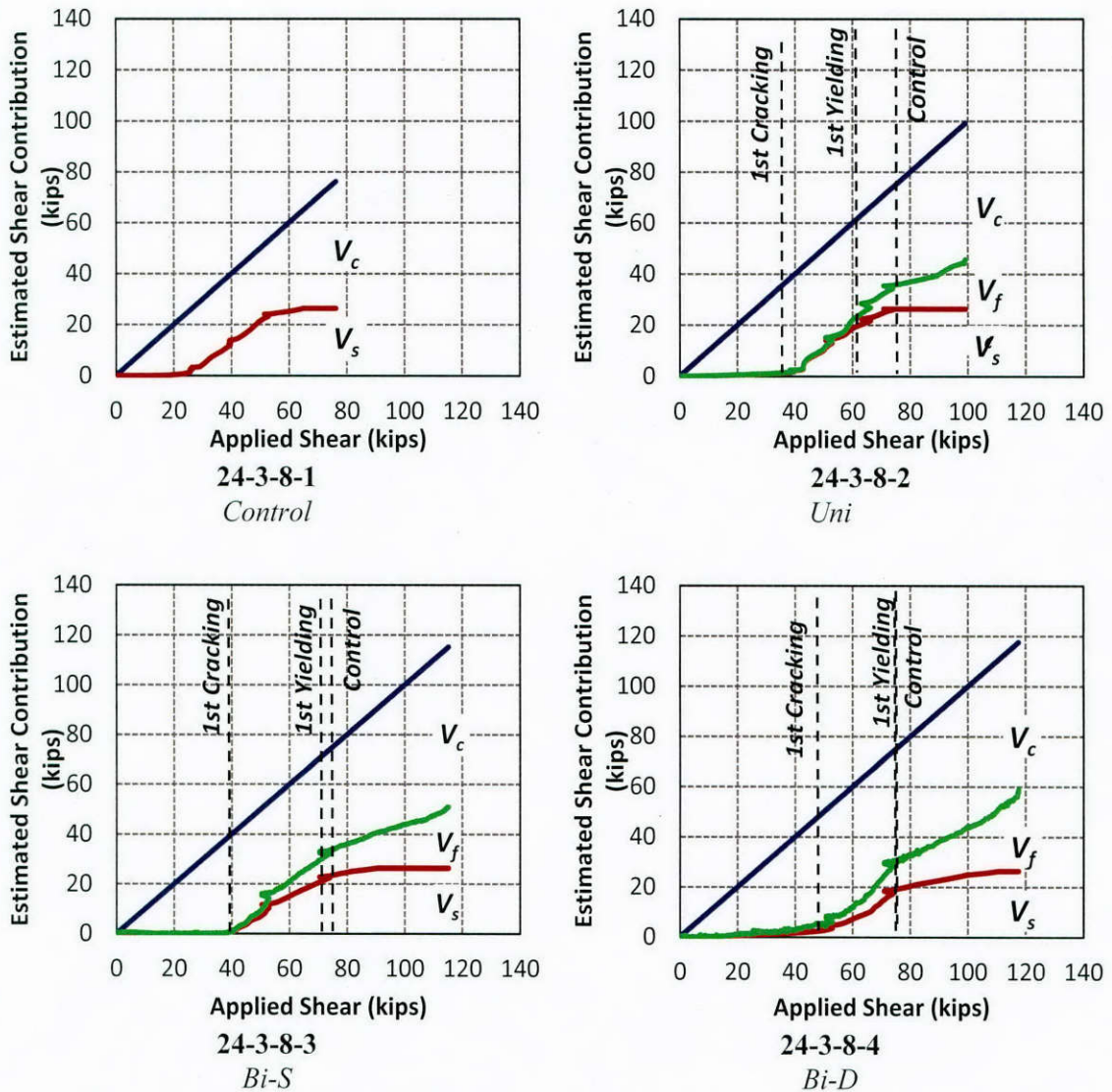


Figure 3-31: Shear contributions of 8-in. web with a/d of 3

3.4.4 Strain Variations in Transverse Reinforcement

Strains in the steel stirrups were monitored by strain gages. The measured strains in the transverse steel may not be the maximum strains developed in the steel depending on the location of the strain gage relative to the critical crack. However, in most cases, measured strains are reported from the strain gages that were close to the critical crack. In all strain data, figures are presented such that the x-axis represents the distance from the applied load to where the strain was measured. Figure 3-32 shows the strains developed in the stirrups at different load stages of two specimens with 14-in. webs, one strengthened uni-directionally and the other strengthened bi-directionally.

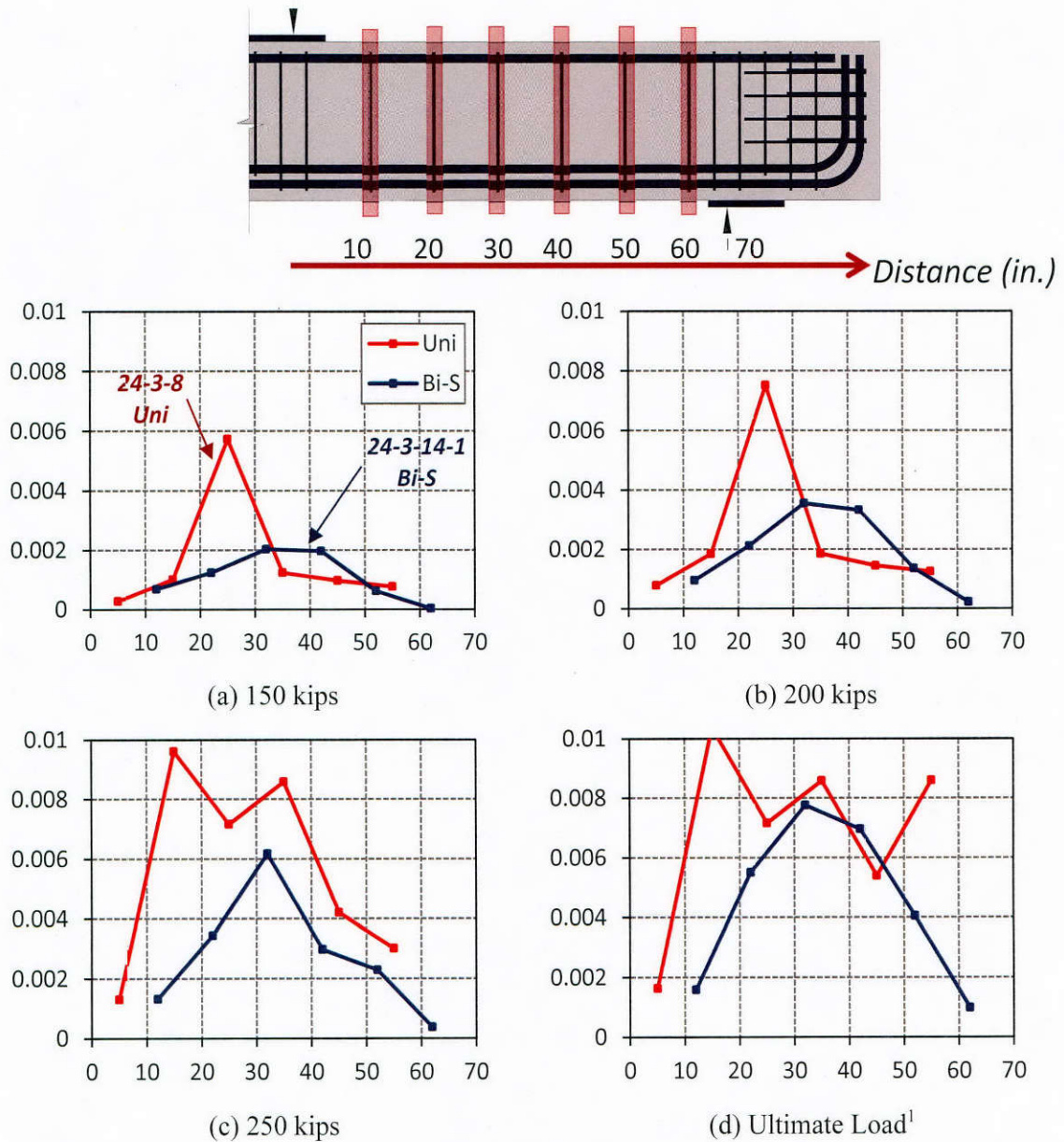


Figure 3-32: Strains in stirrups at different loading stages of 24-3-8 (Uni) and 24-3-14-1 (Bi-S)

A reduction in the transverse steel strains was observed in bi-directionally strengthened specimens in comparison to uni-directionally specimens under the same applied load. From tests conducted on bi-directionally strengthened specimens, it was observed that most of the transverse steel within the test region and all transverse steel crossing the critical crack yielded before the ultimate load was reached. This is in agreement with assumptions made in most design guidelines and code provisions.

3.4.5 Steel-CFRP Interaction in Uni-Directional Layout versus Bi-Directional Layout

Strains in the CFRP strips were monitored using the optical measurement system that is described in Section 6.2.4.1. The vertical strips in the bi-directionally strengthened specimen

experienced lower strains than in the uni-directionally strengthened specimens. Strains developed in steel stirrups and CFRP strips of beams with 8-in. webs are compared in Figure 3-33.

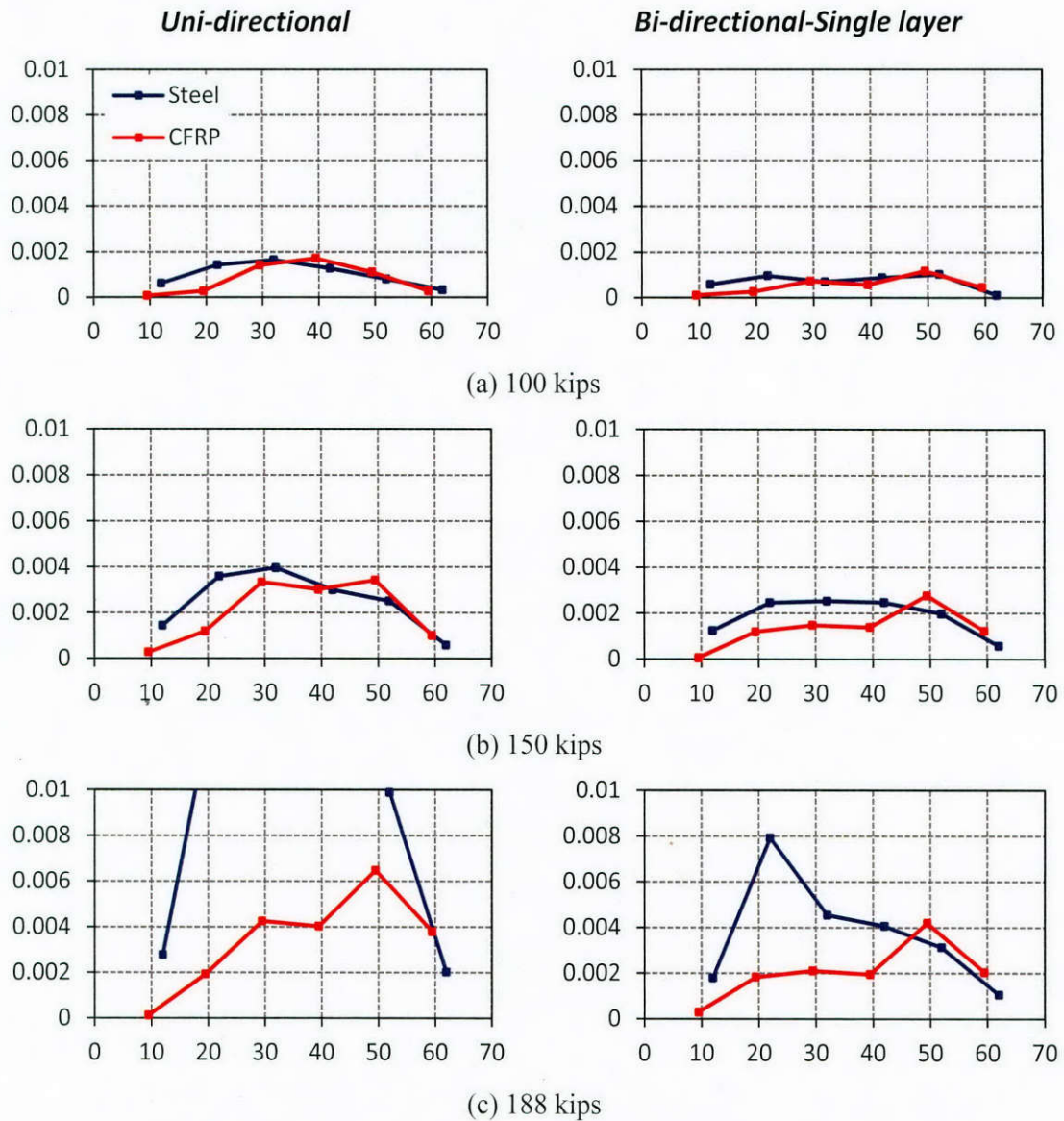


Figure 3-33: Strain variations in steel and CFRP, 24-3-8-2 (left), 24-3-8-3 (right)

The addition of the horizontal strips in the bi-directional application was found to reduce the strain level in the transverse steel and the CFRP. This can be attributed to the fact that horizontal strips contributed to reducing the crack width and delaying its propagation.

3.4.6 Analysis of Contributions of Concrete, Steel, and CFRP to Shear Strength

As mentioned earlier, to eliminate the effect of concrete compressive strength variations, the concrete contribution to the shear strength was normalized by the concrete strength of the control specimen. A normalized shear capacity was then achieved by adding the normalized concrete contribution to the steel and CFRP contributions. The shear contributions of transverse steel and CFRP strips were estimated based on the measured strains, while the concrete contribution was assumed as the difference between the shear strength of the beam and the steel and CFRP

components. For specimens with 14-in. webs and span-to-depth ratio of 3, the normalized shear contributions are summarized in Table 3-5. A comparison of the contribution of each component to the shear capacity is presented in Figure 3-34.

Table 3-5: Shear contributions of 14-in. web beams with a/d of 3

Specimen	CFRP Layout	Normalized Shear Capacity	Steel Contribution V_s	CFRP Contribution V_f	Normalized Concrete Contribution $V_{c,normalized}$	$\frac{V_{test}}{V_{control}}$
24-3-2*	Control	105.3	42.4	-	62.8	0
24-3-8*	Uni	152.7	43.5	29.0	80.2	1.45
24-3-14-1	Bi-S	161.3	39.5	27.2	94.6	1.53
24-3-14-2	Bi-D	170.9	39.6	57.3	74.0	1.62

* Tested in TxDOT Project 0-6306

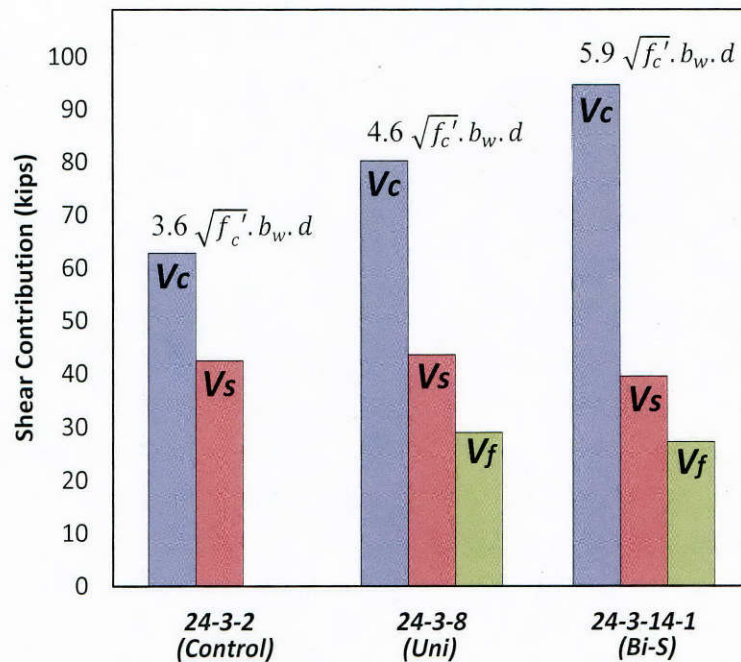


Figure 3-34: Shear contributions of 14-in. web beams with a/d of 3

The increase in the concrete contribution observed in 24-3-8 and 24-3-14-1 is attributed to the fact that (V_c) of the control specimen was only $3.6\sqrt{f'_c} \cdot b_w \cdot d$ and $V_n = 6.1\sqrt{f'_c} \cdot b_w \cdot d$, which is well below code limits. For 24-3-8 and 24-3-14-2, the steel contribution was nearly the same but with the addition of the CFRP, the concrete contribution increased considerably with $V_n = 8.9\sqrt{f'_c} \cdot b_w \cdot d$ and $10\sqrt{f'_c} \cdot b_w \cdot d$; values that approach code limits. These results confirm that the shear resisted by steel (V_s) for strengthened beams can be assumed to be the same as that of the unstrengthened beams. The shear resisted by vertical CFRP strips (V_f) in 24-3-8 and 24-3-14-1 was found to be similar.

Similarly, for specimens with 8-in. web, the results of normalized shear capacity and gain in the shear strength are presented in Table 3-6.

Table 3-6: Shear contributions of 8-in. web beams with a/d of 3

Specimen	CFRP Layout	Normalized Shear Capacity	Steel Contribution V_s	CFRP Contribution V_f	Normalized Shear Contribution $V_{c,normalized}$	$\frac{V_{test}}{V_{control}}$
24-3-8-1	Control	76.2	26.4	-	49.8	0
24-3-8-2	Uni	99.1	26.4	19.3	53.4	1.30
24-3-8-3	Bi-S	106.1	26.4	24.5	55.1	1.39
24-3-8-4	Bi-D	109.2	26.4	32.4	50.3	1.43

An evaluation of the contribution of each component to the shear capacity for the thin web specimens is presented in Figure 3-35.

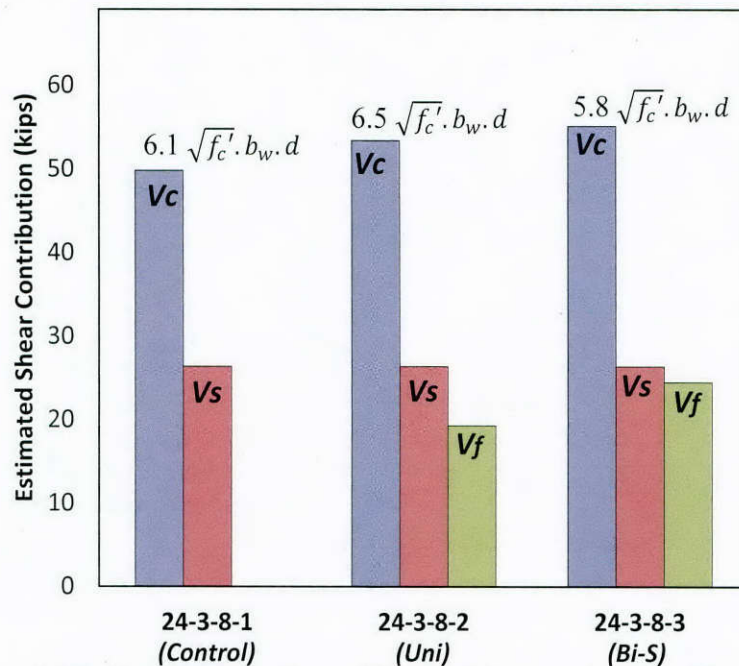


Figure 3-35: Shear contributions of 8-in. web beams with a/d of 3

A small increase was observed in the concrete contribution due to the addition of the horizontal strips for this series. This can be attributed to the fact that the concrete contribution in 24-3-8-1 was $6.1 \sqrt{f'_c} \cdot b_w \cdot d$, which is approximately twice the concrete contribution of 24-3-2. Additional shear contribution from the concrete should not be expected since the maximum concrete contribution reported in the 14-in. web specimens was 95 kips, which is equivalent to $5.6 \sqrt{f'_c} \cdot b_w \cdot d$. Therefore, the addition of the horizontal strips increases the concrete contribution from 53.4 kips ($6.5 \sqrt{f'_c} \cdot b_w \cdot d$) for test 24-3-8-2 to 55.1 kip ($5.8 \sqrt{f'_c} \cdot b_w \cdot d$) for test 24-3-8-3. The reduction in $\sqrt{f'_c} \cdot b_w \cdot d$ term is due the variation in f'_c between the two tests. It may be important to mention here that ACI 318-11 code provisions limit the concrete contribution to the shear strength of conventional reinforced concrete members to $3.5 \sqrt{f'_c} \cdot b_w \cdot d$.

Test results confirm that the steel contribution to shear capacity was not affected by the external application of CFRP material (uni-directionally or bi-directionally); as long as steel stirrups yielded prior to failure. However, the steel contribution to the shear resistance was found

to be delayed by the external application of CFRP material. As shown in Figure 3-36, in all test specimens the steel contribution to the shear capacity was the same; however, this contribution was developed at higher applied shear as the amount of CFRP crossing the critical crack increased.

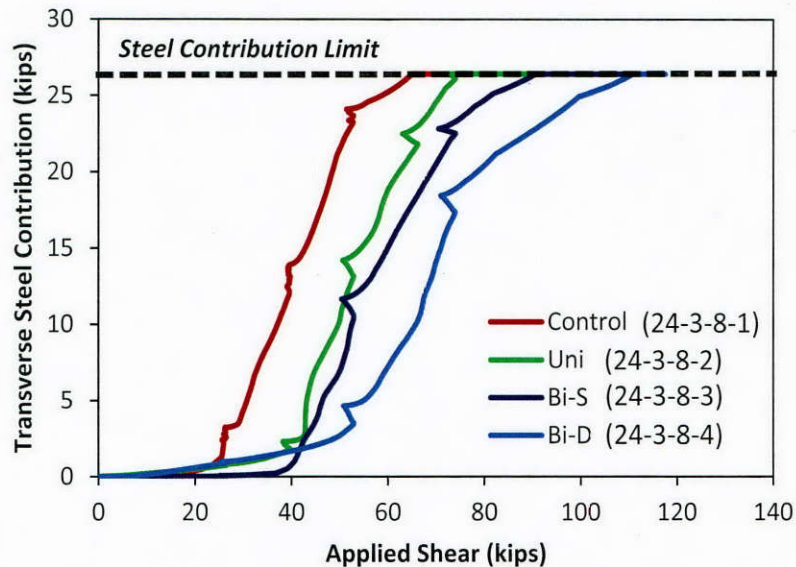
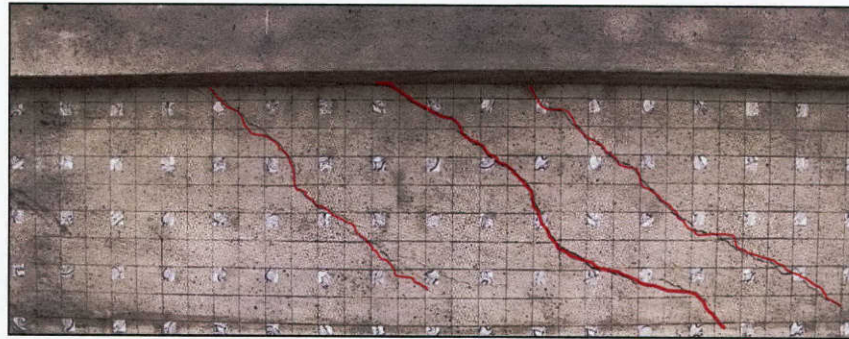


Figure 3-36: Steel contribution to shear capacity for 8-in. web beams

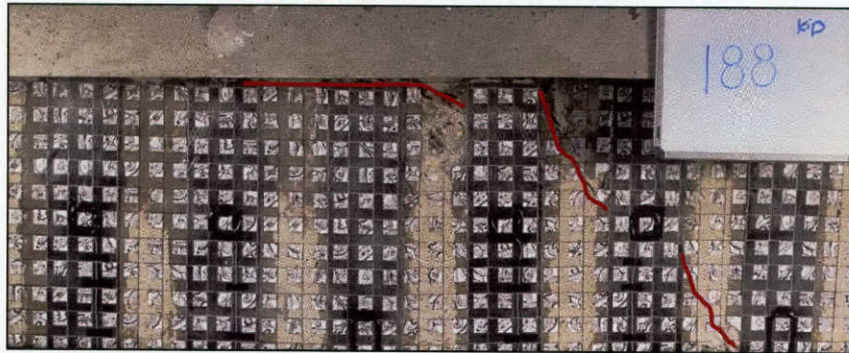
3.4.7 Observations on Cracking Behavior

The dominant failure mode of all test specimens was shear. The failure was always caused by a critical shear crack that passed through the web of the beam. In several cases, when a specimen was strengthened bi-directionally, the principal crack was found to develop along the flange-web interface before it propagated to the support. To examine the influence of the strengthening system on the cracking behavior of a reinforced concrete beam, the vertical and horizontal CFRP strips were removed after each test for visual evaluation.

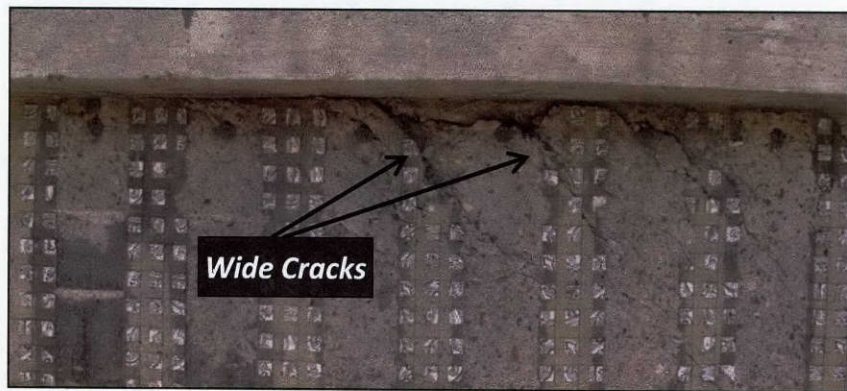
Specimen 24-3-8-1 failed after developing a typical shear tension failure where the failure was caused by a principal shear crack with two minor cracks in parallel to the major crack. The crack angle of the principal shear crack that caused the failure of 24-3-8-1 was in the range of 30° to 35°. Specimen 24-3-8-2 failed by a major crack that started horizontally at the flange-web interface, and then was inclined at 45°. It was observed that cracking after the removal of the CFRP was well-distributed (Figure 3-37). Specimen 24-3-8-3 exhibited narrower cracks and a lower angle of inclination than 24-3-8-2.



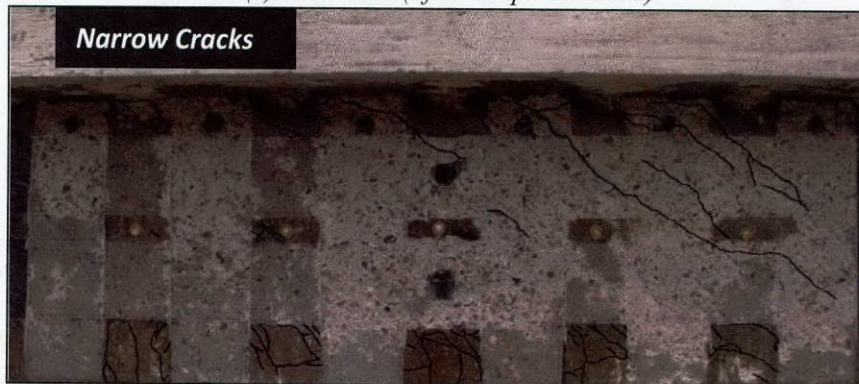
(a) 24-3-8-1



(b) 24-3-8-2 (before strips removed)



(c) 24-3-8-2 (after strips removed)



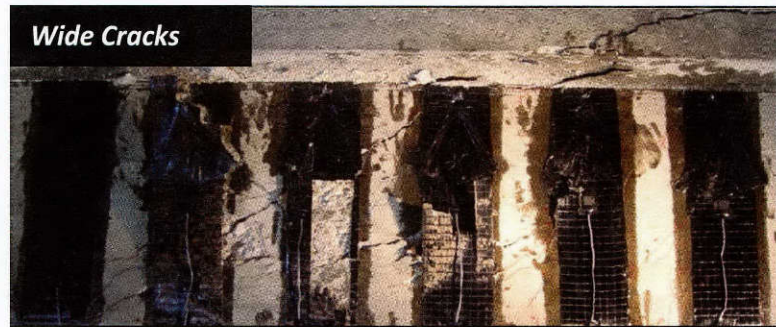
(d) 24-3-8-3 (after strips removed)

Figure 3-37: Cracking pattern of 8-in. web beams

Similar cracking was observed in the 14-in. web specimens (Figure 3-38).



(a) 24-3-2



(b) 24-3-8



(c) 24-3-14-1 (after strips removed)

Figure 3-38: Cracking pattern of 14-in. web beams

Specimen 24-3-2 developed two major shear cracks. Specimen 24-3-8 failed by a principal shear crack with distributed minor cracks. In the bi-directionally strengthened specimen (24-3-14-1), the cracking pattern at failure consisted of distributed narrow cracks (visible after the strips were removed) when compared with 24-3-8.

3.5 TEST RESULTS OF 48-IN. DEEP T-BEAMS

3.5.1 Test 48-3-14-1 (Control)

Ten tests were conducted on 48-in. deep T-beams. The first test 48-3-14-1 was conducted to determine the base shear capacity of the 48-in. section. Although, data available from TxDOT project 0-6306 indicated that the base shear strength of a 48-in. deep section tested was 147 kips it was decided that an additional control test was needed.

Shear failure of 48-3-14-1 occurred at a shear force of 122 kips. Diagonal shear cracking initiated at the middle of the web of the specimen after reaching an applied shear of approximately 74 kips. As the load continued to increase, a principal crack formed at an angle of 42° and propagated simultaneously toward the support and the flange as shown in Figure 3-39.

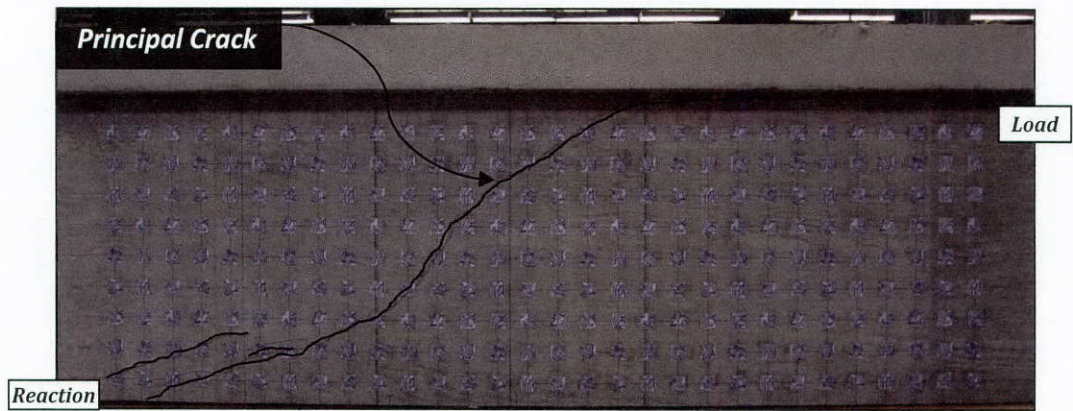


Figure 3-39: Cracking of 48-3-14-1

The internal transverse reinforcement started yielding at 105 kips. All measured strains on stirrups crossing the critical crack (C, D, E, and F) were above yield. At ultimate, the crack width was 0.25-in. (7mm) as shown in Figure 3-40.

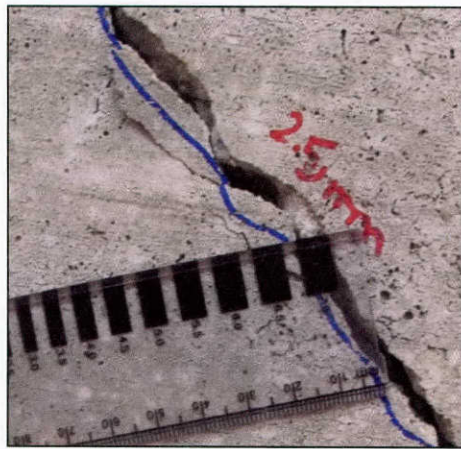


Figure 3-40: Crack width measurement of 48-3-14-1

The shear response of test 48-3-14-1 (control) is shown in Figure 3-41. The diagonal shear crack formation, stirrup yielding, and ultimate capacity are marked in Figure 3-41 with a strain profile of each event (determined by the optical measurement data). A reduction in stiffness can be clearly seen at shear crack formation and at yielding of the reinforcement.

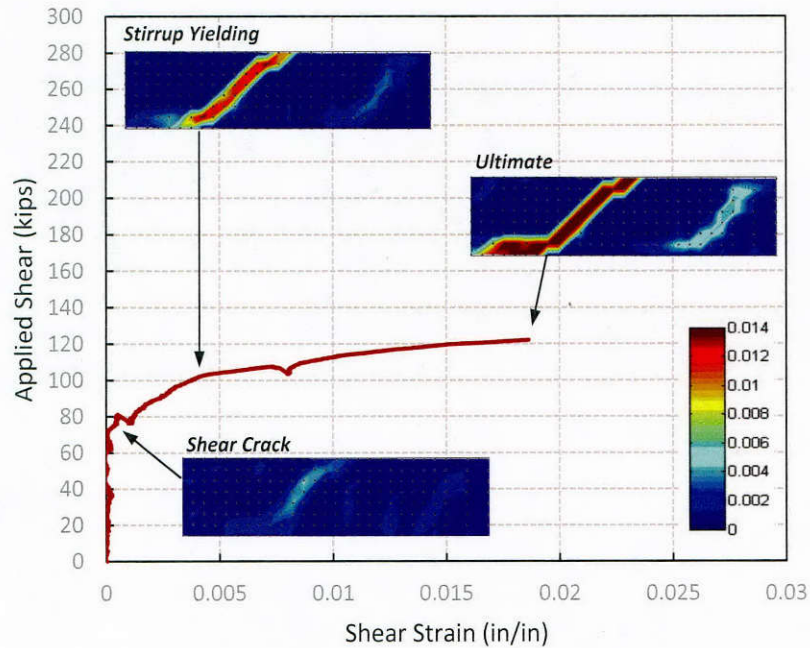


Figure 3-41: Shear response of test 48-3-14-1 (control)

3.5.2 Test 48-3-14-2 (Uni-Directional / 10-in. Strips)

In test 48-3-14-2, six 10-in. wide vertical strips at 20-in. on center were installed to form a uni-directional strengthening scheme. The test was similar to test 48-3-2, which was conducted as part of TxDOT project 0-6306. The difference between these two tests is the thickness of CFRP material. Test 48-3-2 was strengthened with 0.011-in. thick CFRP material while test 48-3-14-2 was strengthened with 0.02-in. thick CFRP material.

During the initial loading, small flexural-shear cracks initiated on the lower end of the web after reaching a shear of 60 kips. As the load increased, these cracks propagated vertically until they reached the middle of the web. At a shear of 100 kips, diagonal shear cracks were observed on the middle of the web. More diagonal cracks were observed at shears of 120 kips and 150 kips. At this load stage, debonding started to initiate along the length of vertical strips. As the load continued to increase, a principal crack formed at an angle of 40° and a secondary crack formed at an angle of 30° . Both propagated simultaneously toward the support and the flange, resulting in failure of the beam at an applied shear of 230 kips. Shear failure was initiated by explosive rupture of strips 3, 4, and 5. Figure 3-42 shows test 48-3-14-2 at a shear force of 175 kips and after failure.

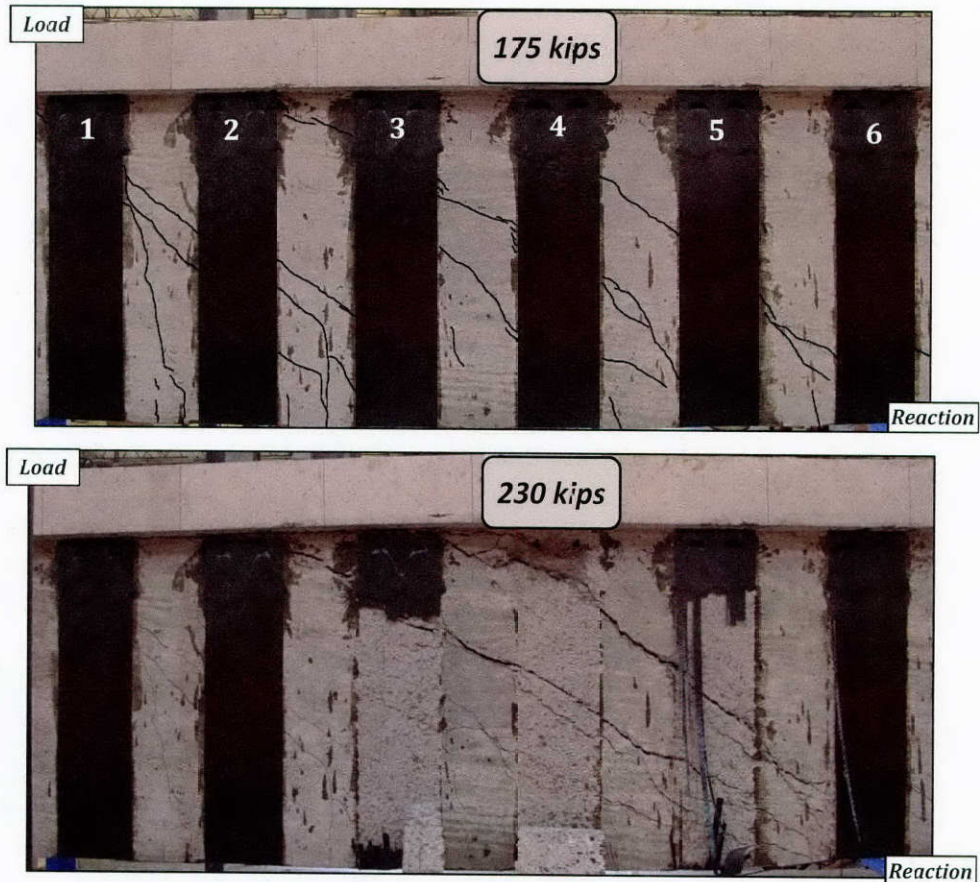


Figure 3-42: Test 48-3-14-2, cracking (top), failure (bottom)

The shear response of test 48-3-14-2 is shown in Figure 3-43. Major events in the applied shear versus shear strain response are labeled. Diagonal shear cracking occurred at a shear of about 100 kips. At 150 kips, all stirrups across the critical crack yielded. The stiffness of the beam substantially decreased after complete debonding of strips crossing the critical crack. At that point, strains were uniformly distributed over the length of the strip. At a shear of 225 kips, strips 4 and 5 were carrying most of the load until the critical crack passed through one of the anchors in strip 4. The anchors pulled out slightly and strains in strip 4 reduced. The forces in strip 4 were then redistributed to strips 5 and 6. The principal strain contours for test 48-3-14-2 at major events mentioned above are shown in Figure 3-44 clearly show the effects of debonding and loss of capacity of strip 4.

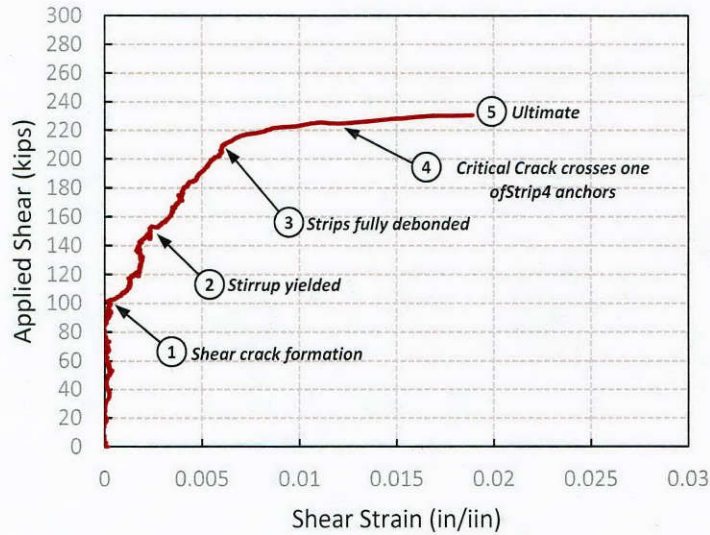


Figure 3-43: Shear response of test 48-3-14-2 (uni-10'')

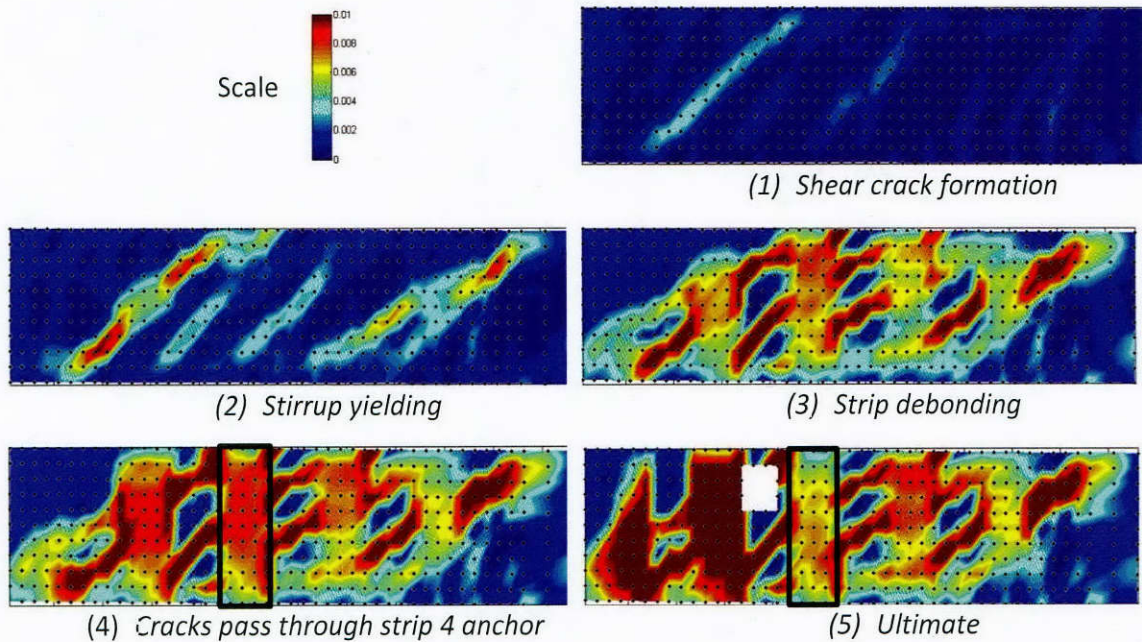


Figure 3-44: Principal strain profiles of test 48-3-14-2

The reduction in inclined crack widths with the shear strengthening system was significant. The control test (48-3-14-1) exhibited a principal shear crack that was 0.25-in. wide at failure (shear of 122 kips) while test (48-3-14-2) exhibited only flexural-shear cracks at the same applied shear (122 kips) as shown in Figure 3-45. While the intent of the project was shear strengthening, the addition of the CFRP strips also improved the cracking serviceability of the beams.

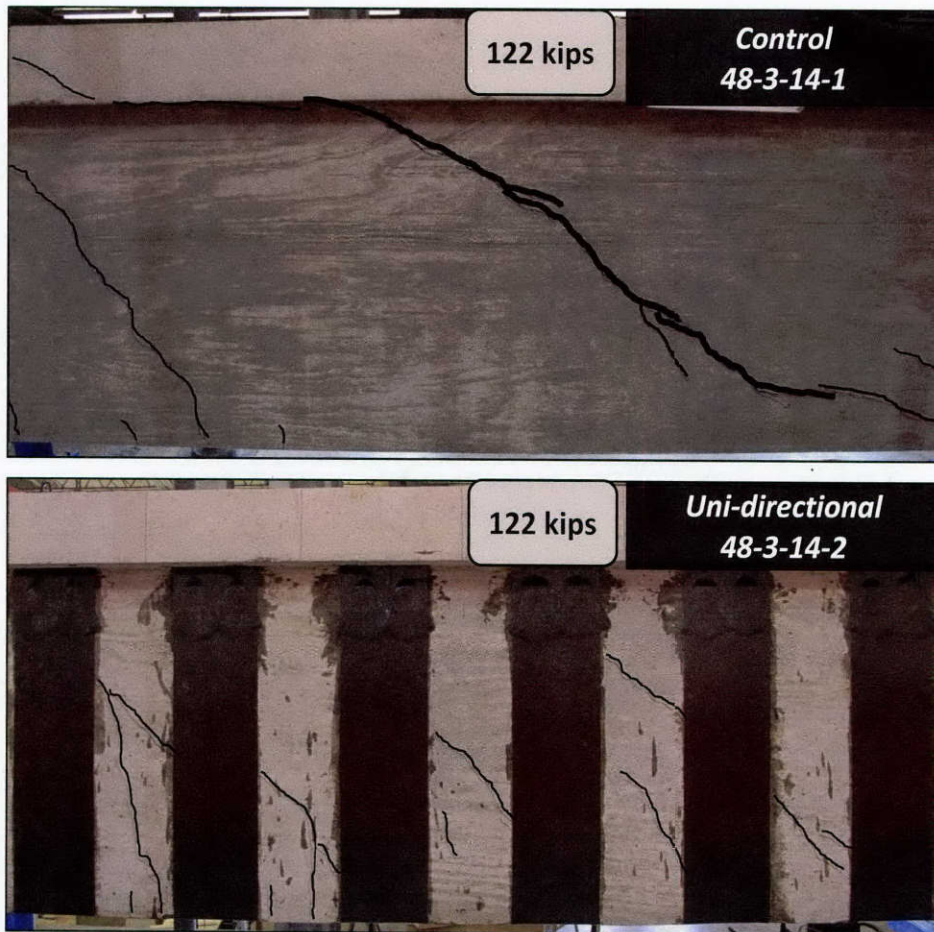


Figure 3-45: Failure of 48-3-14-1 (top), cracking of 48-3-14-2 (bottom), under equivalent load

3.5.3 Test 48-3-14-3 (Uni-Directional / 5-in. Strips)

The goal of the third test (48-3-14-3) was to investigate the efficiency of different uni-directional layouts in shear strengthening applications. The amount of CFRP material used in 48-3-14-2 and 48-3-14-3 is identical. Test 48-3-14-2 was strengthened with six 10-in. wide strips spaced at 20-in. on center, while test 48-3-14-3 was strengthened with twelve 5-in. wide strips spaced at 10-in. on center.

The shear load versus shear deformation response of test 48-3-14-3 is shown in Figure 3-46. At the initial loading, small vertical flexural-shear cracks initiated on the lower portion of the web after reaching a shear of 67 kips. At around 90 kips, diagonal shear cracks were observed in the middle portion of the web. More diagonal cracks were observed at a shear of 120 kips. As the shear increased to 148 kips, debonding of several strips was observed. Additional shear cracks formed and existing shear cracks continued propagating toward the flange at a shear of 175 kips. At an applied shear of 242 kips, the test was stopped as the load-deformation curve started to flatten out.

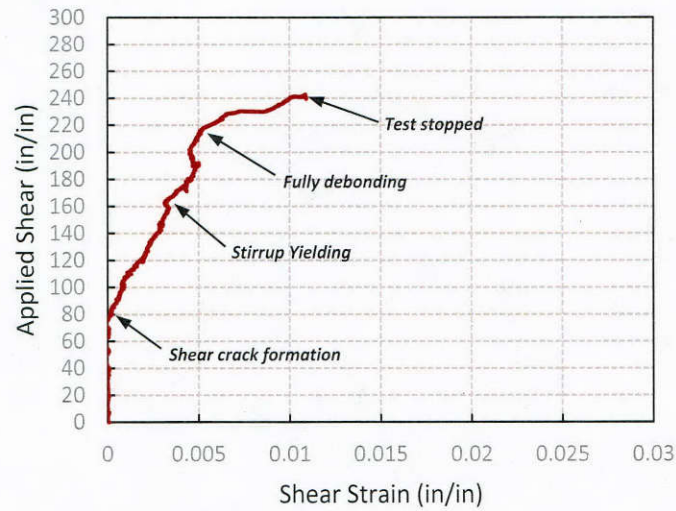


Figure 3-46: Shear response of test 48-3-14-3

At about 220 kips, the strips were fully debonded (Figure 3-47) and the stiffness of the beam dropped dramatically. After unloading the beam, the measured crack width was 0.1 in. Figure 3-48 illustrates the cracking pattern of 48-3-14-3.



Figure 3-47: Debonding of strips in 48-3-14-3



Figure 3-48: Cracking pattern of 48-3-14-3

3.5.4 Test 48-3-14-4 (Bi-Directional / Wide Spacing)

Test 48-3-14-4 had a bi-directional layout of CFRP strips. The beam was strengthened with six 5-in. wide strips at 20-in. on center vertically and two 5-in. wide strips at 12-in. on center horizontally. The horizontal strips had anchors at each end and at the mid-length of the strips. The test has the same amount of material as 48-3-14-2 and 48-3-14-3; however, the CFRP material in this test was distributed in both directions. Material in the vertical strips was reduced and was used to provide the horizontal strips.

At initial loading, small vertical flexural and shear cracks initiated on the lower portion of the web after reaching a shear of 67 kips. As the applied shear was increased to 94 kips, both flexural and shear cracks continued to extend. At 120 kips, new flexural and shear cracks were observed.

More diagonal cracks were observed at the upper portion of the web (passing through the anchor of strip 4) at a shear of 145 kips. As the load continued to increase, shear cracks propagated toward the flange and the beam failed at an applied shear of 195 kips. The principal crack formed at an angle of 42° at the upper part of the web and propagated to the support at approximately 27° . The crack opening resulted in rupturing strips 5 and 6. The applied shear versus shear deformation response is shown in Figure 3-49. The member stiffness decreased when diagonal shear cracks formed, when stirrups crossing the critical crack yielded, and when CFRP strips completely debonded.

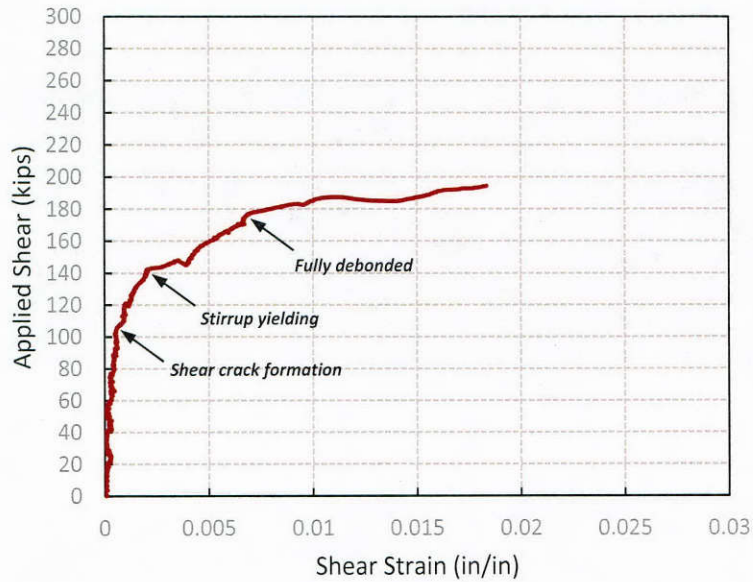


Figure 3-49: Shear response test 48-3-14-4

The steel transverse reinforcement started yielding at a shear of 119 kips. In Figure 3-50, the failure of test 48-3-14-4 is shown. With a wide spacing of vertical strips, the critical shear crack was crossed by only one strip. This test shows that a maximum spacing limit for vertical CFRP strips must be specified in order to prevent the critical crack from forming at a steep angle and intersecting only a few (or one) CFRP strips. A maximum spacing between vertical strips of $d/4$ seems reasonable for an effective layout.

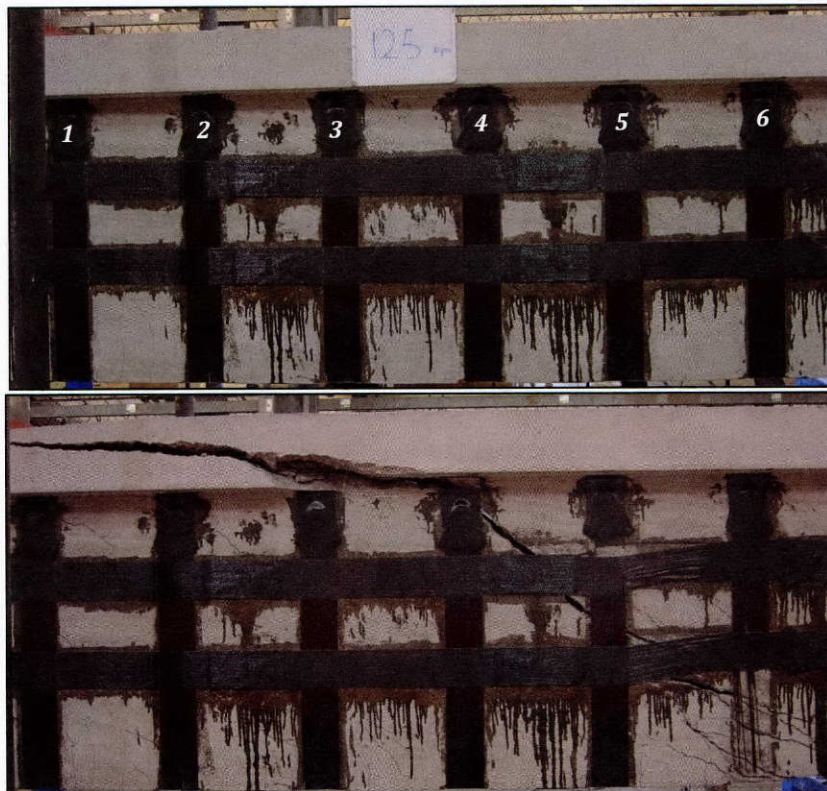


Figure 3-50: Test 48-3-14-4 before (top) and after (bottom) failure

3.5.5 Test 48-3-14-5 (Bi-Directional / 10-in. Strips)

The specimen was strengthened bi-directionally with 10-in. wide vertical CFRP strips spaced at 20-in. on center and 10-in. wide horizontal strips spaced at 14-in. on center. The CFRP layout of this test is shown in Figure 3-3. The test had the same vertical layout of CFRP as Test 48-3-14-2.

The applied shear versus shear deformation response of 48-3-14-5 is shown in Figure 3-51. Major events where a change in shear stiffness was observed are labeled within the figure.

At the initial loading stage, flexural cracks formed at a shear of 66 kips. Flexural cracks extended as the load increased and turned into inclined cracks. Web shear cracks formed at a shear of 120 kips. The measured crack widths at shears of 156 kips and 182 kips were 0.025 in and 0.035 in, respectively. The transverse reinforcement crossing the critical crack yielded at 203 kips. The test was stopped at a shear of 253 kips after fracture of strip 4, as can be seen in Figure 3-52. Continued loading could have resulted in a destructive failure that would have prevented testing the other sections in the beam. At ultimate, the strains were 0.008 and 0.0055 at vertical CFRP strips 4 and 5, respectively.

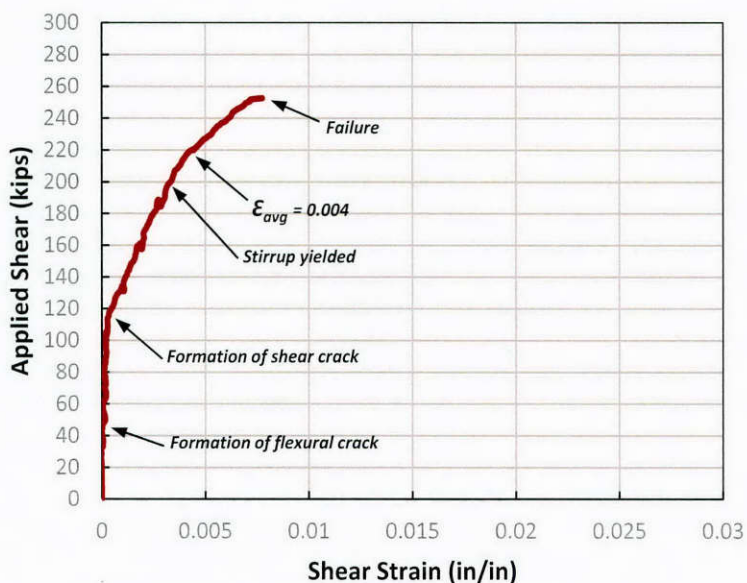


Figure 3-51: Shear response of test 48-3-14-5

Figure 3-53 shows the shear contribution of transverse steel and CFRP. After transverse reinforcement across the critical crack yielded, the shear contribution of the CFRP strips increased substantially.

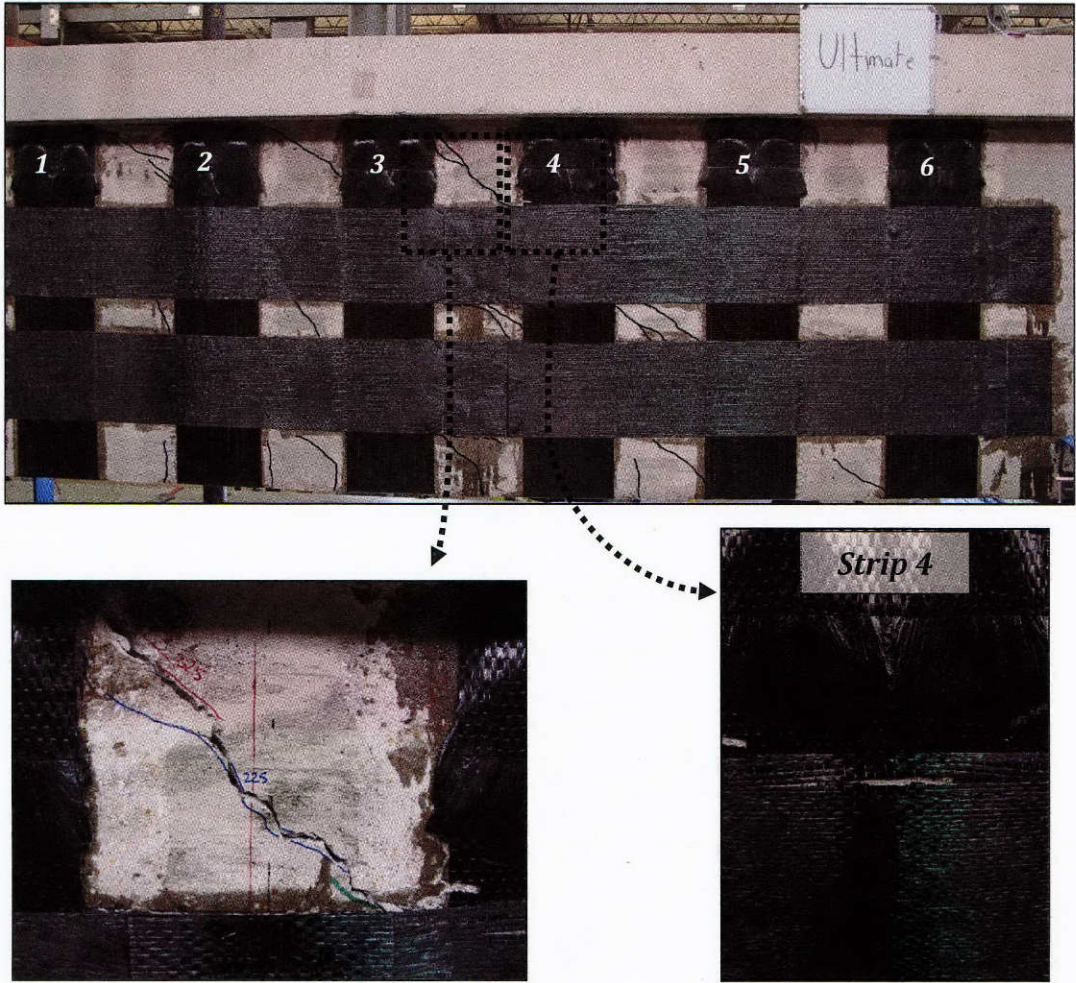


Figure 3-52: Cracking and failure of 48-3-14-5

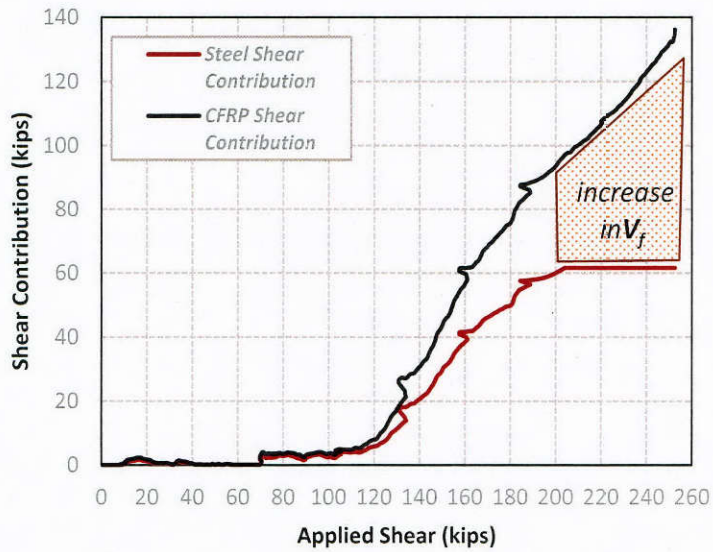


Figure 3-53: Shear contribution of steel stirrups and CFRP strip of test 48-3-14-5

3.5.6 Test 48-3-14-6 (Bi-Directional / 5-in. Strip)

This test had a bi-directional layout that consisted of 5-in. wide vertical CFRP strips spaced at 11-in. on center and 5-in. wide horizontal strips spaced at 7.5-in. on center. The CFRP layout of this test is shown in Figure 3-3.

Flexural cracks initiated at a shear of 66 kips. As load was increased, the flexural cracks extended vertically into the web. Web shear cracks formed at a shear of 123 kips. The measured crack widths at 129, 156, and 182 kips were 0.008-in., 0.016-in., and 0.03-in., respectively. The transverse reinforcement crossing the critical crack yielded at 190 kips. Shear failure was initiated by fracture of CFRP strip 6 at a shear of 275 kips. The test was stopped to prevent an explosive failure that would have prevented testing of the remaining test span. The applied shear versus shear deformation response is shown in Figure 3-54. Major events during the course of loading are labeled.

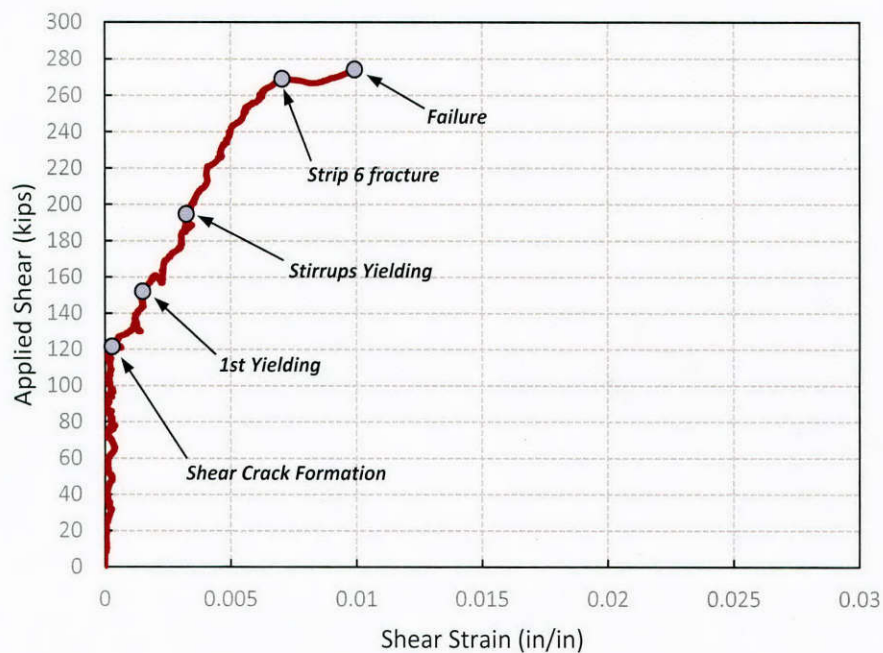
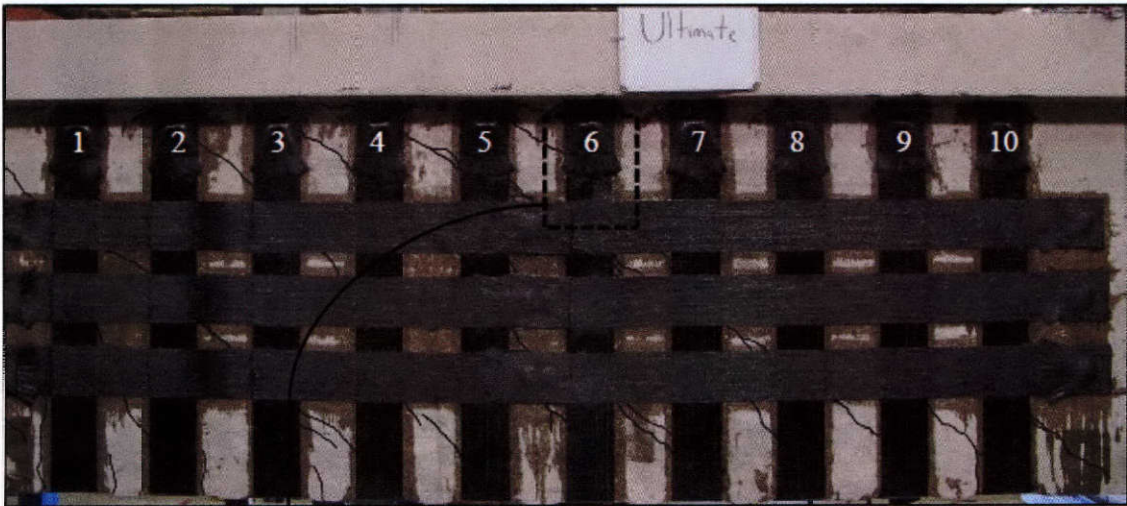
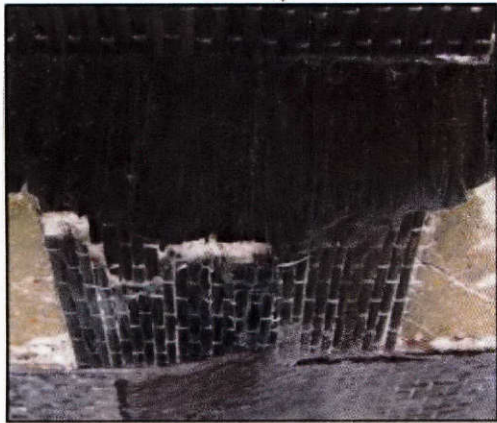


Figure 3-54: Shear response of test 48-3-14-6

The cracking pattern and failure mode are illustrated in Figure 3-55. At ultimate, the average strain in the CFRP strips was 0.007. As in the previous test, the data indicates that after transverse reinforcement across the critical crack yielded, the shear contribution of the CFRP increased substantially.



(a) Cracking pattern



(b) Strip 6 fracture (west side)



(c) Strip 6 fracture (east side)



(d) Critical crack



(e) Debonding horizontal strip

Figure 3-55: Cracking pattern and failure of test 48-3-14-6

3.5.7 Test 48-3-14-7 (10-in. Stirrups Spacing / Uni-Directional)

While the first six tests had a stirrup spacing of 18-in., this test was conducted on a specimen with a 10-in. stirrup spacing. The base shear capacity of this section without CFRP strengthening was 228 kips as measured by (Kim, 2011). The specimen was strengthened uni-directionally with 10-in. wide vertical CFRP strips spaced at 20-in. The CFRP layout was the same as test 48-3-14-2 which has a stirrup spacing of 18-in. A similar test was conducted in TxDOT project 0-6306; however, the specimen failed at 255 kips (with only a 12% strength gain) due to anchor rupture and no strips fractured. To evaluate the ability of the anchored CFRP system in strengthening heavily reinforced sections, this test was repeated with an improved CFRP anchor detail.

Since this test was the third and last test of a 40-ft long specimen (Figure 3-7 (b)), the test exhibited early cracking due to the tests conducted on both sides of this test span. However, cracking from the previous loadings did not affect the overall structural behavior of this test.

The shear response of the beam is shown in Figure 3-56. Shear and flexural cracks were observed at a shear below 66 kips. Flexural cracks extended and turned into inclined cracks as the load increased. The crack width was 0.02-in. when the transverse steel started yielding at a shear of 188 kips. At 325 kips, all transverse steel crossing the critical crack yielded, and the average strain in vertical strips 4 and 5 was 0.0075. Contour plots of principle tensile strains at major events are presented in Figure 3-57. The beam failed due to fracture of strip 4 at an applied shear of 336 kips (Figure 3-58). At failure, the strain in strip 4 was 0.011.

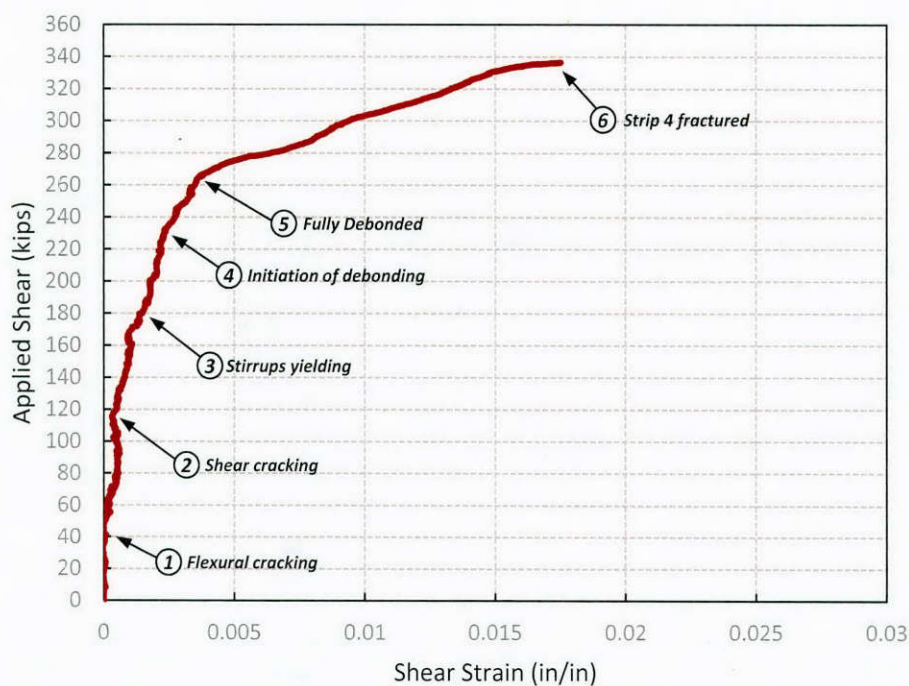


Figure 3-56: Shear response of test 48-3-14-7

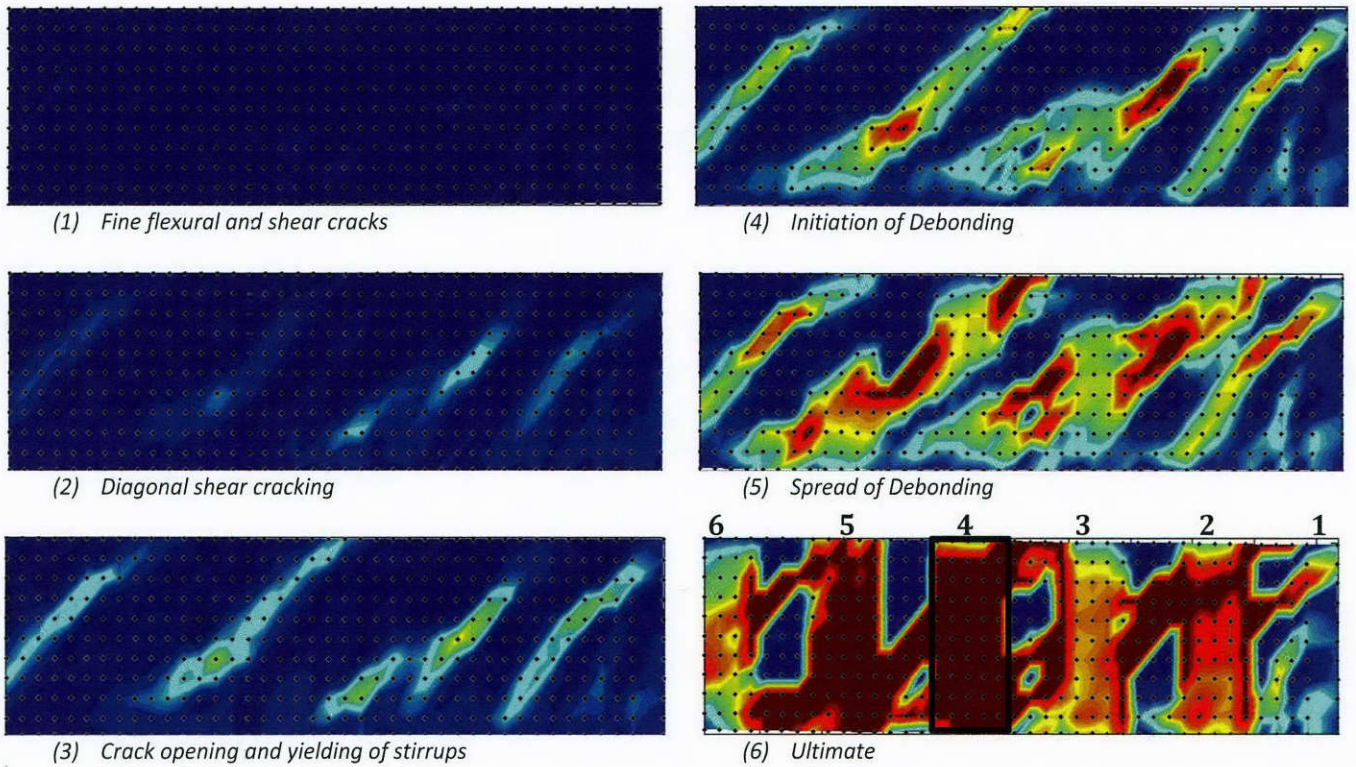


Figure 3-57: Principal strain profile of test 48-3-14-7 at major events [east side]

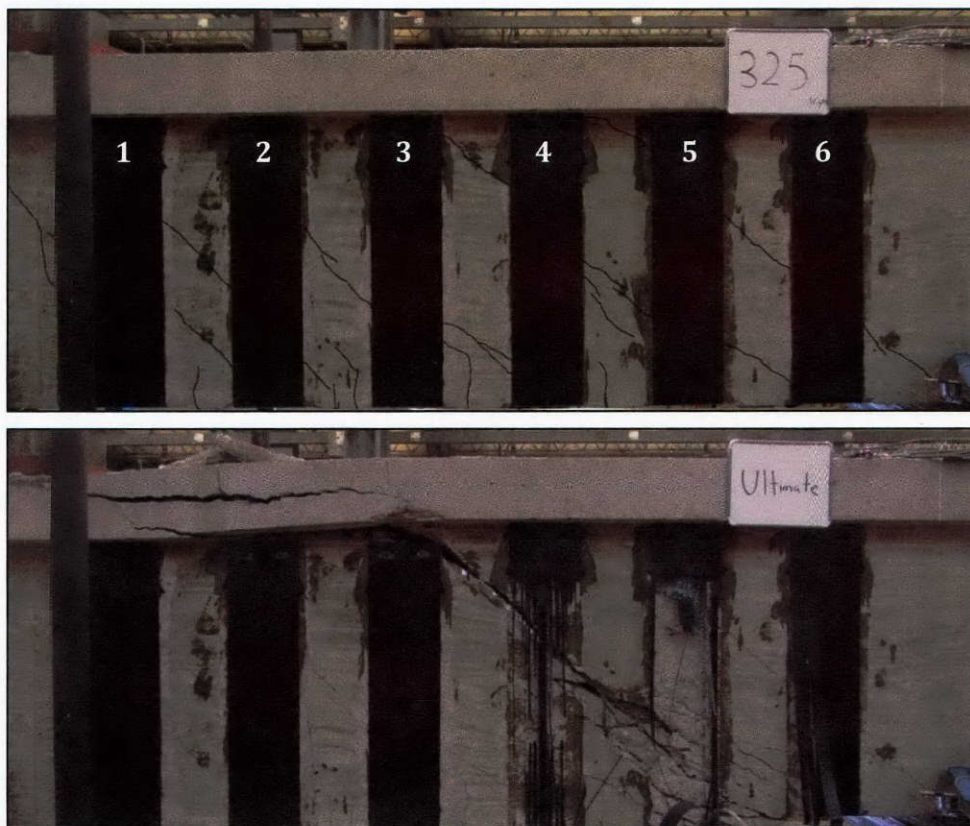


Figure 3-58: Test 48-3-14-7 before (top) and after (bottom) failure [west side]

3.5.8 Test 48-3-14-8 (Uni-Directional / Double Layers)

The specimen was strengthened uni-directionally with double layers of 10-in. wide vertical CFRP strips spaced at 20-in. on center. The CFRP layout of this test is shown in Figure 3-3. The CFRP layout was the same as that of test 48-3-14-2 but with twice the amount of CFRP material. The amount of CFRP material in the anchor was adjusted to maintain a ratio of two between the anchor-to-strip material area. The anchor fan length could have been adjusted following anchor design recommendations; however, the fan length was kept the same to evaluate the efficiency of the anchors under extreme conditions.

Flexural cracks were observed at a shear of 66 kips. Flexural cracks extended and turned into shear cracks as the load was increased. The shear response of test 48-3-14-8 is presented in Figure 3-59. Diagonal shear cracking was observed at 120 kips. The crack width was 0.025-in. when transverse steel start yielding at 186 kips. At a shear of 210 kips, strip 4 and 5 started to debond causing a reduction in stiffness. At 228 kips, all transverse steel crossing the critical crack yielded, and the average strain in vertical strips 4 and 5 was 0.0035. Loading stopped at 297 kips. The average strain in strips at ultimate was 0.0045, and the maximum recorded strain was 0.006. Figure 3-60 shows the condition of the strips when the test was stopped.

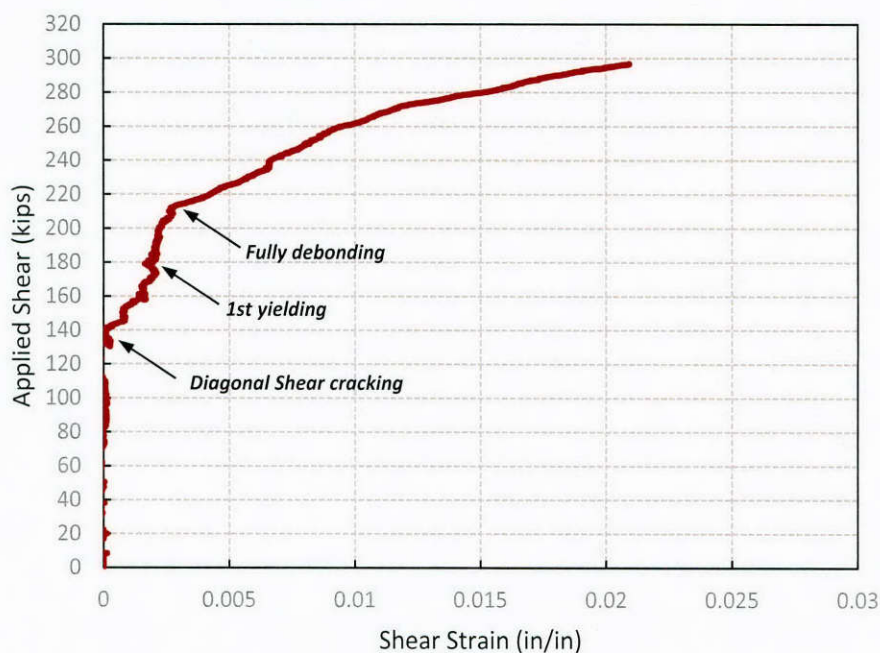


Figure 3-59: Shear response of test 48-3-14-8

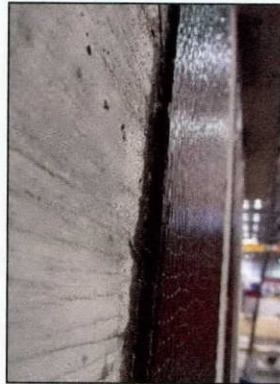
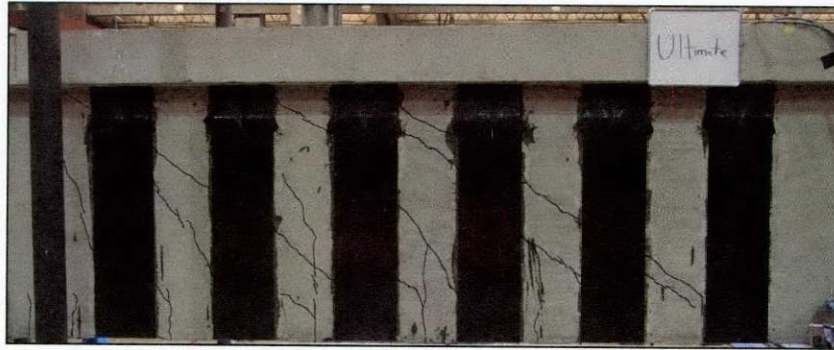


Figure 3-60: Failure of test 48-3-14-8

3.5.9 Test 48-3-14-9 (Bi-Directional / Double Horizontal)

The CFRP layout was similar to that of test 48-3-14-6 except that twice the amount of CFRP material was provided in the horizontal strips. The CFRP layout consisted of 5-in. wide vertical CFRP strips spaced at 11-in. on center and 5-in. wide horizontal strips spaced at 9.25-in. on center. The CFRP layout of this test is shown in Figure 3-3.

The shear response with major events is presented in Figure 3-61. Flexural cracks initiated at an applied shear of 66 kips. As load increased, the flexural cracks extended vertically into the web. Web shear cracks formed at 122 kips. The maximum measured crack widths at 129, 156, and 182 kips were 0.011-in., 0.016-in., and 0.02-in., respectively. The transverse reinforcement crossing the critical crack yielded at a shear of 206 kips. Prior to failure, the average strain in vertical CFRP strips was 0.0075. The principal tensile strain profiles of the major events are illustrated in Figure 3-62. Shear failure was initiated by rupture of CFRP strips at 273 kips (Figure 3-63) followed by explosive diagonal shear tension failure.

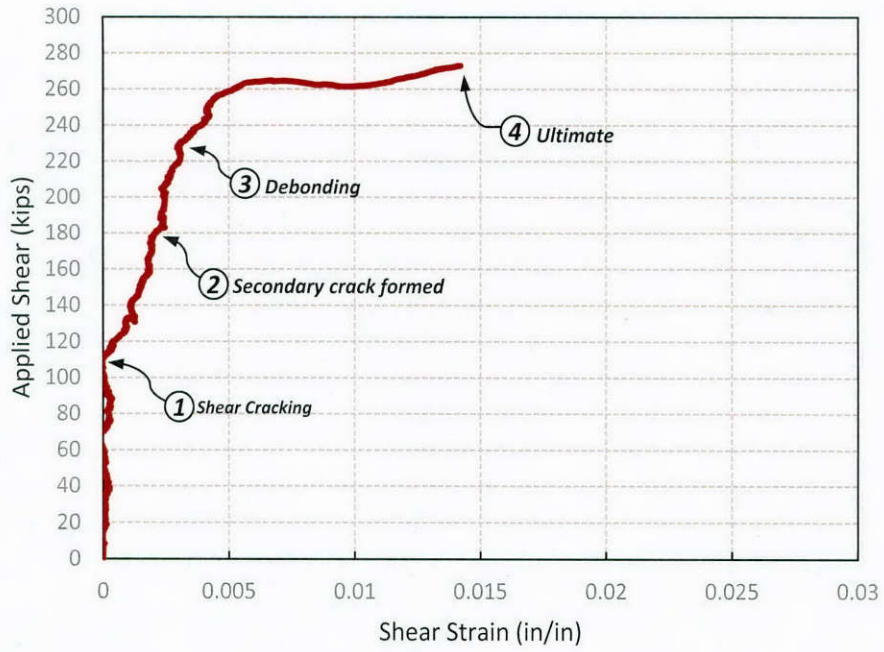


Figure 3-61: Shear response of test 48-3-14-9

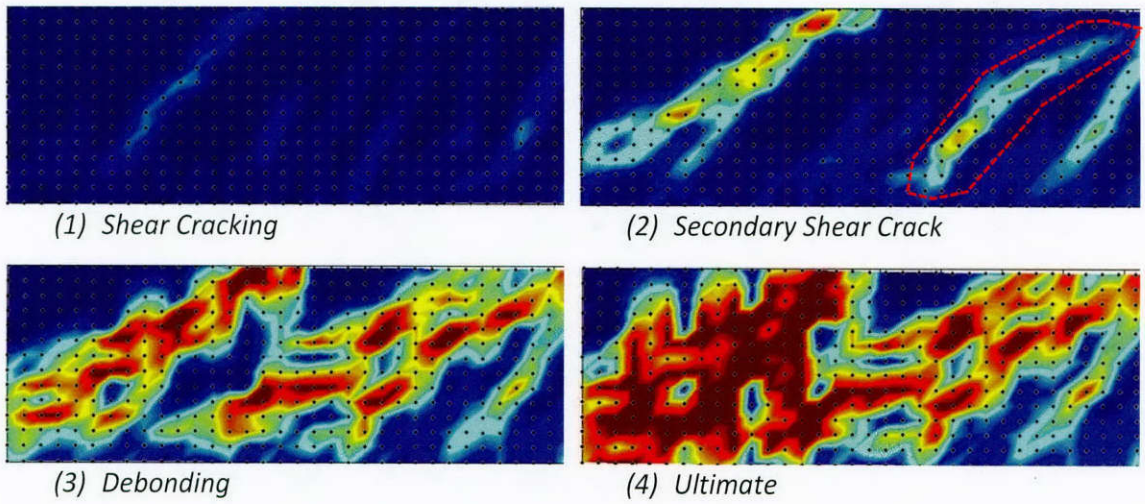


Figure 3-62: Principal tensile profile of test 48-3-14-9 at major events



Figure 3-63: Test 48-3-14-9 before failure (top) and after failure (bottom)

3.5.10 Test 48-3-14-10 (10-in. Stirrup Spacing / Bi-Directional)

This specimen had stirrups spaced at 10-in. and was strengthened bi-directionally with 5-in. wide vertical strips spaced at 11-in. on center and 5-in. wide horizontal strips spaced at 9.25-in. on center. The layout of this test is shown in Figure 3-3. The shear capacity was expected to be equivalent or lower than that of test 48-3-14-7 (336 kips) due to severe damage of an adjacent test span tested previously. The shear response is shown in Figure 3-64. Flexural cracks were observed at an applied shear of 66 kips. New flexural cracks formed as load was increased while previous cracks extended deeper into the web turning to shear cracks at 95 kips. The maximum measured crack widths at 129, 156, and 182 kips were 0.012-in., 0.014-in., and 0.018-in., respectively. The transverse reinforcement crossing the critical crack yielded at 238 kips. Shear failure was initiated by rupture of CFRP strips 7, 8, and 9 simultaneously. At the same time, the anchor of strip 7 on the east side fractured at 305 kips as shown in Figure 3-65. At ultimate strength, the average strain in vertical CFRP strips crossing the critical inclined crack was 0.0086. The reduction in the shear capacity in this test is attributed to the severe damage from previous testing of the adjacent test sections.

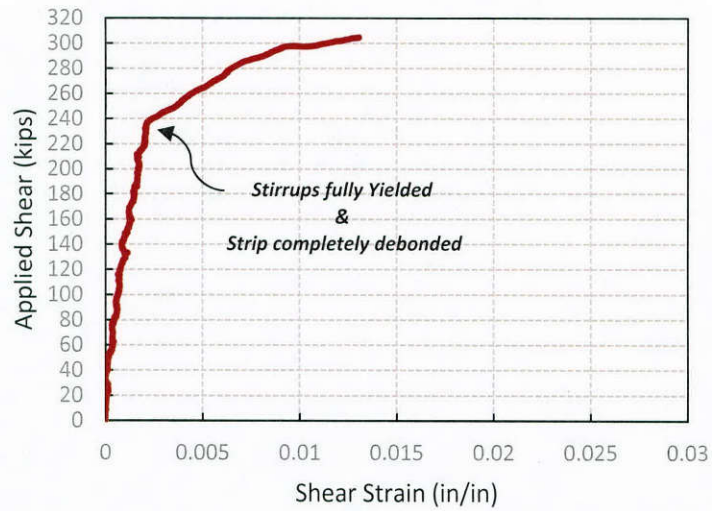


Figure 3-64: Shear response of test 48-3-14-10

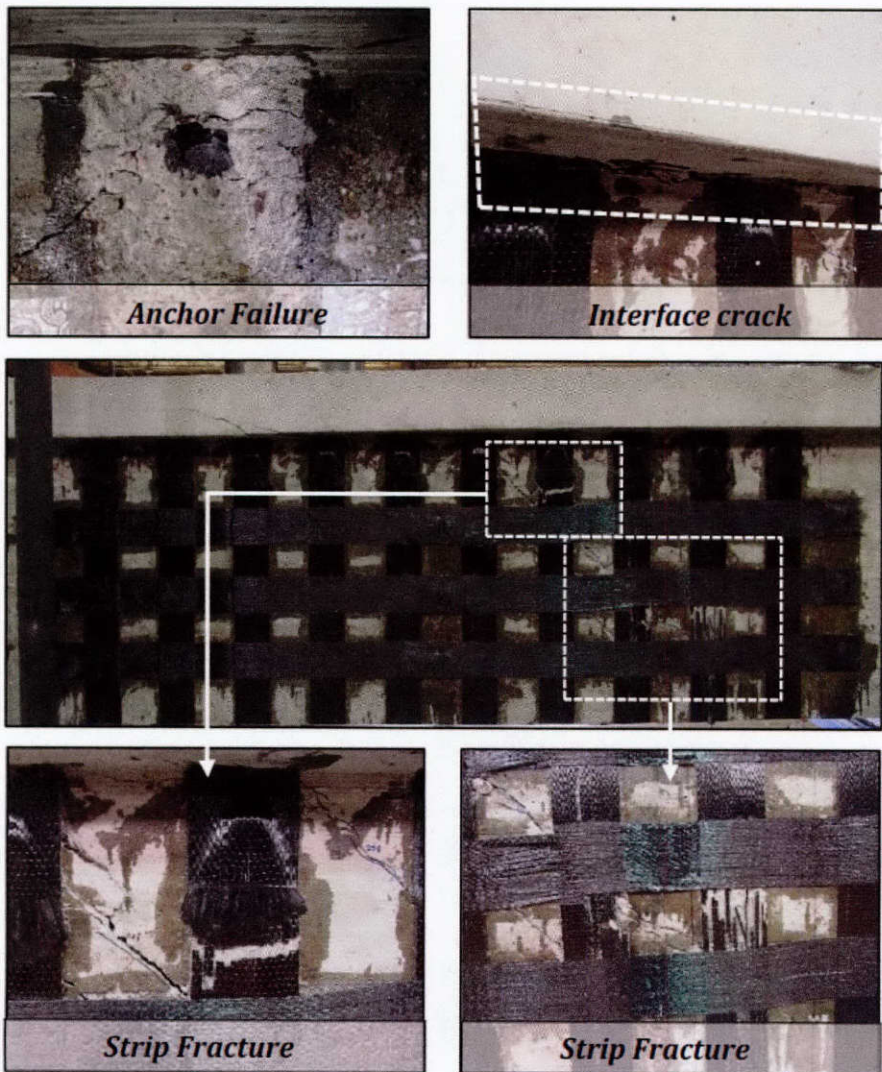


Figure 3-65: Failure of test 48-3-14-10

3.6 SUMMARY OF TEST RESULTS OF 48-IN. DEEP T-BEAMS

The test results of the 48-in. deep T-beams is summarized in Table 3-7. Test results confirm the efficiency of CFRP anchor system in shear strengthening of large scale members. Test specimens with stirrup spacing of 10-in. are highlighted in grey. Shear strength gains were calculated based on control test of TxDOT 0-6306 (147 kips), which is higher than the control test conducted in this program (48-3-14-1) that may have been stopped before the peak load was reached.

Table 3-7: Test results of 48-in. deep T-beam series

Test Name	CFRP Layout	Stirrup Spacing (in)	Concrete Strength ^{f_c} (psi)	Cracking Shear (kips)	Shear Capacity (kips)	Disp. at Ultimate (in)	Cracking Shear Increase	Shear Strength Gain	Normalized Concrete Contribution V_c (kips)	Normalized Shear Strength Gain
48-3-14-1	-	18	3900	73	122	0.49	-	-	59	-
48-3-14-2	U	18	3900	102	231	1.04	41%	57%	51	57%
48-3-14-3	U	18	5400	100	243	0.89	38%	65%	66	57%
48-3-14-4	B	18	5400	112	195	0.80	54%	32%	83	22%
48-3-14-5	B	18	4530	125	253	0.93	72%	72%	108	66%
48-3-14-6	B	18	4530	120	275	0.97	66%	87%	125	81%
48-3-14-7	U	10	4530	NA	337	1.39	NA	48%	129	43%
48-3-14-8	U	18	4570	126	297	1.06	74%	102%	103	96%
48-3-14-9	B	18	4570	119	273	1.01	65%	86%	103	80%
48-3-14-10	B	10	4570	NA	305	1.19	NA	34%	107	30%

In all tests, the CFRP anchor system was able to fully utilize the tensile capacity of the CFRP strips causing the strips to rupture. Table 3-7 shows a substantial strength gain up to 96% was achieved when CFRP anchors were used to provide essential anchorage after debonding. The CFRP anchor system was effective in strengthening of sections that were heavily reinforced with stirrups (10-in. stirrup spacing).

3.7 ANALYSIS OF TEST RESULTS

3.7.1 Control vs. Uni-Directional

The applied shear versus shear deformations for a control and a strengthened beam is presented in Figure 3-66 to illustrate the effect of CFRP strengthening on the overall shear response. The strengthened member exhibited a higher shear cracking load (41% increase) than the control beam. After cracking, the anchored CFRP strips maintained a higher member stiffness. Localized debonding of the strip started at the critical crack at a shear of about 150 kips. Debonding continued to spread as load was increasing until strips that cross the critical crack were fully debonded. After stirrups yielded at about 220 kips, additional loading was carried by the CFRP strips. The strengthened beam resisted an additional applied shear of (109 kips or a 57% increase over the control test. The failure initiated with fracture of one of the strips and produced a brittle failure since the forces could not be resisted or redistributed to other elements that were already highly

stressed. Overall, the strengthened beam exhibited higher strength and stiffness, and failed at a slightly higher shear deformation.

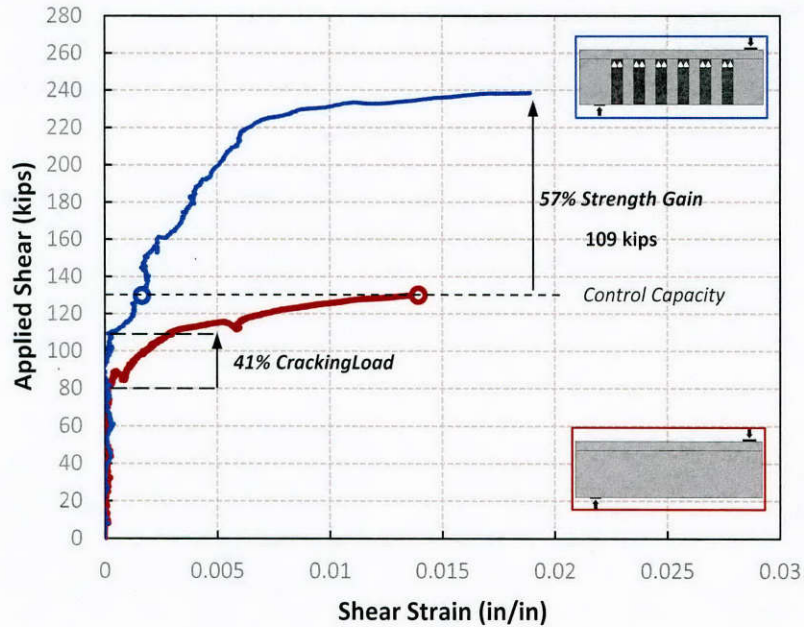


Figure 3-66: Comparison of shear response of test 48-3-14-1 (control) and 48-3-14-2 (uni 10'')

The principal tensile strain profiles for the control and uni-directional tests are presented in Figure 3-67. Strains were localized along the critical crack as expected in an ordinary reinforced concrete beam. As load increased the crack width increased causing yielding of transverse reinforcement and then loss of aggregate interlock with shear failure at a shear of about 130 kips. In contrast, the strengthened beam was stiffer because the CFRP strips provided better crack control that allowed the aggregate interlock mechanism to be maintained as the load increased. A larger number of cracks formed as a result and as the strips debonded, large strains (around 0.01) developed in strip 2, which fractured and resulted in failure of the beam. The primary shear crack formed at the same location in both tests.

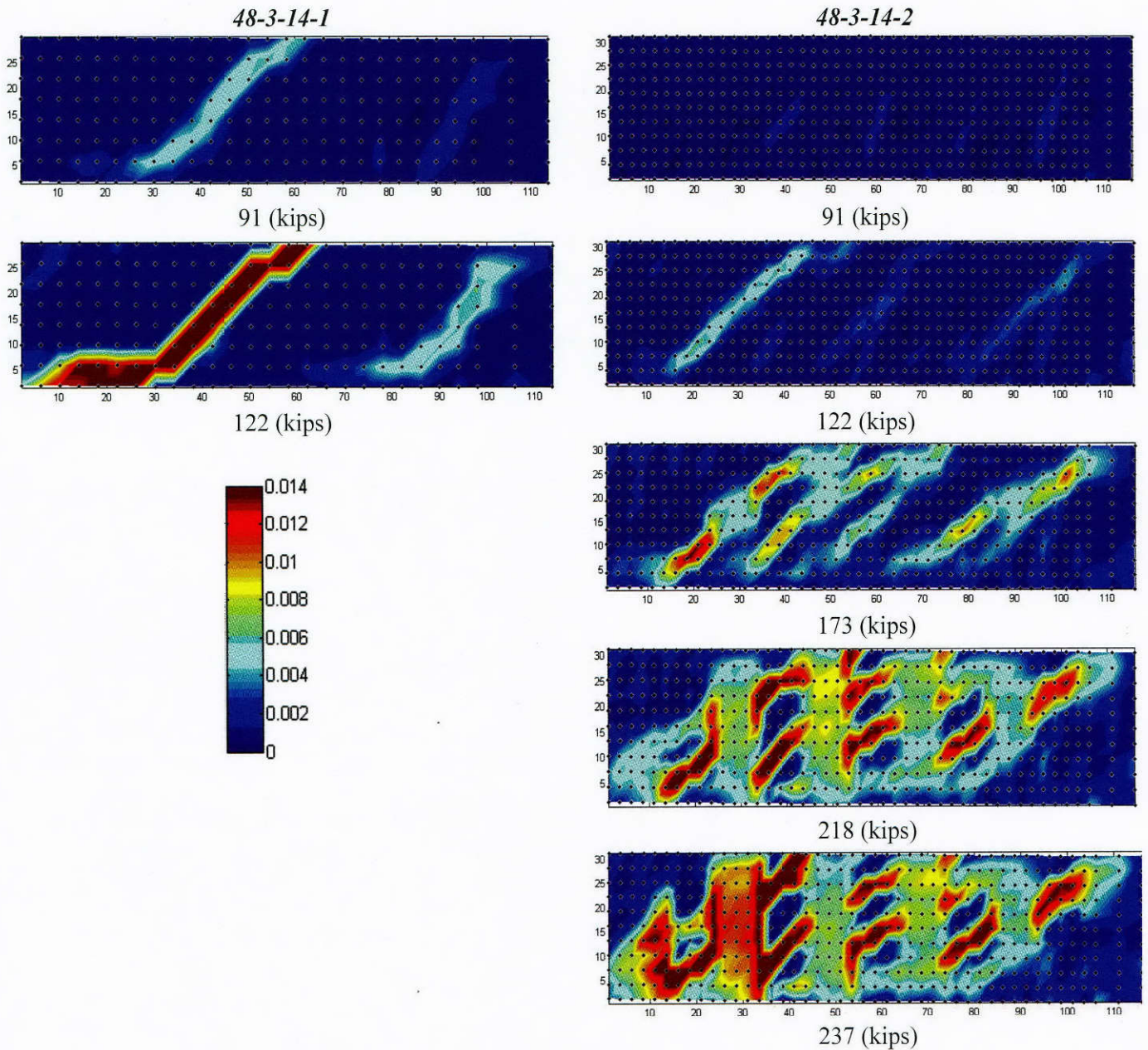


Figure 3-67: Principal tensile strain of 48-3-14-1 (control-left) and 48-3-14-2 (uni-directional-right)

Measured strains from strain gages on the transverse reinforcement and from the optical measurement system were used to measure the contribution of transverse reinforcement and CFRP strips to the shear strength. Figure 3-68 shows the shear contribution of each component for test 48-3-14-1 (control) and test 48-3-14-2 (strengthened). For the control test, transverse steel started to carry loads after the diagonal cracks formed at a shear of 80 kips. At 103 kips, all transverse steel crossing the critical crack yielded and shortly after that, the beam reached its shear capacity. In the strengthened beam, diagonal cracking occurred at a higher shear (103 kips). Similarly, yielding of transverse reinforcement occurred at 153 kips. Shear strengthening resulted in a 22% increase in cracking shear load due to the restraint to cracking provided by the bonded CFRP strips. A 33% increase in load was required to yield the transverse steel. This is attributed to the fact that the CFRP anchors provided enough anchorage to activate the CFRP reinforcement earlier and thus

delayed yielding of the transverse steel reinforcement. Figure 3-68 shows that CFRP shear contribution increased significantly after yielding of the transverse steel.

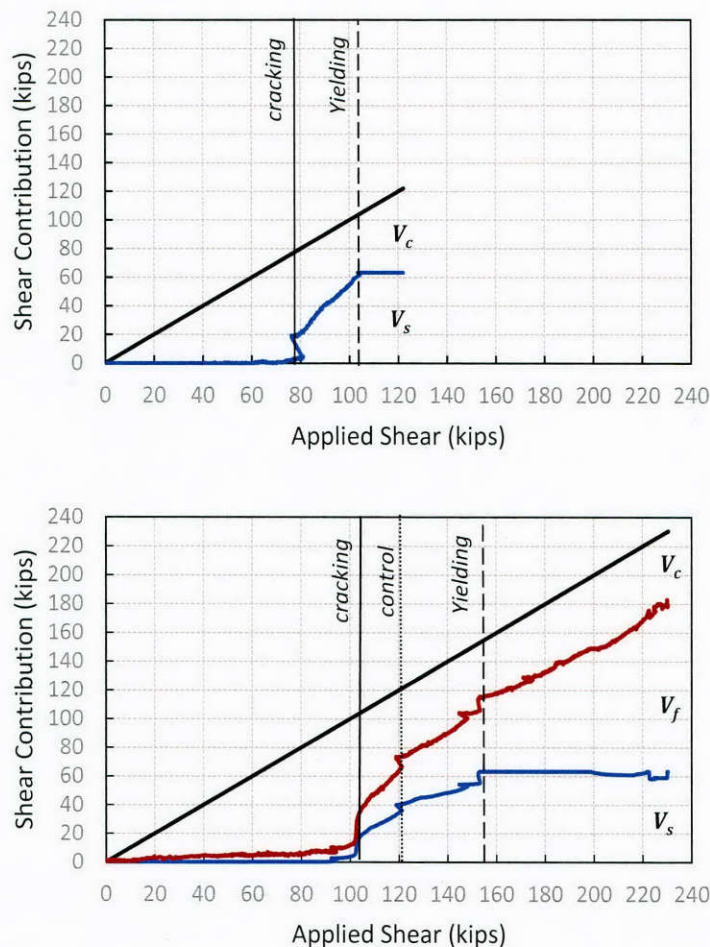


Figure 3-68: Shear contributions of control test (top) and uni-directional test (bottom)

3.7.2 Uni-Directional vs. Bi-Directional

The applied shear force versus shear strain for control, uni-directional, and bi-directional tests are shown in Figure 3-69. Bi-directional strengthening layouts resulted in shear strength gains up to 81%. The beam strengthened with a bi-directional layout exhibited a higher shear cracking load than the beam strengthened with uni-directional layout because the bi-directional layout provides an additional direction of restraint to the development of cracks. After cracking, the beam strengthened bi-directionally was stiffer than the beam with the uni-directional layout. The difference in stiffness can be attributed to the difference in the progression of debonding. In the uni-directional layout, vertical strips debonded over their total length so the strains were distributed over that length. However, in bi-directional layouts, the horizontal strips provided additional anchorage to vertical strips delaying the debonding process and resulting in higher CFRP strains concentrated near the diagonal crack. Therefore, the total shear deformation at failure in the bi-directional test was approximately half the shear deformation of the uni-directional test.

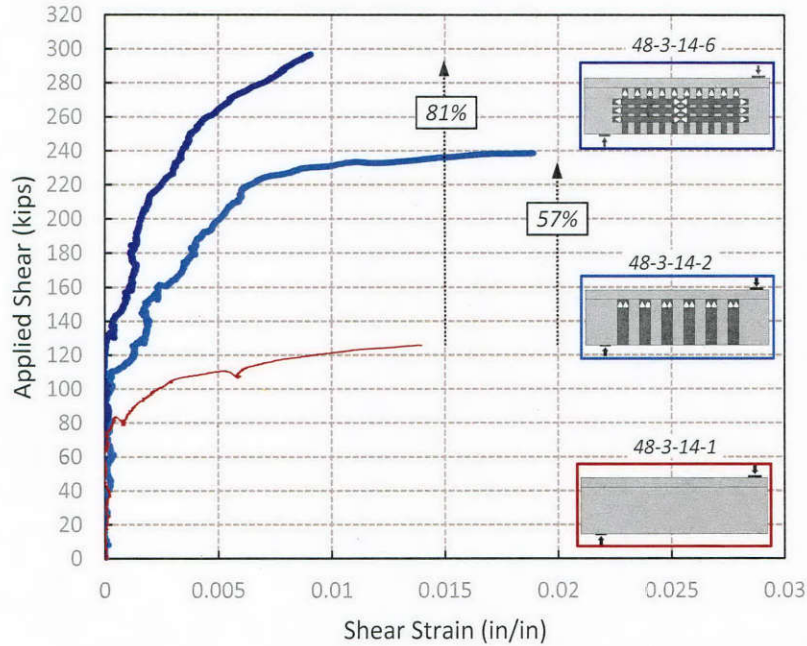


Figure 3-69: Shear versus shear deformations of control, uni-directional, and bi-directional tests

Although both tests failed by strip fracture, failure of test 48-3-14-6 was not as explosive as test 48-3-14-2. In a uni-directional layout, after fracture of a strip, the load dropped dramatically because the strip completely peeled off the concrete surface. However, in the bi-directional layout, horizontal strips provided some anchorage for the vertical strips after they fractured and allowed the beam to maintain a portion of the load after the strip fractured. In Figure 3-70, the restraint provided by the horizontal strip in the bi-directional layout prevented loss of anchorage along the full length of the vertical strips after they fractured. In Figure 3-71, strips on both faces of the uni-directional test 48-3-14-2 peeled off entirely at failure.

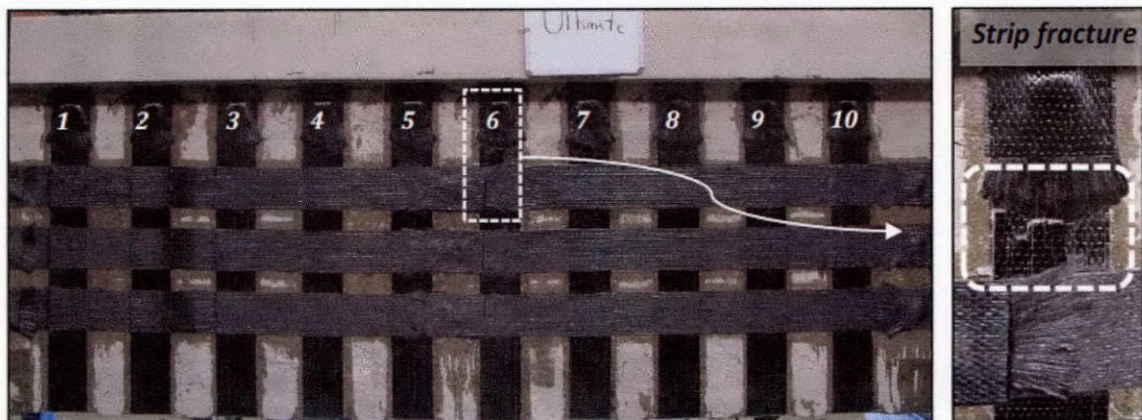


Figure 3-70: Failure of bi-directional test 48-3-14-6

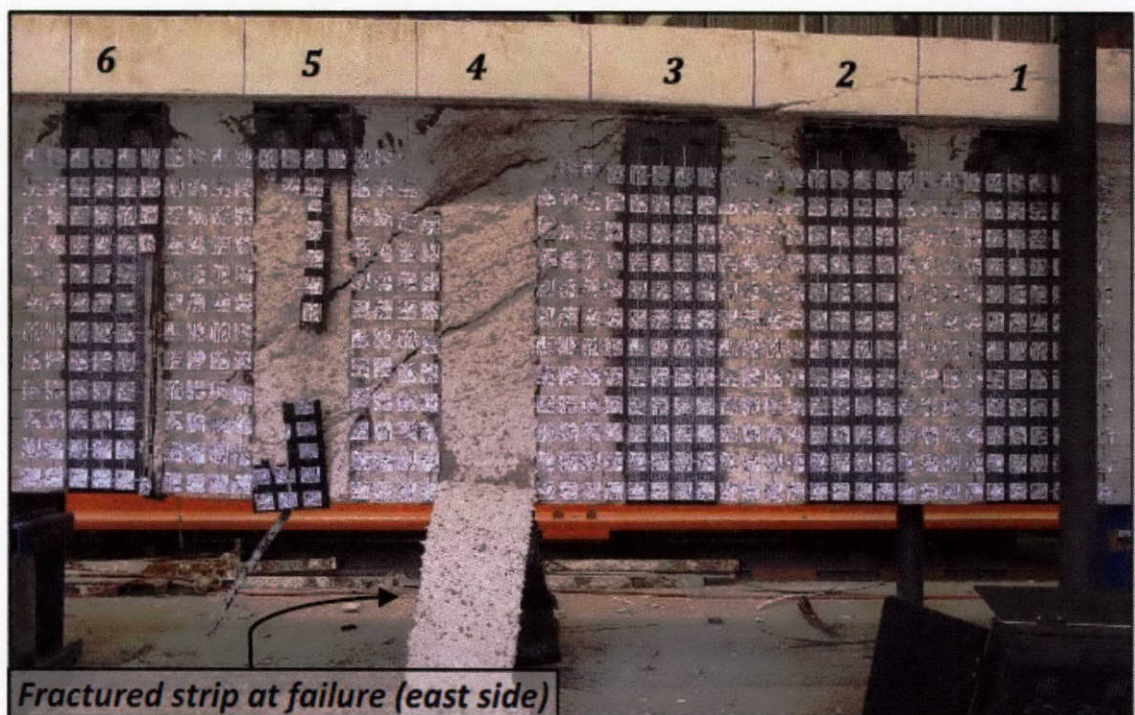


Figure 3-71: Failure of uni-directional test 48-3-14-2, west side (top) and east side (bottom)

The transverse reinforcement contribution to the shear resistance is determined by the number of stirrups that cross the critical crack. Previous studies on CFRP shear strengthening systems showed that transverse reinforcement did not reach yield before shear failure occurred due to strip debonding (Chen and Teng, 2003; Pellegrino and Modena, 2006). This is not completely accurate for two reasons: 1) these studies were conducted on unanchored strengthening systems while in CFRP anchored systems, the anchors prevent failures due to debonding and the transverse steel can develop its yield strength where it crosses the critical crack, 2) measured strains may not be as precise due to the fact that the critical crack may not cross the strain gages. In this experimental program, the optical measurement system was used, in addition to strain gages, to provide a more accurate measure of strains in transverse reinforcement.

In Figure 3-72, the transverse steel contribution to the shear resistance for control, uni-directional, and bi-directional test is shown. All transverse reinforcement crossing the critical crack fully yielded before failure. The slight difference in the maximum steel shear contribution is due to the difference in the yield strength of transverse reinforcement used in fabrication. The bi-directional layout delayed the development of the steel shear contribution more than in the uni-directional layout, even though the ultimate steel shear contribution is similar for both cases. For instance, at an applied shear of 140 kips, transverse steel contributed 48 kips to the shear resistance in the uni-directional layout while it contributed 22 kips in the bi-directional layout. This shows that the horizontal strips inhibited the opening of the crack and increased the concrete shear contribution provided by aggregate interlock.

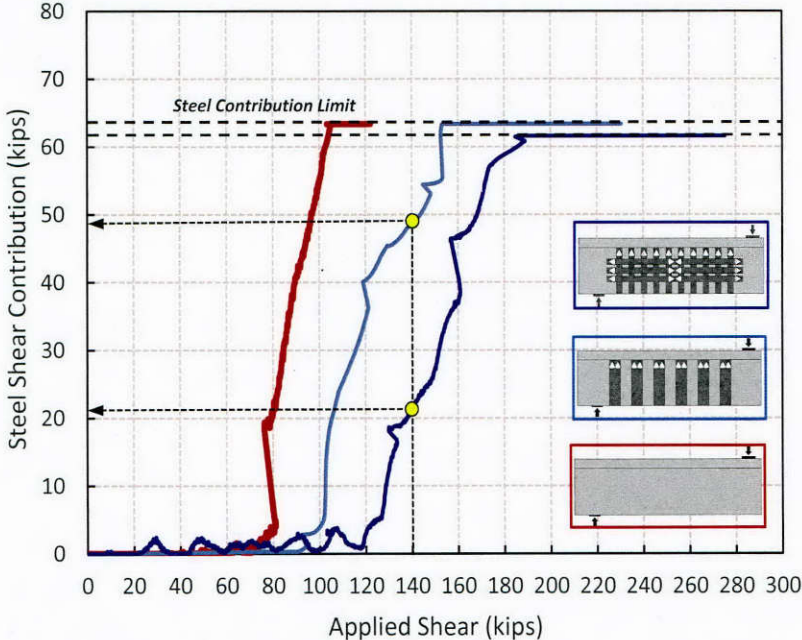


Figure 3-72: Transverse steel contribution to the shear strength of control, uni-directional, and bi-directional tests

The optical measurement system also was used to determine the crack widths. Figure 3-73 shows applied load versus crack widths of control, uni-directional, and bi-directional tests. As can be seen, the bi-directional layout provided better crack control than the uni-directional layout. The maximum crack width in the web of the beam that was bi-directionally strengthened is less than half the maximum crack width in the uni-directionally strengthened beam. By controlling the crack better, the concrete shear contribution of the beam strengthened with a bi-directional layout was higher than that of the beam strengthened with a uni-directional layout.

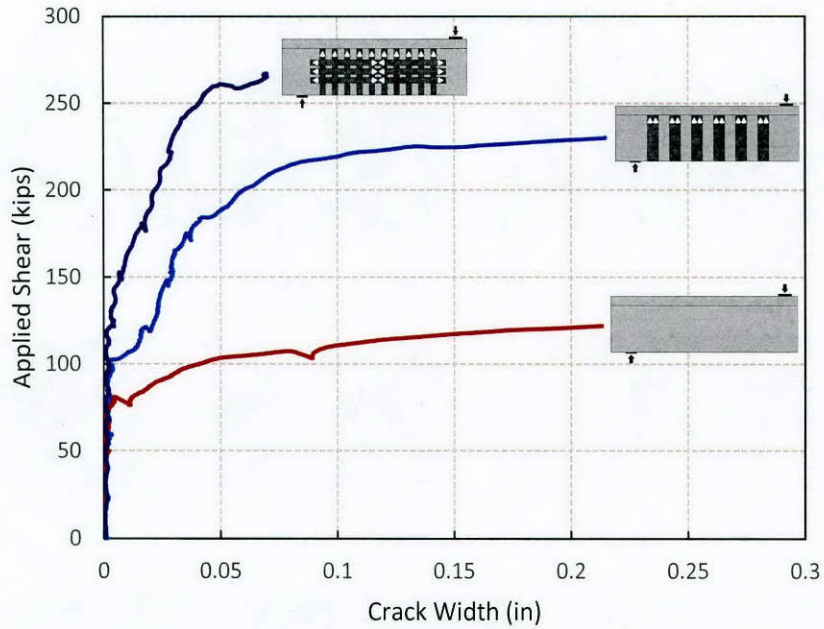


Figure 3-73: Crack width at mid-depth of control, uni-directional and bi-directional tests

The principle tensile strain contours for uni-directional and bi-directional tests at different load stages are shown in Figure 3-74. The contour plots show that the primary shear crack formed in the uni-directional test at an applied shear of 122 kips, while in the bi-directional test, only the initiation of the shear crack can be noticed at the same load. As the load increased, secondary shear cracks formed in both tests with wider cracks in the uni-directional test. With further loading, debonding began earlier in uni-directional tests since horizontal strips in bi-directional layout helped provide anchorage for the vertical strips.

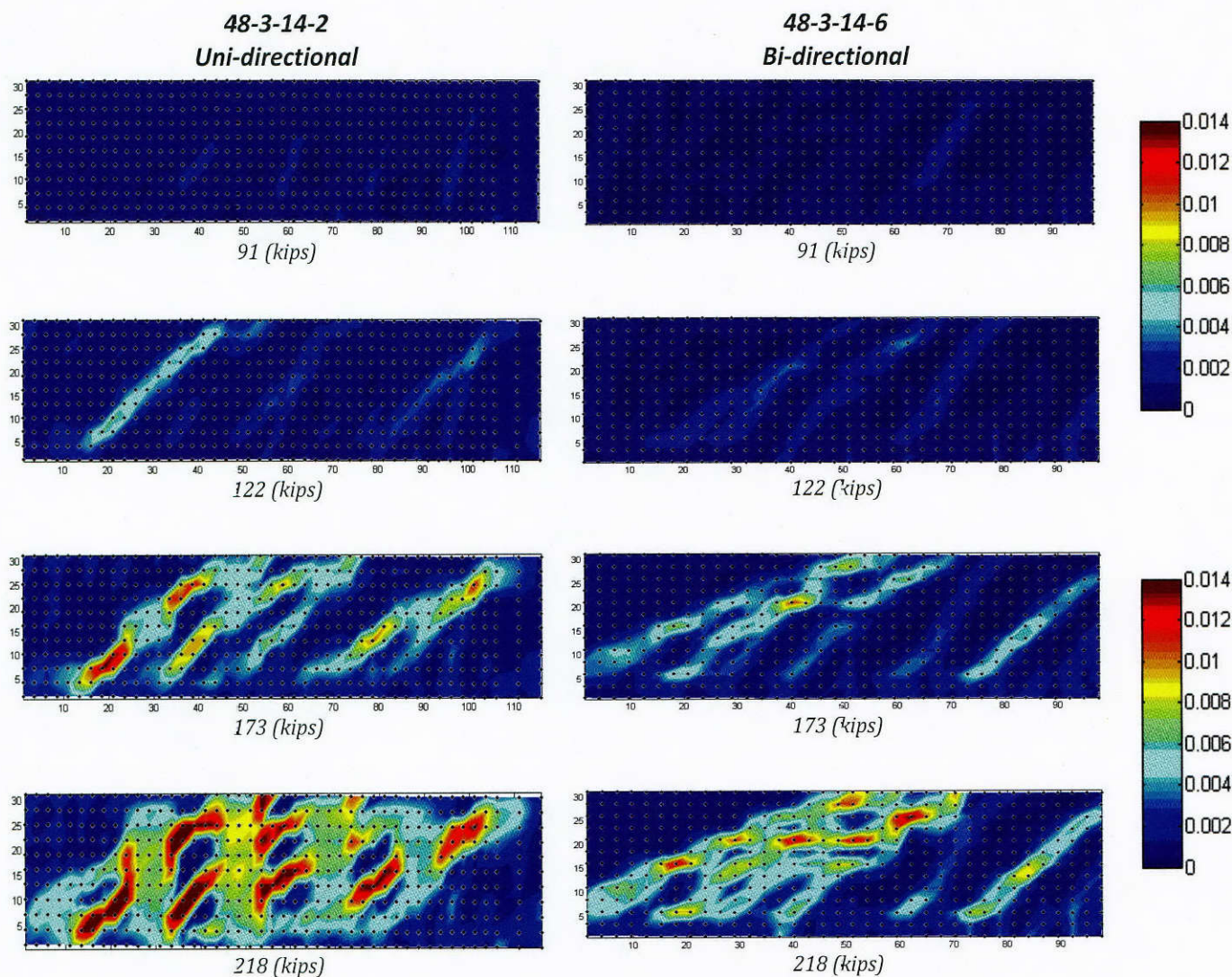


Figure 3-74: Principal tensile strain profile for uni-directional test (left) and bi-directional test (right)

The shear contributions of concrete, steel reinforcement, and CFRP for control, uni-directional, and bi-directional tests are shown in Figure 3-75. As can be seen in Figure 3-75, in the bi-directional layout, the shear cracking load increased, and yielding of transverse steel was further delayed. It also illustrates the effect of the bi-directional layout on the concrete shear contribution. The concrete shear contribution is roughly the same in the control and uni-directional tests; however, the concrete shear contribution is about doubled in the bi-directional layout. The steel shear contribution is the same for all tests and indicates that all transverse steel crossing the critical crack yielded in CFRP anchored systems.

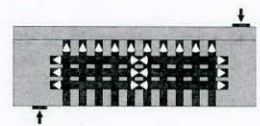
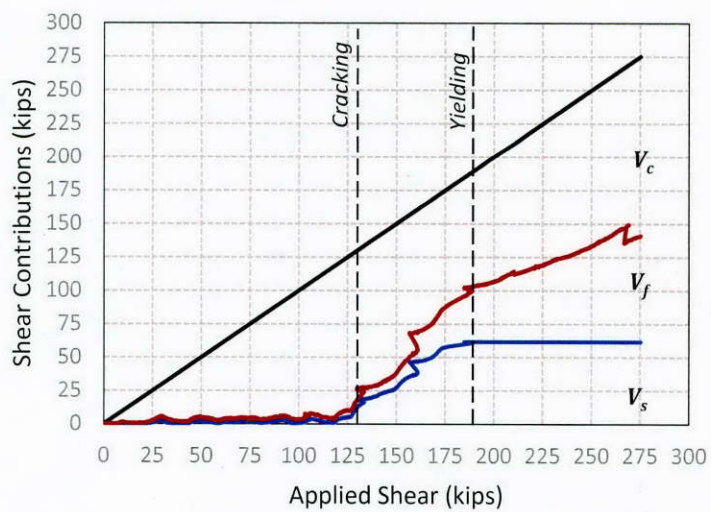
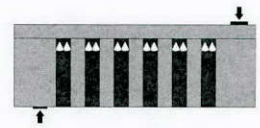
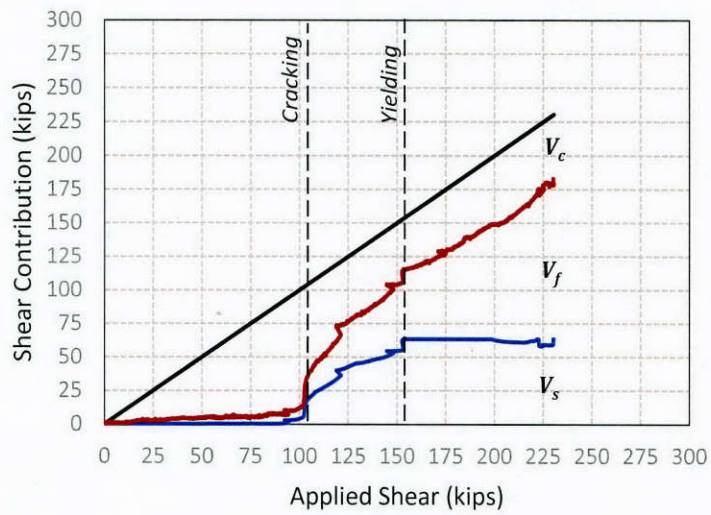
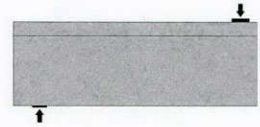
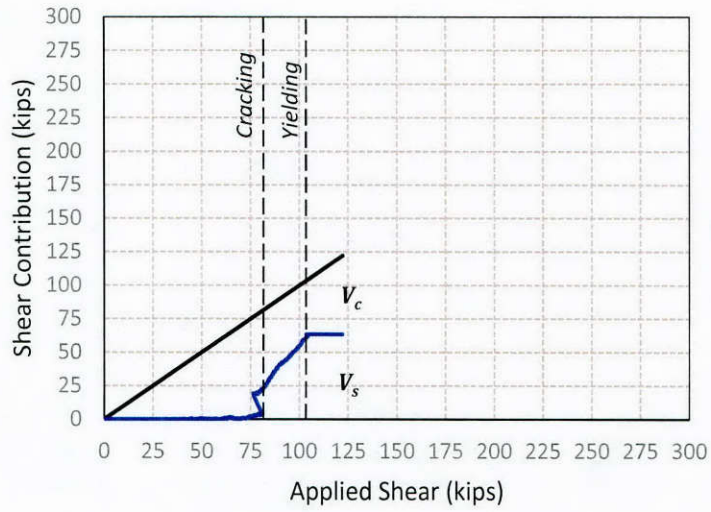


Figure 3-75: Shear contributions of control, uni-directional, and bi-directional tests

3.8 CONCLUSIONS

A total of eighteen tests were conducted on large-scale T-beams to investigate the effect of bi-directional applications of CFRP strips and CFRP anchors for strengthening reinforced concrete (RC) members in shear. Eight tests were performed on 24-in. deep T-beams and ten tests were performed on 48-in. deep T-beams. The effects of various parameters were investigated, including:

- 1) shear span-to-depth ratio (1.5 and 3),
- 2) amount of CFRP material (single layer and double layers),
- 3) web width (14-in. and 8-in),
- 4) CFRP layout (5-in. and 10-in. strips),
- 5) transverse reinforcement ratio.

The findings from the 24-in. deep T-beam tests can be summarized as follows:

- The bi-directional application of CFRP had a negligible effect on the shear capacity of beams with a/d of 1.5. The use of uni- or bi-directional CFRP layouts for strengthening of beams with $a/d \leq 1.5$ is not recommended because the tests indicated that load was transferred to the support through compression struts in the concrete and the CFRP did not have any measurable influence on the strength of the struts.
- The bi-directional application of CFRP had a substantial effect on the shear capacity of beams with a/d of 3. For the beams with 14-in. webs, a shear strength gain up to 62% was achieved with a bi-directional layout. With a uni-directional layout that had the same amount of vertical CFRP reinforcement, a 45% shear strength gain was achieved.
- The shear capacity of beams with 8-in. webs was governed by concrete web crushing due to high shear stresses (up to $12 \sqrt{f'_c} b_w d$ in psi units) that exceeded the maximum shear stresses permitted in most codes.
- In all tests, the steel stirrups crossing the critical inclined crack yielded. The steel contribution to the shear capacity was not affected by the type of external application of CFRP (uni-directional or bi-directional). However, the steel contribution was reached at higher loads in bi-directional than in uni-directional applications.
- There was a considerable reduction in strains in the steel stirrups and the CFRP strips in beams strengthened with bi-directional layouts in comparison with beams strengthened with uni-directional layouts at the same load.
- The cracking pattern of the bi-directionally strengthened beams was different than uni-directionally strengthened beams. The use of bi-directional layouts resulted in a more distributed cracking pattern with smaller crack widths compared with uni-directional application.
- The performance of lap splicing vertical CFRP strips under the web was comparable to the performance of wrapping a single vertical CFRP strip around the web. Therefore, the difficulty of wrapping vertical CFRP strips around the web of reinforced concrete girders in the field can be eliminated by lap splicing the vertical strips under the web of the beam.

The finding from the 48-in. deep T-beams can be summarized as follows:

- The use of anchored CFRP layouts on full-scale RC beams was found to be very effective and resulted in substantial shear strength increases up to 96% for lightly reinforced beams ($d/2$ stirrup spacing) and up to 43% for heavily reinforced beams ($d/4$ stirrup spacing).

- Specimens strengthened with bi-directional layouts exhibited up to an 81% increase in shear capacity while specimens strengthened with uni-directional layouts that had the same amount of vertical CFRP reinforcement exhibited up to a 57% increase.
- Specimens strengthened with bi-directional layouts exhibited shear strengths gains that were 10% to 24% larger than specimens strengthened with uni-directional layouts that had the same amount of CFRP reinforcement in the vertical direction.
- Strengthening with narrow CFRP strips resulted in: 1) simplified CFRP handling and installation, 2) enhanced concrete shear contributions, and 3) fewer stress concentrations in the CFRP strips compared to strengthening with wider strips.
- Specimens strengthened with bi-directional layouts were found to have 1) stiffer post cracking responses, 2) narrower shear crack widths, 3) lower shear deformations at failure, and 4) a higher concrete shear contribution compared to specimens strengthened with uni-directional layouts that had the same amount of CFRP reinforcement in the vertical directions.
- The shear contribution of the CFRP reinforcement was not proportional to the amount of CFRP material used for strengthening.
- As in the 24-in. deep T-beam series, the bi-directional layouts delayed the shear contribution of the steel reinforcement. Although horizontal CFRP reinforcement is not accounted for in current shear strengthening design guidelines, it does increase the shear capacity if proper anchorage is provided. However, a bi-directional layout is less effective than a uni-directional layout at increasing the shear capacity of a member when the same amount of CFRP material is used.
- The addition of anchored horizontal strips in bi-directional layouts prevented the sudden loss of load carrying capacity by providing anchorage for the vertical CFRP strips. This allowed the beams to maintain higher post-peak load after the vertical CFRP strips fracture.
- The application of uni-directional layouts required less labor compared to the bi-directional layouts.

Chapter 4. I-Beam Tests

4.1 OVERVIEW AND OBJECTIVE

Previously, in project 0-6306, four 54-in. deep I-beams were tested. The tests indicated that bi-directional CFRP layouts were able to significantly increase the I-beam's shear capacity compared to the uni-directional layouts. Unfortunately, a reason for the bi-directional layout's superior performance could not be drawn due to the lack of available test data. Therefore, additional tests were proposed to investigate the shear behavior of full-scale I-beams strengthened with various bi-directional CFRP layouts.

A large number of I-beam tests were initially envisioned. However, it soon became apparent that the I-beam tests were not a priority to the Project Panel since the in-field I-beams were not experiencing shear deficiencies. Consequently, the I-beam tests were scaled back when only one suitable I-beam could be procured from the fabrication plants in Texas. As a result, the I-beam tests were delayed about six months.

4.2 EXPERIMENTAL PROGRAM

4.2.1 Test Specimen

The Project Panel provided assistance in procuring a 100-ft. long Tx46 I-beam located at Bexar Concrete in San Antonio, TX. A drawing of the beam is shown in Figure 4-6. The beam was originally rejected from service because of consolidation problems in the bottom flange. However, the voids in the bottom flange were deemed insignificant for the planned shear tests.

The 100-ft. long beam was cut in two equal sections prior to being shipped to Ferguson Structural Engineering Laboratory. Once received, the honeycombed area was repaired using a patching material. The damaged and repaired flange can be seen in Figure 4-1 and the location of the damage can be seen in Figure 4-6.



(a) Before repair



(b) After repair

Figure 4-1: Honeycomb repair

Figure 4-2 shows the cross-section of the longitudinal tendon locations at the end and middle sections of the original 100-ft. I-beam. Note that some of the tendons had a draped longitudinal profile. A total of 64 1/2-in. low-relaxation strands were used in the I-beam. The ultimate tensile stress of the strands was 270-ksi.

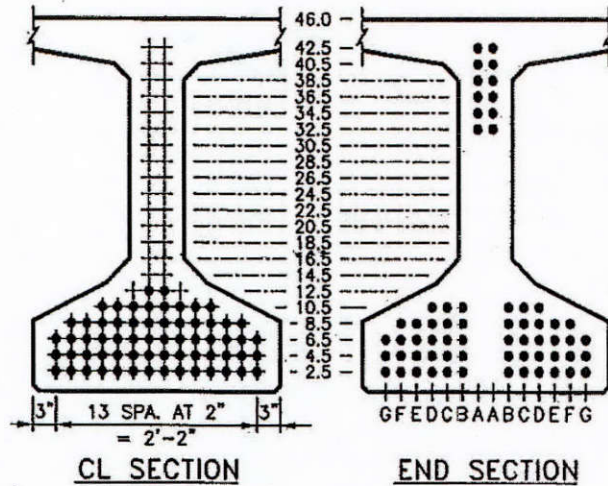


Figure 4-2: Tendon profile

Table 4-1 shows the design and measured concrete strength at various key stages of the beam's life. The strength at testing was evaluated by taking cores from undamaged portions of the beam.

Table 4-1: Concrete strength

	Concrete Strength (psi)
Release	5,900
28-day Design	6,500
Measured Test Day	11,400

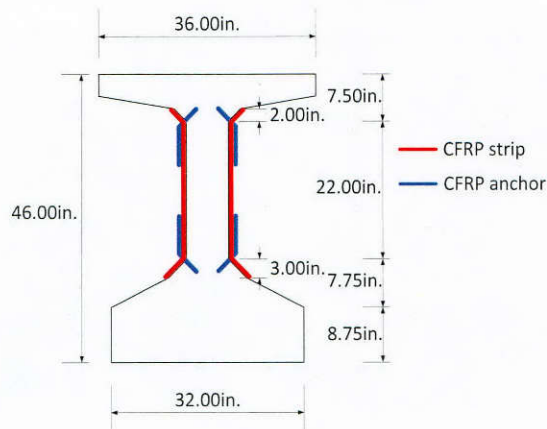


Figure 4-3: CFRP strengthening

Figure 4-3 shows the CFRP placement on the web of the Tx46 I-beam. CFRP strips and anchors were placed in the web region of the I-beam. Since the I-beam had a narrow web-width, the 4-in. deep anchor holes were angled upward to avoid having opposing holes intersect. The first 50-ft. section of the I-beam was reinforced with only uni-directional CFRP layouts while the other section was reinforced with bi-directional layouts.

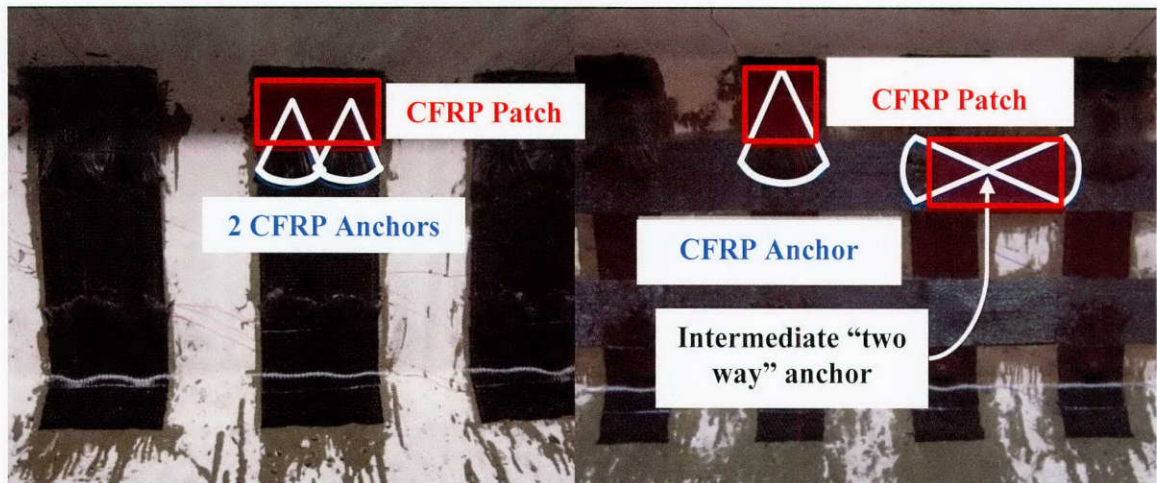
4.2.2 Test Variables

Table 4-2 shows the variables that were investigated in each of the tests. The nomenclature used to identify each test is comprised of the type of CFRP layout (control, uni-, or bi-directional) and the steel stirrup center-to-center spacing. In the uni-directional layout, 10-in. wide strips at an 18-in. center-to-center spacing were used. As can be seen in Figure 4-4(a), each strip was anchored with two 5/8-in. diameter CFRP anchors at each end of the strip. In the bi-directional layout, 5-in. wide CFRP strips were spaced at 12-in. on center. One CFRP anchor was installed at each end of the vertical strip (Figure 4-4(b)). The horizontal strips were also 5-in. wide but spaced at 10-in. on center. Each horizontal strip was anchored at its ends and intermediately by two equally spaced “two-way” anchors.

Table 4-2: I-beam test matrix

Nomenclature	CFRP Layout	CFRP Spacing (in.)		CFRP Strip Width (in.)		Stirrup Spacing (in.)
		Vertical	Horizontal	Vertical	Horizontal	
Control-18	None	None	None	None	None	18
Uni-18R	Uni-direction	18	None	10	None	18
Uni-12						12
Uni-8						8
Bi-18	Bi-direction	12	10	5	5	18
Bi-12						12

Note: “R” indicates a repaired specimen (i.e., pre-cracked)



(a) Uni-directional CFRP layout

(b) Bi-directional CFRP layout

Figure 4-4: CFRP anchor installation for uni- and bi-directional CFRP layout

In Figure 4-5, the area of CFRP material used to strengthen each specimen is shown. The areas shown include the CFRP strips, patches, and anchors. The various layout details, such as strip width and spacing, were specified so that each test would have nearly equal area of CFRP.

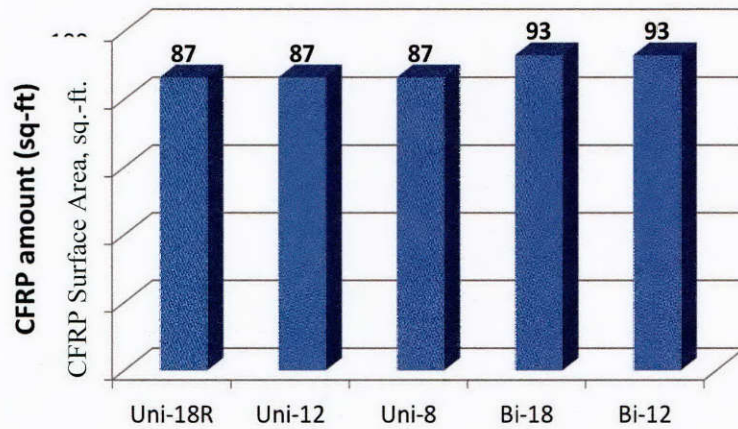
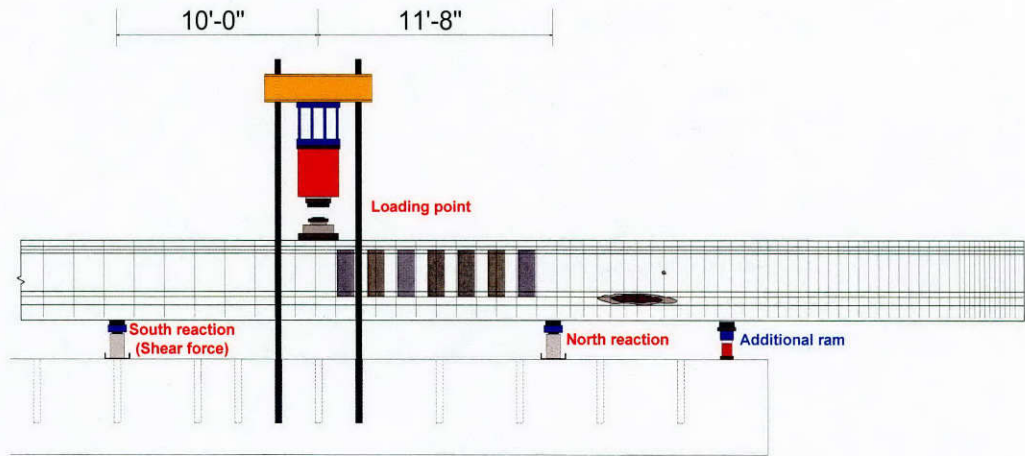


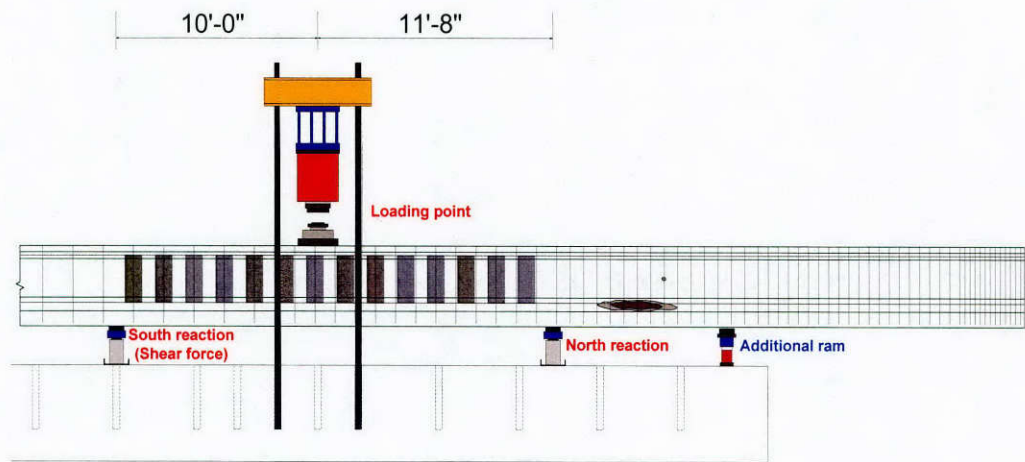
Figure 4-5: CFRP area comparison

4.2.3 Test Setup

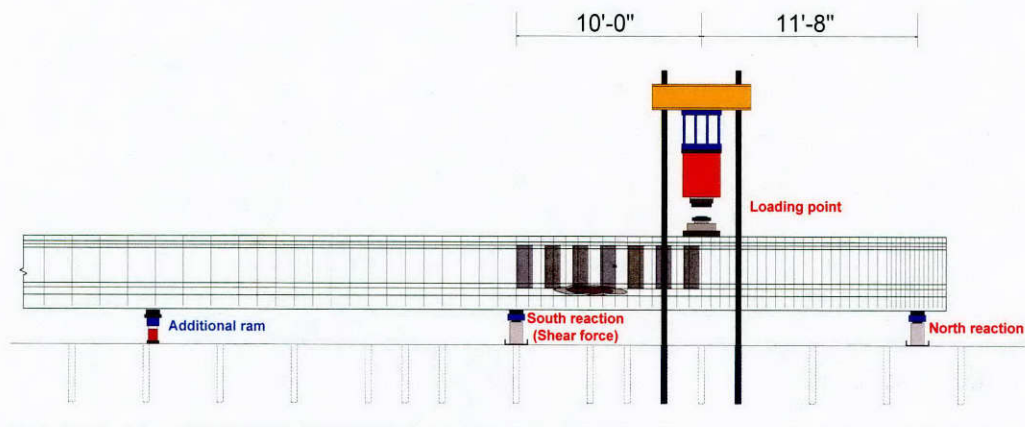
Figure 4-6 shows a schematic of the test setup for the I-beams. Two 1,000-kip load cells were used to monitor each reaction point and a 1,000-kip load cell was placed at the loading point. Details of the test setup are shown in Figure 4-7. All the tests had a 120-in. shear span (a_v) measured from the center of the load to the center of the reaction. The back span of the beam, between the north reaction and the loading point, was increased to 140-in. to reduce the applied shear and prevent failure outside of the test span.



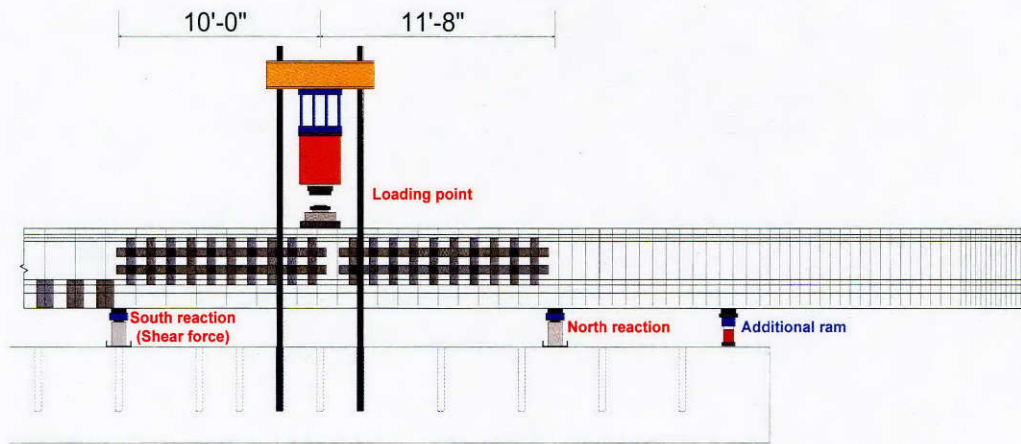
(a) Control-18 and Uni-18R



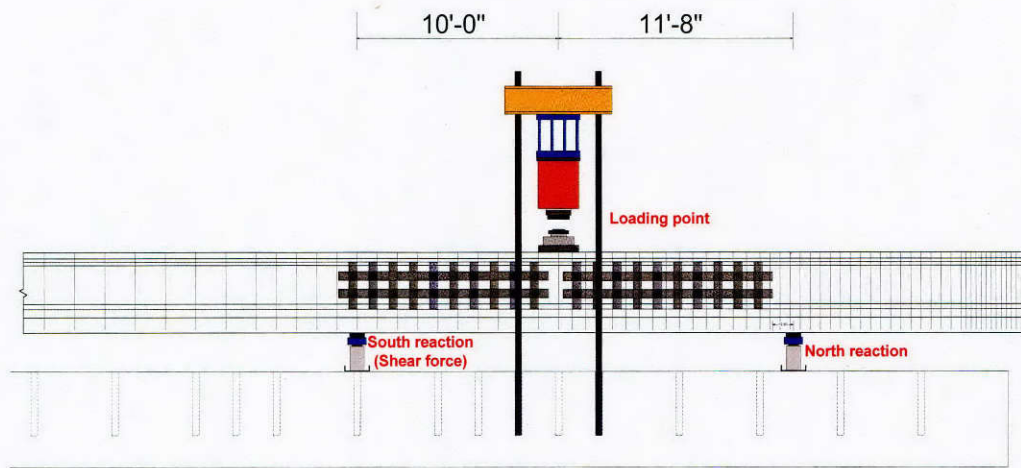
(b) Uni-12



(c) Uni-8



(d) Bi-18



(e) Bi-12

Figure 4-6: Test setup

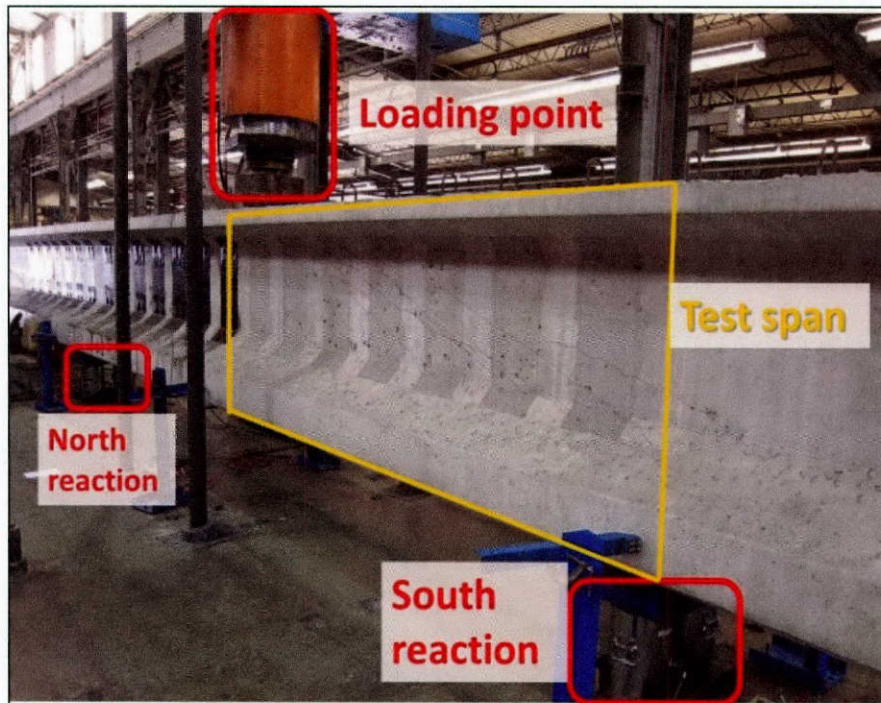


Figure 4-7: View of test setup showing load cells and hydraulic ram

In the case of Control-18, Uni-18R, Uni-8, and Bi-18, an additional ram was used to eliminate the negative moment that was produced by the self-weight of the cantilevered portion of the beam. The self-weight of the overhang was calculated and an appropriately scaled load was applied through an additional ram to produce zero moment at the north reaction.

4.3 TEST RESULTS

4.3.1 Overview of the Test Results

Four tests, including a control test, were conducted on the first I-beam section while two tests were conducted on the other section. A summary of the test results are displayed in Table 4-3. Unfortunately, the ultimate shear capacity could not be obtained for at least half of the tests due to tendon anchorage failures at the cut-end of the sections where transverse confinement was not provided. The anchorage failures occurred before the CFRP strips fractured. Figure 4-8 shows the premature anchorage failure of Uni-12. The failure propagated outside of the test span causing a reduction in flexural capacity of the beam and failure before the shear capacity was reached (Figure 4-8(b)).

The cut end of the second 50-ft. I-beam section was strengthened with three anchored CFRP strips and two steel beams to help confine the end region and prevent the bond cracks from propagating (Figure 4-9). Unfortunately, the failure could not be prevented with the CFRP strips and the external clamp. Figure 4-10 and Figure 4-11 show the condition of each test span after the failure load was reached. Considering the shear crack that extended into the anchorage zone of Bi-18, it is likely bond problems related to the tendons reduced the failure load.

The beams' inability to fracture the CFRP strips did not render the test data unusable. Insight into the behavior of different layouts may be obtained by comparing the strain distributions in the webs prior to failure.

Table 4-3: Summary of the test results

Nomenclature	Applied Load (kips)	Shear Force (kips)	Ratio of Shear/Control	Failure Mode
Control-18	700	377	-	Shear
Uni-18R	774	417	1.11	Shear
Uni-12	648	349	-	Bond
Uni-8	610	328	-	Bond
Bi-18	781	420	1.12	Shear
Bi-12	553	298	-	Bond



(a) Reaction end of beam
(Cut at mid-section of 100-ft. beam)

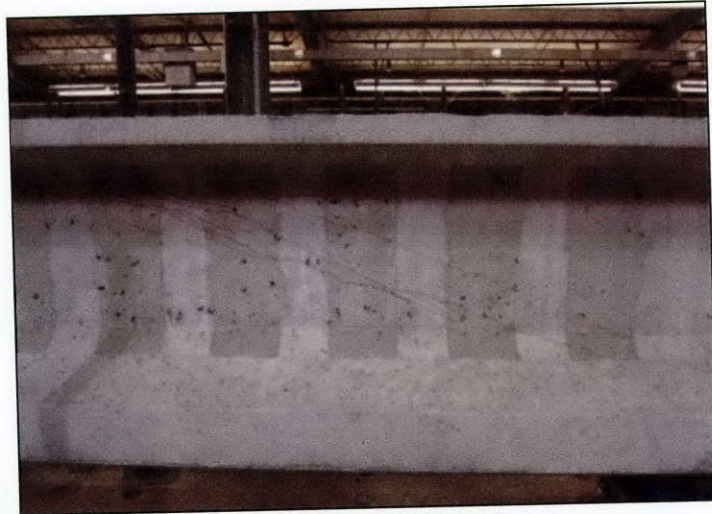


(b) Propagation of bond cracks from cut end

Figure 4-8: Anchorage failure of the tendons



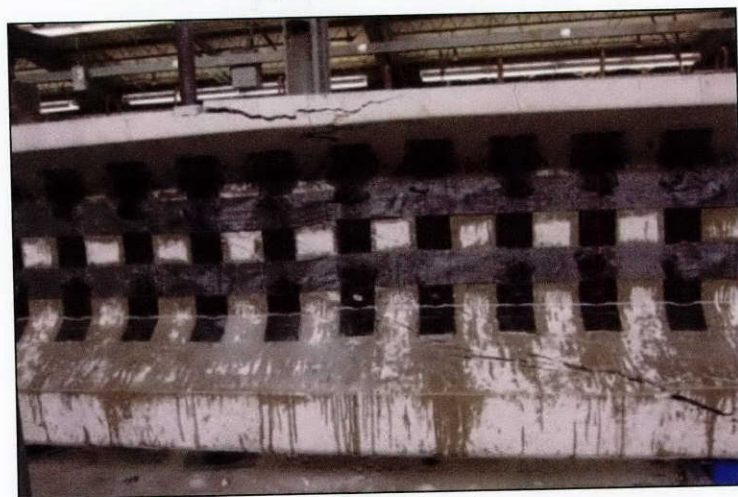
Figure 4-9: Strengthening of the cut end



(a) Control-18 (shear)

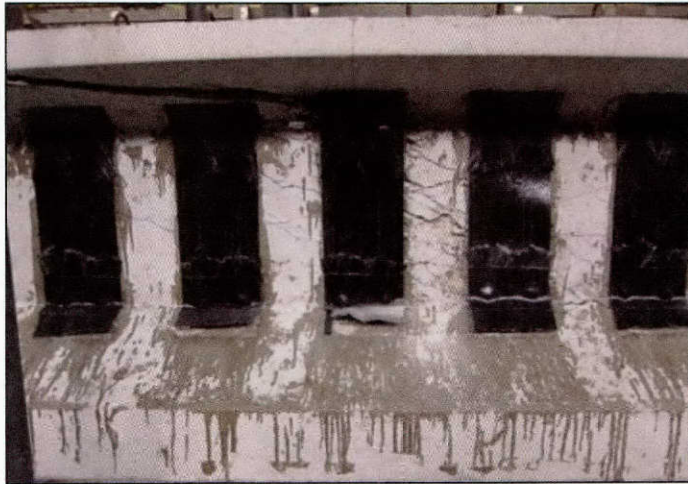


(b) Uni-18R (shear)



(c) Bi-18 (shear)

Figure 4-10: Appearance of test span after shear failure



(a) Uni-12 (bond)



(b) Uni-8 (bond)



(c) Bi-12 (bond)

Figure 4-11: Appearance of test span after bond failure

4.3.2 Effect of CFRP Layout

The size, shape, and location of a shear crack tend to change depending on the amount of transverse reinforcement (steel and/or CFRP). Therefore, a consistent method for comparing the test results had to be established. Since an optical measurement system was used to monitor the I-beam surface displacements, an average shear strain across the web could easily be calculated using Equation 4-1. However, the gage length of the horizontal (ϵ_x) and vertical (ϵ_y) strains had to be the same between all of the tests to be able to compare the results appropriately. Figure 4-12 shows the relative gage length of the strains used for the shear strain measurements, as well as the assumed strain rosette's orientation.

$$\gamma = \frac{\epsilon_\theta - (\epsilon_x \cos^2 \theta + \epsilon_y \sin^2 \theta)}{\cos \theta \sin \theta} \quad \text{Equation 4-1}$$

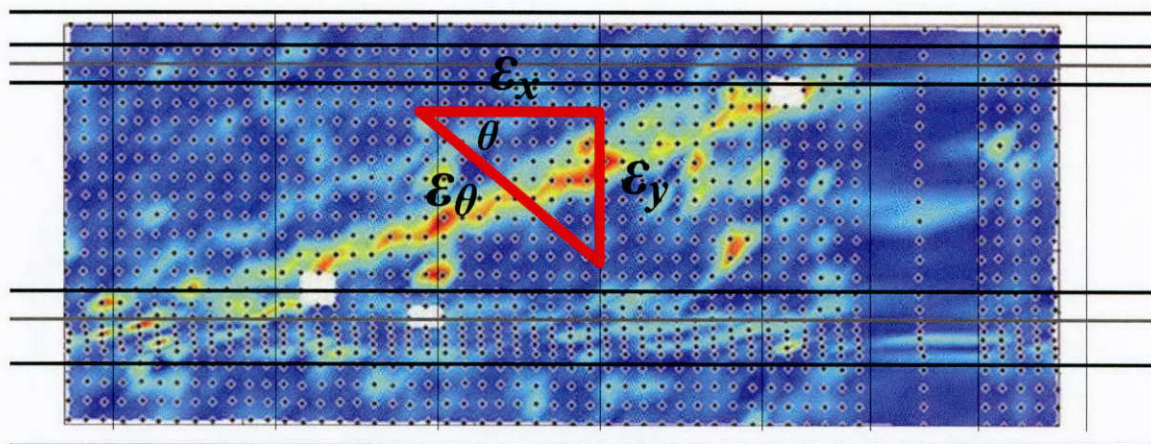


Figure 4-12: Shear strain calculation

The shear strain responses for the I-beams that failed in shear are displayed in Figure 4-13. Control-18 had a cracking shear load of 176-kips and an ultimate shear capacity of 377-kips, which is noted in Figure 4-13 by a dashed blue line. Since Control-18 was rehabilitated with a uni-directional layout there was no cracking load for Uni-18R. The application of the uni-directional layout to the pre-cracked beam resulted in approximately an 11% increase in the shear capacity. Uni-18R reached a higher peak shear load compared to Control-18 as expected but at a lower initial stiffness due to the pre-existing shear cracks.

As previously mentioned, Bi-18 was strengthened using approximately the same area of CFRP material as Uni-18R. The bi-directional layout was able to increase the cracking load 16% to 204-kips compared to Control-18. The ultimate shear capacity of Bi-18 was nearly the same as Uni-18R. A higher load was expected but it is likely that the concrete bond failure adversely limited the shear load that could be applied to Bi-18.

However, it should be noted that the bi-directional layout exhibited significantly lower shear strains compared to the uni-directional layout. Shear deformations of the bi-directional layout were better controlled than with the uni-directional layout.

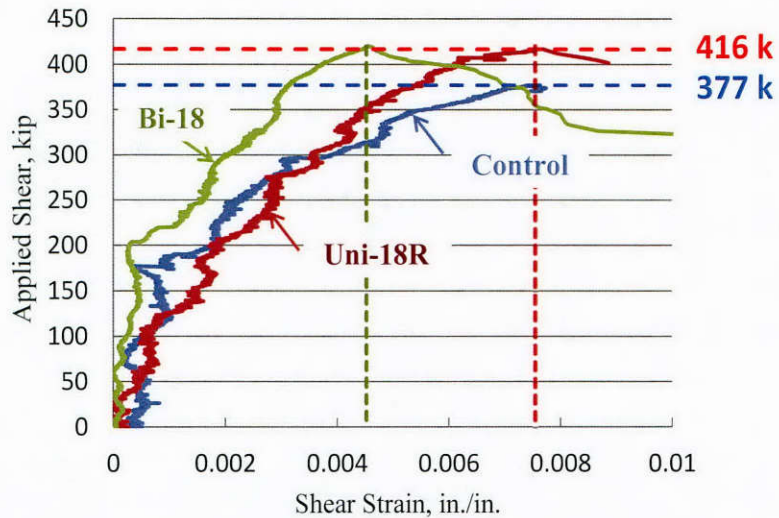
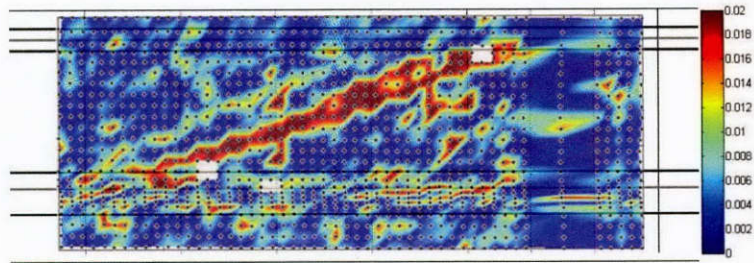


Figure 4-13: Shear strain response of I-beams with different CFRP layouts

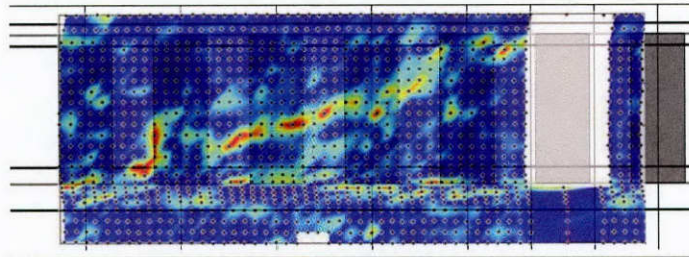
Figure 4-14 shows the tensile principal strain contours for three tests that failed in shear plotted at the failure load of Control-18. The reduction in the principal strains between the three tests indicates that the CFRP layouts were efficient in distributing the shear cracks and controlling the crack widths.

In Control-18, nearly all of the shear deformation was concentrated at a single shear crack, which eventually caused the shear failure. Uni-18R had the same crack distribution as Control-18. The principal tensile strains were reduced, as well as the crack widths. While the uni-directional CFRP strips did not fracture, the measured maximum strain in the strips was close to the CFRP fracture strain [0.01-in./in.]. Bi-18 had smaller but more distributed shear cracks compare to Control-18 and Uni-18R. All of the critical shear cracks were found to have angles ranging between 40 and 45-degrees.

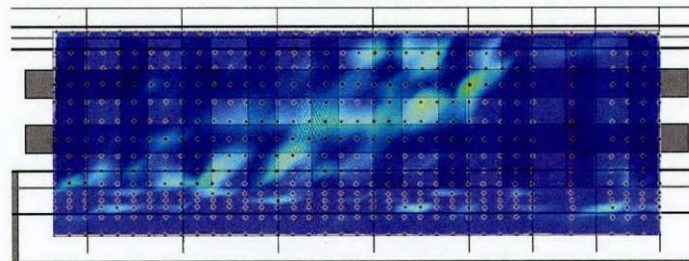
Principal tensile strain contours were also plotted at 416-kips to amplify the differences between the uni- and bi-directional layouts (Figure 4-15). Again, the strains measured for Bi-18 were significantly lower than Uni-18R when the ultimate shear capacity was reached.



(a) Control-18

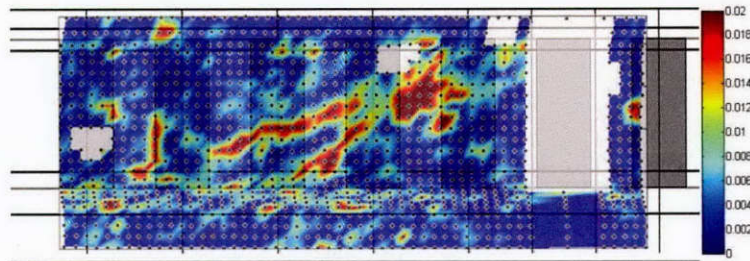


(b) Uni-18R

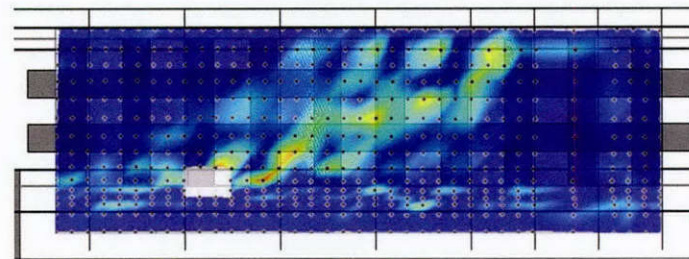


(c) Bi-18

Figure 4-14: Principal tensile strain contours for an applied shear of 377-kips



(a) Uni-18R



(b) Bi-18

Figure 4-15: Principal tensile strain contours for an applied shear of 416-kips

Figure 4-16 represents the concrete, steel, and CFRP shear contributions for the strengthened beams. The red curve is the shear contribution of the CFRP. Since Uni-18R was previously cracked, the transverse reinforcement and the CFRP began to contribute to the shear

resistance immediately. However, for Bi-18, there was a delay in the steel and CFRP contributions until the shear crack formed. Even though the CFRP layouts were different, Uni-18R and Bi-18 had similar CFRP strip contributions at a shear equal to 416-kips.

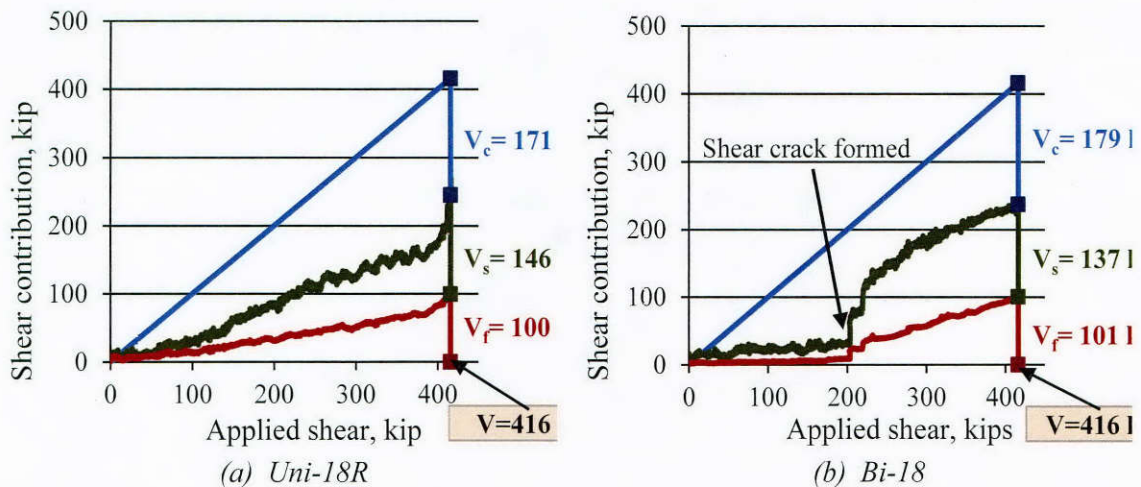


Figure 4-16: Shear contribution of CFRP, steel, and concrete (Uni-18R and Bi-18)

4.4 CONCLUSIONS

- A higher cracking load was obtained using the bi-directional CFRP layout compared to the control test.
- The bi-directional CFRP layout provided better crack control, indicated by the lower and more uniformly distributed tensile principal strains, relative to the comparable uni-directional CFRP layout.
- It was not possible to compare peak shear capacities for the uni- and bi-directional layouts because the tendon anchorage failures controlled the capacity of the specimens.

4.5 SUMMARY COMMENTS

Unfortunately, the behavior of strengthening I-beams with CFRP could not be clearly established due to unexpected anchorage failures. However, it was found that the Tx46 shape is not an ideal section for CFRP shear strengthening. The two reentrant corners between the web and the flanges make anchoring the CFRP strips difficult (see Figure 4-2 and Figure 4-3). Each reentrant corner, or abrupt change in the beam's geometry, requires the use of CFRP anchor(s) to prevent the CFRP strip from pulling away from the beam's surface. Therefore, if a U-wrap CFRP layout is used additional CFRP anchors would be required; thus complicating the installation process. Moreover, the beam's constant thickness web height is relatively short, which poses detailing and efficiency problems for bi-directional layouts.

Only considering the three tests that exhibited shear failures, the uni-directional layout resulted in an 11% increase in strength, which is similar to the bi-directional layout (12%). The increase in strength of the uni-directional layout was similar to the increases observed in Project 0-6306. A larger increase in the bi-directional layout's shear strength was expected but the Tx46 short web depth and the influence of anchorage problems at the cut end resulted in a reduction of the capacity and modes of failure not related to shear.

Chapter 5. Pile Cap Girder Tests

5.1 OVERVIEW AND OBJECTIVE

Task 1d was originally intended to demonstrate the viability of strengthening full-scale prestressed U-beams using bi-directional CFRP strips and CFRP anchors. However, the Project Panel decided that shear distress in U-beams had not been observed in the field. Conversely, shear distress (in the form of shear cracks) were observed in a number of pile cap girders (Figure 5-1). As a result, the Project Panel suggested that the U-beam test program be redirected to investigate the shear strengthening of large-scale pile cap girders.

The main objective of the pile cap girder test program was to determine the feasibility of strengthening wide-webbed reinforced concrete members for shear. Pile cap girders are bridge elements that support the superstructure of a reinforced or prestressed concrete bridge. In certain locations, pile cap girders can be fully wrapped with CFRP strips; whereas in other locations, where the pile cap girders support the bridge beams, a U-wrap CFRP scheme that utilizes CFRP anchors would be required.



Figure 5-1: Shear crack in pile cap girder

5.2 EXPERIMENTAL PROGRAM

5.2.1 Test Specimens

After reviewing TxDOT plans for typical pile cap girders, it was observed that pile cap girders are nearly as wide as they are deep, have minimal transverse reinforcement, have short shear spans, and produce both positive and negative moments, which results in double curvature loading. However, since pile cap girder web widths were significantly larger than any members previously tested, it was decided to conduct a simple span (single curvature) test on one of the girders. The intent of testing one girder in single curvature was to provide a means of relating the pile cap girder results with the T-beam and I-beam tests. The remaining pile cap tests were subjected to anti-

symmetrical double curvature loading to determine if the direction of the moment would adversely affect the member's behavior- especially the performance of CFRP anchors.

The pile cap girder geometry was designed to test as large a specimen as possible within the constraints of the facilities at Ferguson Structural Engineering Laboratory. As a result, a cross-sectional dimension of 32-in. by 32-in. and a total length of 27'-8" was selected.

Standard ASTM A615 reinforcing steel was used for both the transverse and longitudinal reinforcement. The transverse reinforcement consisted of Grade 60 No.5 reinforcing bars spaced at 18-in. on center. The measured yield strength of the transverse reinforcement was 60.6-ksi. The size of the transverse reinforcement was selected based on TxDOT drawings, which followed A.A.S.H.O 1957 specifications, while the spacing was selected to meet current minimum transverse reinforcement requirements (AASHTO, 2014). The flexural reinforcement consisted of Grade 75 No.11 longitudinal reinforcing bars. The strength and layout of the No.11 reinforcing bars was selected so that the flexural strength would exceed the shear capacity of the strengthened girders and would not yield at peak shear capacity. The layout of the flexural reinforcement resulted in similar longitudinal strains between the single and double curvature specimens when the peak shear capacities were reached. Furthermore, the anti-symmetrical double curvature loading required that the amount of longitudinal tension and compression reinforcement be equal for the double curvature specimens, whereas the amount of compression reinforcement placed in the single curvature specimen was selected so that the compression zone would not prematurely crush. A 2-in. concrete clear cover was provided for all specimens.

Figure 5-2 illustrates the longitudinal reinforcement layout, while Figure 5-3 illustrates the transverse reinforcement and loading points for the single and double curvature girders. Mid-way through the test matrix, the double curvature's bundled longitudinal reinforcement was shifted inward to the red reinforcing bar locations, shown in Figure 5-2 (b), due to unexpected bond demand issues.

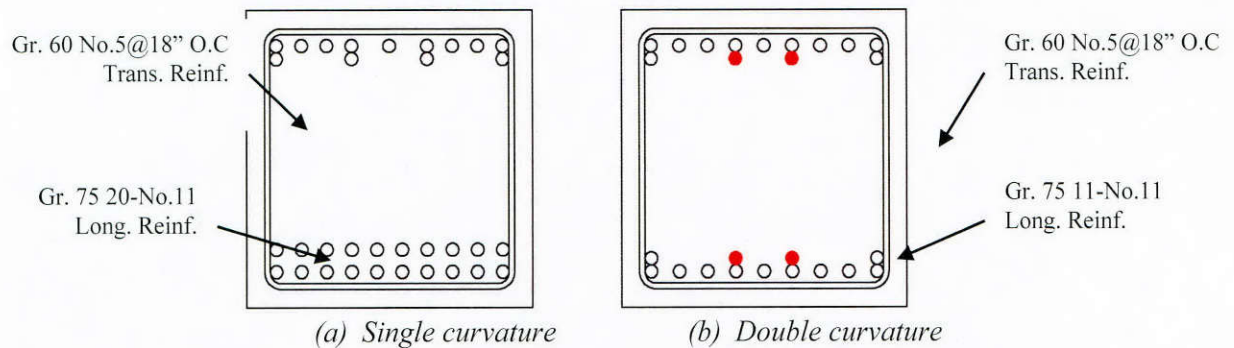


Figure 5-2: Longitudinal reinforcement

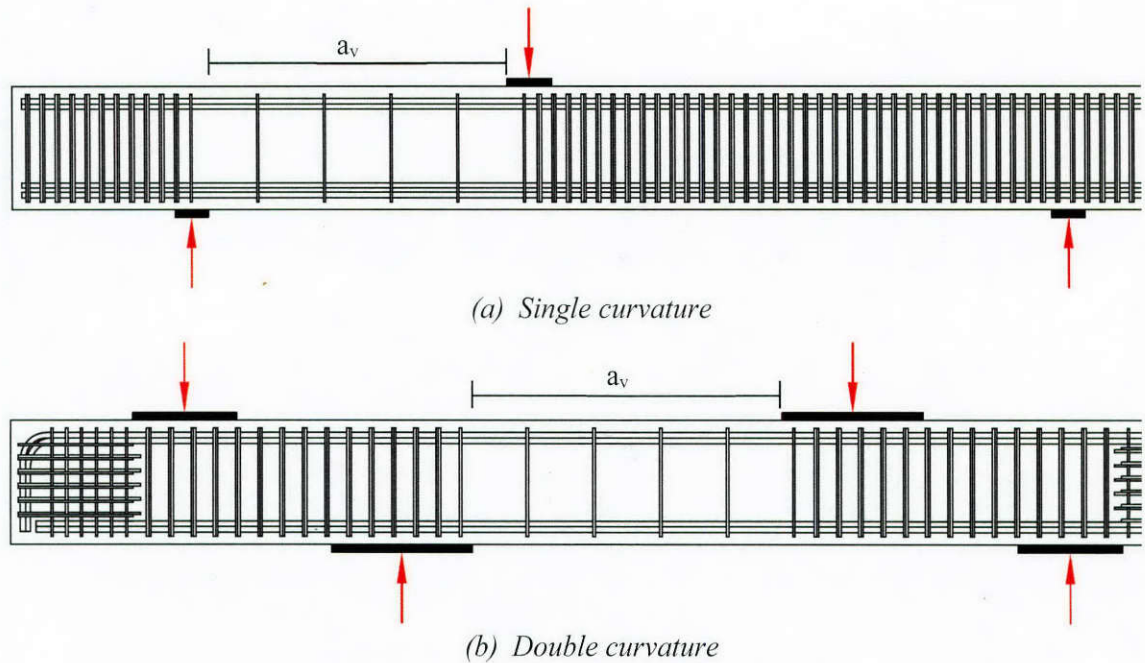


Figure 5-3: Transverse reinforcement

The shear span in the test region, a_v , was determined by ensuring that the span-to-depth (a_v/d) ratio equaled three. A span-to-depth ratio of three indicates that the girder should exhibit sectional shear behavior (AASHTO, 2014). The shear span for these girders was defined as the clear distance between the loading and reaction plates where a constant shear acts. Had the shear span been defined as the distance between the center of the applied load to the face of the reaction, as AASHTO (2014) specifies, the span-to-depth ratio of the single curvature specimen would change to 3.2 whereas the span-to-depth ratio of the double curvature specimen would change to 3.7 due to the large reaction plate. Moreover, the span-to-depth ratio for a concrete member loaded in double curvature is implied to be halved due to the existence of a point of inflection between the negative and positive moments (ACI, 2014). However, this definition would indicate that the girder should have behaved like a deep beam rather than a sectional beam. However, such behavior was not observed.

The constant shear span in the test region was 80.75-in. for the single curvature specimen and 83.5-in. for the double curvature specimens. The slight differences in the constant shear span between the two reinforcement layouts stemmed from minor differences in the member's effective depth (d). Specifically, the single curvature specimen had an effective depth equal to 27-in., whereas, the double curvature specimen had an effective depth equal to 28-in.

A typical 28-day concrete compressive strength for a pile cap girder of 4,500 psi was specified. A ready mix concrete supplier provided a concrete mixture with the following characteristics:

- 4-3/4 Sacks of Portland Cement
- 25% Fly Ash Class F
- 1-in. Maximum Aggregate Size, Crushed Limestone
- 8-in. Slump

The congestion within the pile cap girder reinforcement cages required the use of a superplasticizer, as well as, a retarder to increase the concrete mixture's slump, workability, and to delay the concrete initial set time. The test day concrete strength of the pile cap girders ranged from 4,400 to 5,100 psi.

5.2.2 Test Variables

The pile cap girder tests were proposed to evaluate the effectiveness of strengthening wide-web reinforced concrete members in shear using CFRP strips and anchors. Moreover, the loading conditions were chosen to reflect in-situ conditions, which could result in anchors being placed in flexural tension zones. Therefore, a test matrix was derived that addressed the following topics:

- Effects of loading conditions
- Efficiency of retrofitting uncracked and cracked sections
- Placing CFRP anchors in known flexural tension regions
- Efficiency of CFRP anchors relative to fully wrapped systems
- Effectiveness of fully wrapped and anchored uni- and bi-directional layouts

Figure 5-4 illustrates the resulting test matrix. As previously mentioned, two test configurations were used: single and double curvature. The target test day concrete strength and transverse reinforcement layouts were identical for all of the girders. Six girders were constructed resulting in nine shear tests (including the control shear capacity tests). The girders that provided the control shear capacities were rehabilitated using anchored and fully wrapped uni-directional CFRP layouts.

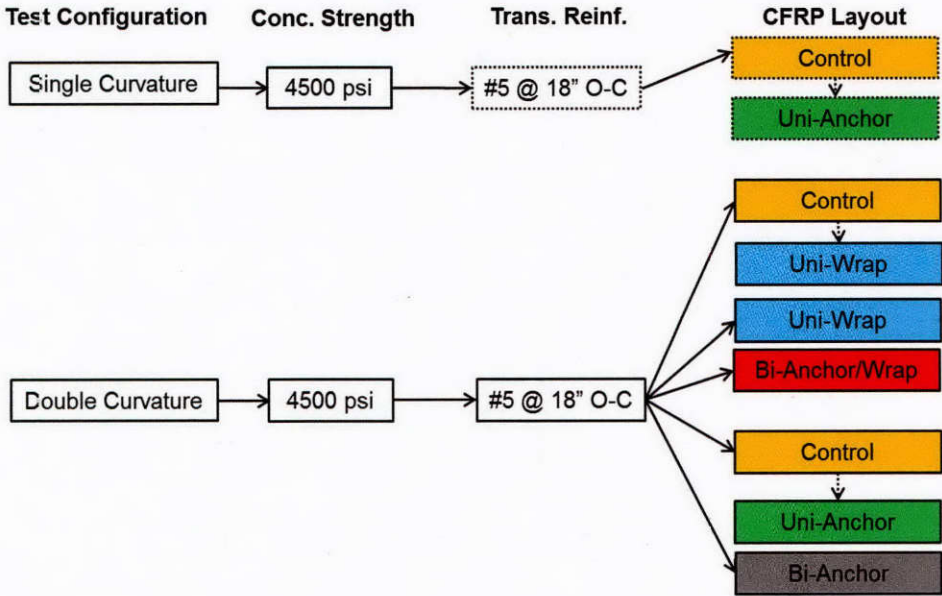


Figure 5-4: Experimental test matrix

A nomenclature system was developed to help quickly identify each test based on various defining parameters. A graphical representation of the nomenclature can be seen in Figure 5-5. The first designator indicates how the girder was tested. The second designator indicates if the girder was previously tested and thus pre-cracked. The third and fourth group of designators indicates whether vertical or horizontal strips existed and if so, how the CFRP strips were configured so that their fracture strength could be utilized. Table 5-1 provides the nomenclature and a short description for each test.

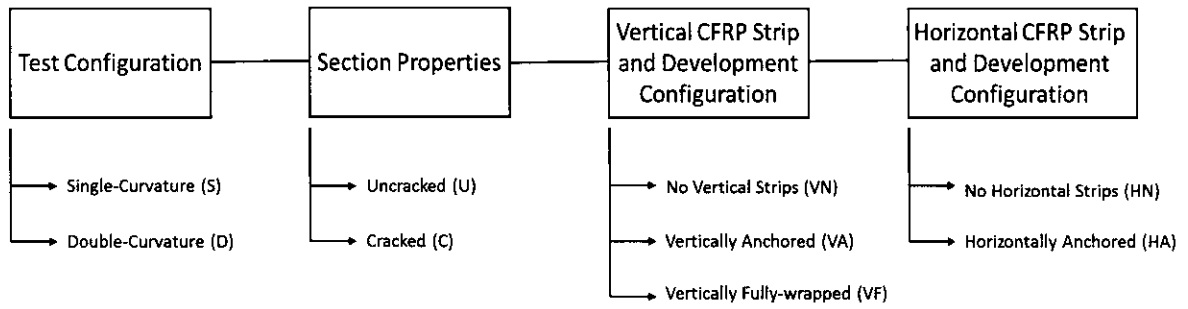
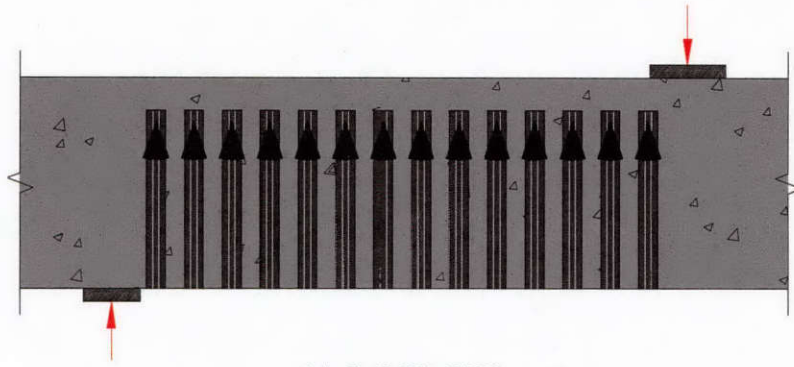


Figure 5-5: Test nomenclature

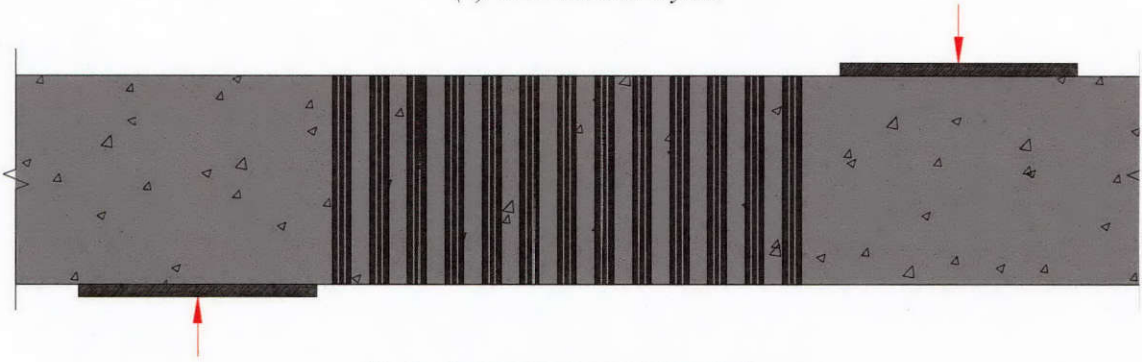
Table 5-4: Nomenclature description

Nomenclature	Description
S-U-VN-HN	Control
S-C-VA-HN	Anchored Uni-directional, Cracked
D-U-VN-HN	Control
D-C-VF-HN	Fully Wrapped Uni-directional, Cracked
D-U-VF-HN	Fully Wrapped Uni-directional, Uncracked
D-U-VF-HA	Fully Wrapped Vertically and Anchored Horizontally, Uncracked
D-U-VN-HN*	Redundant Control
D-C-VA-HN	Anchored Uni-directional, Cracked
D-U-VA-HA	Anchored Bi-directional, Uncracked

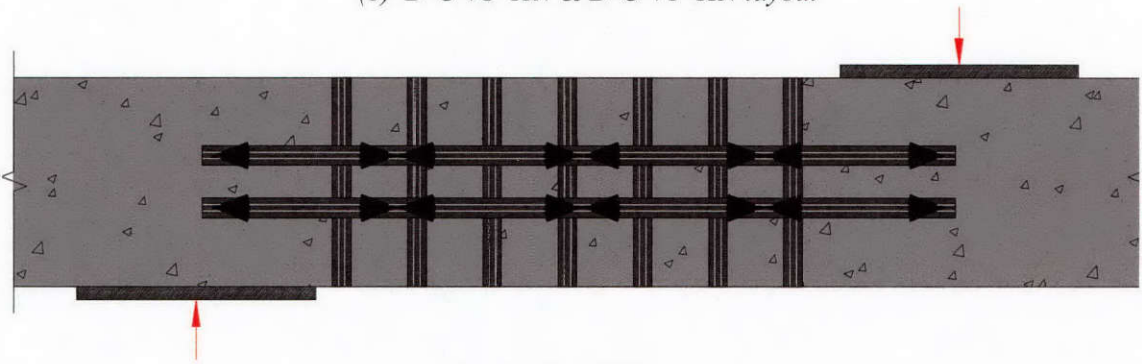
* indicates redundant tests



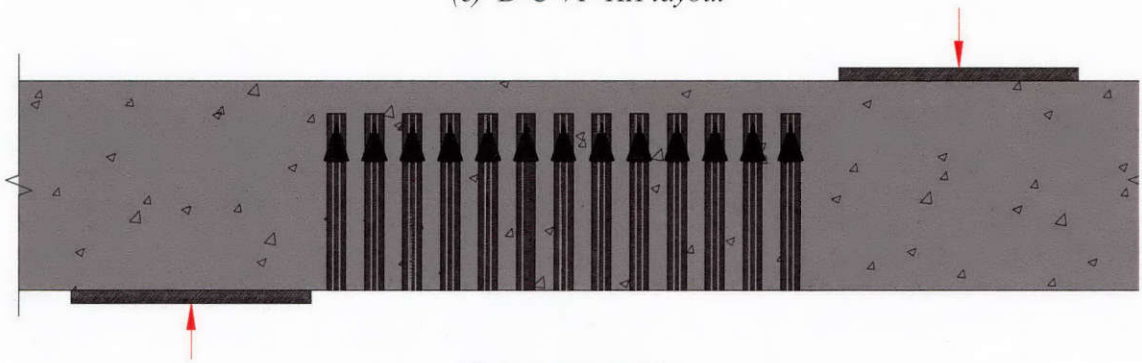
(a) *S-C-VA-HN layout*



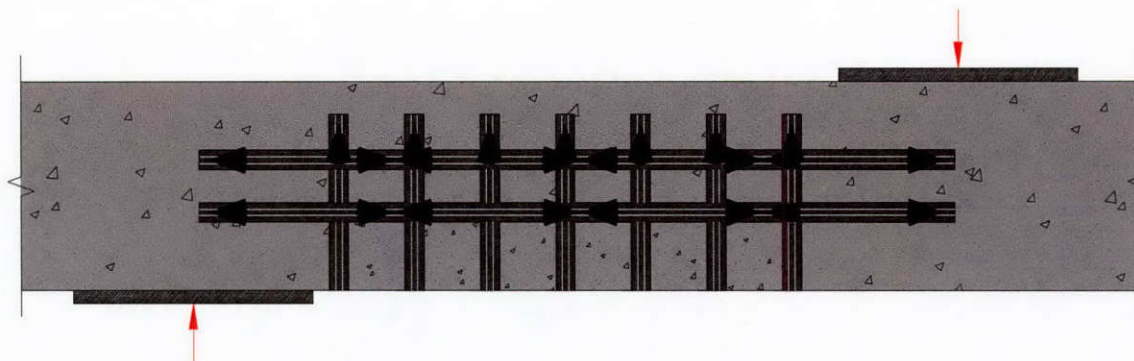
(b) *D-C-VF-HN & D-U-VF-HN layout*



(c) *D-U-VF-HA layout*



(d) *D-C-VA-HN layout*



(e) D-U-VA-HA layout

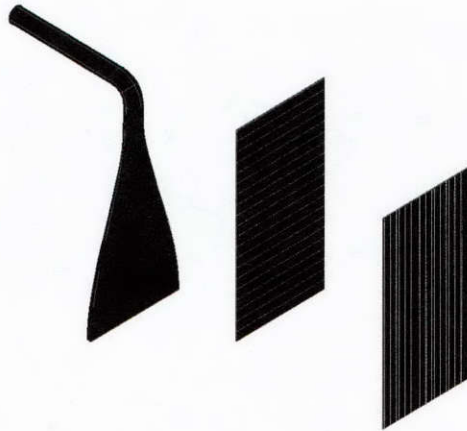
Figure 5-6: Various CFRP strip layouts

Prior to the installation of the CFRP strips, the concrete surface was lightly cleaned with a grinding wheel, thus exposing the aggregate. All corners were rounded to a minimum bend radius of 1/2-in. to avoid stress concentrations in the CFRP strips. All of the CFRP strips had a nominal 3-in. width and 0.02-in. laminate thickness. The various CFRP layouts that were used are illustrated in Figure 5-6.

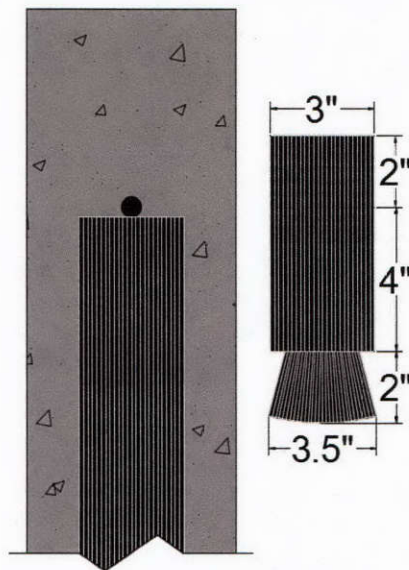
The vertical strips ranged in length from 45 to 73-in. The strip lengths were sized so that each CFRP strip location would be comprised of two individual CFRP strips spliced together. Anchored U-wrap layouts were spliced only on the bottom of the girder, whereas, fully wrapped layouts were spliced on the bottom and top of the girder. All splices had at least an 8-in. overlap length. Splicing the CFRP strips simplified the installation process. The vertical strips were spaced at 6-in. on center (measured from center to center of the strips) and positioned so some of the CFRP strips would overlie the transverse reinforcement in the test span.

For the bi-directional layouts only, half of the vertical CFRP area used in the uni-directional layout was installed and half was placed in the horizontal direction so that an assumed 45-degree shear crack would cross nearly the same area of CFRP material as the uni-directional layout. Since half of the vertical strips were removed, the CFRP strips overlie only half of the transverse reinforcement within the test span. The vertical CFRP was installed one day prior to the installation of the horizontal CFRP to simplify the placement of each direction.

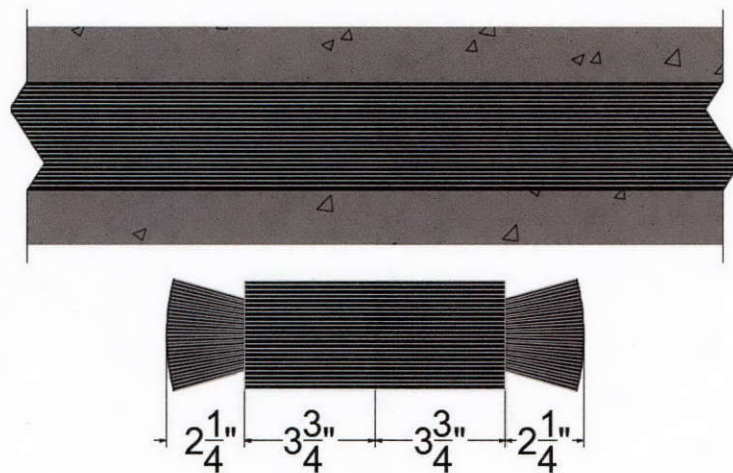
The horizontal CFRP strips were 120-in. long, spaced 8-in. on center, and were equidistant from the top and bottom of the girder ($>d/4$). Thus, the strips were concentrated around the center of the girder within a $d/2$ distance where the shear crack widths tend to be greatest. The horizontal strips were extended and anchored within the peak moment regions for the double curvature tests.



(a) Typical anchor installation at end of strip



(b) Vertical CFRP strip and boundary anchor detail



(c) Continuous horizontal CFRP strip and intermediate anchor detail

Figure 5-7: CFRP anchor details

Figure 5-7 depicts the CFRP anchor details. The CFRP anchors that were used on the pile cap girders were purchased from the CFRP supplier. The 1/2-in. diameter anchors that were used at the ends of the CFRP strips provided an anchor-to-strip ratio of 2.9. Three equidistant intermediate anchors (spaced approximately d away from each other) were installed on each horizontal strip as a means of minimizing the strip elongation and reducing shear crack widths. The intermediate horizontal strip anchors had a 5/8-in. diameter and provided an anchor-to-strip ratio equal to 2.4 after the anchors had been divided into two fans that were splayed in opposing directions over the strip. The intermediate anchors were placed through a continuous horizontal CFRP strip (Figure 5-7(c)). However, the modified detail in Figure 5-7(b) could have used. All anchors were 10-in. long with an embedment of 4-in. into the concrete.

The vertical strip anchors were positioned slightly below the upper longitudinal steel. The 4-in. deep anchor holes were 9/16-in. and 3/4-in. diameter for the 1/2-in. and 5/8-in. diameter anchors, respectively. The depth of the hole was selected so that 2-in. of the anchor penetrated into the concrete core. In all of the pre-cracked girders, at least a few anchor holes, and thus anchors, were drilled through shear or bond cracks. All of the anchor holes were rounded to a minimum radius of a 1/2-in. so that the anchor bend would not fracture the anchor before the strip strength was developed.

A modified anchor detail was utilized for the anchors on the boundary of the CFRP layouts. In the modified detail, the CFRP strips were stopped short of the anchor holes rather than extending beyond, which causes holes to be covered. This detail greatly accelerated the installation process since the anchor holes were easily found and the anchors did not need to pass through the CFRP strips. Not only can the modified detail speed up the installation process, but it can also affect the way CFRP layouts are installed. For instance, in specimen D-U-VA-HA, the anchors for the vertical CFRP strips were installed at the same time as the horizontal strips and anchors, one day after the vertical CFRP strips were installed. Hence, the modified detail allows for the installation of the CFRP anchors after the CFRP strips have partially cured.

All of the anchors were designed to overlap the CFRP strips a minimum of 6-in. After the anchors were installed, two patches were laid over the anchors in a perpendicular and parallel fiber direction. The patches on the boundary anchors were 3-in. wide and extended 4-in. over the anchor and 2-in. beyond the center of the anchor hole. The intermediate patches were 7.5-in. long by 3-in. wide and were centered over the anchor.

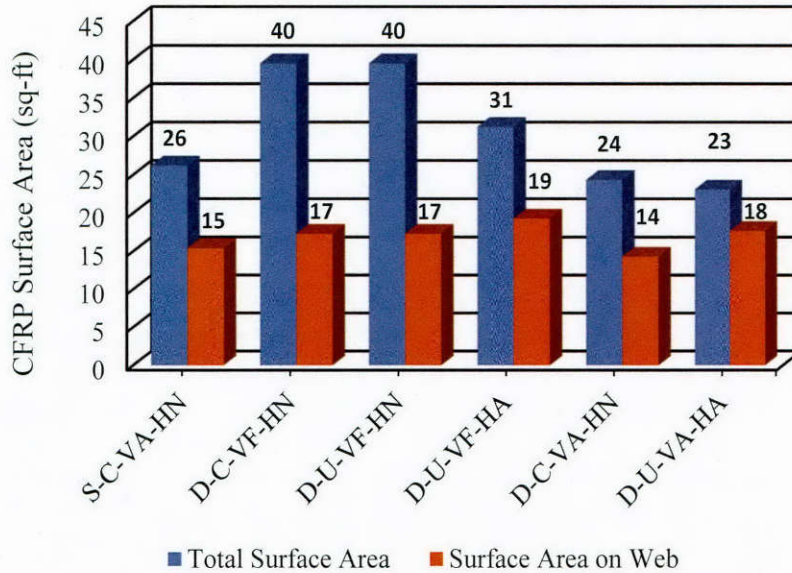


Figure 5-8: CFRP surface area comparison

Unlike the I-beam tests, the total area of CFRP material used in each test could not be held constant. Girders that utilized fully wrapped CFRP strips will naturally require more CFRP material compared to anchored systems. However, Figure 5-8 indicates that the area of CFRP material on the girder webs was nearly the same for all of the tests.

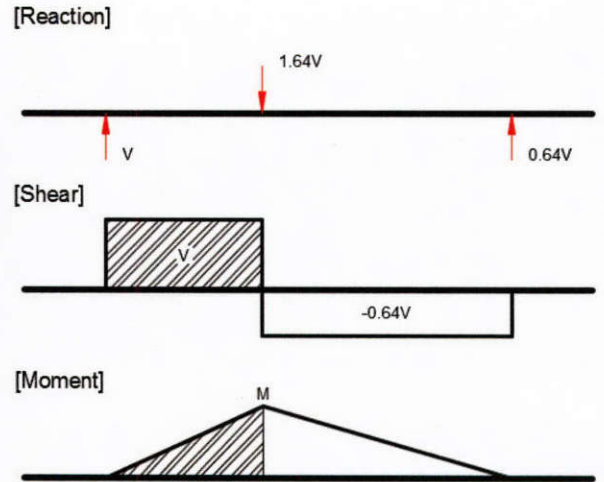
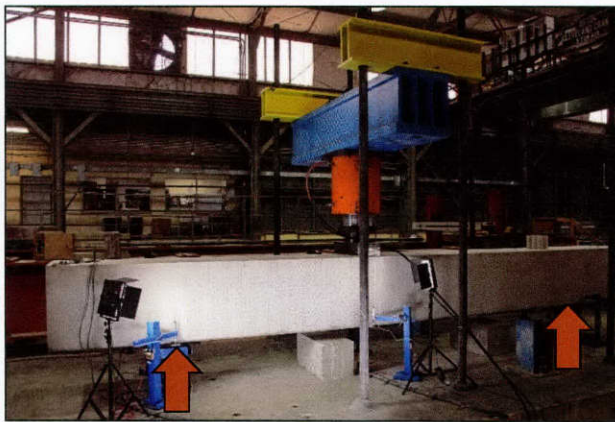
5.2.3 Test Setup

As previously mentioned, the pile cap girders were tested under two different types of loading conditions: single and double curvature. While the two test setups produced different shear and moment conditions, the components that comprised both setups were similar. For instance, both setups utilized load cells with various capacities to directly measure the applied shear force, loading frame(s), ram(s), spherical head(s), linear potentiometers, strain gages, and a high resolution optical measurement system to measure full-field displacements and strains.

5.2.3.1 Single Curvature

Shear tests are typically conducted using single curvature, or simple span, test setups. The single curvature test setup that was utilized is shown in Figure 5-9 (a). The corresponding shear and moment diagrams can be seen in Figure 5-9 (b). The hatched lines indicate the test span.

Two reaction points supported the pile cap girder. Each reaction point was comprised of two 1000-kip capacity load cells, a loading plate, and a typical 9-in. long by 21-in. wide by 3-in. thick elastomeric bearing pad (Figure 5-10). A ram with a 2000-kip capacity applied the load to a spherical head by reacting against the loading frame and consequently the anchored 3.5-in. diameter rods. The intent of the spherical head was to accommodate any differential rotation between the ram and the girder. A 12-in. long by 28-in. wide loading plate was placed between the spherical head and the girder to help distribute the applied forces so that local concrete crushing would not occur (Figure 5-11). The shear demand on the girder was directly measured by the reaction at the end of the test span.



(a)

(b)

Figure 5-9: Single curvature test setup and statics



Figure 5-10: Reaction in the test region (2-1000 kip load cells)

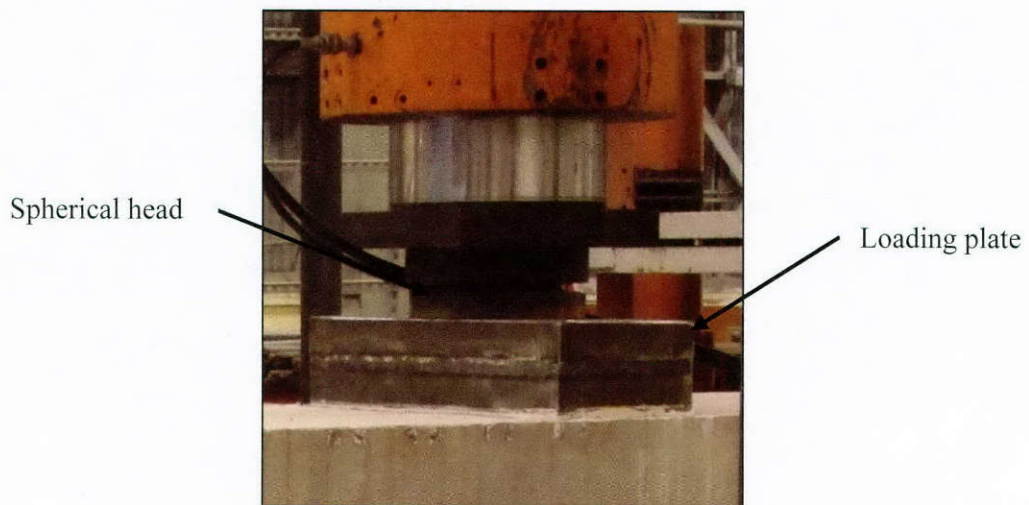


Figure 5-11: Applied load

The displacements at the reactions and under the point load were monitored by linear potentiometers. Conversely, strains within the transverse and longitudinal reinforcement were

monitored using strain gages. The concrete's surface displacements and strains were monitored at discrete locations using the aforementioned optical measurement system.

5.2.3.2 Double Curvature

The double curvature test setup load application was similar to the single curvature test setup. However, the double curvature setup has one additional loading point as seen in Figure 5-12 (a). The fundamental difference between the two test setups is that the double curvature setup produced equal positive and negative moments. To achieve this type of moment distribution, one of the rams had to apply twice as much load as the other, causing one of the reactions to carry twice as much load as the other. The resulting reaction and moment diagrams will be anti-symmetrical while the shear force diagram is symmetrical. The aforementioned diagrams are depicted in Figure 5-12 (b). Again, the hatched lines indicate the test span.

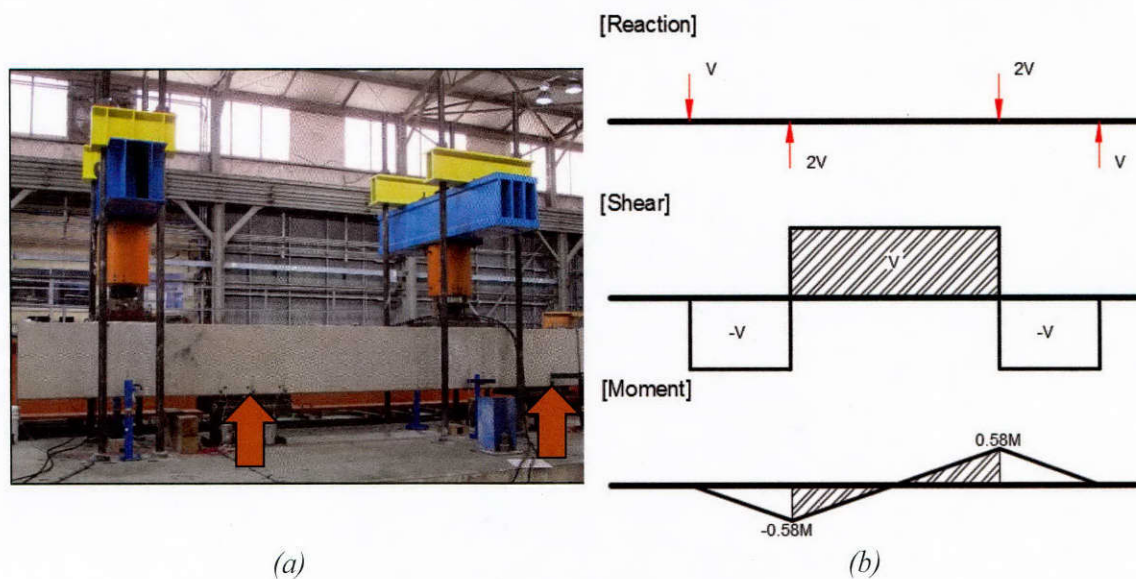


Figure 5-12: Double curvature test setup and statics

The load ratio between the rams was attained by using a load maintainer. Unfortunately, the load maintainer did not consistently produce a load ratio exactly equal to two throughout the test. Therefore, the shear in the test span needed to be calculated as the larger reaction minus the load applied by the smaller ram. A flat load cell was placed under the ram that applied the smaller load to facilitate this calculation (Figure 5-13).

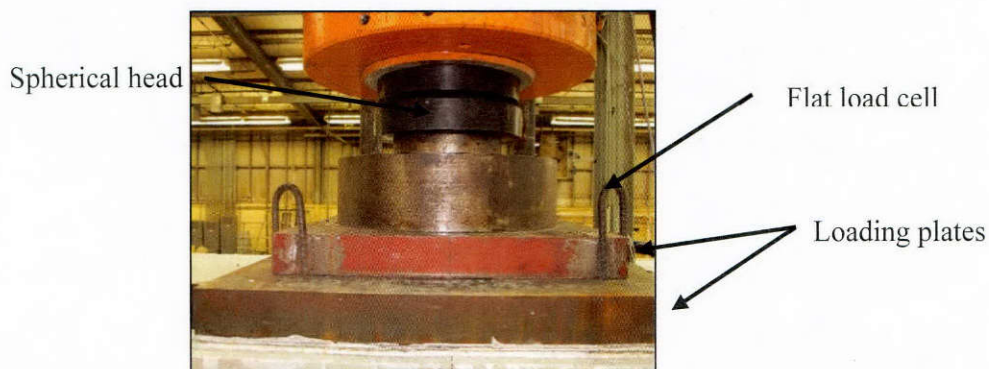
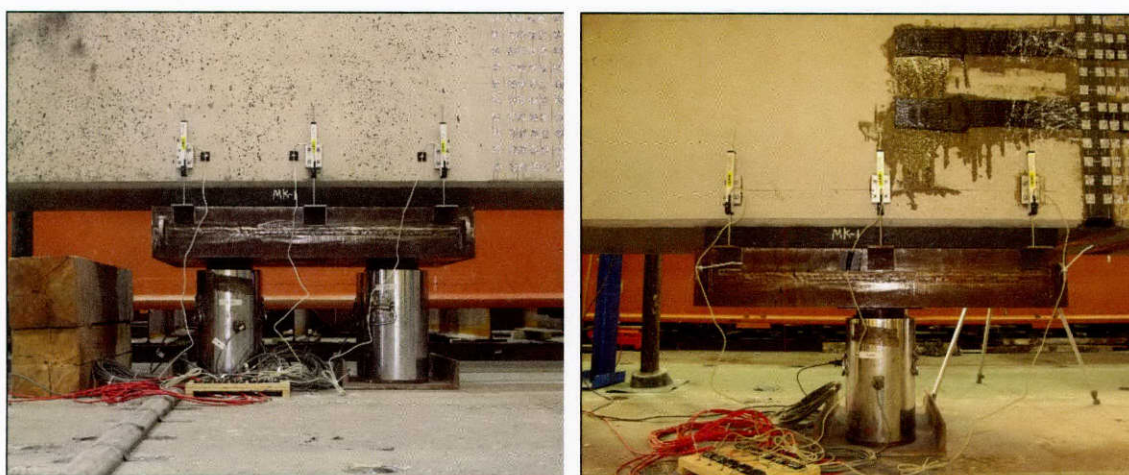


Figure 5-13: Small applied load

Between each ram and reaction point (outside of the test span) are two short spans that had span-to-depth ratios less than 1.5 and had higher shear capacities than the test span. It was imperative that the shorter spans did not fail or exhibit significant inelastic deformations before the test span reached its capacity. Therefore, large loading and reaction plates were used to prevent concrete crushing at the critical locations. At the high load point, a 38-in. long by 32-in. wide steel loading plate was used and at the other load point a 28-in. long by 30-in. wide loading plate was used. The girder was then supported on a 38-in. by 31-in. by 2.1-in. elastomeric bearing pad at the larger reaction and 28-in. by 30-in. by 2.1-in. bearing pad at the smaller reaction. While these plates and bearing sizes were large, they represented dimensions comparable to a prestressed I-beam that rests on top of a cap girder and a reaction column that frames into a cap girder.

The large reaction was originally designed using four 1000-kip load cells. Any differential rotation between the girder and the underlying reaction plate was assumed to be accommodated by the elastomeric bearing pad. However, the bearing pad could not overcome girder rotations; resulting in the centroid of the reaction force to shift. The reaction was modified by removing one set of load cells. The remaining load cells had rounded ends that allowed rotation of the plates and accommodated the girder rotation. Changing the support configuration did not affect the shear capacity of the girders. Figure 5-14 shows the original and modified support conditions.

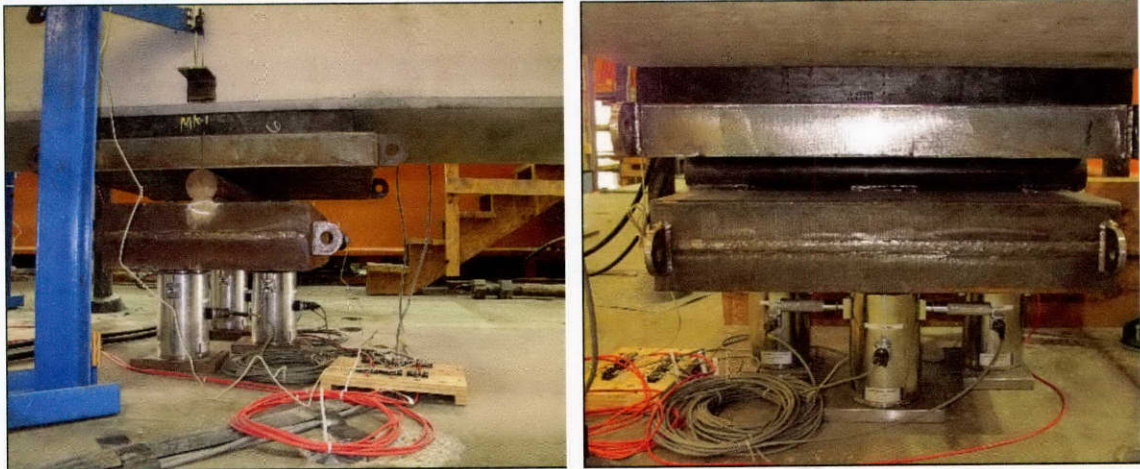


(a) Original 4 load cell reaction

(b) Modified 2 load cell reaction

Figure 5-14: Large reaction

The smaller reaction utilized a 3-in. diameter steel roller that was welded to a 6-in. thick loading plate. A second loading plate was placed above the welded roller and was free to rotate. A bearing pad was placed between the second loading plate and the girder. The reaction was supported by three 500-kip load cells placed in a triangular formation. The bearing pad accommodated for any lateral displacement induced by flexural deformation. The resulting behavior of the reaction is similar to a roller support. Various views of the smaller roller support are shown in Figure 5-15.



(a) Small reaction—side view

(b) Small reaction—front view

Figure 5-15: Small reaction

Displacements and strains of the double curvature girders were monitored in a similar fashion as the single curvature girder tests.

5.3 TEST RESULTS

5.3.1 Overview of the Test Results

Shear failures were observed in all of the tested pile cap girders. In the single and double curvature control tests, the shear failures initiated once the transverse reinforcement that crossed the critical shear crack began to yield, resulting in shear tension tie failures. The control capacity for the single curvature test was 295-kips while the control capacities for the double curvature tests were 293-kips and 313-kips. In comparison, the single and double curvature control capacities are relatively close. Based on the similar control capacities and the fact that the double curvature tests did not form direct compression struts from the applied load to the reaction, it can be concluded that the double curvature tests exhibited sectional shear behavior.

The shear failures for the CFRP retrofitted single and double curvature girders initiated when one or more CFRP strip reached its ultimate tensile capacity, causing the strips to fracture. The strips were able to develop their tensile strength from the provided lap splices and/or CFRP anchors. The various CFRP layouts increased the single curvature shear capacity by 24% and the double curvature shear capacity by 56%.

From the test data, a more in-depth comparison and understanding could be obtained. Figure 5-16 shows the concrete (V_c), transverse steel (V_s), and CFRP's (V_f) shear contributions at the cracking and ultimate shear capacity normalized relative to the square root of the concrete's strength ($\sqrt{f'_c}$), web width (b_w), and effective depth (d).

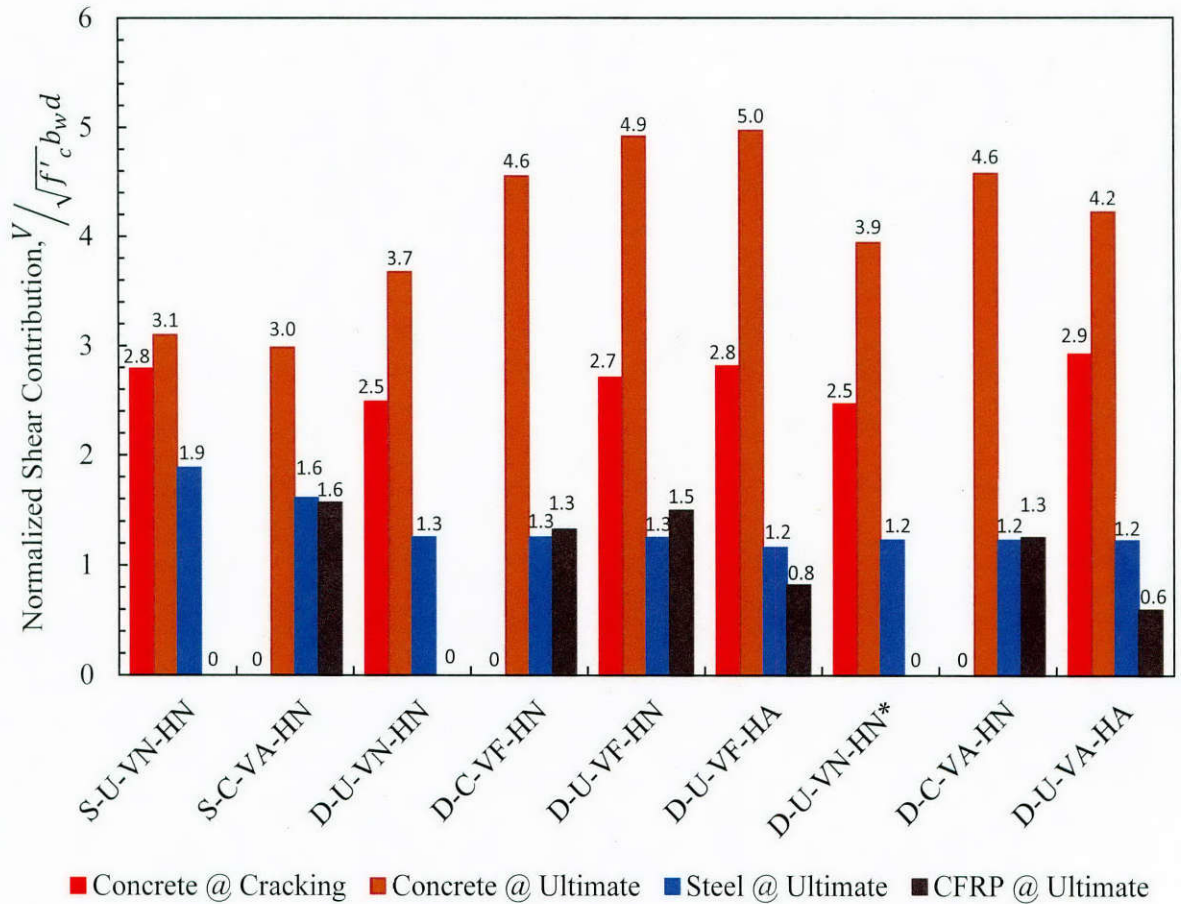


Figure 5-16: Normalized shear contributions at cracking and ultimate shear capacity

Based on Figure 5-16, several observations can be made regarding the single and double curvature tests. One observation is that the single curvature test formed a shear crack at a higher shear load compared to the double curvature tests. On the other hand, the double curvature girders exhibited higher concrete contributions at the ultimate shear capacity. Another observation is that the single curvature tests experienced higher steel contributions compared to the double curvature tests. This difference is because the shear crack in the single curvature tests were shallower and thus crossed more transverse reinforcement than the double curvature tests. Since the single and double curvature tests performed inherently different, their test results are separated and discussed independently.

5.3.2 Single Curvature Results

The shear load-displacement plot for the single curvature control and anchored uni-directional tests can be seen in Figure 5-17. The small drops in shear load, not highlighted by markers, are caused by pausing the tests to measure crack widths. However, the drop in load (red marker) is due to the formation of the critical shear crack in S-U-VN-HN. Similarly, the small load reduction in S-C-VA-HN (highlighted by the black marker) is associated with the internal shear forces trying to redistribute as small strands within the CFRP strips began to fracture. Once the forces were able to redistribute, the shear applied to the rehabilitated girder was able to increase slightly prior to failure.

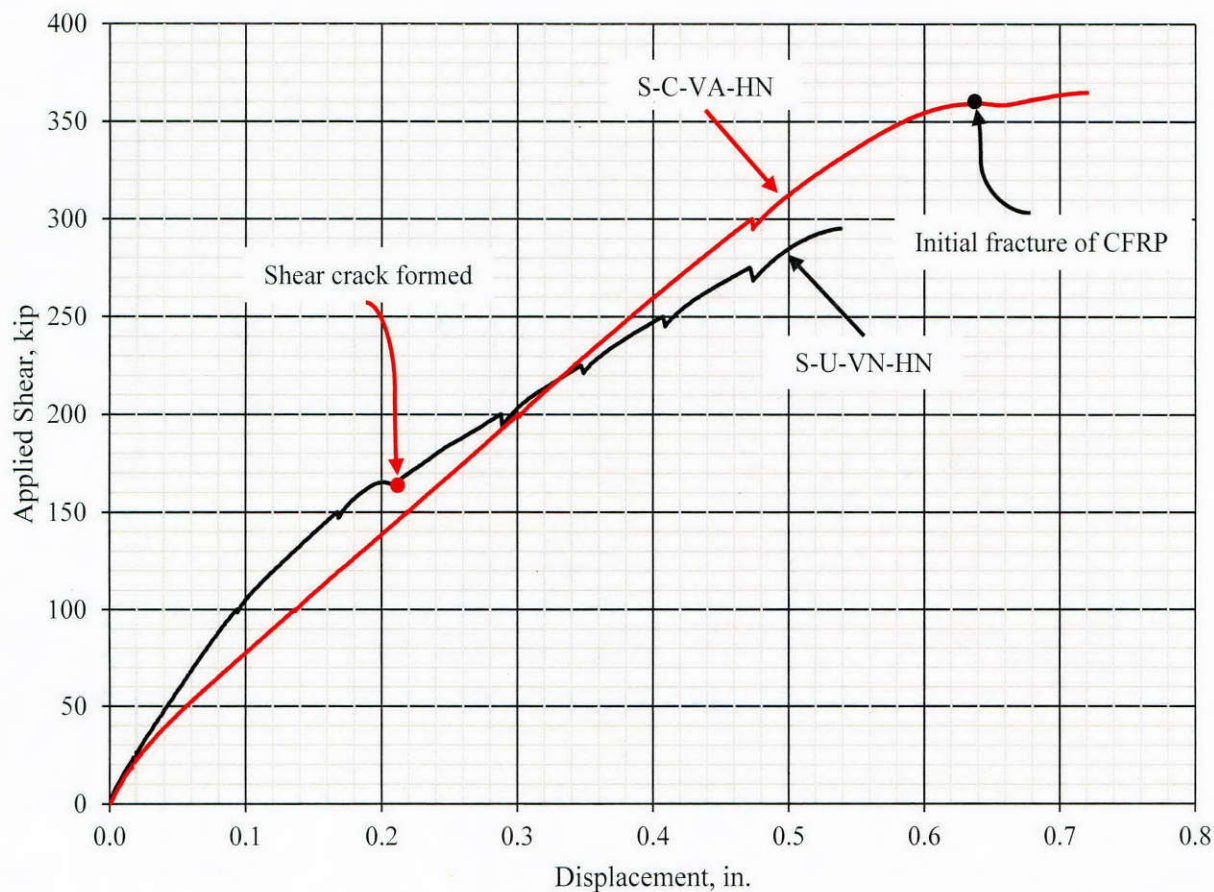


Figure 5-17: Single curvature shear load-displacement curves

Note that S-C-VA-HN had a lower initial shear stiffness when compared to S-U-VH-HN. The lower initial stiffness was caused by the pre-existing shear cracks from the control test (Figure 5-18). However, notice that the nearly constant shear stiffness of S-C-VA-HN is larger than the post-cracking stiffness of S-U-VH-HN, which indicates that an anchored uni-directional layout provided significant increases to the shear stiffness of wide-webbed pre-cracked members. Moreover, S-C-VA-HN exhibited 24% more capacity and a larger ultimate deformation when compared to the control test. However, not all of the transverse steel that crossed the critical crack of S-C-VA-HN reached yield prior to failure that was triggered by a CFRP strip fracture. A summary of the single curvature test data is presented in Table 5-2.



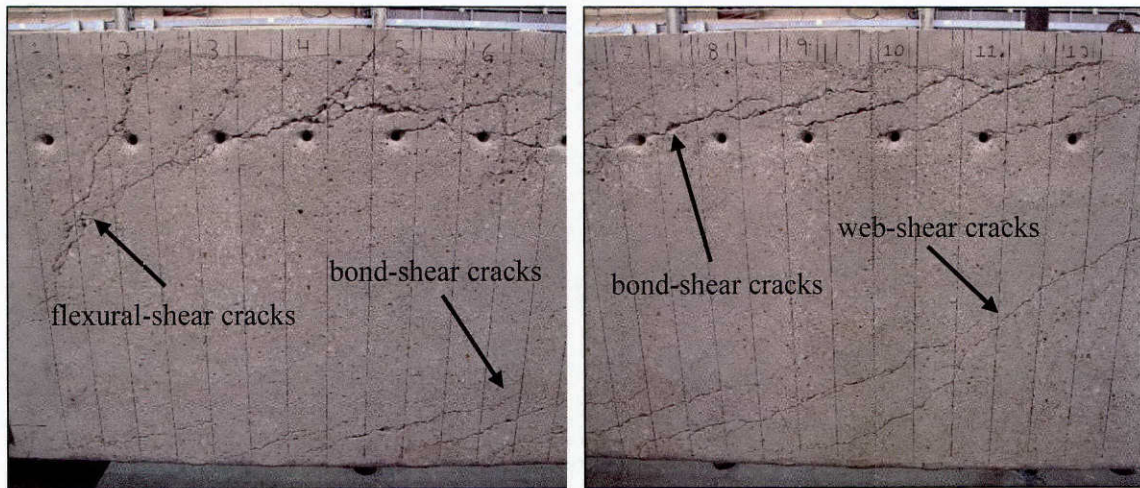
Figure 5-18: S-C-VA-HN crack pattern prior to CFRP installation

Table 5-5: Single curvature test summary

Test Name	Concrete f'_c (psi)	Cracking Shear (kip)	Peak Shear (kip)	Cracking Shear Increase (%)	Peak Shear Increase (%)
S-U-VN-HN	4710	165	295	N/A	N/A
S-C-VA-HN	4710	N/A	365	N/A	24%

5.3.3 Double Curvature Results

The complex behavior of girders tested in double curvature resulted in the unexpected formation of bond-shear cracks at the levels of the longitudinal, or flexural, reinforcement (Figure 5-19). These cracks formed because of a high moment gradient within the test span that created high bond stresses along the flexural reinforcement and the concrete. The bond failure caused the flexural stiffness to reduce slightly due to the loss of the concrete cover. However, the flexural steel was anchored sufficiently at the end regions to continue providing the required flexural resistance. Moreover, the reductions in the concrete cross-sectional area did not result in any concrete inelasticity. Hence, the girders remained elastic but with slightly reduced flexural stiffness (Figure 5-20).



(a) Left test span

(b) Right test span

Figure 5-19: Bond and shear cracks

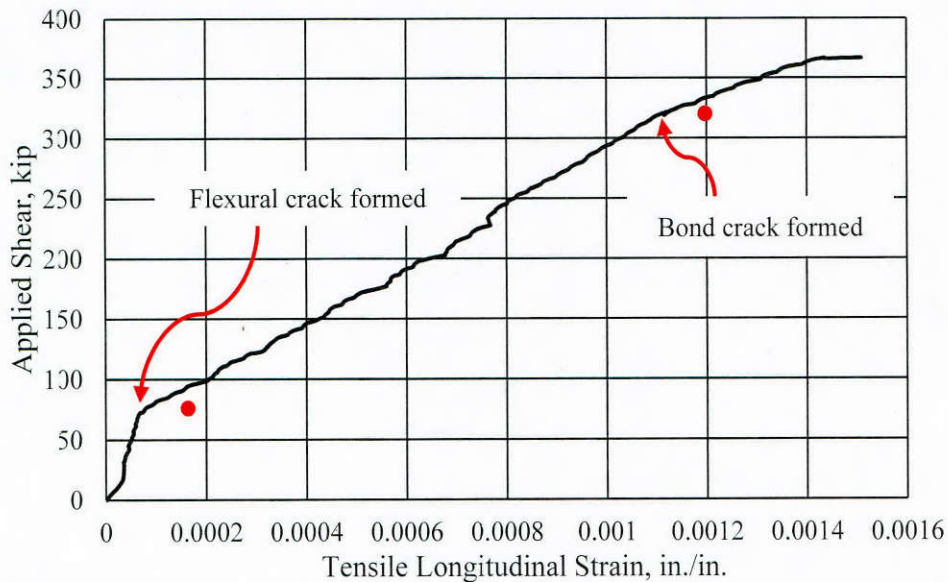


Figure 5-20: D-U-VA-HA flexural stiffness reduction

The effects of high bond stresses were observed after more than half of the double curvature girders were constructed. The flexural reinforcement was altered by moving the bundled flexural reinforcing bars inward, as shown in Figure 5-2 (b), for the remaining double curvature tests: D-U-VN-HN*, D-C-VA-HN, and D-U-VA-HA. The intent of changing the flexural reinforcement layout was to anchor more reinforcing bars away from the concrete corners. Unfortunately, the design change did not resolve the problem.

Since the cross-sectional design of the pile cap girders changed, an additional control test was conducted. The control test for the modified cross-section, D-U-VN-HN*, resulted in a slightly higher shear stiffness and shear capacity compared to D-U-VN-HN. Therefore, strength gains will be compared between tests with similar cross-sectional designs.

Unlike the single curvature tests, the double curvature tests formed two shear cracks. A flexural-shear crack formed in the left portion of the test span (negative moment). The negative moment created a flexural crack that eventually turned into a shear crack. Hence, the crack in the left span was the first shear crack to form. Based on an analysis of the girders, it was found that the

flexural-shear crack exhibited strains predominantly in the horizontal direction (ϵ_x). The flexural-shear crack eventually turned into a bond-shear crack. A web-shear crack formed in the right portion of the test span (positive moment). The web-shear crack formed because of high principal tensile stresses within the girder's web. Even though the web-shear crack was the last shear crack to initiate, it was always the crack that initiated the shear failure (i.e., critical shear crack).

Since two different types of shear cracks formed at different shear loads, a definition for the cracking shear load had to be established. Therefore, the cracking shear load was defined as the shear load that caused the shear carrying mechanism to change. This definition implies that the cracking shear load is the load at which the transverse reinforcement, across the critical crack, began to carry some of the applied shear.

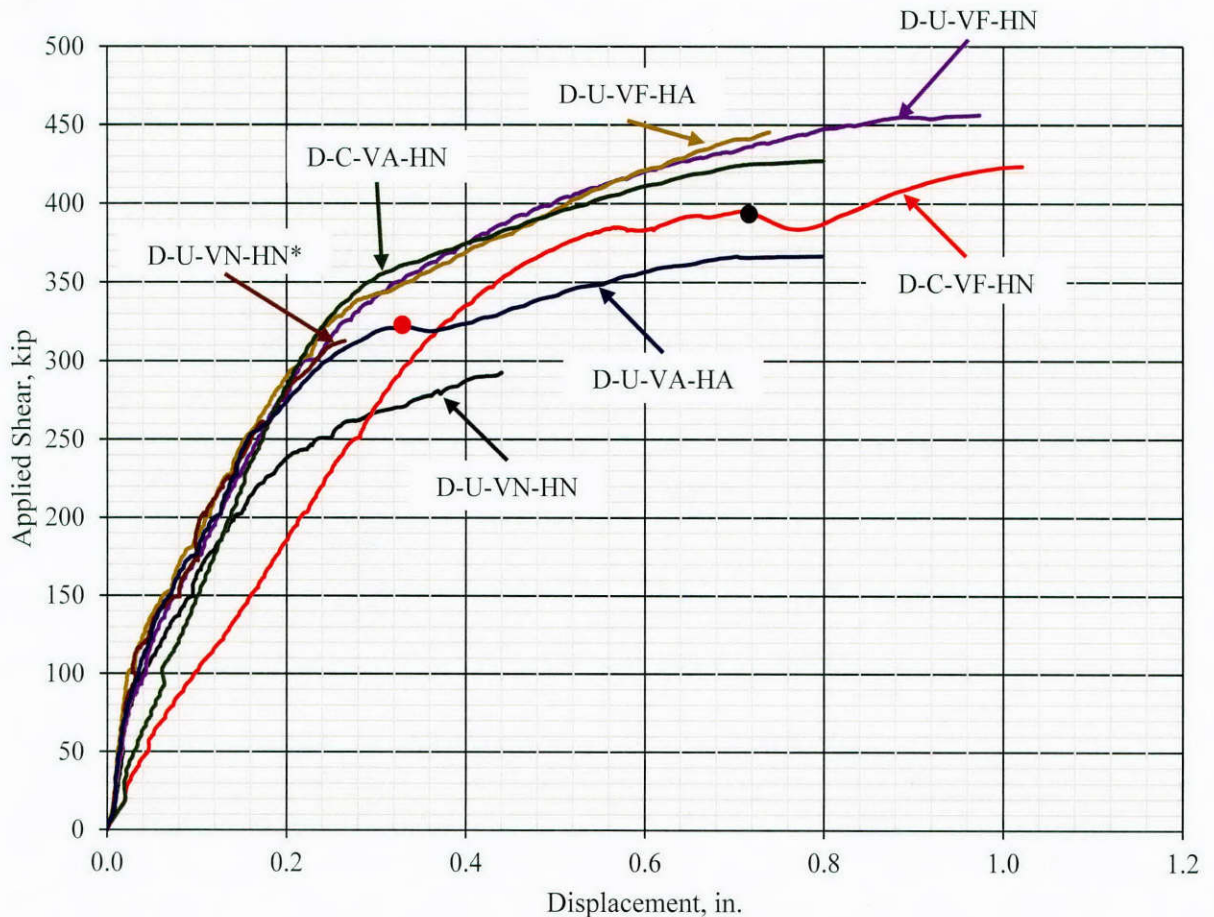


Figure 5-21: Double curvature shear load-displacement curves

The shear load-displacement curves for the double curvature tests can be found in Figure 5-21. Based on these curves, several key observations about shear stiffness can be made. As previously mentioned, changing the location of the flexural reinforcement did affect the control specimens' post-cracking shear stiffness. Hence, the original design experienced a significantly higher ultimate displacement. Moreover, the various CFRP layouts were able to increase the girder's cracked shear stiffness similar to the single curvature tests. The drastic changes in shear stiffness for the rehabilitated girders, shown in Figure 5-21, is the result of the CFRP strips debonding from the concrete surface. Even though the CFRP strips had debonded, additional shear load could be applied because of the lap splices and/or the CFRP anchors. The debonding of uncracked girders typically began at a load near the ultimate shear capacity of the control specimen.

The shear load-displacement curves also allude to an unexpected drop in the applied shear load for D-C-VF-HN (black marker) caused by an inadvertent change to the load ratio. The unbalanced loads yielded the longitudinal steel in the negative moment region before the load ratio was adjusted. The tests ultimate shear capacity was not affected.

On the other hand, the drop in the applied shear load for D-U-VA-HA (red marker) was the result of a poor CFRP layout and anchor detail. Since the pile cap girder web depth is relatively short, the vertical strip anchors had to be placed over the upper horizontal strip. In some cases, the intermediate horizontal strip anchors were placed on top of the vertical strip anchors. Moreover, the horizontal strips were extended and anchored into the peak moment regions. As a result, the horizontal strips not only bridged the flexural-shear crack, but they also bridged the flexural cracks. Thus inducing additional horizontal tensile strains. The upper horizontal strips fractured between the vertical and horizontal strip anchors, shown in Figure 5-22, due to a strain concentration between the anchors. The fracturing of the upper horizontal strips caused the applied shear load to drop temporarily. The applied shear load was able to redistribute and increase before eventually causing the vertical CFRP strips in the right span to fracture. The poor CFRP detailing likely influenced the failure of D-U-VA-HA. A summary of the double curvature test data is presented in Table 5-3.

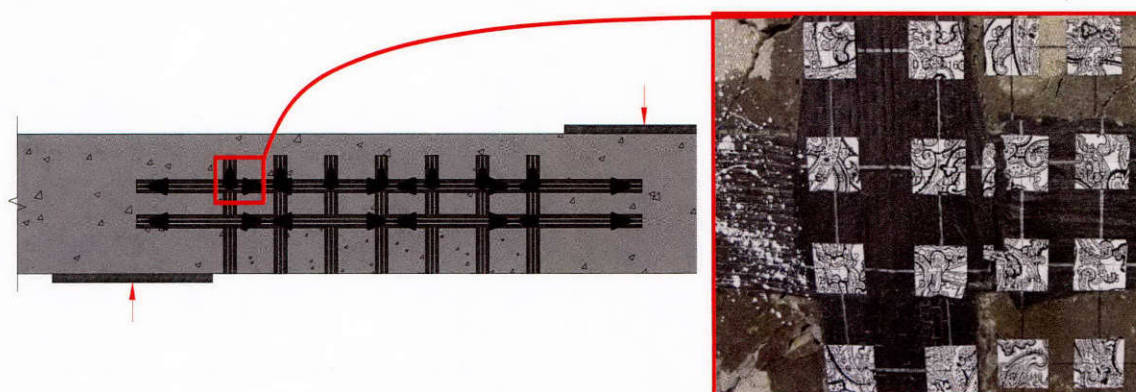


Figure 5-22: D-U-VA-HA premature horizontal strip fracture

Table 5-6: Double curvature test summary

Test Name	Concrete f'_c (psi)	Cracking Shear (kip)	Peak Shear (kip)	Cracking Shear Increase (%)	Peak Shear Increase (%)
D-U-VN-HN	4400	148	293	N/A	N/A
D-C-VF-HN	4400	N/A	424	N/A	45%
D-U-VF-HN	4410	161	456	9%	56%
D-U-VF-HA	5110	180	446	22%	52%
D-U-VN-HN*	4560	149	313	N/A	N/A
D-C-VA-HN	4560	N/A	427	N/A	37%
D-U-VA-HA	4580	177	367	19%	17%

5.3.4 Effects of CFRP

The increase in shear strength was found to be directly related to the influence of the layouts on crack widths, which are directly related to principal tensile strains. Using the optical measurement system, the principal tensile strains on the concrete's surface were measured and converted into crack widths. The width of a typical shear crack varies along its depth. The relative

magnitude of a shear crack can be represented by the crack width at mid-height of the web. Therefore, the mid-height shear crack width was used as a means of comparing crack widths.

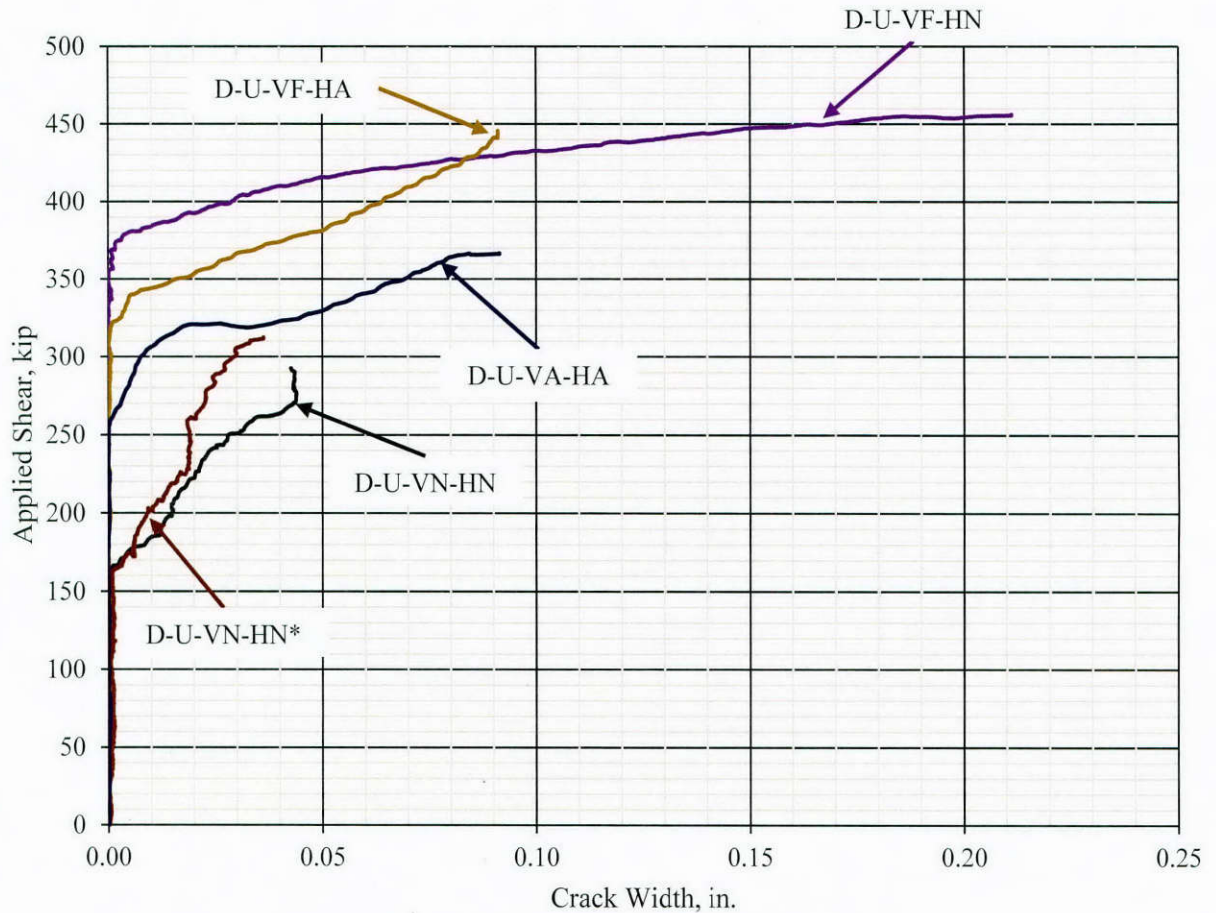


Figure 5-23: Double curvature mid-height crack width comparison

The mid-height crack widths for the various uncracked double curvature tests are plotted in Figure 5-23. The shear loads at the onset of cracking, shown in Figure 5-23, do not represent the cracking shear load. Instead, they represent the applied shear load that caused the mid-height shear crack to form. Both of the double curvature control tests had similar crack widths. However, D-U-VN-HN* exhibited smaller crack widths consistent with the higher shear stiffness compared to D-U-VN-HN. Furthermore, when crack widths are compared with corresponding ultimate shear capacity, it becomes evident that the CFRP layouts that produced the lowest crack widths, for a given applied shear load, also resulted in the highest ultimate shear capacities. However, the bi-directional layout of D-U-VF-HA reached a similar ultimate shear capacity as that of a uni-directional layout, D-U-VF-HN, but had smaller crack widths at failure.

The effects of the CFRP on the pile cap girders' response can be studied further by subdividing the various single and double curvature tests into groups to help determine the efficiency of retrofitting uncracked and cracked sections, the efficiency of CFRP anchors relative to fully wrapped systems, and the effectiveness of fully wrapped and anchored uni- and bi-directional layouts. The efficiency and effectiveness of CFRP can be explained by investigating the concrete, steel, and CFRP shear contributions for each group of tests. Since the single and double curvature tests produced significantly different responses, they are discussed independently.

5.3.4.1 Single Curvature

Figure 5-24 and Table 5-3 show the shear contributions for the two single curvature tests. Since the CFRP was applied to a previously tested girder, the concrete response was nearly linear. Moreover, the pre-existing shear cracks caused the CFRP strips to contribute to the shear capacity immediately. Near the ultimate capacity of S-C-VA-HN, the steel and CFRP contributions rose steeply resulting in the concrete contribution to reduce by an equivalent amount. Unlike S-U-VN-HN, the transverse steel in the test span of S-C-VA-HN did not yield prior to the CFRP strips fracturing. Some of the transverse reinforcement did not yield in S-C-VA-HN because the transverse reinforcement was near the end of the shear crack, which was well controlled by a CFRP strip at that location that also limited the steel strains. It is likely that the transverse reinforcement at this location should not have been included in the steel crossing the critical crack.

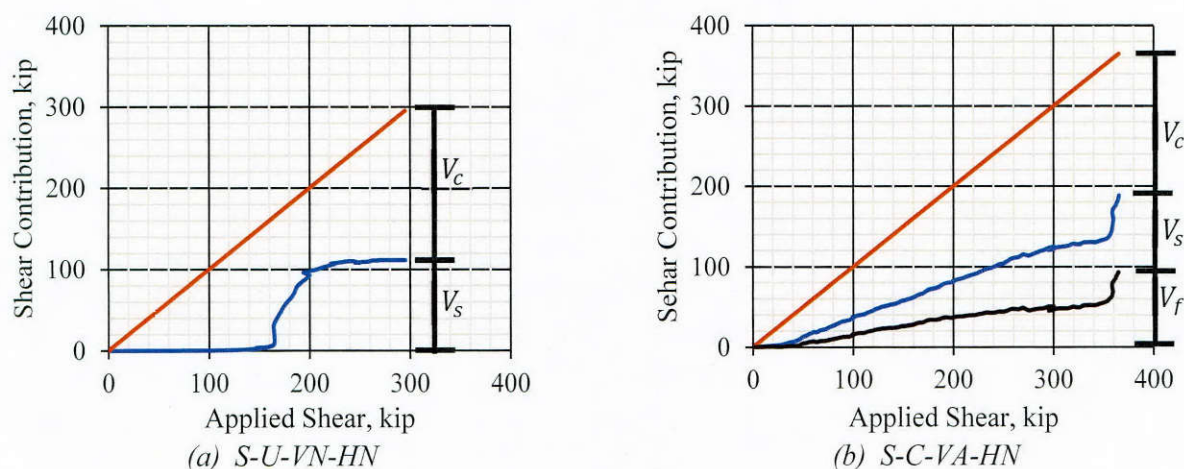


Figure 5-24: Single curvature anchored uni-directional

Table 5-7: Single curvature shear contributions

Test Name	Concrete Contribution (kip)	Steel Contribution (kip)	CFRP Contribution (kip)
S-U-VN-HN	184	112	0
S-C-VA-HN	177	95	93

5.3.4.2 Double Curvature

Figure 5-25 shows that D-U-VF-HN and D-C-VF-HN had similar ultimate shear contributions indicating that uncracked and cracked members can be rehabilitated with the same efficiency. The slight reduction to the concrete contribution for D-C-VF-HN may have been caused by loading the control test (D-C-VN-HN) slightly past failure. As expected, D-U-VF-HN did experience a delay in the steel and CFRP contributions.

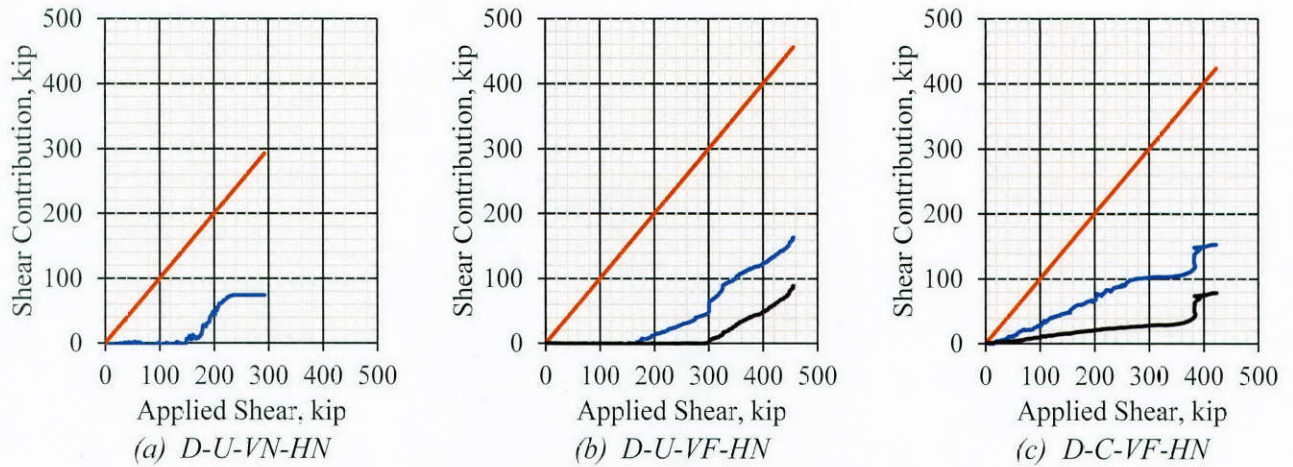


Figure 5-25: Double curvature uni-directional layouts, uncracked and cracked comparison

The similar shear contributions between D-C-VF-HN and D-C-VA-HN, in Figure 5-26, indicates that CFRP anchors are as effective as fully wrapped sections even if the anchors are placed through pre-existing cracks as was done for D-C-VA-HN (Figure 5-19). Thus, the cracks that ran through the anchor holes did not adversely affect any of the anchors' performance.

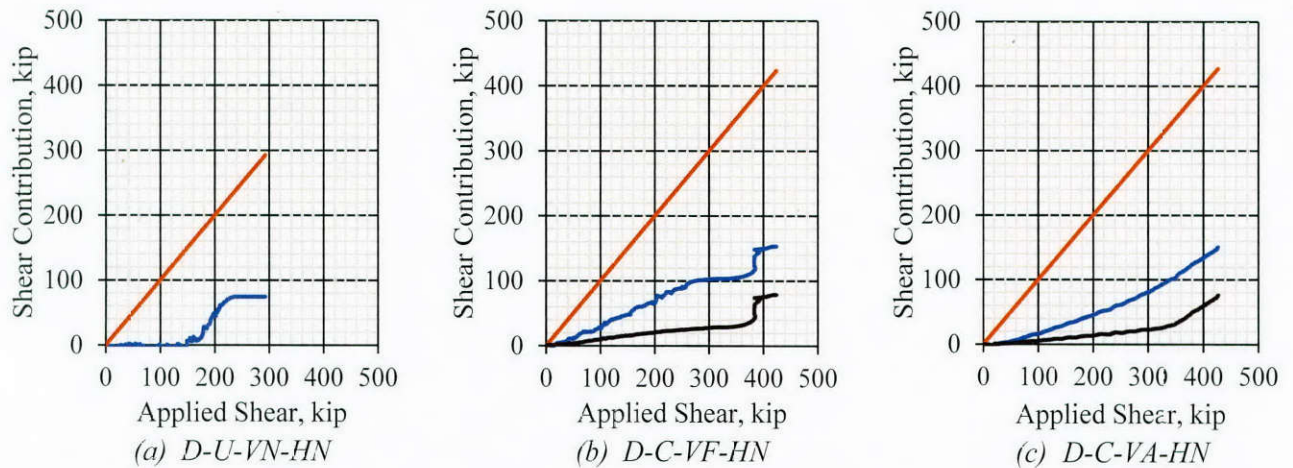


Figure 5-26: Double curvature fully wrapped and anchored uni-directional layouts, cracked sections

One observed advantage to the modified anchor detail was that the edge of the patches would indicate that the CFRP strip had debonded and the anchor was carrying the CFRP strip's load by lifting away from the concrete surface (Figure 5-27). The anchor's integrity remained intact despite the condition of the patches.



Figure 5-27: CFRP anchor post-failure

D-U-VF-HA had half of the vertical CFRP strips compared to D-U-VF-HN. The reduction of CFRP area in the vertical direction is evident in the CFRP shear contribution shown in Figure 5-28. However, since the other half of the CFRP area was placed in the horizontal direction, the concrete contribution for D-U-VF-HA was expected to have been larger than the concrete contribution for D-U-VF-HN, which was not the case. As a result, the bi-directional layout had a marginally lower ultimate shear capacity compared to the uni-directional layout.

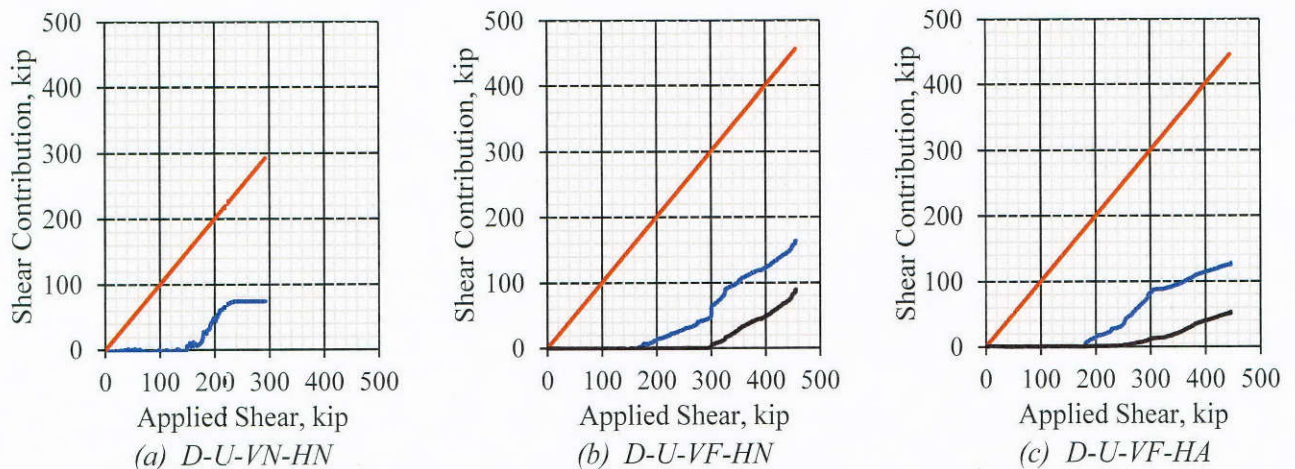


Figure 5-28: Double curvature fully wrapped uni- and bi-directional layouts, uncracked sections

Figure 5-29 shows that D-C-VA-HN outperformed D-U-VA-HA in terms of ultimate shear capacity and shear contribution response. In fact, the concrete contribution for D-U-VA-HA was only slightly larger than D-U-VN-HN* (Table 5-5). However, D-U-VA-HA was able to maintain the applied shear force when one of the CFRP strips fractured by redistributing the internal forces from the CFRP to the concrete as indicated by the nearly vertical drop in the CFRP contribution near the end of the test.

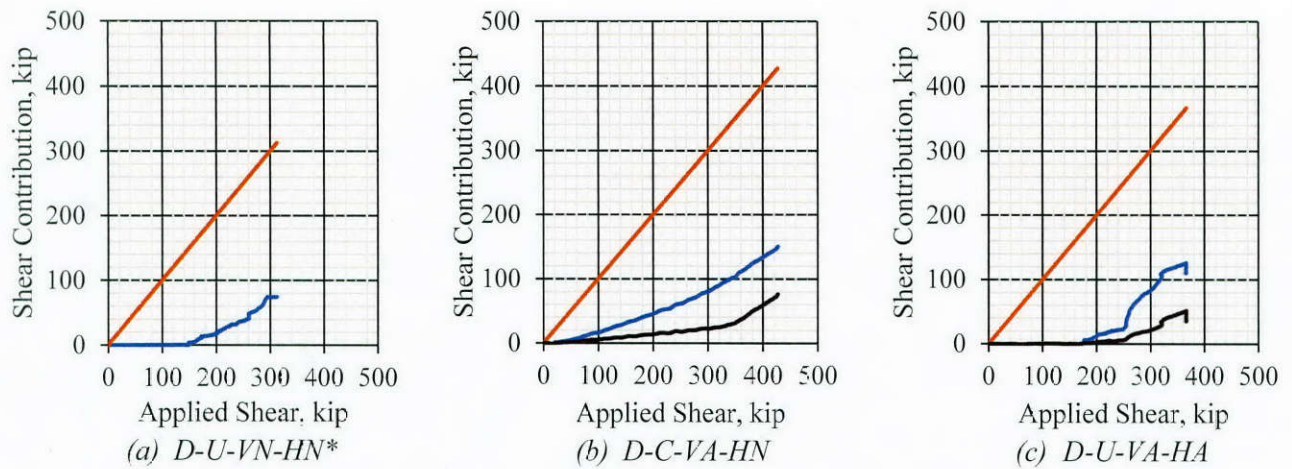


Figure 5-29: Double curvature anchored uni- and bi-directional layouts

Table 5-8: Double curvature shear contributions

Test Name	Concrete Contribution (kip)	Steel Contribution (kip)	CFRP Contribution (kip)
D-U-VN-HN	218	74	0
D-C-VF-HN	271	74	79
D-U-VF-HN	293	74	89
D-U-VF-HA	318	74	53
D-U-VN-HN*	238	74	0
D-C-VA-HN	277	74	76
D-U-VA-HA	256	74	36

5.4 CONCLUSIONS

The pile cap girder tests provided valuable insight into the shear strengthening of wide-webbed girders using CFRP strips and anchors. The test results showed that wide-webbed members could be strengthened effectively with CFRP. However, bi-directional layouts that had an equivalent area of CFRP material on the web as uni-directional layouts were unable to provide strength gains larger than the uni-directional layouts. Even so, the bi-directional layouts were able to increase the shear cracking loads and reduce shear crack widths compared to the uni-directional layouts.

The use of narrow CFRP strips provided more redundancy and tended to result in a more uniform strain distribution across each strip width. Occasionally, some fibers within a strip may fracture due to stress concentrations. With narrow strips, the girders were able to redistribute the internal shear loads to other undamaged strips for additional shear capacity and increase girder deformation.

Finally, the modified anchor detail was proven capable of developing the tensile strength of the CFRP strips. The patches on top of the anchor provided an indication that the CFRP strip had debonded and that the anchor was working properly. The test results also verified that anchors could be placed in regions of tension without adversely affecting the anchor's performance. However, an anchor may pull a cone of concrete from the girder's surface if the anchor is placed between two cracks. Furthermore, the performance of CFRP systems may be degraded if anchors are overlapped or near each other, which may cause unintended stress concentrations.

5.5 SUMMARY COMMENTS

Fully wrapped or anchored uni- and bi-directional CFRP layouts have not been used for strengthening the shear capacity of large pile cap girders. A number of tests on various uni-directional layouts had to be performed for comparison with the bi-directional layouts. Therefore, only a few bi-directional layouts could be tested in the compressed time frame that resulted from a change in Task 1d. Therefore, additional bi-directional tests need to be completed to fully understand how the various bi-directional layouts affect the shear contribution components (i.e., V_c , V_s , and V_f).

Moreover, the tests that were conducted using the double curvature test setup performed less than ideally due to the unintended loss of the longitudinal reinforcement's bond to the concrete. Fortunately, the bond failure did not adversely affect the girder's ability to remain flexurally elastic, albeit at a slightly lower flexural stiffness. The bond failure may have been prevented by reducing the amount of longitudinal reinforcement or lowering the moment gradient in the test span by increasing the tested span-to-depth ratio. However, a typical pile cap girder is designed to have the flexural capacity govern. As a result, the longitudinal reinforcement ratio is generally much lower than the ratio that was used for these pile cap girder tests.

Chapter 6. Small-Scale Beam Tests

6.1 OVERVIEW AND OBJECTIVE

Small-scale beams tests were conducted to achieve the objectives of Tasks 2a and b.

The objective of Task 2a was to develop a simple reliable test that can be used to qualify a particular CFRP material and anchored CFRP design, as well as provide means by which the quality of an installation and installer can be verified. The standard three-point load beam specimen and testing procedure of ASTM C293 (ASTM, 2007) were selected, but with the beam strengthened using an anchored CFRP system. Benefits of adopting the standard beam test are: 1) it is widely used in structural engineering laboratories so most laboratories have the necessary equipment to conduct the tests; 2) the beam is (6-in. tall by 6-in. wide by 24-in. long) making it easily maneuverable by two people without the need for lifting equipment; 3) the proposed test can easily be used for on-site evaluation by requiring contractors to install anchored CFRP on several beam specimens for each batch of epoxy; and 4) given the other benefits, the cost of conducting such tests would be relatively low.

The objective of Task 2b was to optimize anchor design by identifying critical parameters that affect anchor strength and setting optimal design limits for those parameters. The same small-scale beam tests that were used to develop the quality control test specimen and procedures for Task 2a, were also used to optimize anchor design. Beam tests were conducted with varying anchored CFRP-system parameters, which produced the data necessary for developing design guidelines for CFRP anchors. Due to the overlap in the experimental portion of the two sub-tasks, the experimental results for both sub-tasks are presented and discussed in this chapter.

6.2 EXPERIMENTAL PROGRAM

6.2.1 Overview of Experimental Program

Four series of small-scale beam tests were conducted to complete Tasks 2a and b.

- Series 1: Modified ASTM C293 beam specimens with through-strip CFRP anchors
- Series 2: Modified ASTM C293 beam specimens with through-strip GFRP anchors
- Series 3: Modified ASTM C293 beam specimens with CFRP anchors adjacent to strip
- Series 4: Larger beam specimens with CFRP anchors adjacent to strip

Series 1 and 2 had anchors installed through the CFRP strip (Figure 6-1a). For ease of construction, Series 3 and 4 had anchors installed adjacent to the CFRP strip (Figure 6-1b). The latter anchor layout proved to perform as well as the through-strip layout, but avoided the difficulty of pushing the anchor through the strip during installation. Series 1, 3, and 4 had CFRP anchors while Series 2 explored GFRP anchors.

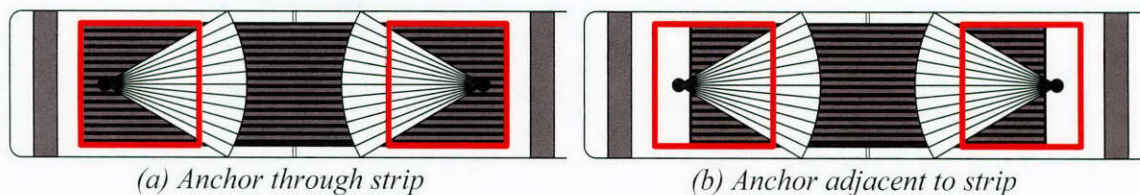


Figure 6-1: Anchor layouts

The beam geometry for Series 1 to 3 was based on the standard concrete beam used for modulus of rupture tests and described in ASTM C293 (ASTM, 2007). For the first three series,

beam specimens had dimensions of 6-in.x6-in.x24-in. A notch was cut at mid-span of the tension face to control the location of flexural cracking. Holes were drilled on the tension face of the beam for installing CFRP anchors (Figure 6-2). A CFRP strip anchored at the holes was applied to the tension face of beam specimens. Beams did not have any steel reinforcement but had side CFRP strips added to reduce the likelihood of shear failures.



Figure 6-2: Beam specimen before CFRP installation (Series 1 to 3)

For Series 4, larger beams were tested under three-point loading to evaluate the behavior and strength of larger anchored CFRP systems. This series was undertaken based on findings from the first three series, in which significant size effects were observed in CFRP strips and CFRP anchors. The larger beams were 12-in. tall by 12-in. wide by 68-in. long. The new dimensions were selected to test CFRP strips up to 10-in. wide, which is considered to be the largest practical field installation width. Similarly to the smaller beams, a notch was cut at mid-span and holes were drilled on the tension face for the placement of anchors (Figure 6-3).

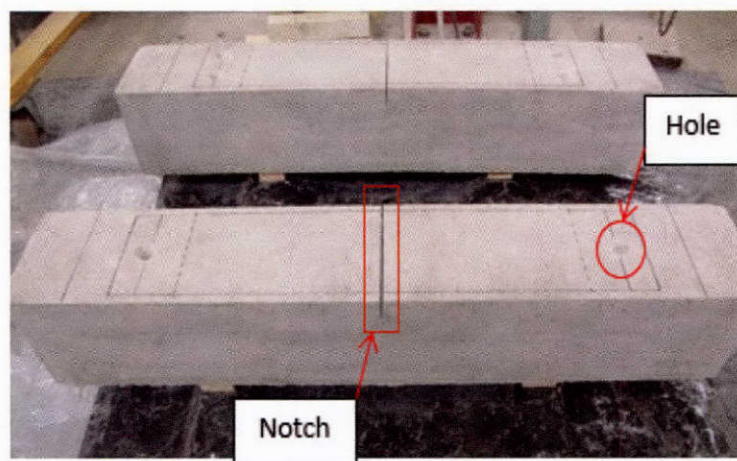


Figure 6-3: Large beam specimens before CFRP installation

Three-point loading was applied to the test specimens as is done in modulus of rupture tests. The loading induced tension forces in the CFRP strip and anchors as seen in Figure 6-4. When CFRP is used for strengthening and rehabilitation, the primary tension force in the strip is caused by widening of cracks in a concrete member (Figure 6-4). Similar loading was generated on the CFRP system in the small-scale beam specimens (Figure 6-5).

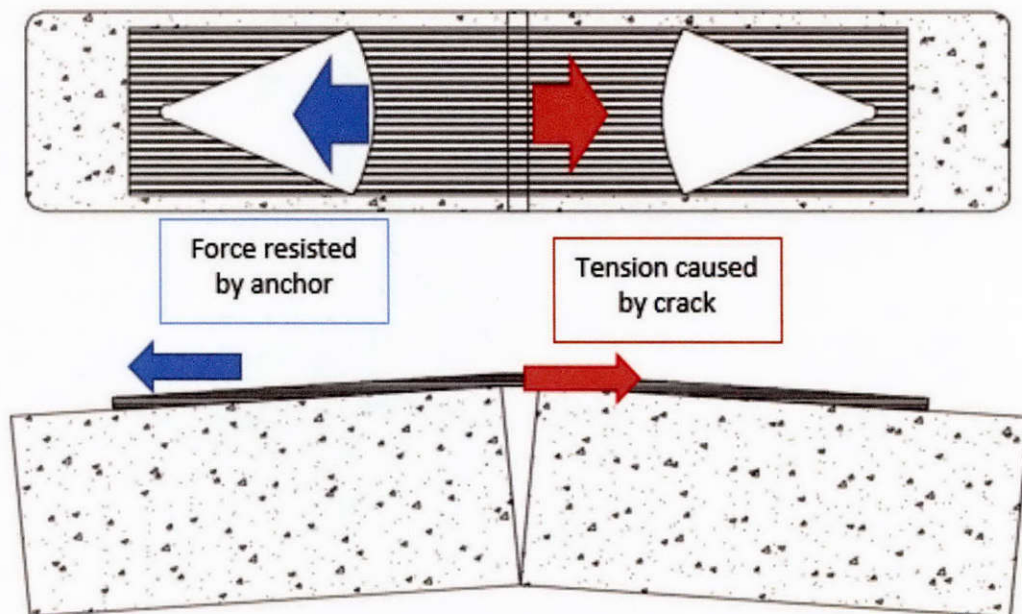


Figure 6-4: CFRP system loading in a three point load beam test

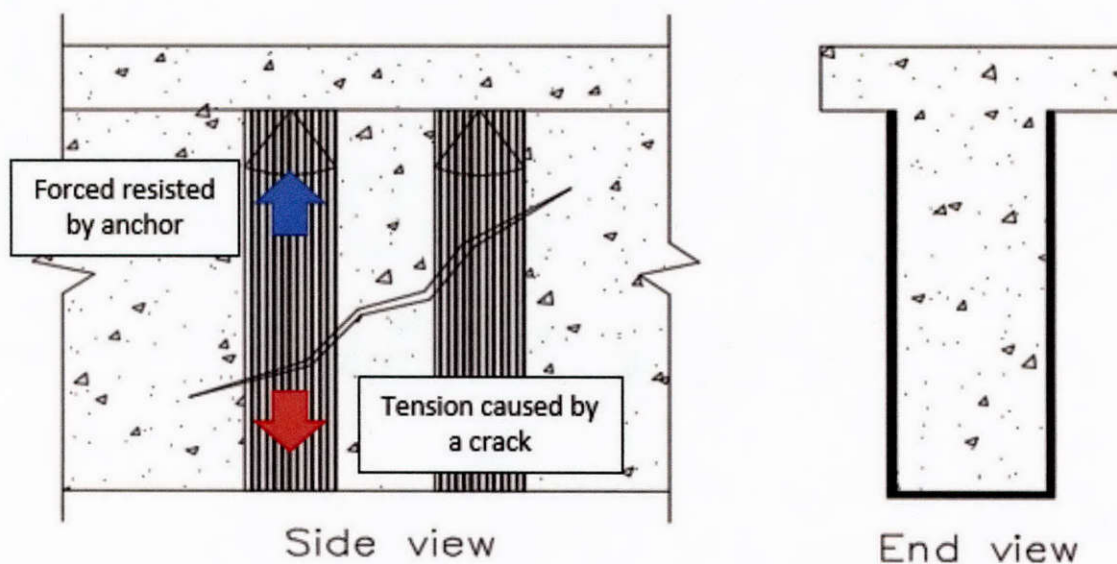


Figure 6-5: CFRP system loading in a concrete beam with inclined cracking

6.2.2 Typical Specimen Preparation and Strengthening

The same specimen preparation and CFRP installation procedures were used for the smaller and larger beams. These procedures are discussed briefly in the following sections. Additional details can be found in the final reports of TxDOT projects 0-6306 and 5-6306 (Kim et al., 2012 and Garcia et al., 2014).

6.2.2.1 Specimen Preparation

The concrete surfaces, anchor holes, specimen corners and mid-span notch were prepared before installation of CFRP U-wraps, CFRP strip, and CFRP anchors. To improve bond between concrete and CFRP, the concrete surfaces that contacted CFRP were prepared by grinding off

laitance and removing all dust and residue (Figure 6-6 (a)). Two holes were drilled to a depth of four inches on both ends of the beam tension face for anchor installation (Figure 6-6 (b)). The anchor holes were rounded to avoid premature CFRP anchor failure (Figure 6-6 (c)). Compressed air or a vacuum cleaner were used to remove the dust from the anchor holes (Figure 6-6 (d)).



(a) Grinding a concrete surface



(b) Drilling holes



(c) Rounding hole edge



(d) Cleaning holes with compressed air or vacuum cleaner
Figure 6-6: Specimen preparation before CFRP installation

As shown in Figure 6-7, the corners of the beams were rounded to a radius of 0.5-in. so that U-wrapped CFRP strips would not fail at sharp corners. Beam corners were rounded by grinding or through form inserts. Finally, a notch was cut at mid-span to control the location of concrete flexural cracking. The notch was 1-in. deep in the smaller beams and 2.5-in. deep in the larger beams.

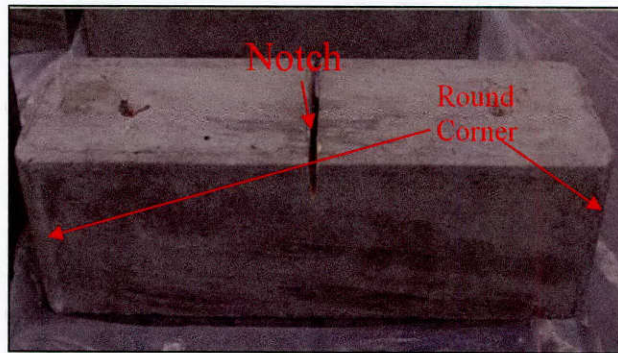


Figure 6-7: Typical prepared specimen

6.2.2.2 Installation of CFRP Strips and Anchors

Anchors and CFRP strips were prepared as shown in Figure 6-8. Epoxy was prepared and mixed following the supplier's instructions (Figure 6-9). Anchor holes and beam surfaces where CFRP strips were to be installed were saturated with epoxy (Figure 6-10). CFRP strips were then saturated with epoxy and applied to beam side and tension surfaces as shown in Figure 6-11. Putty knives and rollers were used to remove air bubbles and excess epoxy.

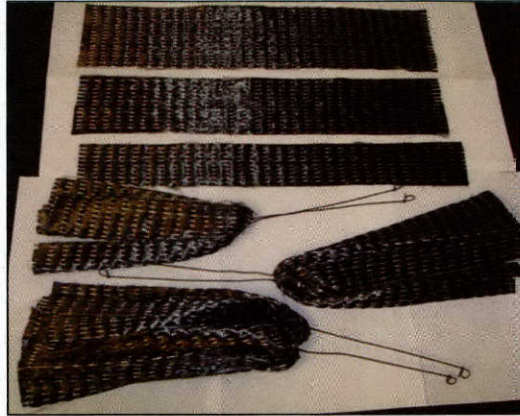


Figure 6-8: CFRP anchors and CFRP strips (Huaco, 2009)



Figure 6-9: Mixing the epoxy components (Huaco, 2009)



Figure 6-10: Saturating holes and surfaces (Hauco, 2010)



Figure 6-11: Applying CFRP strips

Two anchor layouts were used in the small beam tests as illustrated in Figure 6-1. For Series 1 and 2, the anchors were inserted through the CFRP strip, while in Series 3 and 4 the anchors were installed adjacent to the CFRP strip for ease of construction. In both cases, a saturated CFRP anchor was inserted into the hole and the anchor material sticking out of the hole was fanned out (Figure 6-12) to provide force transfer from the entire width of the strip to the anchor. Two patches of CFRP were then applied over the center of each anchor to reduce stress concentrations in the anchors and achieve better load transfer between the strip and the anchors. The fiber direction of the first patch was perpendicular with the CFRP strip, while the fibers of the second patch were parallel to the strip fibers. A completed installation is shown Figure 6-13.



Figure 6-12: Fanning the anchor

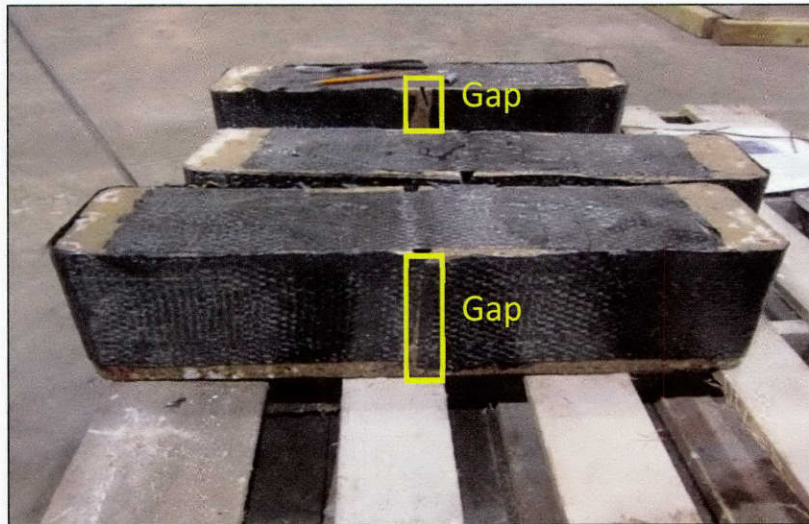


Figure 6-13: Specimens with CFRP installed

6.2.3 Test Matrix Details

6.2.3.1 Series 1

This series of tests was undertaken to achieve a reliable test specimen and test methodology for controlling the strength and the quality of installation of anchored CFRP systems (Task 2a). Specimen details were modified throughout this test series to preclude undesirable failure modes in the concrete specimen that were observed in previous work by Huaco (2009). This test series was also used to optimize anchor design by identifying critical parameters that affect anchor strength (Task 2b). Beam tests were conducted with varying anchored CFRP-system parameters, which produced the data necessary for developing design guidelines for CFRP anchors. In all, 39 standard-size beams were tested in Series 1, with varying CFRP strip and anchor details, as well as varying side-wrap details.

6.2.3.1.1 Specimen Details

Specimens consisted of a strengthened standard concrete beam described in ASTM C293 (2007), and typically used for the evaluation of the modulus of rupture of concrete. Specimen dimensions were 6-in. by 6-in. by 24-in. (Figure 6-14). A 1-in. deep notch was cut at mid-span to initiate the cracking, the beam side corners were rounded, and two holes were drilled for installing CFRP anchors (Figure 6-14).

An insufficient anchor embedment depth (or anchor hole depth) provides less contact area between CFRP anchor and its surrounding concrete element. It will reduce the capacity of anchorage systems, and the anchor may pull out before the CFRP strip fractures. A 4-in. embedment depth was suggested by Huaco (2009) and was used in all small-scale beam specimens (Figure 6-14).

The edge of the anchor hole in the direction of the anchor fan was rounded to prevent stress concentrations in the anchor at the edge and premature anchor fracture. A ½-in. chamfer radius was used as recommended by Pham (2009) and was used in this test series (Figure 6-14).

Too large or too small a hole diameter is prone to making the installation more difficult and lower the installation quality as well as the capacity of anchors. The area of hole was suggested to be at least 1.4 times larger than the area of the CFRP anchor based on the equivalent area of a laminate having the same CFRP fiber area as the anchor (Kim et al., 2012). In order to determine the equivalent laminate area of an anchor, CFRP strips and anchors are converted to unit weights

of dry fiber per unit length of fiber. Because both strips and anchors are of the same material, the weight per unit fiber length can be converted to an equivalent laminate area. Manufacturers typically provide the dry fiber weight per square surface area of a laminate ($\gamma_{s,Exp}$). While for pre-manufactured anchors, typically the dry fiber weight per unit length is provided (λ_A). The equivalent laminate anchor area can therefore be evaluated using the following equation:

$$A_{Eqv} = \text{Eqv. laminate area of anchor} = \frac{\lambda_A}{w_f \gamma_{s,Exp}} (w_f t_f) \quad \text{Equation 6-1}$$

With w_f = strip width and t_f = strip laminate thickness

All anchor fans covered the full width of the CFRP strip as seen in Figure 6-15

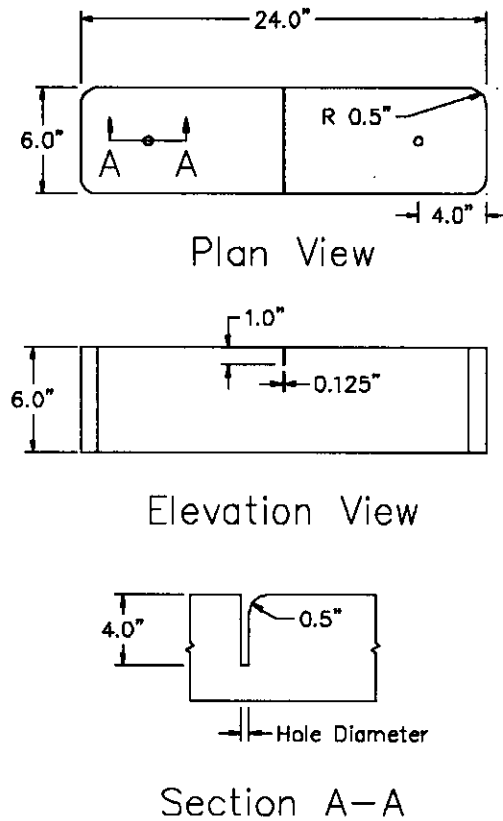
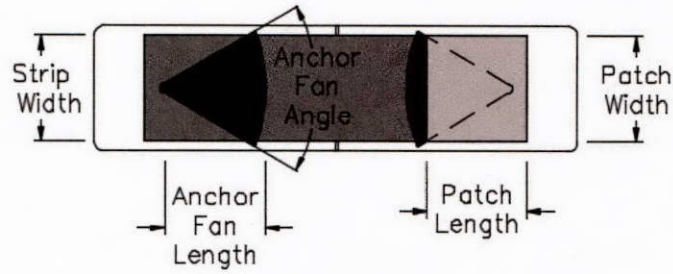
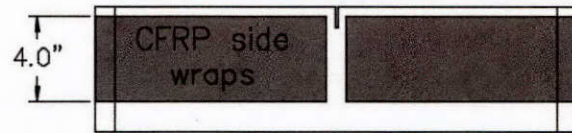


Figure 6-14: Detailed drawings of concrete specimen



Plan View



Elevation View

Figure 6-15: Detailed drawings of specimen with CFRP

Of particular concern in Series 1 was achieving a beam design that would fail the CFRP strip or the anchors but not the concrete. Specimen details were adjusted throughout Series 1 to achieve a reliable test specimen for quality control of FRP materials and installation. More specifically, the undesirable concrete shear/tension failure mode observed in previous work by Huaco (2009), was targeted (Figure 6-16 and Figure 6-17). Steel reinforcement was found to be of limited benefit in the smaller beams (Series 1 to 3) due to the limited development length available for the bars. Side-face CFRP U-wraps were, however, found to provide a sufficient margin of safety against concrete failure and develop the strength of the anchored CFRP strengthening system (Figure 6-13).

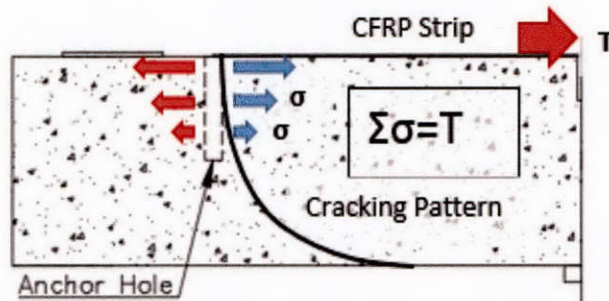


Figure 6-16: Shear/tension failure mode in small beams



Figure 5-17: Concrete beam shear failure (Huacc, 2009)

6.2.3.1.2 CFRP Anchor and Strip Variables

In this series, the following parameters were held constant across all specimens:

- The anchor embedment depth was 4-in.
- The chamfer at the anchor hole edge had a radius of 1/2-in.
- The area of the anchor holes was 1.4 times larger than the area of the anchor.
- The anchor fan length was 6-in.
- The anchor patch dimensions were 5 by 5-in.

Based on work completed in TxDOT project 0-6306 (Kim et al., 2012), the following specimen and CFRP parameters were varied in this test series:

1. Material ratio of CFRP anchors to CFRP strip = equivalent anchor laminate area / strip laminate area
2. CFRP strip width
3. Anchor fan length/angle
4. Concrete strength
5. Contribution of epoxy bonding on load transfer mechanism (Bonded vs. Unbonded).

The sectional area of CFRP anchors is an important parameter in determining the force being transferred at the anchor from the CFRP strip into the concrete substrate (Kim et al., 2012). An insufficient amount of CFRP material in the anchors leads to rupture of the anchors before fracture of CFRP strips. This premature failure due to anchor rupture reduces the effective tensile capacity of the CFRP strips.

The anchor material ratio (AMR) is defined as the equivalent laminate cross-sectional area of the anchor (Eq. 6-1) divided by the laminate cross-sectional area of the strip it is developing (Figure 6-18). The nominal anchor diameter provided by the manufacturer should not be used to determine the anchor area as it is not an exact measurement. Figure 6-18 illustrates an anchor material ratio of 2.4. Two examples are provided for how anchor material ratios are calculated, 1) if anchors are made from the sheet material used in the strips, and 2) if using premanufactured anchors.

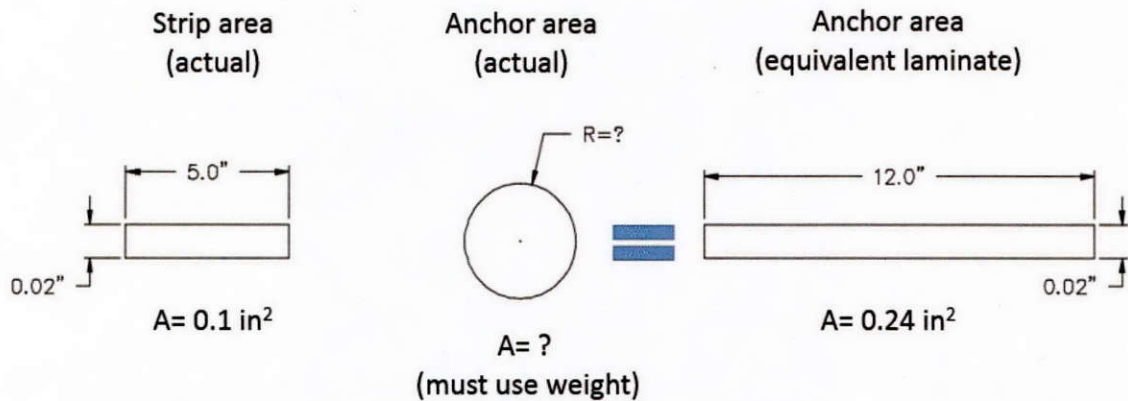


Figure 6-18: Equivalent anchor area and anchor material ratio

6.2.3.1.2.1 Example 1: Making anchors from CFRP sheets used for the strip

This process is simple because the anchor is being made from the strip sheet material. Therefore simply multiplying the strip width by $\frac{1}{2}$ the anchor material ratio provides the equivalent width of strip that needs to be cut and turned into an anchor. The ratio is multiplied by $\frac{1}{2}$ because the strip should be cut twice as long as needed and folded in half, therefore doubling the area. Assume the CFRP layout has a 5-in. wide strip with a desired material ratio of 2.4. The anchor would be made from a strip that was $5 * (2.4/2) = 6$ -in. wide and folded in half, making its area 2.4 times that of the strip.

6.2.3.1.2.2 Example 2: Using premanufactured anchors

This process is more involved because dry fiber weights per unit fiber length need to be evaluated. The anchor equivalent laminate area can be evaluated using Equation 6-1. The Anchor material ratio is then given by:

$$\text{Anchor material ratio (AMR)} = \frac{A_{Equ}}{A_{strip}}$$

For example, given the following manufacturer data:

Weight of strip laminate per surface area ($\gamma_{s,Exp}$) = 0.005 oz/in²

Weight of anchor per length (λ_A) = 0.06 oz/in.

Strip width (w_s) = 5-in.

Strip thickness (t_f) = 0.02-in.

$$A_{Eqv} = \frac{\lambda_A}{w_f \gamma_{s,Exp}} (w_f t_f) = \frac{0.06}{0.005} * 0.02 = 0.24$$

$$A_{strip} = w_f * t_f = 5 * 0.02 = 0.1$$

$$\text{Anchor material ratio} = \frac{A_{Eqv}}{A_{strip}} = \frac{0.24}{0.1} = 2.4$$

The area of CFRP material in anchors was suggested by Kim (2008) and Orton (2007) to be 1.5 to 2 times the area of CFRP material in the strips. To install CFRP anchors, the area of holes was suggested to be 1.4 times larger than the area of FRP material in the anchor (Garcia et al., 2014 and Kim et al., 2012). On the other hand, a CFRP anchor with a large material area may be hard to

install and may reduce the quality of the installation. The anchor to strip material ratio was varied from 1.06 to 2.0 in Series 1.

CFRP strip widths of 3-in. and 5-in. were selected to investigate the influence of width on the load transfer mechanism between the CFRP strip and anchors.

The length of the anchor fan is directly related to the angle of the fan for full coverage of the CFRP strip width. Considering that the tensile capacity of CFRP composite is mostly determined by the fiber, load transfer in the outer fibers of a fan with a large angle is less effective than the center fibers in the same direction. A reduction of anchor capacity therefore may occur when a large fan angle is used. A fan anchor angle less than 60° was suggested by Kim (2011). The anchor fan length and associated anchor fan angle were selected in this study to investigate their influence on the load transfer mechanism. Anchor fan lengths of 4-in. to 7.5-in. with associated angles from 64° to 37° were used on 5-in. CFRP strips. Fan lengths from 2.4-in. to 4.5-in. with associated angles from 64° to 37° were used with 3-in. CFRP strips.

Two concrete compressive strengths were used for the beam specimens, a lower strength of 5.4 ksi and a higher strength of 11.5 ksi. The concrete strength was varied to investigate its influence on the bonding mechanism between CFRP strips and concrete substrate, and the load transfer mechanism between CFRP strip and anchors.

In order to investigate the capacity of CFRP anchor to fully develop the strength of the CFRP strip without the assistance of bond stress between the strip and concrete, a plastic film was attached on the concrete surface of some specimens to prevent any bond between the concrete surface and the CFRP strip as shown in Figure 6-19. Unbonded tests were compared with bonded tests to determine the contribution of epoxy resin on the load transfer mechanism of anchorage system.



Figure 6-19: Layout of unbonded specimens

6.2.3.1.3 Nomenclature

Specimen nomenclature is shown in Figure 6-20.

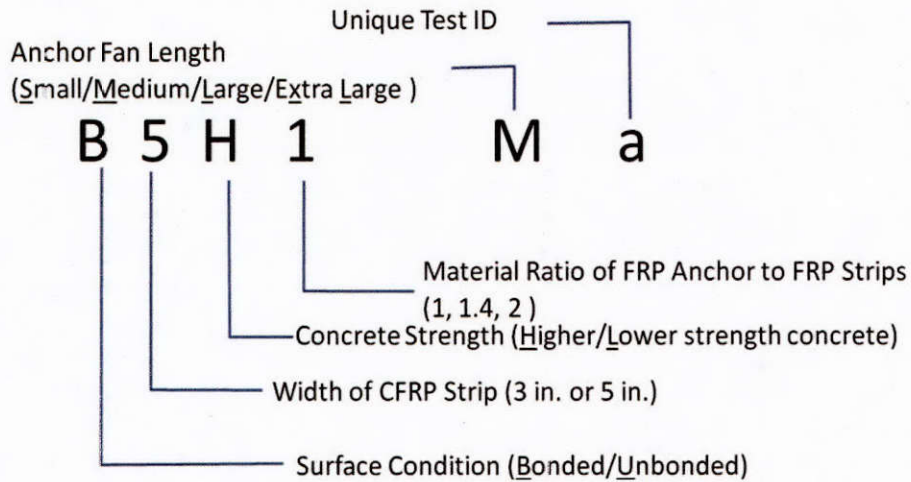


Figure 6-20: Specimen nomenclature

The first character B or U refers to the bonded or unbonded specimens. The second number refers to the width of the CFRP strip. Considering the width of specimens is 6-in., two widths of CFRP strip, 3-in. and 5-in., were investigated in this series. The third character refers to the concrete compressive strength. Two concrete strengths were used and will be referred to using the letters H, for the higher strength of 11.5 ksi, and L for the lower strength of 5.4 ksi). The fourth number refers to the ratio of the CFRP anchor material to the CFRP strip material. This series investigated anchor material ratios ranging from 1.06 which is represented by 1 in the nomenclature to 2.0. The fifth character refers to the anchor fan length described and illustrated in Table 6-1. The last character is a unique identifier required to distinguish between redundant tests having identical parameters. Several redundant tests were conducted in this series to evaluate the inherent variability in results generated by the test methodology. The details of the 39 tests conducted in Series 1 are presented in Table 6-2.

Table 6-1: Details for anchor fans

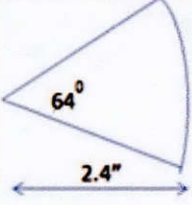
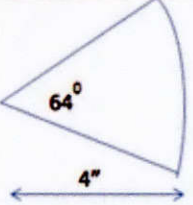
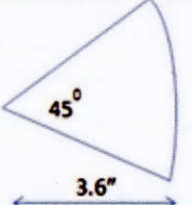
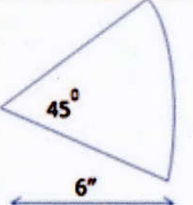
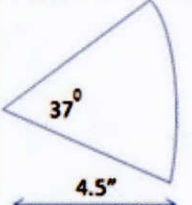
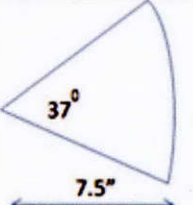
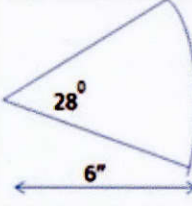
Anchor fan length	3-in. strip	5-in. strip
S		
M		
L		
XL		

Table 6-2: Test details

Test number	Specimen	Concrete compressive strength (f'_c) (ksi)	Strip width (in.)	Anchor material ratio	Anchor hole diameter (in.)
1	B5H2Ma	11.5	5	2.0	3/4
2	B5H2Mb	11.5	5	2.0	3/4
3	B5H1.4Ma	11.5	5	1.41	5/8
4	35H1.4Mb	11.5	5	1.41	5/8
5	B5H1.4Mc	11.5	5	1.41	5/8
6	35H1.4Md	11.5	5	1.41	5/8
7	B5H1.4Sa	11.5	5	1.41	5/8
8	B5H1.4Sb	11.5	5	1.41	5/8
9	B5H1.4La	11.5	5	1.41	5/8
10	B5H1.4Lb	11.5	5	1.41	5/8
11	B5L1.4Ma	5.4	5	1.41	5/8
12	35L1.4Mb	5.4	5	1.41	5/8
13	B5L1.4Mc	5.4	5	1.41	5/8
14	35L1.4Md	5.4	5	1.41	5/8
15	B5H1Ma	11.5	5	1.06	5/8
16	B5H1Mb	11.5	5	1.06	5/8
17	B5H1Mc	11.5	5	1.06	5/8
18	B5H1Md	11.5	5	1.06	5/8
19	B5L1Ma	5.4	5	1.06	7/16
20	B5L1Mb	5.4	5	1.06	7/16
21	B5L1Mc	5.4	5	1.06	7/16
22	B5L1Md	5.4	5	1.06	7/16
23	B5L1Me	5.4	5	1.06	5/8
24	B5L1Mf	5.4	5	1.06	5/8
25	B5L1Mg	5.4	5	1.06	5/8
26	B5L1Mh	5.4	5	1.06	5/8
27	U5H2Ma	11.5	5	2.0	3/4
28	U5H1.4Ma	11.5	5	1.41	5/8
29	U5H1.4Mb	11.5	5	1.41	5/8
30	B3H1.4Sa	11.5	3	1.41	5/8
31	B3H1.4Sb	11.5	3	1.41	5/8
32	B3H1.4Ma	11.5	3	1.41	5/8
33	B3H1.4Mb	11.5	3	1.41	5/8
34	33H1.4La	11.5	3	1.41	5/8
35	33H1.4Lb	11.5	3	1.41	5/8
36	B3L1.4XLa	5.4	3	1.41	5/8
37	B3L1.4XLb	5.4	3	1.41	5/8
38	B3L1XLa	5.4	3	1.06	5/8
39	B3L1XLb	5.4	3	1.06	5/8

6.2.3.2 Series 2

Series 2 investigated the use of glass fiber anchors with carbon fiber strips. Glass fiber materials are substantially cheaper than carbon fiber materials and considered by some to be easier to work with. However, the strength and stiffness of glass fibers are lower than those of carbon fibers, which is why carbon fiber strips were used in this series but anchored with the cheaper glass

fiber anchors. Several anchor parameters were varied in this series of tests. In all, nine small-scale beam tests were conducted in Series 2.

Concrete beam specimens having the same dimensions and details as those used in Series 1 were used in Series 2.

In this series, the following parameters were held constant across all specimens:

- The anchor embedment depth was 4-in.
- The chamfer at the anchor hole edge had a radius of ½-in.
- The area of the anchor holes was 1.4 times larger than the area of the anchor.
- The anchor fan length was 6-in.
- The anchor patch dimensions were 5 by 5-in.

The parameters varied in this test series were:

1. Width of the CFRP flexural sheet
2. Size of the anchor (ratio of anchor to strip capacity)
3. Bonded and unbonded CFRP sheets

These three parameters were also varied in Series 1.

Similarly to Series 1, 3-in. and 5-in. wide CFRP strips were applied on the beam tension face in this series.

Varying the anchor size was aimed at finding the minimum size necessary for reliably developing the full capacity of the anchored CFRP strip. To do this, the manufacturer specified expected tensile strength of GFRP anchors were normalized by the expected tensile strength of the CFRP strips they anchored to obtain the anchor strength ratio. The GFRP anchor strength ratios used in Series 2 were 1.95, 2.38, and 3.25.

Some beam specimens were installed with a plastic film between the CFRP and the concrete to simulate a fully debonded CFRP strip, while other beams were installed with the CFRP strip fully bonded to the concrete. Exploring the difference between bonding and debonding of the flexural strip provided indication direct measure of the strength of the anchors by removing the beneficial contribution of bond forces.

6.2.3.2.1 Anchor Design for GFRP

Since the size of the GFRP anchors were based on commercial availability, there was little flexibility in manipulating anchor to sheet ratios to achieve the same strength ratios that were used in the research on CFRP anchors. The CFRP anchors used in the previous tests were made in-house, allowing control of the size and amount of material in each anchor. As a result, the CFRP anchor sizes were varied to achieve material ratios of 1.06, 1.41, and 2.0. The material ratio relates the amount of anchor material to the amount of material in the flexural sheet, which is indicative of the strength of the anchor compared to the force the anchor needs to resist in the sheet. In other words, the ratio provides the capacity of the anchor normalized by the capacity of the sheet and will be referred to as the design ratio of the anchor.

In past research, the design ratio was obtained by calculating the cross-sectional area of a CFRP anchor to the cross-sectional area of a CFRP sheet. This was possible because the same CFRP materials were used in the anchor and sheet. To determine a similar ratio for a GFRP anchor, which has different properties than CFRP, the strength of the GFRP needs to be taken into account. As a result, cross-sectional areas are no longer sufficient. Instead, GFRP anchor strength ratios are determined by computing the tensile strength that can develop in the GFRP anchor divided by the tensile capacity the anchor needs to resist in the CFRP sheet. For instance, a design ratio of 2.0 signifies an anchor that has twice the strength of the flexural strip. Equation 6-2 describes how the ratio of anchor strength to flexural sheet strength is calculated.

$$\text{Design Ratio} = \frac{\text{Strength of Anchor}}{\text{Strength of CFRP strip}} = \frac{f_{CFRP} * A_{GFRP}}{f_{CFRP} * A_{CFRP}} \quad \text{Equation 6-2}$$

Where f_{GFRP} and f_{CFRP} represent the manufacture specified expected tensile strength of GFRP and CFRP materials, respectively, in ksi, and A_{GFRP} , represent the equivalent cross-sectional areas of GFRP and CFRP laminates, respectively, in in.².

Example calculation of anchor strength ratio for specimen 9-5-5/8-B1:

	<u>GFRP</u>	<u>CFRP</u>
	Anchor size: 5/8-in.	flexural sheet: 5-in.
	$f_{GFRP} = 470$ ksi	$f_{CFRP} = 550$ ksi
	$A_{GFRP} = 0.0935$ in ²	$A_{CFRP} = 0.041$ in ²
Anchor strength ratio:	$\frac{470 \times 0.0935}{550 \times 0.041} = 1.95$	

6.2.3.2.2 Nomenclature

Specimen nomenclature is shown in Figure 6-21 while a summary of the details of all 9 tests in this series is provided in Table 6-3.

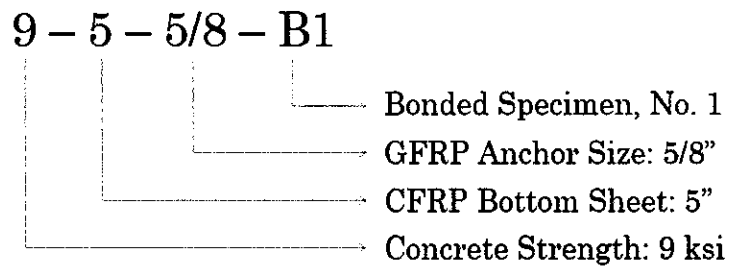


Figure 6-21: Description of specimen nomenclature for Series 2

The parameters in Table 6-3 are explained as follows:

- $f'c$: Concrete compressive strength
- *Width of bottom strip*: Width of CFRP strip reinforcement on the tension face of the beam
- *Width of horizontal strip*: Width of CFRP U-wraps reinforcing the sides of the beam
- *Anchor size*: Nominal diameter of the GFRP anchor provided by the manufacturer
- *Anchor hole diameter*: Inner diameter of the anchor hole
- *Plastic film*: Adhesive sheet introduced to unbond the anchored CFRP strip; “Yes” indicates a plastic film was present, “No” indicates no plastic film was present
- *Anchor strength ratio*: Ratio of the tensile capacity of the anchor to the tensile capacity of the CFRP tensile reinforcement.

Table 6-3: Test details

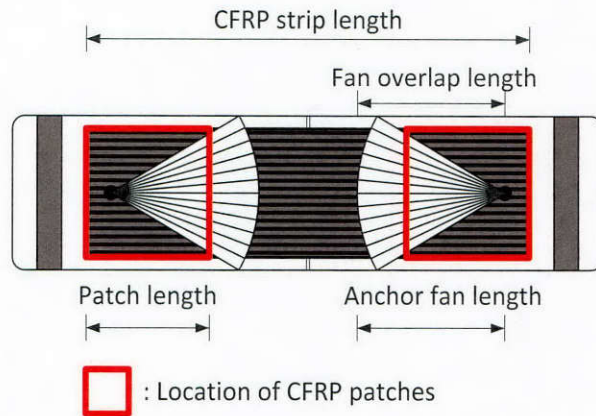
Specimen Name	f'c (ksi)	Width of CFRP strip (in)	Manufacturer provided anchor size (in)	Anchor hole diameter (in)	Plastic film	Anchor strength ratio
9-3-1/2-B1	9	3	1/2	5/8	No	2.38
9-3-1/2-B2	9	3	1/2	5/8	No	2.38
9-3-5/8-B1	9	3	5/8	3/4	No	3.25
9-3-5/8-B2	9	3	5/8	3/4	No	3.25
9-3-5/8-D1	9	3	5/8	3/4	Yes	3.25
9-3-5/8-D2	9	3	5/8	3/4	Yes	3.25
9-5-5/8-B1	9	5	5/8	3/4	No	1.95
9-5-5/8-B2	9	5	5/8	3/4	No	1.95
9-5-5/8-D1	9	5	5/8	3/4	Yes	1.95

6.2.3.2.3 Installation

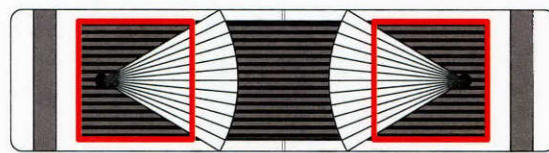
Both preparation of specimens and installation of GFRP/CFRP materials were conducted using the same methodology as in Series 1.

6.2.3.3 Series 3

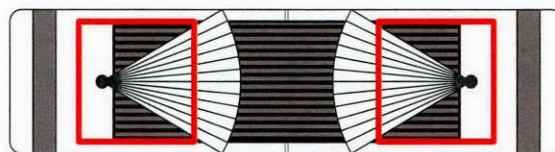
The main objective of this series of test was to explore a new anchor detail. When an anchored CFRP system was installed in a field implementation project as part of the 5-6306 project, it was stated in report FHWA/TX-13/5-6306-01-1 that installation proved to be difficult due to trying to find the anchor hole once the CFRP sheet was placed. There were many suggestions but none were agreed upon at that time. Because of this difficulty in installation, a new detail was explored in which the CFRP sheet stopped just before the anchor hole (Figure 6-22), allowing for easier installation which would save both material and time. Investigation into how well this new detail would work was needed to provide a comprehensive anchor design guideline, which would also be easy to implement in the field. Series 3 consisted of 14 tests that investigated the new anchor detail.



(a) Illustration of parameters



(b) 18-in. long CFRP strip installation with through strip anchor



(c) 15-in. long CFRP strip installation with anchor adjacent to strip

Figure 6-22: Test parameters for Series 3 beams

The same concrete beam design and detailing used in Series 1 and 2 were used in this series of tests. Fixed parameters in this series were as follows:

- The anchor embedment depth was 4-in.
- The bend radius of the anchor hole edge was $\frac{1}{2}$ -in.
- The area of the hole was 1.4 times larger than the equivalent laminate area of the anchor.
- The anchor fan length was 6-in.

The parameters varied in this series were:

1. CFRP strip and anchor fan lengths
2. Bonded and unbonded CFRP sheets

The CFRP strip length was varied and governed the anchor layout as well as the length of the anchor patches. Strip lengths of 32-in., 18-in., 15-in. and 12-in. were selected for this series. The 32-in. strips are longer than the tension face of the concrete beams and wrapped around beam sides. This allowed for the strip strength to be fully developed without anchors and with boundary conditions that minimized uneven stress distributions across the strip width. The performance of this unanchored fully developed layout was compared with those of various anchored layouts to determine whether the anchors were able to fully develop the strength of the CFRP strip without causing premature fracture due to stress concentrations. The 18-in. strip length is shown in Figure 6-22 (b) and corresponds to the anchor layout used in Series 1 and 2. The 15-in. strip length is the new anchor detail where the strip stops just short of the anchor (Figure 6-22 (c)). For the 15-in. strip length, anchor fan length was maintained at 6-in. while the anchor patch dimensions were

maintained at 5-in. square. The 15-in. strip stopped a ½-in. short of the center of the anchor hole. Lastly, the 12-in. strip length provided a layout where the strip was stopped 2-in. away from the center of the anchor hole. The same anchor fan length of 6-in. was used with the 12-in. strip length giving a reduce fan/strip overlap length of 4-in. The anchor patch length, however, was extended in some of the 12-in. strip specimens by 2-in. to maintain a 5-in. overlap length between the patches and the strip.

As in the previous two series, bonded and unbonded conditions were investigated to observe the effect of bonding on anchor and strip strengths

Specimen nomenclature is shown in Figure 6-23. The details of all 14 tests are shown in Table 6-4.

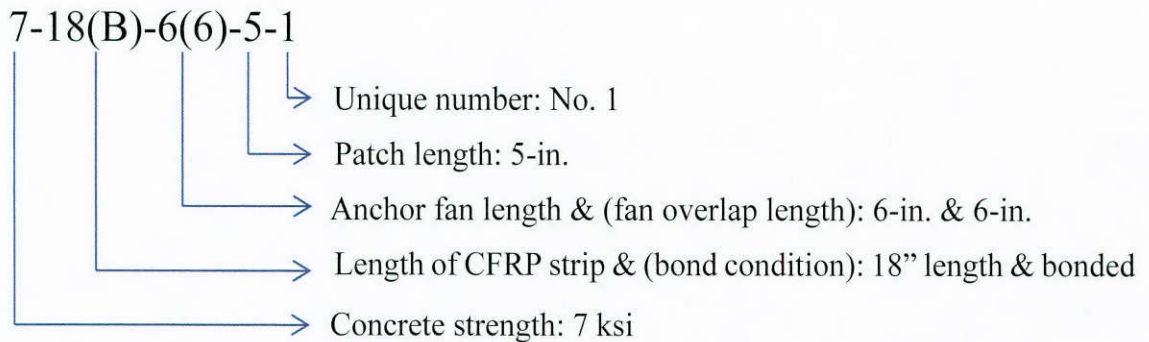


Figure 6-23: Description of specimen nomenclature for Series 3

Table 6-4: Test details

Concrete compressive strength (ksi)	CFRP strip length (in.)	Bond condition	Anchor fan length (in.)	Fan overlap length	Anchor patch length (in.)	Nomenclature
7	32	Bonded (B)	N.A. (N)	N.A. (N)	N.A. (N)	7-32(B)-N-1
						7-32(B)-N-2
		Unbonded (U)				7-32(U)-N-1
						7-32(U)-N-2
	18	Bonded (B)	6	(6)	5	7-18(B)-6(6)-5-1
						7-18(B)-6(6)-5-2
	15	Bonded (B)	6	(6)	5	7-15(B)-6(6)-5-1
						7-15(B)-6(6)-5-2
		Unbonded (U)				7-15(U)-6(6)-5-1
						7-15(U)-6(6)-5-2
	12	Bonded (B)	6	(4)	5	7-12(B)-6(4)-5-1
						7-12(B)-6(4)-5-2
					7	7-12(B)-6(4)-7-1
						7-12(B)-6(4)-7-2

6.2.3.4 Series 4

In series 4, larger beam specimens were used to 1) develop a test for qualifying larger anchorage systems than possible with the smaller beams, and 2) assess the strengths of wider CFRP strips and larger anchors given the size effects uncovered in Series 1.

6.2.3.4.1 Specimen Details

The larger beam specimens followed the same basic design as the smaller beams. The drawings in Figure 6-24 and Figure 6-25 provide the dimensions and details of the beam specimens of this series. The larger beams had dimensions of 12-in.x12-in.x68-in. (Figure 6-24). The new dimensions were selected such that CFRP strips up to 10-in. wide could be tested. The specimen preparation and CFRP installation followed the same procedure followed in the other test series.

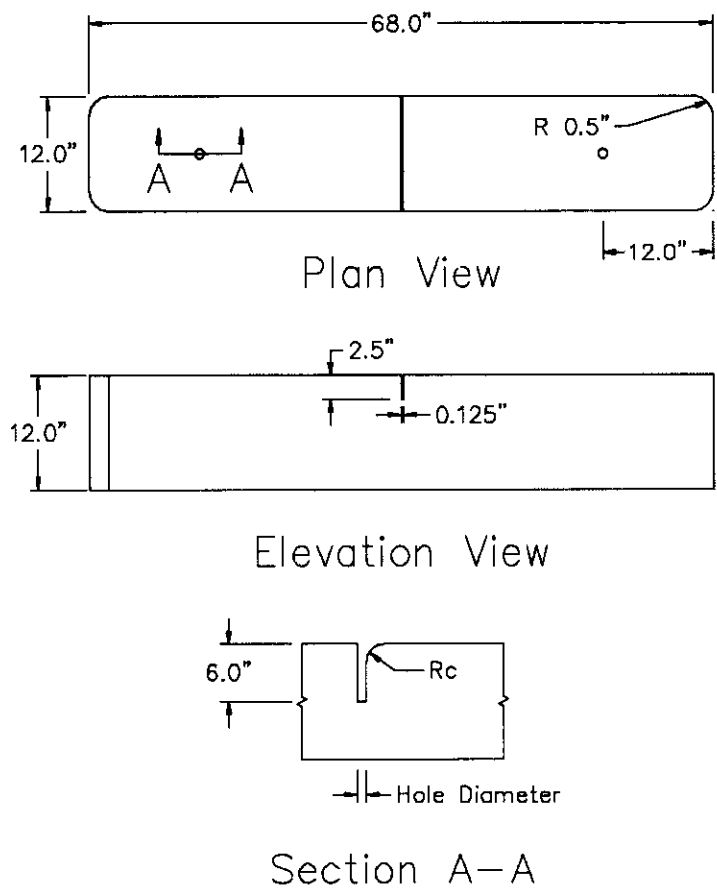


Figure 6-24: Detailed drawings of concrete specimen

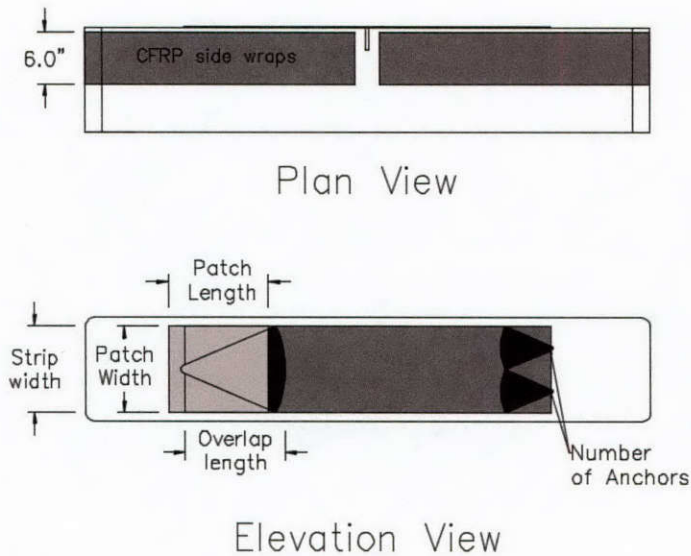


Figure 6-25: Detailed drawings of concrete specimen

At first, steel reinforcement was not used in the beams. However, after one specimen sustained an undesirable concrete failure (Figure 6-26), steel reinforcing cages were added to the specimens (Figure 6-27). The steel cages did not cross the mid-span of the beams and therefore did not affect their flexural strength. Without steel reinforcing, the specimen sustained a concrete failure at $1.38\sqrt{f'_c} * b_w d$ (in psi units), which is much lower than the design value of $2\sqrt{f'_c}$ for concrete in shear. This indicated that the concrete failure was not a pure shear failure but rather a tension failure in the concrete at the anchor edge (Figure 6-28). Therefore, the primary reinforcement was designed to resist the maximum force in the strip. This force was expected to be at most 60 kips for a test specimen with two layers of 10-in. wide strips having a laminate thickness of 0.02-in. and an expected fracture stress of 143 ksi. 6 - #4 bars with a specified yield stress of 60 ksi were introduced as U bars (Figure 6-28) to provide sufficient strength to prevent the tension failure at the anchor edge. Side CFRP U-wraps were also added in the larger beam specimens. Figure 6-28 shows the layout of reinforcing bars used in most of the test specimens in Series 4.



Figure 6-26: Beam specimen failure

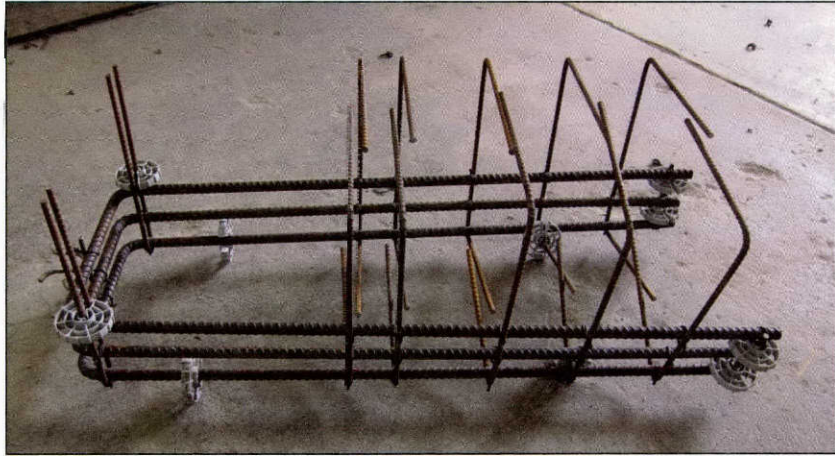


Figure 6-27: Typical steel reinforcing cage used in the larger specimens of Series 4

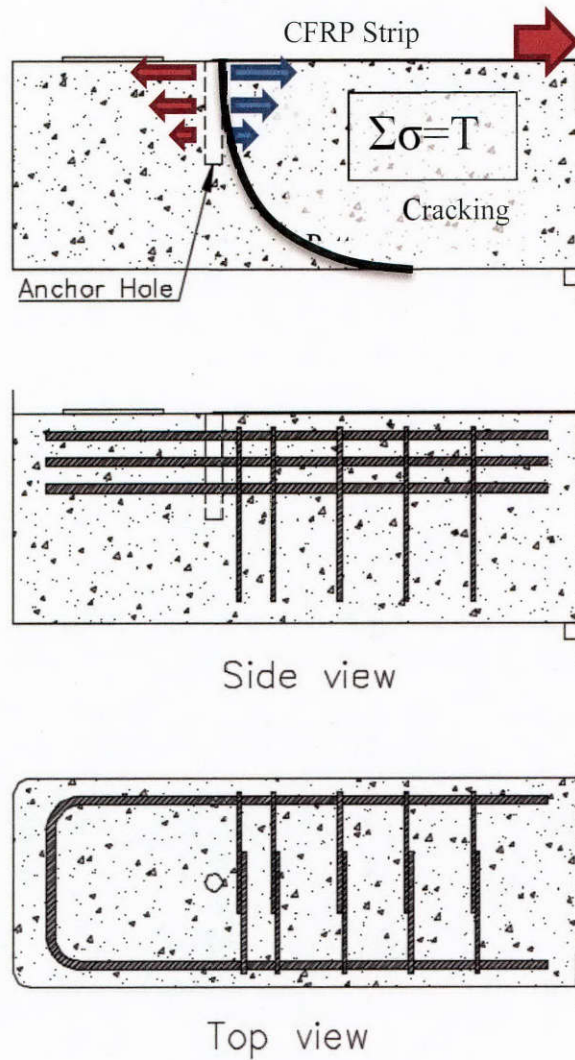


Figure 6-28: Diagram of forces and reinforcing bar layout

6.2.3.4.2 Test Parameters

The following primary parameters were varied in this series:

1. Width of CFRP strip
2. Number of layers of CFRP strips
3. Number of anchors per strip width
4. Ratio of anchor to strip materials
5. Anchor fan overlap length
6. Chamfer radius of anchor hole

These parameters are illustrated in Figure 6-24.

In Series 1, it was observed that increasing the strip width from 3-in. to 5-in. resulted in a lower ultimate tensile stress at strip fracture. In Series 4, this trend was further investigated using strip widths of 5-in., 8-in., and 10-in.

Multiple layers of CFRP strips can be used in applications where a large CFRP tensile strength is required. Single, double, and triple CFRP strip layers were used in this series to evaluate the strength of multi-layer layouts.

The number of anchors per strip width or the effective width of CFRP strip developed by an anchor can affect anchor strip strength in this series, one or two anchors were used over the width of 10-in. wide strips.

The effects of the ratio of anchor to CFRP strip cross-sectional material were investigated further in this series to determine whether size affect anchor performance and the required ratio to fully develop wide strips. Three ratios were used in this series, 1.7, 2, and 2.8.

A 6-in. anchor fan overlap length over the CFRP strip was used in Series 1 through 3. While this length worked well for a single layer of CFRP, it did not for multiple layers. The anchor fan length was increased when developing multiple CFRP layers to maintain the interface bond stress between anchors and strips to below the manufacturer recommended bond strength of 500 psi.

Chamfers of one-half inch radius were recommended in the last project for all holes. This was acceptable for the size of anchors being used in the prior series and project. However, for the fourth series of tests, chamfers were based on a formula of 1.4x radius of hole. This was compared to one test which keeps the 0.5-in. radius recommendation which was about half of what would be recommended based on 1.4x radius of hole.

The following test parameters were either held constant or varied as a function of the primary varied parameters:

- All CFRP strips were fully bonded to the concrete beam tension face
- Anchor patch length and anchor hole size were each varied according to the sectional area of anchor material. Patch length was the same as the anchor overlap length, while hole size was selected as 1.4 times the equivalent anchor laminate area.
- A hole depth of 4-in. was used in some tests, but when larger anchor sizes and chamfer radii were used, a longer hole depth of 6-in. was selected.
- Lastly, the concrete compressive strength varied due to the use of different mixes for the test specimens. Concrete strength ranged from 3.6 to 9.9 ksi.

Specimen nomenclature is shown in Figure 6-29. The details of all 12 tests conducted in this series are shown in Table 6-5.

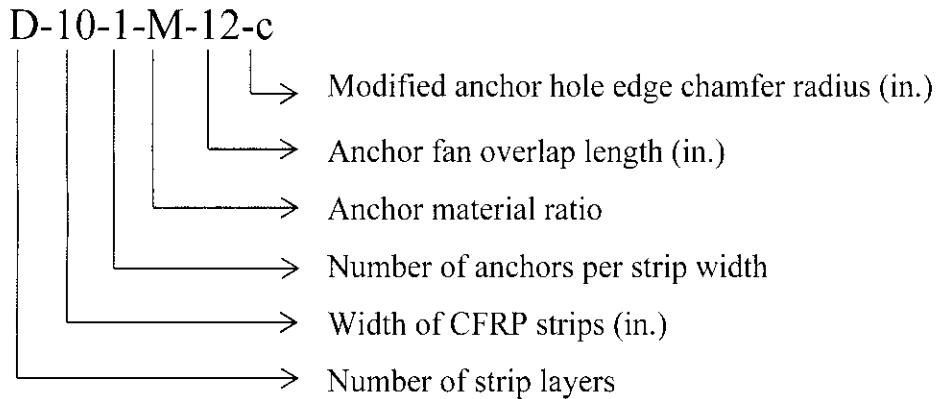


Figure 6-29: Specimen nomenclature

Explanation of nomenclature:

-Number of strip layers: S: Single = 1 layer, D: Double = 2 layers, T: Triple = 3 layers

-Width of CFRP strips: Width of CFRP strips on the tension face of the beam

-Number of anchors per strip width: Configurations with 1 and 2 anchors per strip width are shown in Figure 6-24.

-Anchor material ratio: S: Small = 1.72, M: Medium = 2, L: Large = 2.8

-Anchor fan overlap length: Length of overlap between anchor fan and strip (in.)

-Anchor hole edge chamfer radius: All chamfer radii were 1.4* Hole radius, except for test 11 in which a smaller 0.5-in. chamfer radius was used.

Table 6-5: Test variables for Series 4

Test Variables								
Test #	Number of CFRP strip layers	Width of strip (in.)	Number of anchors per strip width	Anchor material ratio	Anchor fan overlap length	Anchor hole edge chamfer radius (in.)	Concrete Strength (ksi)	Nomenclature
1	1	5	1	1.72	6	0.5	8.8	S-5-1-S-6
2	1	8	1	2	7	0.625	9.0	S-8-1-M-7
3	1	10	2	1.72	6	0.5	9.0	S-10-2-S-6
4	2	5	1	2.8	6	0.75	9.9	D-5-1-L-6
5	1	10	1	2	9	0.625	9.9	S-10-1-M-9
6	2	10	2	2.8	6	0.75	9.9	D-10-2-L-6
7	2	5	1	2.8	12	0.75	5.1	D-5-1-L-12
8	2	10	1	2.8	12	1.125	5.1	D-10-1-L-12
9	2	10	2	2.8	12	0.75	5.1	D-10-2-L-12
10	2	10	1	2	12	0.875	3.6	D-10-1-M-12
11	2	10	1	2	12	0.5	3.6	D-10-1-M-12-c
12	3	5	1	2	18	0.875	3.6	T-5-1-M-18

6.2.4 Data Collection and Processing

6.2.4.1 Instrumentation

For all four series, the same three-point loading configuration was used. The applied load was monitored using a load cell placed adjacent to the loading ram at mid-span of each beam (Figure 6-30). Series 1 to 3 utilized a 25 kip capacity load cell, while series 4 used a 100 kip capacity load cell.

A variety of Linear Voltage Displacement Transducers (LVDT) setups were used to monitor specimen deflection in the four test series. Typically, one LVDT was placed at mid-span to measure beam deflection at the load point, and two others were placed at the reaction points to account for the test frame deformations. Figure 6-30 shows a typical test setup. Series 4 had two LVDT at mid-span on each side of the load point.

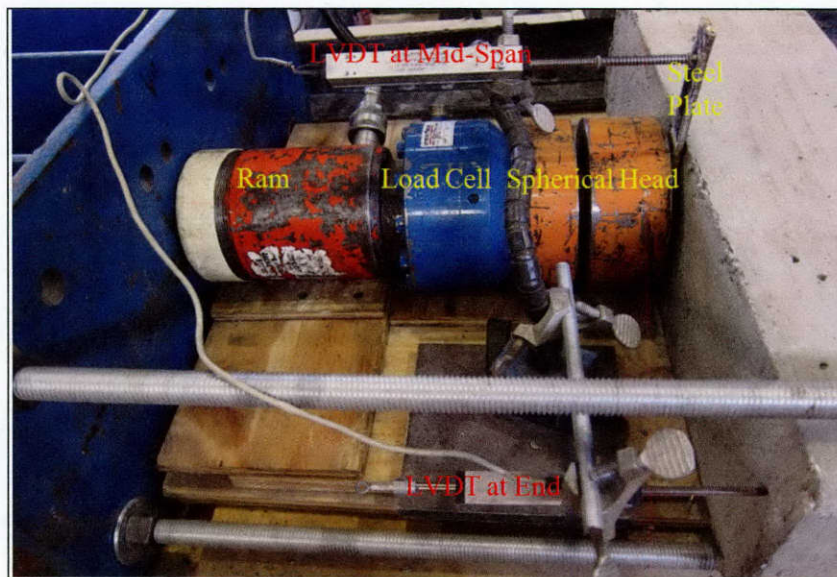
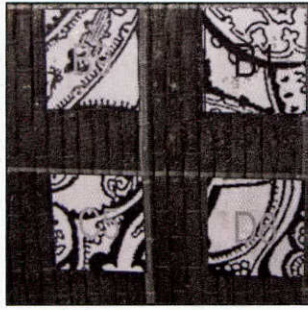


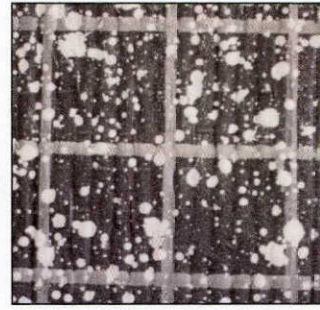
Figure 6-30: Test setup

Strain gauges were applied to measure longitudinal fiber strains at various locations on the surface of the CFRP strips applied to the tension face of beam specimen.

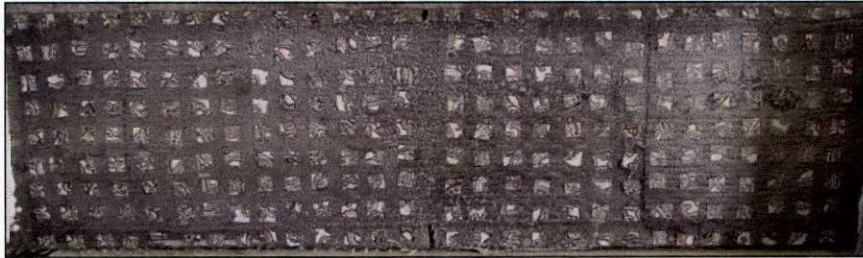
A high-resolution optical measurement system, reported by Sokoli et al. (2014), was used in both Series 1 and 4 to study the 3-dimensional movement and surface strain profiles of the tension face of beam specimens. This system works by using digital image correlation (DIC) to track the three-dimensional movement of targets that are placed on the surface of the beams or CFRP elements. These targets can be either paper squares with high contrast patterns that are glued to the specimen, or a speckle pattern that is painted on (Figure 6-31). Both have been proven to produce reliable measurements, with paper targets providing higher deformation resolution at the expense of longer installation time.



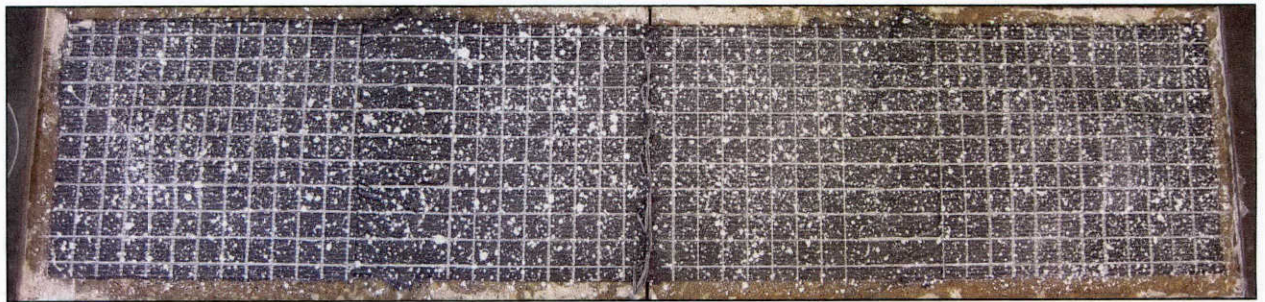
(a) Paper targets



(b) Speckle paint targets



(c) Paper target grid on specimen



(d) Speckle paint target grid on specimen

Figure 6-31: Types of targets

The optical measurement system consisted of two high-resolution cameras (Figure 6-32). The optical measurement system was able to resolve surface strains on the order of 10^{-4} over a gauge length of less than 1-in.

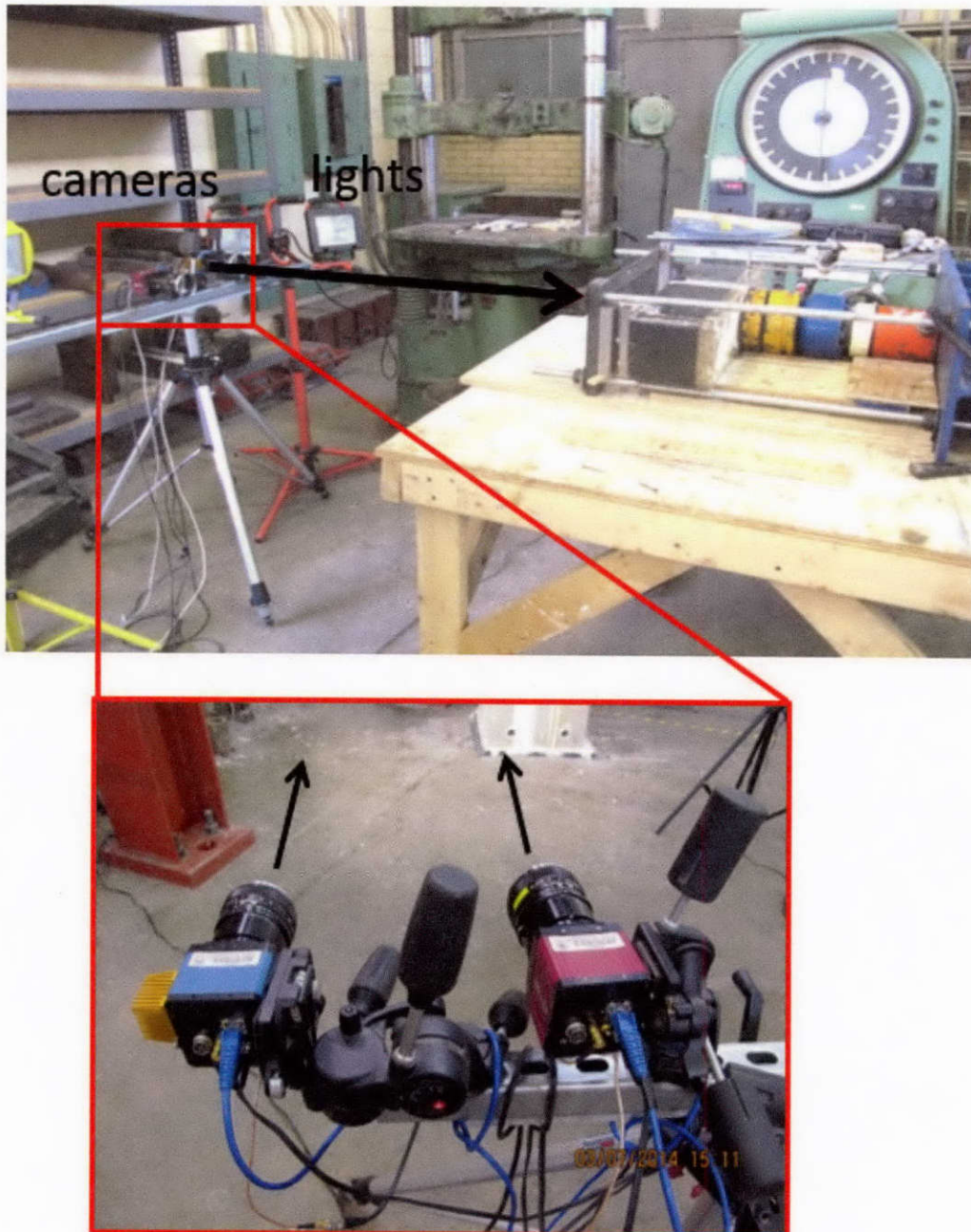


Figure 6-32: Setup of the optical measurement system

6.2.4.2 Data Processing

6.2.4.2.1 Forces

The CFRP strips at the tension face of the beams acted in a similar fashion to flexural steel reinforcement in a concrete beam. The loading setup caused a moment in the beam specimen, which was resisted by a tension force in the strip and a compression-block force in the concrete. Based on the moment applied at mid-span, the force carried by the CFRP in tension was calculated. The average strain in the CFRP was known based on strain gauges or the optical measurement system. Peak strain in the concrete was assumed to be 2.0×10^{-3} . Equation 6-3 through Equation 6-7 were used to find the stress in the strip at failure. These equations can be rearranged into Equation 6-8

where the stress in the strip is the only unknown. For this process, α is assumed to be 0.85, which causes a small error in the stress block depth. However, this assumption greatly simplifies calculations and only causes a minimal error. Because the applied force is known, and the applied moment must equal the internal moment, the equations can be arranged to solve for the tension stress in the strip. Figure 6-33 and Figure 6-34 shows an illustration of forces and strains in the beam specimen.

$$M_a = P * l/4 \quad \text{Equation 6-3}$$

$$M_{int} = j_d * T_f \quad \text{Equation 6-4}$$

$$j_d = h - a/2 \quad \text{Equation 6-5}$$

$$\alpha = \frac{T_f}{0.85 * f'_c * b} \quad \text{Equation 6-6}$$

$$T_f = \sigma_{CFRP} * A_{CFRP} \quad \text{Equation 6-7}$$

$$\frac{P * l}{4} = \left[h - \frac{\sigma_{CFRP} * A_{CFRP}}{2 * 0.85 * f'_c * b} \right] * (\sigma_{CFRP} * A_{CFRP}) \quad \text{Equation 6-8}$$

Where:

M_a : Applied moment calculated based on statics of test setup, kip-in

P : Applied force, kips

l : Span length, in.

M_{int} : Internal moment caused by concrete compression block and CFRP strip tension, kip-in

j_d : Lever arm between concrete and strip forces, in.

T_f : Tension in CFRP strip, kips

a : Depth of compression block, in.

α : Stress block factor, assumed 0.85

f'_c : Concrete strength, ksi

b : Width of specimen, in

σ_{CFRP} : Stress in CFRP at failure, ksi

A_{CFRP} : Cross-sectional area of CFRP, in².

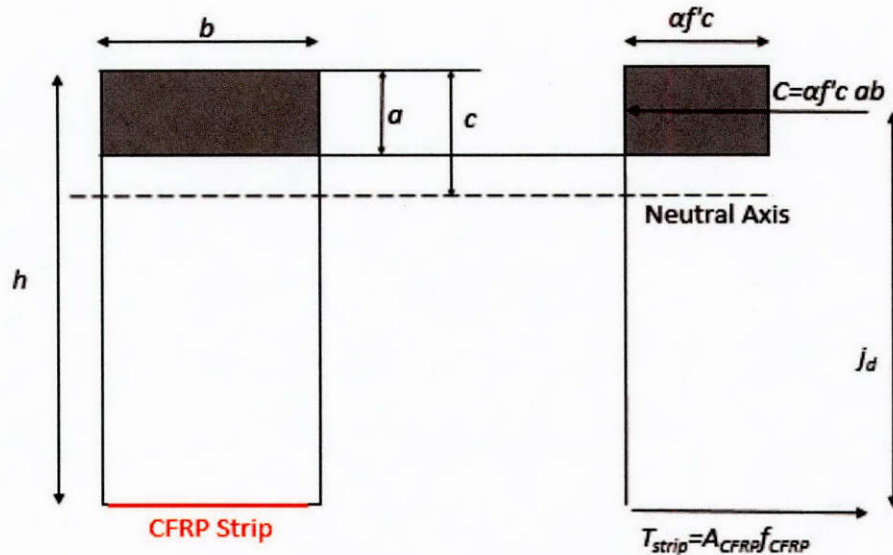


Figure 6-33: Statics of beam specimen

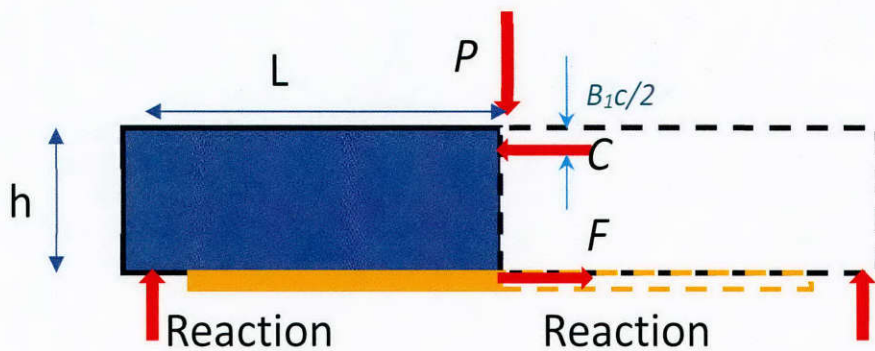


Figure 6-34: Beam equilibrium (Sun, 2014)

6.2.4.2.2 Deformation

LVDTs and the optical measurement system were used to determine the deflection of specimens. In both cases, the deflections of a beam at the reaction points (occurring due to the flexibility of the support rods) was subtracted from the total recorded deflection of the beam at mid-span to obtain the net deflection of the beam between loading and reaction points (Figure 6-35). Additional details on deflection calculations can be found in Sun (2014).

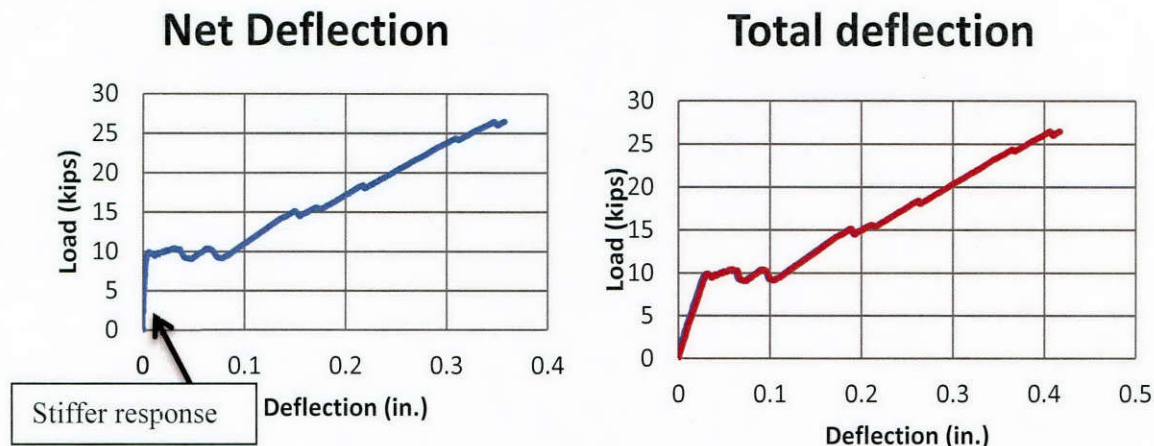


Figure 6-35: Load deflection plots for total and net deflection at midspan

6.2.4.2.3 Strains

Strains were recorded from strain gauges and used to find both average and peak strains. Average strains were calculated by taking the numerical averages of all strain gauges used, and peak was taken as the max strain gauge reading.

Strains at the surface of the CFRP strips were also evaluated using the three-dimensional target location data provided by the optical measurement system. For example, the X-component (or longitudinal) strain ϵ_x in a given frame number (i) is calculated as the change in X-direction distance (Δl_x^i) between two targets divided by the original X-direction distance (Δl) between those two targets (Equation 6-9):

$$\epsilon_x = \frac{\Delta l_x^i}{\Delta l} \quad \text{Equation 6-9}$$

In addition, the targets organized in a grid on the surface were used as nodes to mesh a grid of quad planar elements. The X and Y direction in-plane strains of the elements were calculated through the coordinate changes of four targets assuming linear strain profiles.

Strains were used to evaluate the performance of the CFRP strips and anchors. CFRP surface-strain measurements from the optical measurement system were plotted as contours to locate regions of strain concentrations (Figure 6-36). Surface-strain profiles were also plotted across various sections to better assess strain distributions and associated load paths.

The strain contour plots were analyzed continuously up to failure. At 98% of the maximum recorded load, the maximum CFRP strip strain in the longitudinal fiber direction was extracted ($\max \epsilon_{sx} \text{ mid } 98\% \text{ ult}$). At that same load level, the average longitudinal strain recorded between the edges of anchor fans (Figure 6-37) was also extracted ($\text{mean } \epsilon_{sx} \text{ mid } 98\% \text{ ult}$). Calculating the average strain over the strip area of interest and comparing it to the maximum strain in that same area was useful in examining stress concentrations in CFRP strips. A ratio of maximum strain to average strain was used to quantify the severity of stress concentrations in CFRP strips.

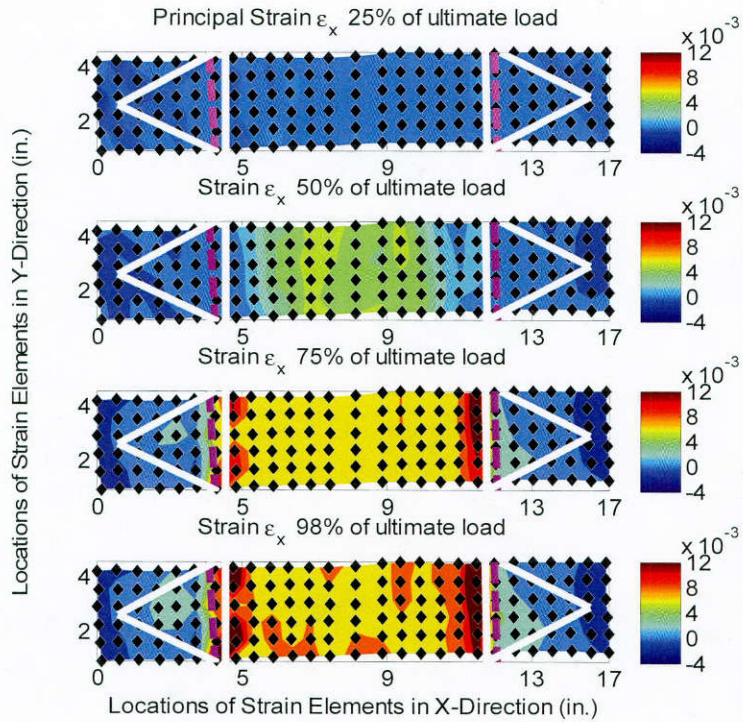


Figure 6-36: Contour plot of strain in the x direction

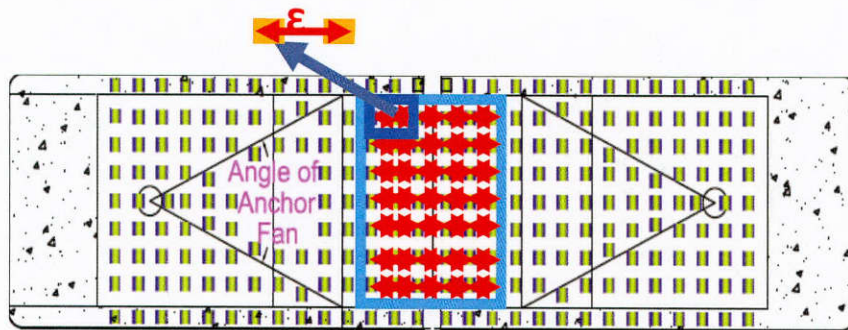


Figure 6-37: Targets used to find average strain and max strain

6.2.5 Material Properties of CFRP and GFRP

All test series used CFRP laminate material to make strips in this study. For series 1, 3, and 4, when CFRP anchors were made, they were made out of this same material, however when premade CFRP anchors were used, they were Composite Anchors. Series 2 used premade GFRP Composite Anchors. Epoxy was used as the adhesive to install FRP material on all specimens. Properties for fiber materials and epoxy are listed in Table 6-6 and Table 6-7 respectively.

Table 6-6: Fiber material properties

Property	CFRP Laminate (Typical test values)	CFRP Laminate (Design values)	Composite Anchors (CFRP)	Composite Anchors (GFRP)
Dry fiber				
Tensile Strength	550,000 psi	-	550,000 psi	470,000 psi
Tensile Modulus	33.4 x 10 ⁶ psi	-	33.4 x 10 ⁶ psi	10.5 x 10 ⁶ psi
Ultimate Elongation	1.7%	-	1.7%	4.5%
Minimum weight per sq. yd.	9.3 oz	-	-	-
Laminate				
Expected Tensile Strength	143,000 psi	121,000 psi	143,000 psi	83,400 psi
Expected Tensile Modulus	13.9 x 10 ⁶ psi	11.9 x 10 ⁶ psi	13.9 x 10 ⁶ psi	379 x 10 ⁶ psi
Expected Ultimate Elongation at Fracture	1%	0.85%	1.2%	2.2%
Thickness	0.02-in.	0.02-in.	-	-

Table 6-7: Epoxy material properties

Property	Epoxy
Tensile Strength	10,500 psi
Tensile Modulus	461,000 psi
Elongation	5%

6.3 TEST RESULTS

In this section, key test results and conclusions from each small-scale beam series are discussed.

6.3.1 Series 1

6.3.1.1 Typical Test

Beam specimens were placed into the testing setup and loaded at mid-span. The beams were placed horizontally on a table for ease of testing as well as allowed for the use of the optical measurement system. Loading was continuous from start to failure. Figure 6-38 shows the typical loading and test setup used for all beams in this series.

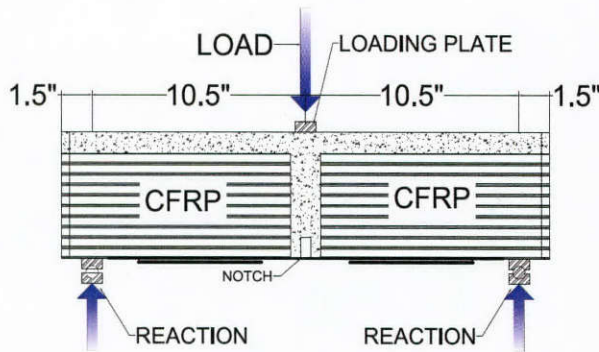


Figure 6-38: Loading and test setup for series 1-3

Typical load deflection plots are shown in Figure 6-39 for specimens with a bonded and anchored CFRP strip. As can be seen in the figure, specimens typically have a linear response up to concrete cracking in flexure. Following cracking, the load-deflection curves experienced a gradual softening due to strip debonding, until most of the load was transferred to the anchors and a nearly linear load-deflection response was again observed. The response was then mostly linearly up to failure. All specimen failures were brittle. Failure modes are discussed in more detail in the next section.

In tests with a bonded tension strip, uniformly distributed longitudinal fiber strains were typically observed prior to beam cracking or 25% of the ultimate load (Figure 6-40). After flexural cracking, debonding between the CFRP strip and the concrete substrate initiated at mid-span and propagated towards the CFRP anchors with increasing applied load, as can be deduced from the increasing CFRP strains spreading away from mid-span with increasing load (Figure 6-40).

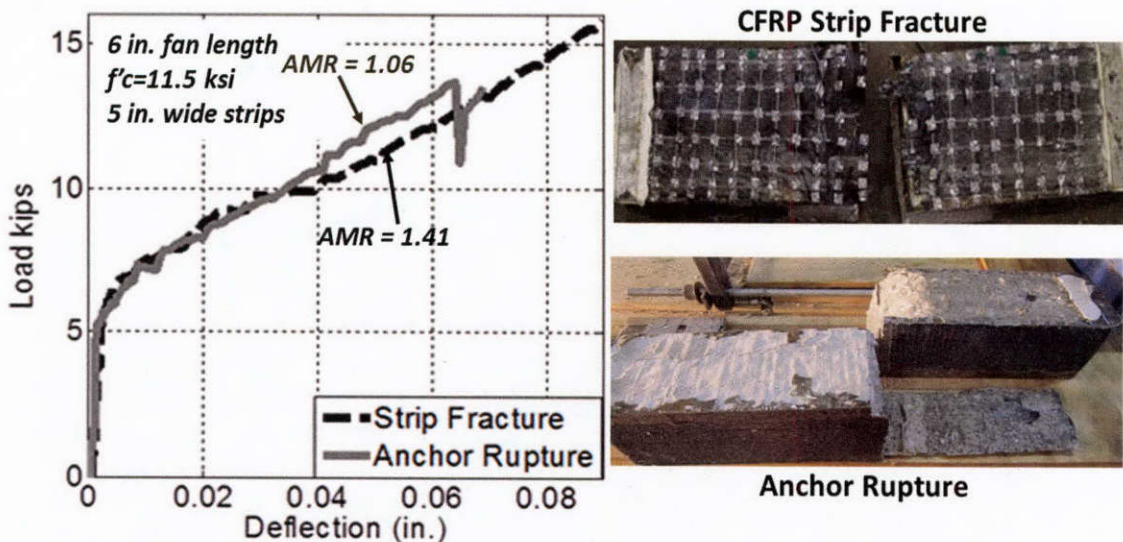


Figure 6-39: Typical load deflection plots for strip and anchor failure modes (Sun 2014)

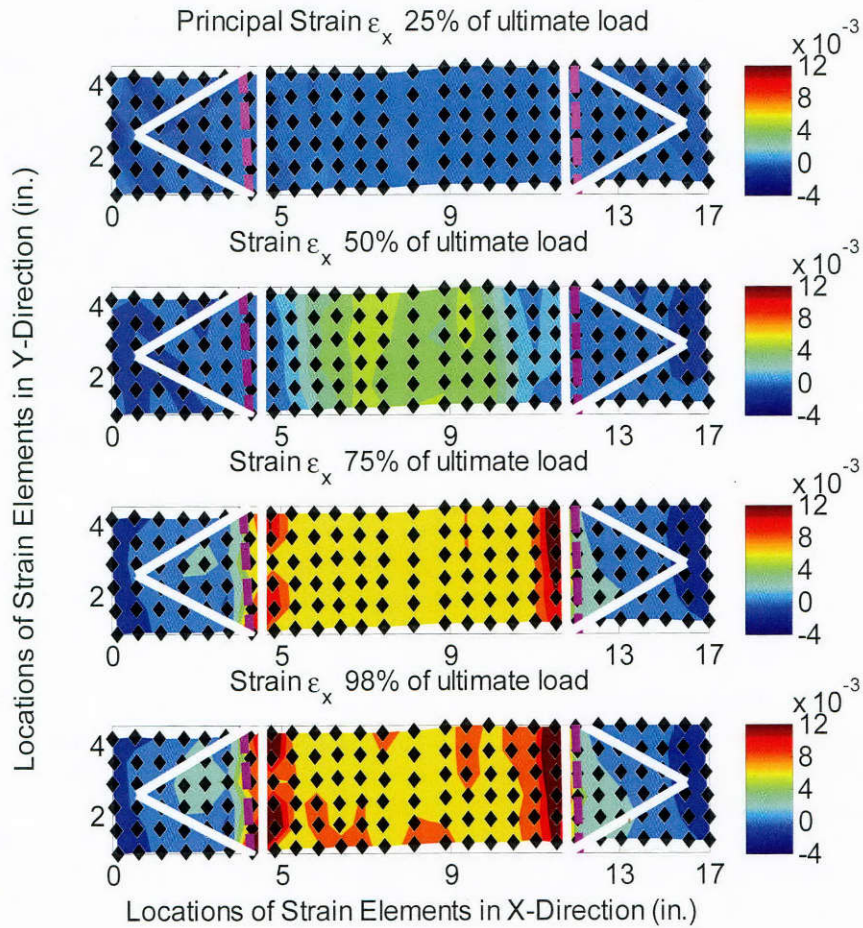


Figure 6-40: Counter plot of strain ϵ_x in the x-direction (longitudinal direction) at various loading stages (Sun 2014)

6.3.1.2 Failure Modes and Implications

Four failure modes were observed for specimens with anchored strips: CFRP strip fracture (Figure 6-39), CFRP anchor rupture (Figure 6-39), concrete failure (Figure 6-41), and delamination between the CFRP strip and the CFRP anchor fans (Figure 6-42).



Figure 6-41: Concrete beam shear failure (Huaco, 2010)

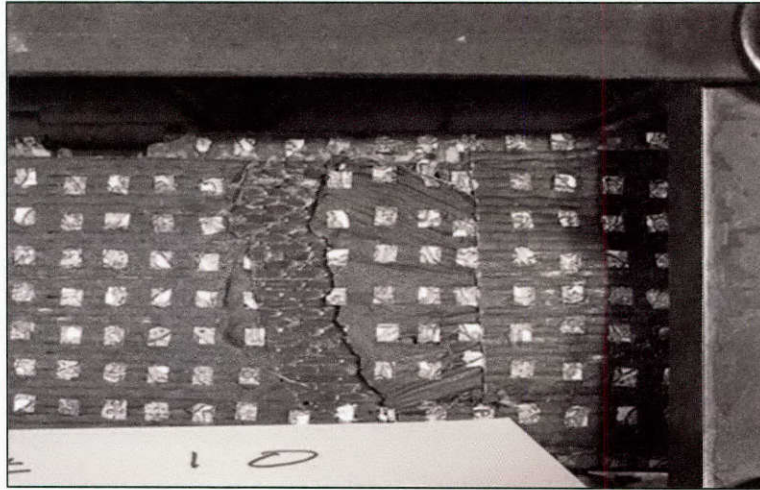


Figure 6-42: Delamination between CFRP strip and anchor

CFRP strip fracture is the most desired failure mode because it results in the highest capacity for a given CFRP strip. This failure mode can only occur if the anchor design and details were adequate to develop the full strength of the strip. CFRP anchor rupture implies the anchor design was not adequate to develop the full force in the strip. These tests are important for quantifying anchor strength. Concrete failures provided valuable information on the capacity of the specimen for quality control tests. The details of the CFRP side U-wraps were gradually improved through this test series to arrive at a design that can reliably develop the strength of a CFRP strip having a tensile strength of up to 14 kips.

Lastly, delamination between the CFRP strip and the CFRP anchor fans indicated that the bond strength between the anchor and strip was not sufficient to fracture the strip. This can happen for two main reasons: 1) the epoxy was of poor quality (e.g., old, contaminated, or poorly mixed epoxy), or 2) an insufficient overlap area was provided between the anchor and strip. This failure mode allows this test procedure to uncover any issues with epoxy quality in field installations.

6.3.1.3 Test Results

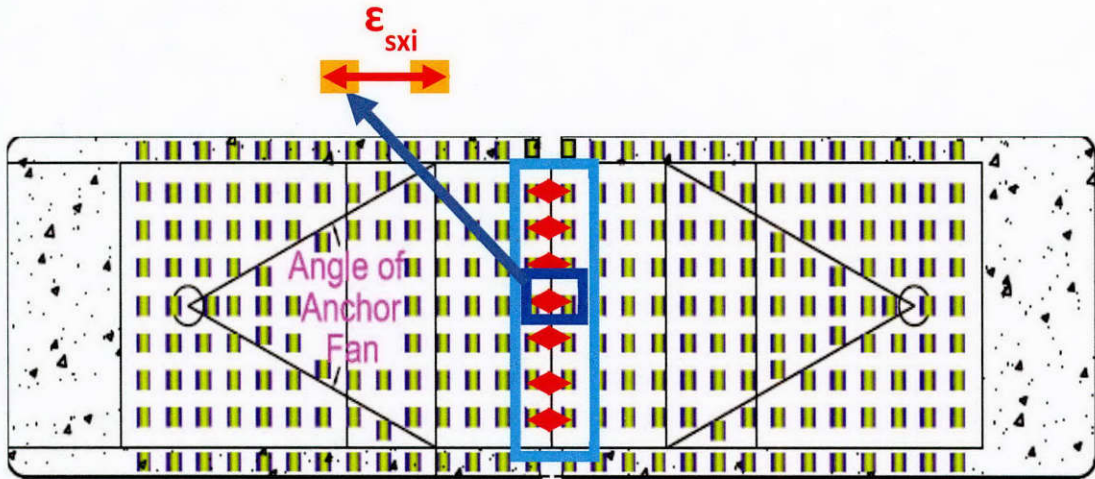
6.3.1.3.1 Overview

Test results were evaluated through the following performance measures: the failure mode, the ultimate applied load from which anchor and strip strengths were derived, and distributed strain measures from which the level of strain concentrations was assessed. A primary objective of this research was to determine characteristics of CFRP anchors that allow them to fully develop the tensile strength of CFRP strips. A qualified CFRP anchorage system is expected to result in the fracture of the CFRP strip. Therefore, the failure mode was used to evaluate the performance of anchorage systems. The ultimate load applied on a beam specimen at failure was also used to evaluate the performance of CFRP anchorage systems. A qualified anchorage system is expected to provide capacities equal to or greater than the expected load at failure derived from the expected CFRP strip strength at failure. Additional details about the Series 1 can be found in Sun (2014).

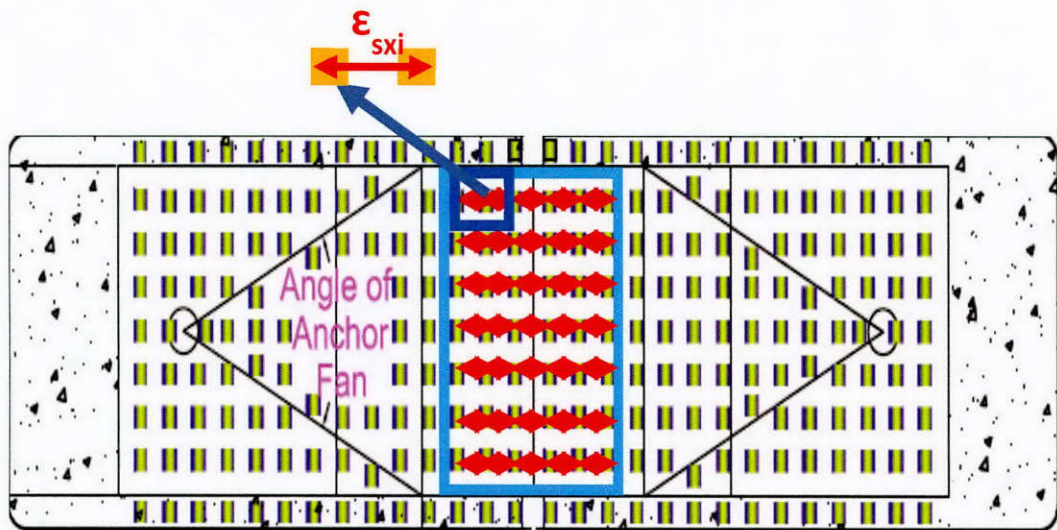
Table 6-8 summarizes the experimental results and main performance measures of the 39 tests conducted, using these notations:

P_{ult}	The ultimate applied load at failure.
P_{des}	The design beam load at failure, which is calculated by equilibrium using the manufacturer specified design stress for the CFRP strip ($\sigma_{des} = 121$ ksi).

P_{exp}	The expected beam load at failure, which is calculated by equilibrium using the expected rupture stress for the CFRP strip provided by manufacturer ($\sigma_{exp} = 143$ ksi).
$F_{f\ mid}$	The strip force at mid-span, which is calculated by equilibrium at ultimate load (P_{ult}) (see 6-2.5.2. Data Processing for derivation).
$\sigma_{fx\ mid\ ult}$	The strip stress at mid-span, which is evaluated at ultimate $load = F_{f\ mid} / A_{CFRP}$ in which A_{CFRP} is the cross-sectional laminate area of the CFRP strip.
$\epsilon_{sx\ mid\ 98\%\ ult} =$	The mid-span strains in the strip fiber direction (X-direction) obtained at 98% of P_{ult} ; measured between the center two targets along the width of the strip at mid-span (Figure 6-43(a)). Its mean value reported in Table 6-8 corresponds to the average strain between targets across the width of the strip.
$\epsilon_{sx\ 98\%\ ult} =$	The strains in the strip fiber direction (X-direction) obtained at 98% of P_{ult} ; measured between adjacent targets over the length between the two anchors along the width of the strip (Figure 6-43(b)). Its mean value reported in Table 6-8 corresponds to the average strain over all target pairs in the measurement area, while the Max values corresponds to the highest individual strain measured between two targets over the same area.



(a) Selected area and targets used to measure the mid-span strip strain $\epsilon_{sx \text{ mid } 98\% \text{ ult}}$



(b) Selected area and targets used to measure the mid-span strip strain $\epsilon_{sx \text{ 98\% ult}}$

Figure 6-43: Area and targets selected for strain measurements

Table 6-8: Summary of experimental results for Series 1

A	B	C	D	E	F	G	H	I	G	K	L
Test Name	Failure Mode	P_{ult} kips	P_{des} kips	P_{ult}/P_{des}	P_{exp} kips	P_{ult}/P_{exp}	$F_{f mid}$ kips	$\sigma_{fx mid ult}$ ksi	Mean $\epsilon_{sx mid 98\% ult}$	Mean $\epsilon_{sx 98\% ult}$	Max $\epsilon_{sx 98\% ult}$
B5H2Ma	Strip Fracture	18.2	13.6	1.34	16	1.14	16.3	163	0.0112	0.0099	0.0158
B5H2Mb	Strip Fracture	18.6	13.6	1.37	16	1.16	16.6	166	0.0109	0.0106	0.0135
B5H1.4Ma	Strip Fracture	15.8	13.6	1.16	16	0.99	14.1	141	0.0101	0.0089	0.0163
B5H1.4Mb	Strip Fracture	16	13.6	1.18	16	1.00	14.3	143	0.0099	0.0106	0.0160
B5H1.4Mc	Delamination	16.1	13.6	1.18	16	1.01	14.4	144	0.0097	0.0092	0.0119
B5H1.4Md	Strip Fracture	16	13.6	1.18	16	1.00	14.3	143	0.0117	0.0101	0.0147
B5H1.4Sa	Concrete Shear	13.4	13.6	0.99	16	0.84	12.0	120	0.0081	0.0079	0.0108
B5H1.4Sb	Anchor Rupture	15.6	13.6	1.15	16	0.98	13.9	139	0.0101	0.0095	0.0151
B5H1.4La	Strip Fracture	18.9	13.6	1.39	16	1.18	16.9	169	0.0113	0.0113	0.0132
B5H1.4Lb	Anchor Rupture	15.6	13.6	1.15	16	0.98	13.9	139	0.0117	0.0117	0.0138
B5L1.4Ma	Strip Fracture	15.8	13.4	1.18	15.6	1.01	14.5	145	0.0097	0.0092	0.0164
B5L1.4Mb	Strip Fracture	14.7	13.4	1.10	15.6	0.94	13.4	134	0.0112	0.0093	0.0134
B5L1.4Mc	Anchor Rupture	17.2	13.4	1.28	15.6	1.10	15.7	157	0.0093	0.0089	0.0111
B5L1.4Md	Delamination	10	13.4	0.75	15.6	0.64	9.1	91	0.0105	0.0089	0.0119
B5H1Ma	Anchor Rupture	15	13.6	1.10	16	0.94	13.4	134	0.0087	0.0087	0.0136
B5H1Mb	Anchor Rupture	15.8	13.6	1.16	16	0.99	14.1	141	0.0102	0.0083	0.0130
B5H1Mc	Anchor Rupture	16.1	13.6	1.18	16	1.01	14.4	144	0.0095	0.0087	0.0126
B5H1Md	Delamination	17	13.6	1.25	16	1.06	15.2	152	0.0118	0.0100	0.0146
B5L1Ma	Anchor Rupture	15.5	13.4	1.16	15.6	0.99	14.2	142	**	**	**
B5L1Mb	Anchor Rupture	11.4	13.4	0.85	15.6	0.73	10.4	104	**	**	**
B5L1Mc	Anchor Rupture	13.7	13.4	1.02	15.6	0.88	12.5	125	0.0089	0.0090	0.0114
B5L1Md	Anchor Rupture	14.8	13.4	1.11	15.6	0.95	13.5	135	0.0087	0.0085	0.0119
B5L1Me	Anchor Rupture	15.4	13.4	1.15	15.6	0.99	14.1	141	0.0105	0.0088	0.0134
B5L1Mf	Concrete Shear	16.9	13.4	1.26	15.6	1.08	15.4	154	0.0103	0.0089	0.0130
B5L1Mg	Concrete Shear	11.1	13.4	0.83	15.6	0.71	10.2	102	0.0088	0.0090	0.0126
B5L1Mh	Anchor Rupture	11.2	13.4	0.84	15.6	0.72	10.2	102	0.0084	0.0085	0.0115
U5H2Ma	Concrete Shear	14.9	13.6	1.10	16	0.93	13.3	133	0.0088	0.0076	0.0126
U5H1.4Ma	Anchor Rupture	14.0	13.6	1.03	16	0.87	12.2	122	0.0082	0.0081	0.0134
U5H1.4Mb	Anchor Rupture	14.8	13.6	1.09	16	0.93	13.2	132	0.0091	0.0087	0.0135

A	B	C	D	E	F	G	H	I	G	K	L
Test Name	Failure Mode	P_{ult} kips	P_{des} kips	P_{ult}/P_{des}	P_{exp} kips	P_{ult}/P_{exp}	$F_{f mid}$ kips	$\sigma_{fx mid ult}$ ksi	Mean $\epsilon_{sx mid 98\% ult}$	Mean $\epsilon_{sx 98\% ult}$	Max $\epsilon_{sx 98\% ult}$
B3H1.4Sa	Strip Fracture	10.4	8.2	1.27	9.7	1.07	9.2	154	0.0090	0.0083	0.0107
B3H1.4Sb	Strip Fracture	11.8	8.2	1.44	9.7	1.22	10.5	174	0.0114	0.0099	0.0128
B3H1.4Ma	Strip Fracture	12.4	8.2	1.51	9.7	1.28	11.0	183	0.0100	0.0106	0.0140
B3H1.4Mb	Strip Fracture	10.4	8.2	1.27	9.7	1.07	9.2	154	0.0099	0.0096	0.0141
B3H1.4La	Strip Fracture	12.6	8.2	1.54	9.7	1.30	11.2	186	0.0096	0.0097	0.0139
B3H1.4Lb	Strip Fracture	10	8.2	1.22	9.7	1.03	8.9	148	0.0103	0.0097	0.0125
B3L1.4XLa	Strip Fracture	10.2	8.1	1.26	9.6	1.06	9.0	151	0.0070	0.0092	0.0148
B3L1.4XLb	Strip Fracture	11	8.1	1.36	9.6	1.15	9.7	162	0.0085	0.0098	0.0123
B3L1XLa	Strip Fracture	10.3	8.1	1.27	9.6	1.07	9.1	152	0.0073	0.0095	0.0145
B3L1XLb	Strip Fracture	11.6	8.1	1.43	9.6	1.21	10.3	171	0.0105	0.0102	0.0155

** Strain data was not available.

6.3.1.3.2 Failure Mode

As shown in Figure 6-44, strip fracture was observed in 18 tests, with only two of those beams failing at a load lower than the expected load, one at 99% and the other at 94% of P_{exp} . Anchor rupture was observed in 14 tests from which only two tests reached the expected load at failure P_{exp} . Delamination between anchors and strips only occurred in three tests and were attributed to a contaminated batch of epoxy. The remaining four tests failed in the concrete. The delamination failures and the two tests with strip fractures that failed to reach the expected load highlight the importance and necessity of developing a standard test methodology for quality control.

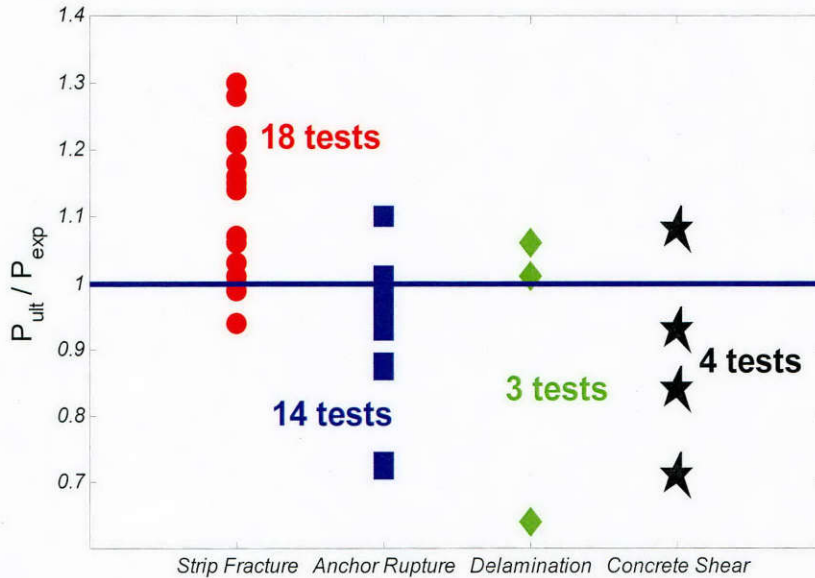


Figure 6-44: P_{ult} / P_{exp} vs. failure modes

6.3.1.3.3 Effects of Width of CFRP Strip

6.3.1.3.3.1 Strip Strength: Directly Comparable Tests

Five directly comparable tests were conducted to investigate the impact of strip width. All parameters except the width of the CFRP strip were kept constant in this comparison. An anchor material ratio of 1.41, high strength concrete and medium anchor-fan lengths were used in all five tests. All tests failed due to strip fracture.

Table 6-9 provides the results of the five directly comparable tests and shows that the wider 5-in. strips developed a mean stress at fracture that is 27 ksi (or 16%) lower than the narrower 3-in. strips. Test results therefore indicate a significant size effect in the strength of anchored CFRP strips.

Table 6-9: Experimental results for effect of strip width on strip fracture

Specimens	Strip Width	$\sigma_{fx \text{ mid ult}} \text{ (ksi)}$	Mean $\sigma_{fx \text{ mid ult}} \text{ (ksi)}$
B5H1.4Ma	5-in.	141	142
B5H1.4Mb		143	
B5H1.4Md		143	
B3H1.4Ma	3-in.	183	169
B3H1.4Mb		154	

In Figure 6-45, the mean and maximum values of $\epsilon_{sx\ 98\% \text{ ult}}$ for the five directly comparable tests are compared. The maximum longitudinal strip strains just prior to strip fracture ranged from 0.0147 to 0.0163 for 5-in. strips. Differences between the maximum and mean strip strains at 98% of the ultimate load ranged from 0.0046 to 0.0074 for 5-in. strips. For 3-in. strips, the maximum strip strains were lower than those for 5-in. strips, and ranged from 0.0140 and 0.0141. Differences between the maximum and mean strip strains in 3-in. strips were significantly lower than those for 5-in. strips, and ranged from 0.0036 to 0.0045. Thus, the wider strips were observed to experience both higher localized maximum strip strains and higher differences between maximum and mean strip strains. These findings indicate that as CFRP strips get wider, strain distributions across their area become less uniform and exhibit higher localized strain concentrations. It should also be noted that one anchor was used at the end of each strip. It is likely that the transfer of stress from the strip to the anchor was less uniform in the wider strips. Since CFRP is a brittle material, higher localized strain concentrations in wider strips may be the cause of their observed weaker strength compared with narrower strips.

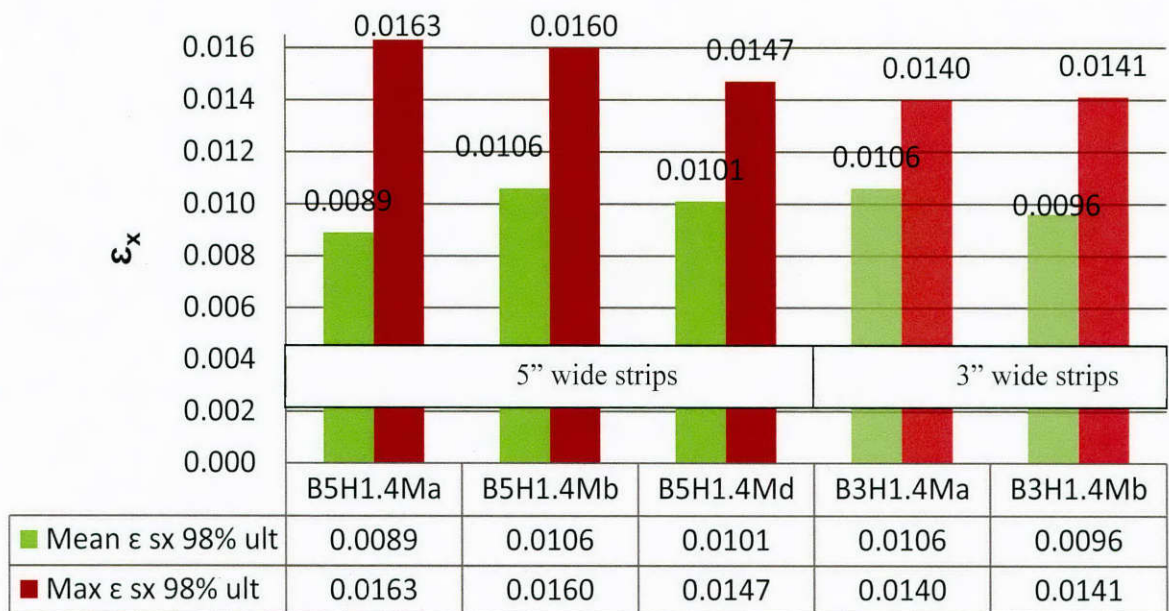


Figure 6-45: Comparison of mean and maximum values of $\epsilon_{sx\ 98\% \text{ ult}}$ for different strip widths

In this series, all CFRP strips were developed by a single anchor at each end. Thus, in this series, the effective width of CFRP strip developed by each anchor increased from 3-in. to 5-in. for the 3- and 5-in. wide strips. Possibly, adding anchors to wider strips to reduce the effective width of CFRP strip developed by each anchor may counter the weaker strength observed in wider strips. Additional tests with wide CFRP strips developed by multiple anchors were conducted in Series 4 to confirm this postulation and will be further discussed in the Series 4 test results.

6.3.1.3.3.2 Strip Strength: Other Tests

Table 6-10 reports strength results for all tests that failed by strip fracture with an anchor material ratio of 1.41. The table contains results for tests with varying concrete strength and fan size, as these parameters were found to have limited influence on strip strength, which will be discussed in later sections. As indicated in Table 6-10, the mean strip stress at strip fracture for six tests with 5-in. strips is 145 ksi; which is 14% lower than that obtained for eight tests with 3-in. CFRP strips (164 ksi).

Table 6-10: Results for tests sustained strip fracture and with an anchor material ratio of 1.41 for different strip widths

Specimens	Strip Width	$\sigma_{fx \text{ mid ult}} \text{ (ksi)}$	Mean $\sigma_{fx \text{ mid ult}} \text{ (ksi)}$
B5H1.4Ma	5-in.	141	145
B5H1.4Mb		143	
B5H1.4Md		143	
B5H1.4La		169	
B5L1.4Ma		145	
B5L1.4Mb		134	
B3H1.4Sa	3-in.	154	164
B3H1.4Sb		174	
B3H1.4Ma		183	
B3H1.4Mb		154	
B3H1.4La		186	
B3H1.4Lb		148	
B3L1.4XLa		151	
B3L1.4XLb		162	

In Figure 6-46 the average for the six tests with 5-in. strips and eight tests with 3-in. strips of the mean and maximum strip strains measured using the optical measurement system are shown. Figure 6-46 corroborates findings observed in Figure 6-45. In Figure 6-46, the wider strips are observed to experience both higher localized maximum strip strains and higher differences between maximum and mean strip strains. The higher localized strip strains may be the cause of the observed lower strip strength in beams with wider CFRP strips.

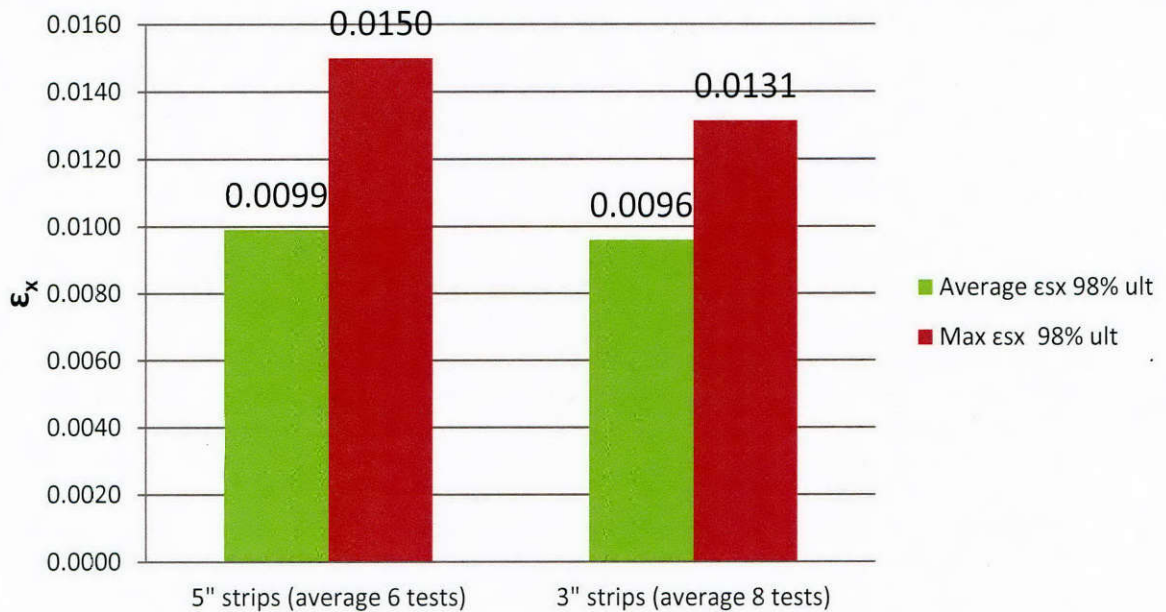


Figure 6-46: Strain comparison between mean and maximum ϵ_{sx} 98% ult for different strip widths tests sustaining strip fracture and with an anchor material ratio of 1.41

6.3.1.3.3 Conclusions

For specimens failing by strip fracture, the ultimate strip stress of all tests using 5-in. strips (145 ksi) was very close to the expected tensile strength provided by the manufacturer of 143 ksi. For tests using 3-in. strips, the ultimate strip stresses at fracture were on average about 15% larger than the expected tensile strength provided by the manufacturer. Strain distributions across the area of a 5-in. CFRP strip were found to be less uniform and exhibited higher localized strain concentrations. The higher localized strain concentrations in wider strips may have caused their observed weaker strength compared with narrower strips. Similar trends were observed when additional tests with 3-in. and 5-in. strip were investigated.

Test results therefore indicate that strength increase of test specimens was less than proportional to the increase in the amount of CFRP material used in the wider strips. Increasing the width of CFRP strips tended to decrease the efficiency of CFRP anchors at developing strip forces. Anchors developing wider strips do not appear to distribute forces as evenly across strips as narrower strips.

6.3.1.3.4 Effects of Material Ratio of CFRP Anchor to CFRP Strip

Tests having anchors with anchor-to-strip material ratios of 1.06, 1.41 and 2.0 were studied to determine the effects of anchor-material ratio on strip and anchor strengths. Twenty-four tests were conducted on 5-in. strips with anchor material ratios of 1.06, 1.41 and 2.0. Another ten tests were conducted on beams with 3-in. strips using anchors with material ratios of 1.06 or 1.41.

6.3.1.3.4.1 Strip Strength: Tests with 5-in. Strips

Five directly comparable tests were conducted on specimens with 5-in. strips and using anchor material ratios of 1.41 or 2.0. All tests had high-strength concrete, medium anchor fan length, and failed by strip fracture. Table 6-11 lists the ultimate strip stress at fracture for the directly comparable tests with 5-in. strips. Results presented in the Table 6-11 indicate that strips with anchors having a material ratio of 1.41 fractured around their manufacturer-provided expected tensile strength of 143 ksi. When anchors having a material ratio of 2.0 are used however, higher strips stresses were observed at fracture by about 14% from those obtained for strips anchored with anchors having a material ratio of 1.41.

Table 6-11: Experimental results for effect of anchor-material ratio on strip fracture

Specimens	Anchor material ratio	P_{ult} (kips)	$\sigma_{fx mid ult}$ (ksi)	Average $\sigma_{fx mid ult}$ (ksi)
B5H1.4Ma	1.41	15.8	141	142
B5H1.4Mb		16	143	
B5H1.4Md		16	143	
B5H2Ma	2.0	18.2	163	165
B5H2Mb		18.6	166	

As can be seen in the Figure 6-47, at the same applied load, anchors with a material ratio of 2.0 had significantly reduced maximum strip strains and differences between maximum and mean strip strains, compared with anchors having a material ratio of 1.41. Therefore, anchors with a larger cross-section are observed to achieve, at a given load, more even strain distributions and lower maximum strains than smaller anchors. Such favorable strain distributions resulted in an increase in the ultimate strip stress at fracture when larger anchors were used.

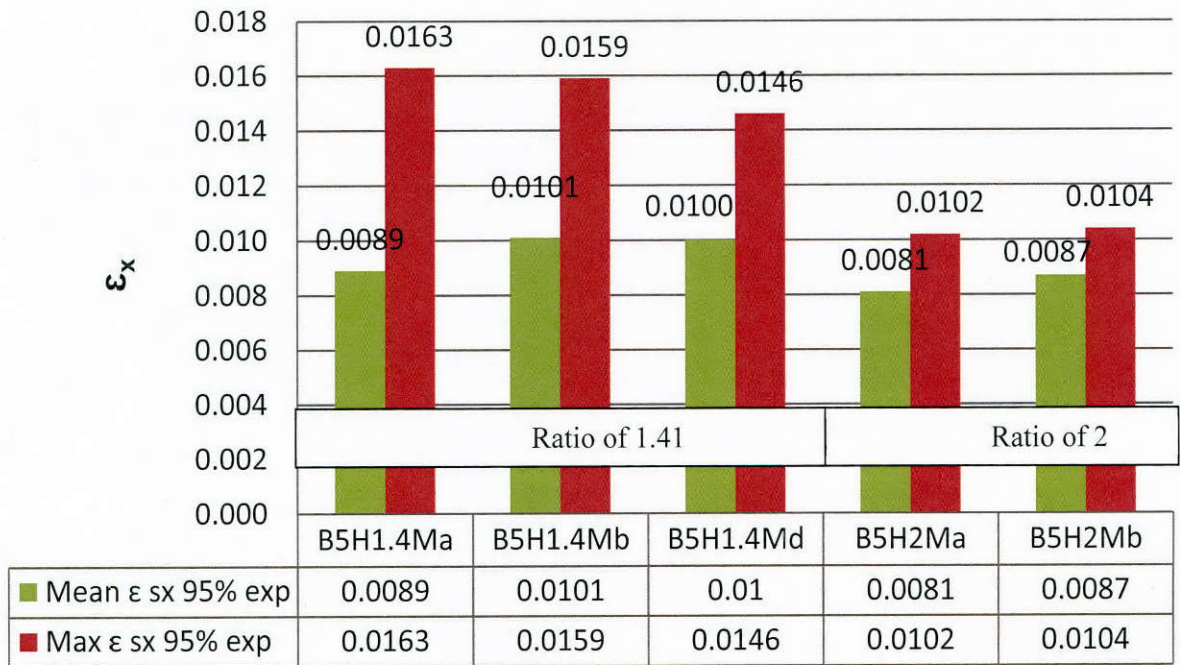


Figure 6-47: Strain comparison between mean and maximum ϵ_{sx} 95% exp for directly comparable tests with 5-in. strips and different anchor-material ratio

Specimens with different concrete strengths and anchor-fan lengths are added to the five directly comparable tests to expand the dataset. As discussed previously, concrete strength and anchor-fan length did not affect strip strength significantly. In Table 6-12, the stress and strain results for two tests with an anchor material ratio of 2.0 and all six tests with anchor material ratio of 1.41 that sustained strip fracture were listed. Results presented in Table 6-12 corroborate findings from the limited set of five tests described above. Overall, increasing the anchor material ratio from 1.41 to 2.0 increased the ultimate strip stress and reduced both the maximum and mean strip strain at a given load.

Table 6-12: Results for strip fracture tests with 5-in. strips

Specimens	Anchor material ratio	$\sigma_{fx\ mid\ ult}$ (ksi)	Average $\sigma_{fx\ mid\ ult}$ (ksi)	Mean ϵ_{sx} 95% exp	Average of Mean ϵ_{sx} 95% exp	Max ϵ_{sx} 95% exp	Average of Max ϵ_{sx} 95% exp
B5H1.4Ma	1.41	141	145	0.0089	0.0097	0.0163	0.015
B5H1.4Mb		143		0.0101		0.0159	
B5H1.4Md		143		0.0100		0.0146	
B5H1.4La		169		0.0110		0.0128	
B5L1.4Ma		145		0.0090		0.0159	
B5L1.4Mb		134		0.0091		0.0130	
B5H2Ma	2.0	163	165	0.0081	0.0084	0.0102	0.0103
B5H2Mb		166		0.0087		0.0104	

6.3.1.3.4.2 Strip Strength: Tests with 3-in. Strips

For tests with 3-in. strips, four directly comparable tests were conducted using anchor material ratios of 1.06 or 1.41. The four tests had normal strength concrete, extra-large anchor fans

lengths and failed by strip fracture. The trend with 5-in. strips was not seen for 3-in. strips. Increasing anchor material ratio from 1.06 to 1.41 for 3-in. strips did not significantly increase the ultimate strip stress. The average ultimate strip stress for tests with anchor material ratio of 1.41 was 157 ksi, which was only 5 ksi less than the average value of tests with anchor material ratio of 1.06. This lack of difference might be attributed to a narrower strip.

6.3.1.3.4.3 Anchor Strength

Anchor rupture occurred only in the tests with 5-in. strips. In Table 6-13, the strip ultimate stress and anchor ultimate stress are listed for six selected tests in which three tests had an anchor material ratio of 1.41 and the remaining three had a ratio of 1.06. Assuming that all the tensile force in CFRP strips at failure was carried by CFRP anchors, the ultimate anchor stress ($\sigma_{ax\ mid\ ult}$) was calculated by $(\sigma_{fx\ mid\ ult} \times A_{CFRP})/A_{anchor}$.

Table 6-13: Results for anchor rupture tests with 5-in. strips and different anchor-material ratios

Specimens	Anchor material ratio	$\sigma_{fx\ mid\ ult}$ (ksi)	Average $\sigma_{fx\ mid\ ult}$ (ksi)	$\sigma_{ax\ mid\ ult}$ (ksi)	Average $\sigma_{ax\ mid\ ult}$ (ksi)
B5H1.4Sb	1.41	139	145	99	103
B5L1.4Mc		157		111	
B5H1.4Lb		139		99	
B5H1Ma	1.06	134	140	126	132
B5H1Mb		141		133	
B5H1Mc		144		136	

Overall, increasing the anchor material ratio from 1.06 to 1.41 slightly increased the average ultimate strip stress at anchor failure from 140 ksi to 145 ksi. The ultimate anchor stress, however, significantly reduced after using anchor material ratio of 1.41. Therefore, increasing the anchor material ratio did not result in a proportional increase in anchor strength.

6.3.1.3.4.4 Conclusions

For beams with 5-in. strips, all with an anchor material ratio of 2.0 failed by strip fracture. Beams with an anchor material ratio of 1.41 sustained strip fractures in six cases, anchor ruptures in three cases, concrete failure in one case, and delamination in the remaining two cases. As for beams with an anchor material ratio of 1.06, none failed due to strip fracture and 75% of the beams were unable to reach the expected load at failure. Test results therefore indicate that an anchor material ratio of 2.0 is needed to reliably fracture 5-in. wide CFRP strips.

For tests with 3-in. strips, the CFRP strip fractured in all ten tests. Eight of these tests had an anchor material ratio of 1.41 and two tests had a ratio of 1.06. All ten tests exceeded the expected load at failure based on a CFRP strip fracture mode of failure. Considering that only two tests had a 1.06 anchor material ratio, it is not possible to estimate the variations that might occur if a larger number of tests had been conducted. Therefore, it is reasonable to suggest that an anchor ratio of 1.41 should be used to reach fracture of 3-in. strips.

For beams with 5-in. strips, those with an anchor material ratio of 2.0 failed at around 115% of the expected load at strip fracture. Increasing the anchor material ratio from 1.41 to 2.0 reduced the strain concentration in a 5-in. strip, which could be observed by the reduction in maximum strip strain as well as the variation between the maximum and mean strip strain. This could be postulated as the reason for a 5-in. strip with anchor material ratio of 2.0 fracturing at a higher ultimate strip stress compared to a ratio of 1.41.

Increasing the anchor material ratio from 1.06 to 1.41 did not result in an increase in 3-in. strip strength

For the tests with 5-in. strips, increasing the anchor material ratio did not lead to a proportional increase in anchor strength when comparing ultimate load at fracture of anchors.

It is interesting to note that no tests in which a 5-in. strip fractured exceeded 120% of the expected load at failure; even when using an anchor material ratio of 2.0. Four tests that fractured a 3-in. strip failed at a greater load than 120% of the expected load at failure. One of them had a 1.06 anchor material ratio, while the remaining three had a ratio of 1.41. It appears that the efficiency of a CFRP anchor at developing the strength of a CFRP strip decreases as the width of the strip increases.

6.3.1.3.5 Effects of Bond

Four directly comparable tests were conducted with the bonding of the CFRP strip to the concrete using epoxy or using a plastic film. In all tests, the anchor-material ratio was 1.41, strips were 5-in. (127 mm) wide, anchor fans were 6-in. (152 mm) long, high-strength concrete was used, and anchor rupture occurred. As shown in Figure 6-48, unbonded specimens failed at ultimate loads lower than the expected applied load at failure (which was 16 kips, 71 kN). In bonded applications, the bond between the CFRP strips and concrete seems to have increased the apparent strength at anchor fracture. The CFRP-concrete bond may distribute anchor stresses more evenly at the anchor area.

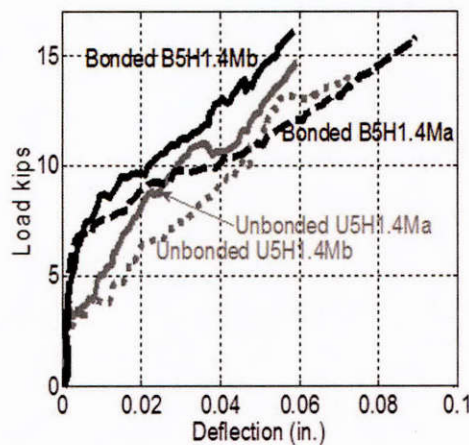


Figure 6-48: Typical load versus deflection responses for tests with different bond condition and $AMR=1.41$ (1 in. = 25.4 mm, 1 kips = 4.45kN)

6.3.1.3.6 Effects of Concrete Strength

6.3.1.3.6.1 Bond Strength

Bond versus slip relations were extracted for tests with 5-in. and 3-in. strips separately. In Figure 6-49, simplified bond versus slip relations between CFRP strips and concrete in test beams are presented. The methodology behind the calculations can be found in Sun (2014) and Sun and Ghannoum (2015). As can be seen in Figure 6-49, the higher strength concrete generates a higher peak bond stress but lower slip at peak stress than the lower strength concrete. The higher peak bond stress and lower slip at peak stress make the ascending slope of the bond vs. slip relation stiffer for higher strength concrete. For the degrading branch, a steeper slope was also observed for specimens with high-strength concrete compared with that of specimens with normal-strength concrete.

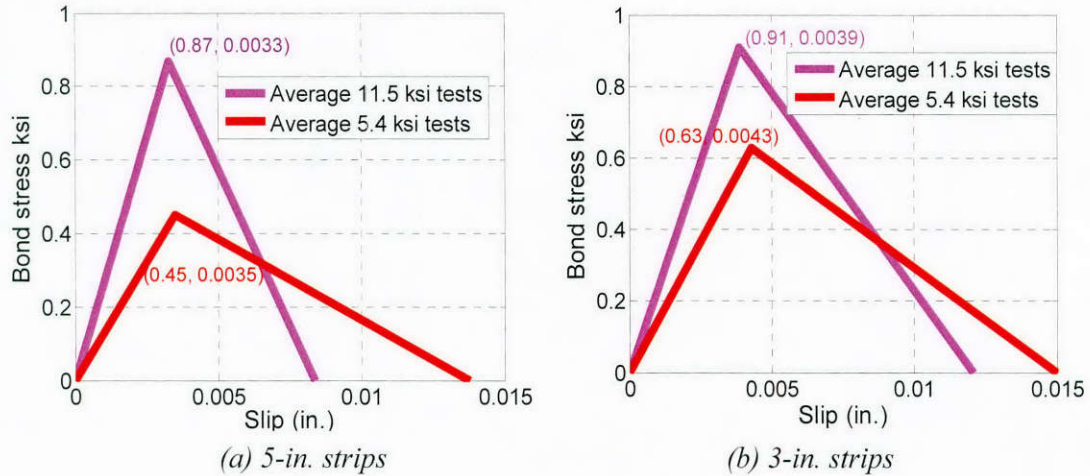


Figure 6-49: Concrete-CFRP bond stress versus slip relations based on the optical measurement data

The peak bond stresses of tests with high-strength concrete were 0.87 ksi and 0.91 ksi, for 5-in. and 3-in. strips respectively. Those values are close to the tensile strength of the high-strength concrete (11.5ksi) which can be estimated as 0.80 ksi. Similarly, the peak bond stress of tests with normal strength concrete (5.4 ksi) were 0.45 ksi and 0.63 ksi, for 5-in. and 3-in. strips respectively, which were close to the tensile strength of the normal concrete (0.55 ksi).

6.3.1.3.6.2 Strip Strength

Five comparable tests were evaluated to study the impact of concrete strength on CFRP strip strength. Every parameter except the concrete strength was kept constant in this comparison. An anchor material ratio of 1.41 was used. CFRP strips were 5-in. wide, and anchor fan lengths were 6-in. in all the tests. All specimens failed by fracture of the CFRP strip. A summary of experimental results for those five tests is presented in Table 6-14.

As shown in Table 6-14, the average ultimate strip stress at mid-span evaluated from beam equilibrium (Average $\sigma_{fx\ mid\ ult}$) was 142 ksi for specimens with high strength concrete and 140 ksi for specimens with normal strength concrete. The concrete strength did not have a significant effect on the CFRP strip fracture stress at failure ($\sigma_{fx\ mid\ ult}$).

Table 6-14: Experimental results for effect of concrete strength on strip fracture

Specimens	f'_c	$\sigma_{fx\ mid\ ult}$ (ksi)	Average $\sigma_{fx\ mid\ ult}$ (ksi)
B5H1.4Ma	11.5 ksi	141	142
B5H1.4Mb		143	
B5H1.4Md		143	
B5L1.4Ma	5.4 ksi	145	140
B5L1.4Mb		134	

6.3.1.3.6.3 Anchor Strength

Seven comparable specimens were evaluated to study the impact of concrete strength on anchor strength. All parameters except the concrete strength were constant. An anchor material ratio of 1.06 was used, CFRP strips were 5-in. wide, and anchor fan lengths were 6-in. in all tests. All specimens failed by anchor rupture. As shown in Table 6-15, the average ultimate strip stress at mid-span evaluated from beam equilibrium (Average $\sigma_{fx\ mid\ ult}$) was 140 ksi for specimens with high strength concrete and 127 ksi for specimens with normal strength concrete. The high strength

concrete resulted in an increase of about 10% in the ultimate strip stress at anchor failure. However, the narrow range of stresses for a small sample of tests is not sufficient to define the role of concrete strength.

Table 6-15: Experimental results for effect of concrete strength on anchor rupture

Specimens	f_c	$\sigma_{fx \text{ mid ult}}$ (ksi)	Average $\sigma_{fx \text{ mid ult}}$ (ksi)	$\sigma_{ax \text{ mid ult}}$ (ksi)	Average $\sigma_{ax \text{ mid ult}}$ (ksi)
B5H1Ma	11.5 ksi	134	140	126	132
B5H1Mb		141		133	
B5H1Mc		144		136	
B5L1Ma	5.4 ksi	142	127	134	120
B5L1Mb		104		98	
B5L1Mc		125		118	
B5L1Md		135		127	

However, as illustrated in Figure 6-50, the tensile force in the CFRP strips can be carried by CFRP anchors and interfacial bond between the CFRP strips and the concrete beams. Possibly, in areas where CFRP strips remain bonded prior to anchor failure, the higher bond strength between the CFRP strips and concrete in high-strength specimens may have increased the apparent strength at anchor fracture. Considering the average peak bond stress were 0.87 ksi for high strength concrete and 0.45 ksi for normal strength concrete, a 13 ksi difference in the average value of ultimate strip stress listed in Table 6-15 may suggest that CFRP strip area around the anchor of about a 3-in.² ($=13 \text{ ksi} \cdot 0.02\text{-in.} \cdot 5\text{-in.} / (0.87 \text{ ksi} - 0.45 \text{ ksi})$) remains bonded until anchor rupture. Due to the speed at which anchor fracture occurs, it is difficult to ascertain experimentally how large a bonded CFRP area is contributing to anchor strength. Another possibility could be that the stiffer higher-strength concrete may help distribute anchor stresses more evenly at the anchor bend.

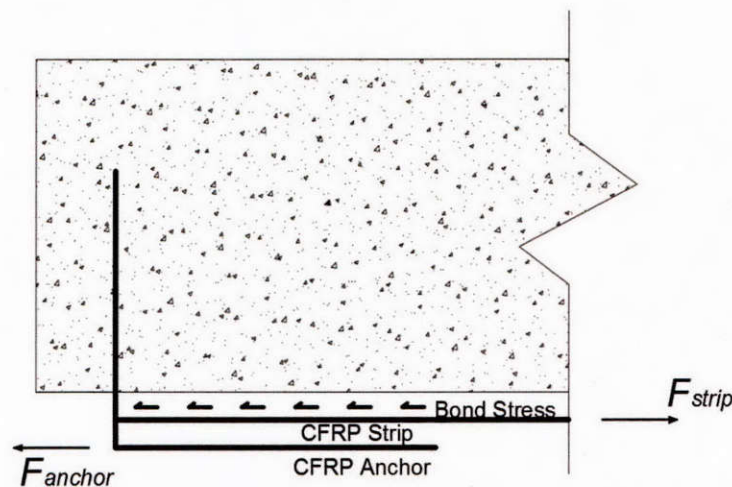


Figure 6-50: Load transfer from CFRP strip to CFRP anchor and concrete

6.3.1.3.6.4 Conclusions

Concrete strength was not found to have a major impact on ultimate CFRP-strip or beam strength. Increasing concrete strength increased the bond strength between CFRP strips and the concrete substrate. Thus, debonding of the CFRP strip occurred at a higher load for higher strength

concrete. A higher concrete strength was found to increase by about 10% the apparent strength of CFRP anchors embedded in it.

6.3.1.3.7 Effects of Anchor Fan length/Anchor Fan Angle

Six comparable tests failing by strip fracture were evaluated to study the impact of anchor fan length/ angle on strip strength. Every parameter except the anchor fan length/angle was kept constant in each group. To effectively develop the strength of CFRP strips, CFRP anchors should be fanned out across the width of CFRP strips. Since strip width was kept the same in each group, the length of the anchor fan determined the anchor-fan angle. All tests had 3-in. wide CFRP strips and high-strength concrete. An anchor material ratio of 1.41 and high-strength concrete were used. A summary of experimental results is presented in Table 6-16.

Table 6-16: Experimental results for effect of fan geometry on strip fracture

Specimens	Fan length/ Angle	$\sigma_{fx\ mid\ ult}$ (ksi)	Average $\sigma_{fx\ mid\ ult}$ (ksi)
B3H1.4Sa	2.4-in.	154	164
B3H1.4Sb	64°	174	
B3H1.4Ma	3.6-in.	183	169
B3H1.4Mb	45°	154	
B3H1.4La	4.5-in.	186	167
B3H1.4Lb	37°	148	

As shown in Table 6-16, all strips fractured at an ultimate strip stress larger than the expected tensile strength provided by the manufacturer (143 ksi). Both the lowest (148 ksi) and highest (186 ksi) ultimate strip stresses were from tests with the large anchor fan length (4.5-in. and 37°). Overall, increasing the fan angle from 37° to 64° did not produce a significant change in the ultimate strip stress at strip fracture.

6.3.1.3.8 Note on Variability in Test Results

Since CFRP is a brittle material and attached on beams made of brittle concrete material, small variations in geometry, material properties, and installation quality can lead to significant variations in overall response. In many cases, several tests were conducted on nominally identical specimens to evaluate such variability.

To illustrate this point, the load versus deflection response of a pair of nominally identical specimens is plotted in Figure 6-51. As can be seen in the figure, responses are typically similar for nominally identical specimens up to concrete cracking. After cracking, variations in installation quality and bond quality and uniformity between the CFRP strips and the concrete surface can result in large differences in beam overall response. Additional information on test variability can be found in Sun (2014).

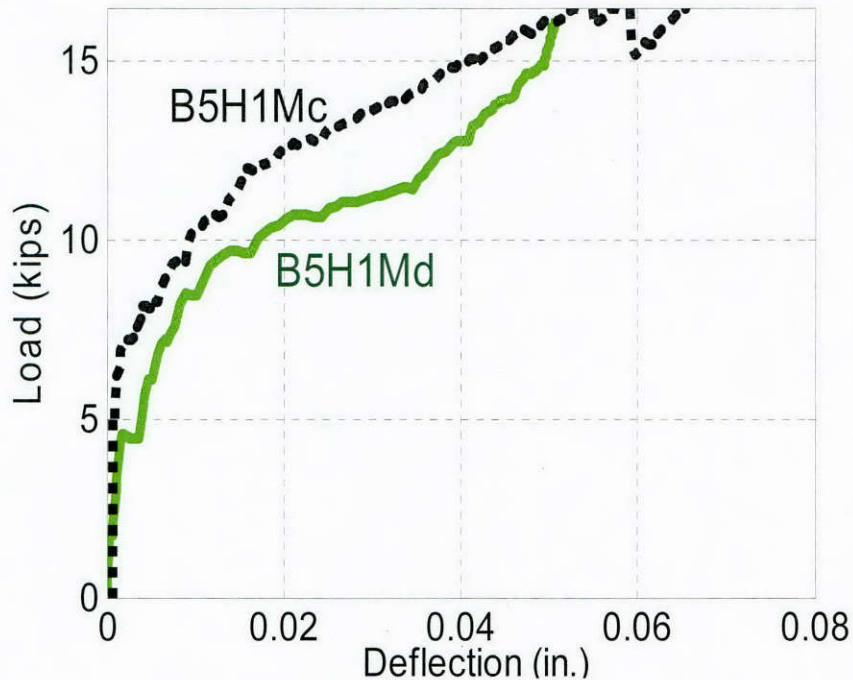


Figure 6-51: Load vs. deflection of nominally identical test specimens

6.3.1.4 Conclusions for Series 1

Failure modes, ultimate load, and strain measurements were used to evaluate the effect of five parameters, 1) width of CFRP strip; 2) anchor-material ratio of CFRP anchor to CFRP strip; 3) bonded and unbonded application 4) concrete strength; and, 5) length/angle of anchor fan, on anchor design.

- Test results have shown that increasing the width of CFRP strips increased strain concentrations, produced a lower ultimate strip stress, and decreased the efficiency of CFRP strips at carrying tensile forces.
- To fracture a 5-in. strip, the anchor material ratio should be no less than 2.0. Increasing the anchor material ratio from 1.41 to 2.0 reduced strain concentrations resulting in higher average ultimate strip stress. An anchor material ratio of 1.41 is recommended for reaching fracture of 3-in. strips.
- Adequately bonding the CFRP strips to the concrete substrate helped to transfer tensile forces from CFRP strips to CFRP anchors, and prevented premature anchor rupture due to strain concentrations.
- Higher concrete strength tended to delay the debonding of CFRP strips from the concrete substrate. Debonding was generally found to occur in the concrete substrate resulting in a layer of concrete adhering to the epoxy as the strip peeled away. A higher concrete strength was found to slightly increase the strength of CFRP anchors embedded in it; however, concrete strength did not affect the ultimate strength of CFRP strips.
- To fully develop tensile strength of a CFRP strip, an anchor-fan angle less than 64° is recommended for anchor design. The application of a smaller anchor-fan angle than 64° (down to 37°), however, had no significant effect on the strength and behavior of the CFRP strengthening system.

6.3.2 Series 2

Series 2 was developed to examine the effectiveness of glass fiber (GFRP) anchors in developing the strength of carbon fiber (CFRP) strips. GFRP strips were not considered due to the relatively low modulus of GFRP compared with CFRP. GFRP anchors were considered as GFRP materials are substantially cheaper than CFRP materials. The specimens were designed to reflect the same parameters as the beams containing CFRP anchors in Series 1. However, the pre-fabricated GFRP anchors used in this project could not be altered to match the exact capacity of previously tested CFRP anchors. CFRP patches were applied over the GFRP anchors in this test Series that consisted of nine beam tests.

6.3.2.1 Typical Test

A typical test in Series 2 was conducted in much the same way as a test in Series 1. The test setup and loading was identical, with major behavioral milestones in Series 2 being similar to those in Series 1. The main difference from Series 1 was that a new failure mode was observed for the GFRP anchors. This failure mode was gradual anchor pullout (Figure 6-52) and was the only mode of failure that was not brittle.



Figure 6-52: Anchor pullout

6.3.2.2 Failure Modes and Implications

The two failure modes observed in this series were CFRP strip fracture (Figure 6-53) and GFRP pullout (Figure 6-54). CFRP strip fracture was observed in four tests—an indication that the GFRP anchor capacity was sufficient to develop the full strength of the CFRP flexural sheet. This is the most desired failure for quality control tests because it acts as the system is designed, with the strip being the weakest link. The other five tests failed by GFRP anchor pullout, a failure mode that was not seen in CFRP anchor systems. In past tests of CFRP anchors, anchor failures occurred by a sudden rupture of the anchor leaving fractured fibers of a CFRP anchor exposed and completely separating the CFRP sheet from the concrete. The GFRP anchors in this specimen failed in a less abrupt manner, pulling out of the concrete instead of rupturing. This difference in failure mode between GFRP and CFRP anchors may result from the differences in their material properties.

GFRP, in its dry fiber form, has significantly more deformation capacity than the dry fibers of CFRP, having a fracture strain of 4.5% compared to the fracture strain of 1.7% of CFRP. Even though saturating the fibers with epoxy reduces the deformation capacity of the materials, the fracture strain of the laminate GFRP is 2.2% and still higher than the laminate CFRP fracture strain of 0.93%. It is possible that the strains occurring in the anchors are large enough to cause rupture of CFRP anchors but are not large enough to cause rupture of GFRP anchors, therefore leading to an elongating behavior.

In an effort to investigate the anchor pull-out failure further, the beams that exhibited pull-out were cut open, and the anchors and hole conditions were examined more closely. The conditions found inside the anchor hole indicated that the GFRP anchors were well bonded to the concrete, stripping off pieces of concrete as the anchor was pulled out of the specimen.

It was noted that epoxy did not seem to fully cover the insides of the anchor, leaving voids in the opening between the anchor fold and possibly throughout the anchor fibers. The presence of voids can contribute to a reduction in anchor strength, causing the anchor to pull out of the specimen. The figures below show the exposed GFRP anchor and the anchor hole condition of several specimens (Figure 6-54 and Figure 6-55). This unexpected failure mode could be due to insufficient use of epoxy during installation, contamination or poor handling of materials, or an indication that a larger anchor is necessary.



Figure 6-53: CFRP strip fracture

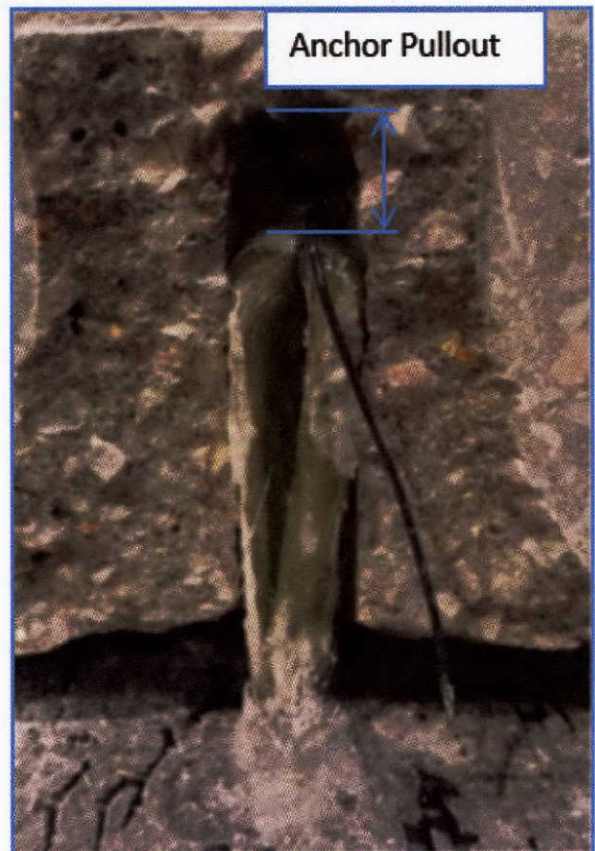


Figure 6-54: GFRP pullout, sectional view

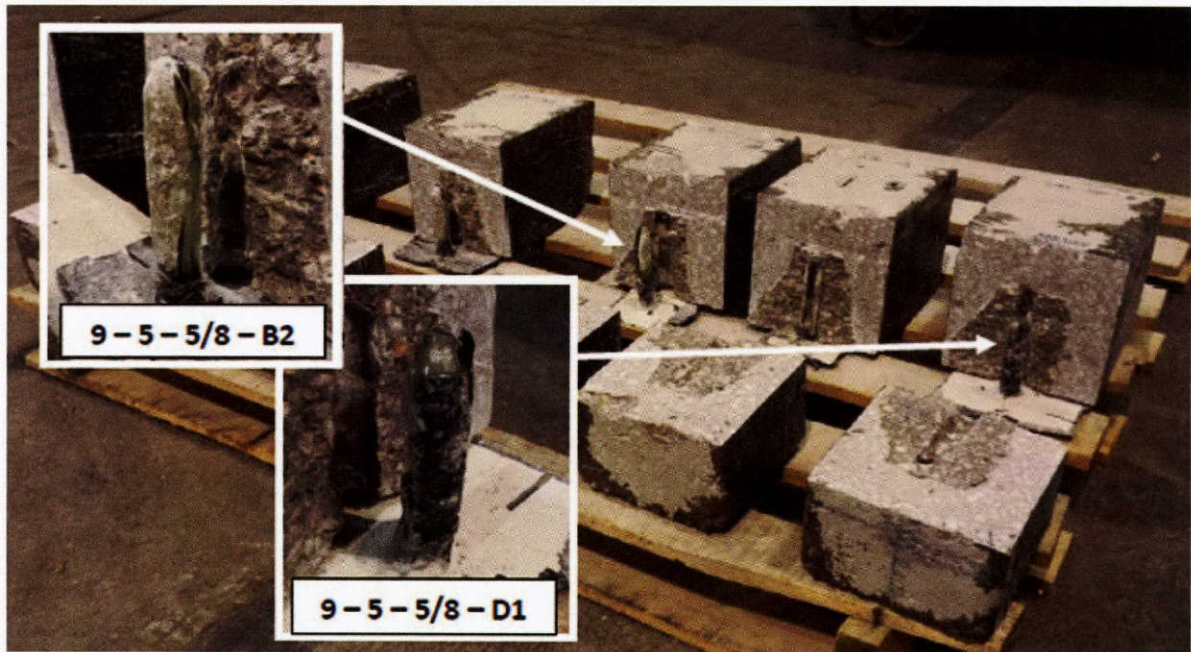


Figure 6-55: Specimens with GFRP anchors exposed

6.3.2.3 Test Results

6.3.2.3.1 Overview

Table 6-17 summarizes the ultimate load and failure mode for all beams tested. The tests can be categorized into four groups: specimens with a bonded 3-in. CFRP strip, specimens with an unbonded 3-in. strip, specimens with a bonded 5-in. strip, and specimens with an unbonded 5-in. strip. Additional details about Series 2 can be found in Wang (2013).

Table 6-17: Summary of experimental results for Series 2

Specimen Number	f'_c (ksi)	Width of CFRP Sheet (in)	Anchor Strength ratio	Expected load (P_{exp}) (kips)	Ultimate Load (P_{ult}) (kips)	P_{ult} / P_{exp}	Failure Mode
9-3-1/2-B1	9	3	2.38	9.5	12.7	1.34	Strip Fracture
9-3-1/2-B2	9	3	2.38	9.5	12.2	1.28	Strip Fracture
9-3-5/8-B1	9	3	3.25	9.5	11.4	1.20	Strip Fracture
9-3-5/8-B2	9	3	3.25	9.5	10.1	1.06	Strip Fracture
9-3-5/8-D1	9	3	3.25	9.5	10.3	1.08	Anchor Pullout
9-3-5/8-D2	9	3	3.25	9.5	9.87	1.04	Anchor Pullout
9-5-5/8-B1	9	5	1.95	17	18.1	1.06	Anchor Pullout
9-5-5/8-B2	9	5	1.95	17	17.8	1.05	Anchor Pullout
9-5-5/8-D1	9	5	1.95	17	14.0	0.823	Anchor Pullout

6.3.2.3.2 Anchor Performance

The load-strain data from beam tests using GFRP anchors and beam tests using CFRP anchors are compared for two categories of beams: beams constructed with bonded 5-in. CFRP strengthening strips and bonded 3-in. CFRP strengthening strips.

6.3.2.3.2.1 Bonded CFRP Strip – 5 in.

Two tests with CFRP anchors using a 5-in. bonded CFRP flexural sheet for an anchor material ratio of 2.0 are compared with two tests having the same parameters but GFRP anchors (9 – 5 – 5/8 – B1 and 9 – 5 – 5/8 – B2). The GFRP specimens had an anchor design ratio of 1.95.

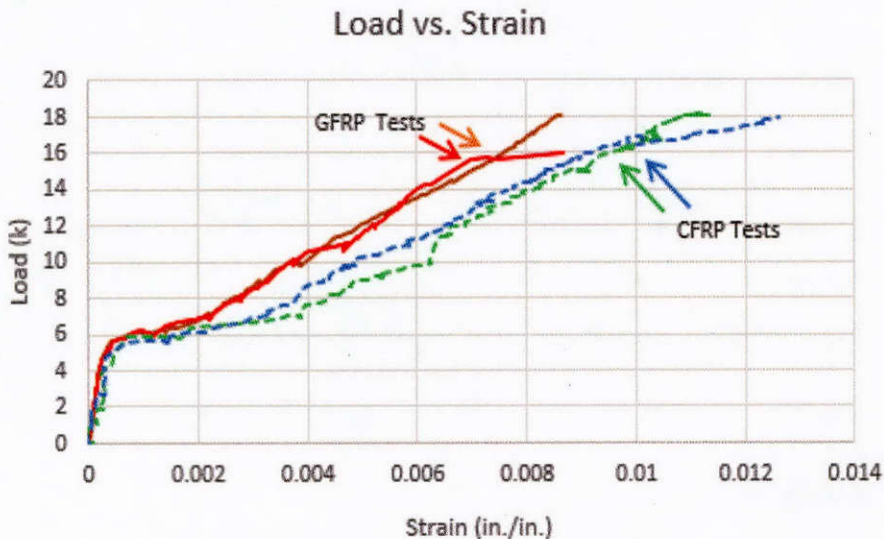


Figure 6-56: Load versus strain for 5-in. bonded specimens

The applied load versus mid-span strain behaviors are compared for the specimens with GFRP anchors and the specimens with CFRP anchors in Figure 6-56. The following comparisons are made using average strain values across the mid-span section, which allows for a better comparison between the multiple specimens.

The four specimens exhibited identical linear behavior until the concrete first cracked. Cracking occurred at around 6 kips, after which a plateau in the plot indicates deformations occurring in the flexural sheet as forces are transferred from the cracked concrete. The force transfer to the CFRP sheets in the specimens occur over approximately the same strain differential. Failure loads are around 18 kips for all specimens. From the comparison of data shown in Figure 6-56, the specimens constructed with CFRP anchors reached larger strains in the flexural sheet for the same loads compared to the specimens constructed with GFRP anchors.

6.3.2.3.2.2 Bonded CFRP Strip – 3-in.

Two tests with CFRP anchors using a 3-in. bonded CFRP flexural strip are compared with GFRP specimens 9 – 3 – 1/2 – B1 and 9 – 3 – 1/2 – B2. The anchor material ratio for the CFRP anchors was 1.41, and the anchor design ratio for the GFRP anchors was 2.38. Specimens having a closer match were not available. The specimens with CFRP anchors in this comparison had varying anchor fan lengths of 2.4 inches and 3.6 inches. Varying the anchor fan length was not a parameter considered in the test of GFRP anchors. However, the effects on anchor performance due to fan length were found to be minimal in Series 1 and thus these tests were determined to be appropriate for comparison. Figure 6-57 shows the load-strain comparison of the four specimens.

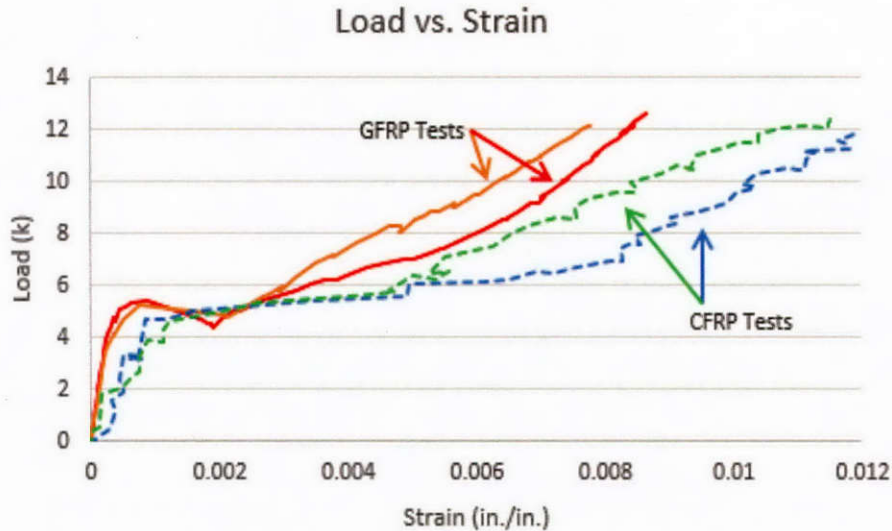


Figure 6-57: Load versus strain for 3-in. bonded specimens

All comparable specimens failed around 12 kips by strip fracture. Again, it is shown that the beams constructed with CFRP anchors reached larger strains in the flexural sheet compared to the specimens constructed with GFRP anchors for the same loads.

While cracking and strength gain behavior appear to differ significantly between 3-in. bonded specimens containing GFRP anchors and those containing CFRP anchors, all of the specimens in this comparison reached a capacity of 12 kips. This suggests that the GFRP anchors are just as capable of developing the full capacity of the flexural strip as CFRP anchors. Failure modes were also consistent among the four specimens, occurring by rupture of the flexural strip, however, GFRP specimens had a much larger anchor material ratio compared to the CFRP specimens. It is also important to note that GFRP anchors resulted in fracturing the CFRP flexural strip at lower recorded strains.

6.3.2.4 Conclusions

From the results in this study, GFRP anchors were able to develop the capacity of externally bonded CFRP reinforcement with common trends in behavior and similar modes of failure as CFRP anchors. However, there are both advantages and disadvantages of using GFRP materials in place of CFRP despite the similarities in performance.

An advantage of using GFRP materials may be attributed to its larger deformation capacity compared to CFRP materials. At more than twice the tensile strain capacity of CFRP, GFRP can be more useful for applications that require bending of the fibers, resulting in lower stress concentrations at the bends and possibly reducing bend radius requirements. During installation, it was also found that GFRP anchors were easier to insert into the anchor hole because the anchors were able to slip through the fibers of the CFRP sheets more easily. In addition to easy handling, it was also observed that anchor failures of GFRP anchors occurred much less abruptly than CFRP anchor failures. Since the GFRP anchors pulled out of the beams instead of rupturing, the CFRP strengthening sheet remained mostly in contact with the concrete.

Despite the positive aspects of using GFRP materials in anchor systems, disadvantages were also apparent. The most obvious disadvantage of GFRP materials is its low tensile strength compared to CFRP. As a result, a greater amount of fibers is needed to design a GFRP anchor of equal capacity to a CFRP anchor. The result is a bulkier anchor that may lead to difficulties during installation, cancelling out the advantages of the smoother installation mentioned above.

It is also important to note that GFRP anchors resulted in fracturing the CFRP flexural strip at lower recorded strains. With CFRP anchors, all CFRP strips that ruptured did so after passing the manufacturer's rupture strain. On the other hand, when GFRP anchors ruptured CFRP strips, the strips fractured below the manufacturer's stated rupture strain. This cannot be explained and would need further investigation to understand the behavior.

Overall, most benefits of GFRP anchors were outweighed by negative consequences, therefore these results suggest CFRP anchors be used until further testing of GFRP anchor prove their usefulness.

6.3.3 Series 3

This series was developed to investigate the effectiveness of anchors placed adjacent, rather than through, a CFRP strip, in developing strip strength. Tests in this series were conducted and unfolded in a very similar manner to tests of Series 1. The test setup and loading protocol was identical, however only strain-gauge and load data were recorded.

In all, 14 tests were conducted in Series 3. The failure modes for this series of tests were strip fracture, anchor rupture, delamination, and concrete failure. All of these failure modes have been previously discussed for Series 1. Two strain gauges were placed at mid-span and symmetric about the centerline of the beam (Figure 6-58). These two gauges were averaged to determine the strain at mid-span across the width of the strip at ultimate load (ϵ_{ult}).

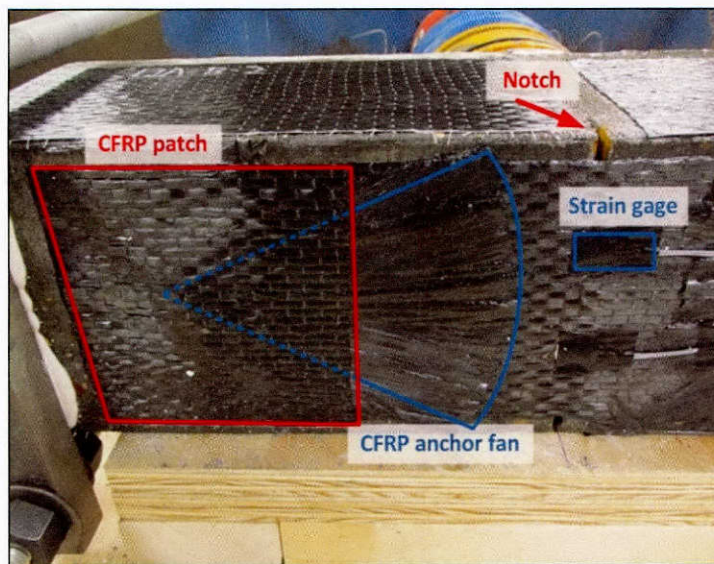


Figure 6-58: Location of strain gauges

6.3.3.1 Test Results

Results for Series 3 are summarized in Table 6-18.

Table 6-18: Summary of experimental results for series 3

	P_{ult} (kips)	ϵ_{ult}	$\epsilon_{ult}/\epsilon_{exp}$	σ_{fult} (ksi)	Failure mode
7-18(B)-6(6)-5-1	16.8	0.012	1.2	152	Concrete
7-18(B)-6(6)-5-2	15.8	0.011	1.1	143	Concrete
7-15(B)-6(6)-5-1	17.2	0.012	1.2	156	Concrete
7-15(B)-6(6)-5-2	16.7	0.015	1.5	151	Strip fracture
7-15(U)-6(6)-5-1	12.8	0.007	0.7	115	Concrete
7-15(U)-6(6)-5-2	8.7	0.007	0.7	77	Anchor rupture
7-12(B)-6(4)-5-1	14.5	0.012	1.2	130	Anchor rupture
7-12(B)-6(4)-5-2	15.6	0.008	0.8	141	Concrete
7-12(B)-6(4)-7-1	17.4	0.011	1.1	158	Concrete
7-12(B)-6(4)-7-2	16.6	0.011	1.1	150	Delamination
7-32(B)-N-1	20.6	0.016	1.6	188	Strip fracture
7-32(B)-N-2	18.5	0.012	1.2	169	Strip fracture
7-32(U)-N-1	21.3	0.012	1.2	195	Strip fracture
7-32(U)-N-2	19.2	0.011	1.1	175	Strip fracture

6.3.3.1.1 Effects of Anchorage Type

The tests in which the CFRP strip was wrapped around the sides provided a more even strain distribution across the strip width and minimized stress concentrations. Table 6-19 compares strip strength results for anchored and wrapped strips for tests having different anchorage details and having failed by strip fracture. Because the specimens with the through-anchor details (or 18-in. strip length) failed in the concrete in this series, Table 6-19 reports the average strip stress and strain values at failure from tests in Series 1 having a 5-in. wide strip, 11.5 ksi concrete, and an anchor material ratio of 1.4 or 2.0 and failing by strip fracture.

All tests reported in Table 6-19 reached a stress in the CFRP tension strip that exceeded the manufacturer expected stress at fracture of 143 ksi. Tests with anchored strips failed at similar stress levels regardless of the anchor type. As expected, however, the unanchored wrapped strips reached a higher stress at fracture than anchored ones, confirming the hypothesis that wrapping the strip along the edges provided a more even strain distribution in the strip.

Table 6-19: Effects of anchorage type

	Tests	Average values		
		P_{ult} (kips)	σ_{fult} (ksi)	ϵ_{ult}
Through-Strip Anchor Detail	Average Series 1 Tests*	17.3	154.2	0.0149
Adjacent to Strip Anchor Detail	7-15(B)-6(6)-5-2	17.0	153.5	0.0135
Unanchored Wrapped Strips	Average for all tests with wrapped strips	19.6	178.5	0.014

*Average values from tests in Series 1 having a 5-in. wide strip, 11.5 ksi concrete, and an anchor material ratio of 1.4 or 2.0.

6.3.3.1.2 Effects of Strip Length in the Adjacent to Strip Anchor Detail

The strip and patch overlap was found to play an important role in the modified adjacent to strip anchor detail. A 15-in. strip stopped just short of each anchor hole on the beam specimen, while a 12-in. strip stopped about 1.5-in. short of each anchor hole. Table 6-18 indicates that the shorter 12-in. strips with short 5-in. patches were vulnerable to anchor failures at a significantly lower strip stress level than the manufacturer expect fracture stress. In tests where the patch length was extended 2-in. to make up for the strip stopping 1.5-in. short, however, Table 6-18 also indicates the modified anchor detail will develop stresses in the strips that are larger than their expected fracture stress.

6.3.3.2 Conclusions

The modified anchor detail (adjacent to strip) performed similarly to the through-strip anchor detail and is capable of developing the expected strength of CFRP strips. It is however advised to extend the CFRP strip all the way to the edge of the anchor hole for optimal performance of the modified anchor detail. Given the similar performance observed between the two anchor details and the fact that the new detail is easier to install, it was implemented in Series 4 and large-scale beam tests in this study.

6.3.4 Series 4

Series 4 consisted of 12 tests on larger beam specimen than those used in Series 1 through 3. This series was undertaken to further investigate the size effects observed in Series 1 and develop a quality control test for wider and high-capacity anchored CFRP strips.

6.3.4.1 Typical Test

A typical test for the fourth series of beams was conducted and unfolded in a similar fashion to tests in Series 1, but with larger beam specimens and loading setup. As shown in Figure 6-59 and Figure 6-60, the specimens were loaded with the tension face up and a ram reacting against a strong floor. Loading was continuous from start to end. The most typical failure mode in this series was strip fracture, although anchor rupture, delamination, and concrete failure were also reported.

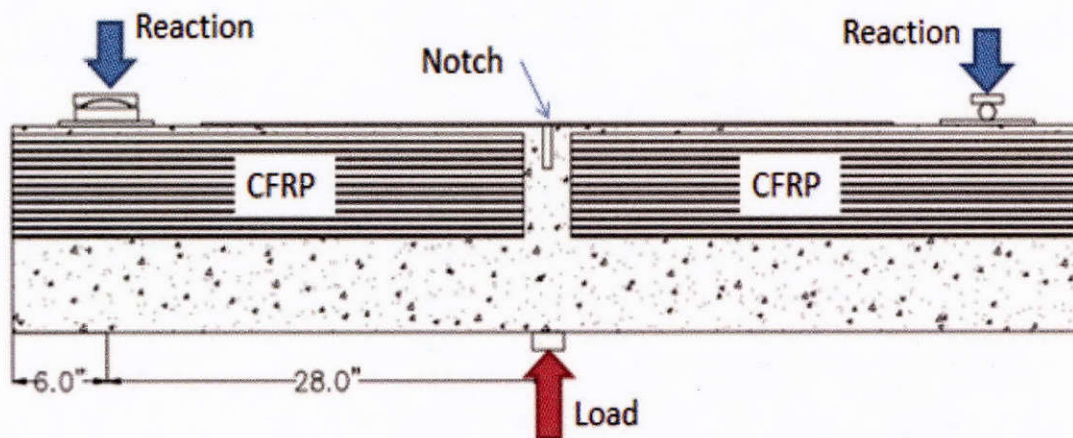


Figure 6-59: Loading diagram

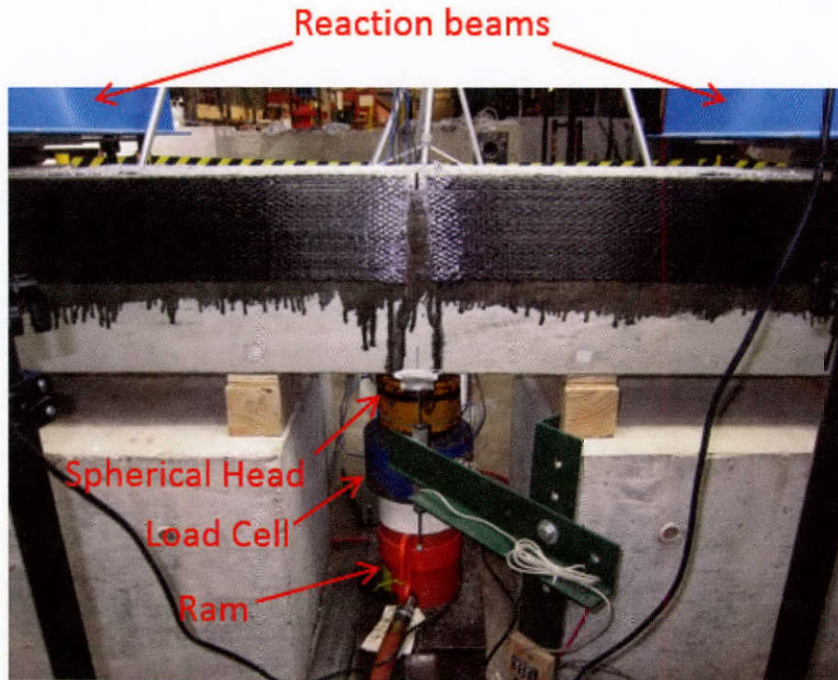


Figure 6-60: Test setup

A typical load deflection response is shown in Figure 6-61 with three characteristic parts. Each load deflection response starts with a very stiff initial linear segment up to cracking of the concrete in flexure, followed by plateau, which comes from debonding of the CFRP strip from the concrete substrate. Lastly, after the entire strip has debonded and the anchors become fully engaged, the response becomes mostly linear again up to failure. This response is similar to what was observed in the other test series.

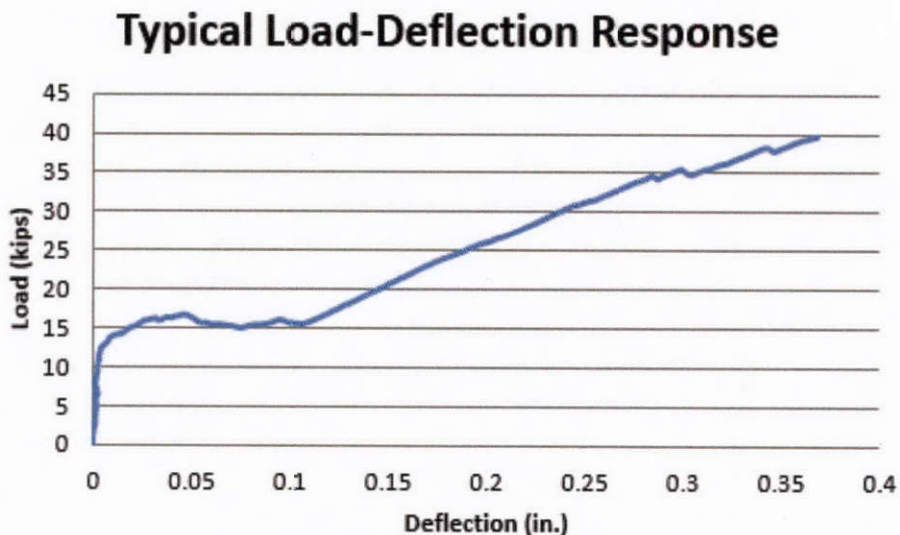
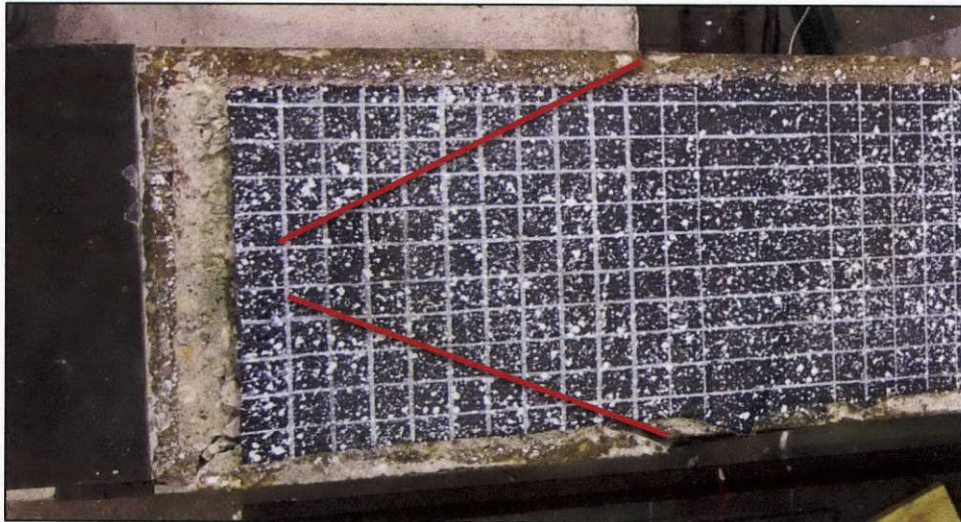


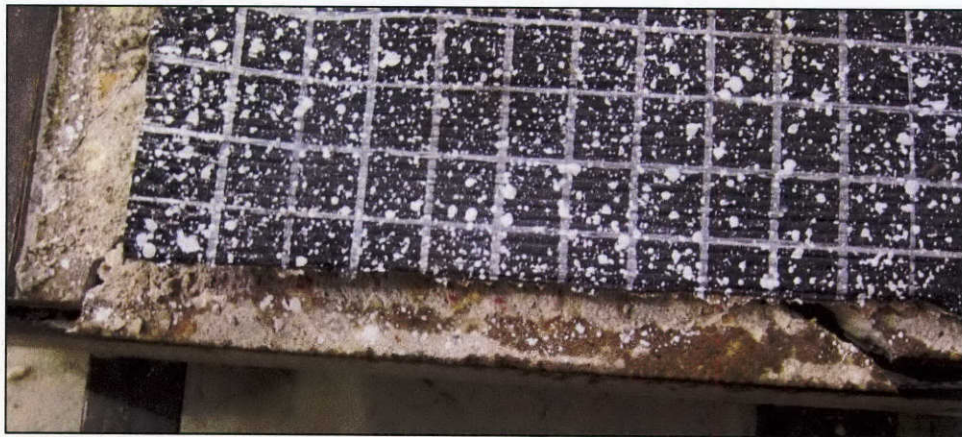
Figure 6-61: Typical load-deflection response for a test in Series 4

6.3.4.2 Failure Modes and Implications

Failure modes for this series are strip fracture, anchor rupture, delamination, and failure of the concrete specimen. These failure modes have been described in previous sections for the first three series. In this series, two distinct concrete failure modes were observed. One concrete failure mode was similar to those observed in the other test series with the concrete beam failing in a shear/tension manner (Figure 6-16). The other failure mode involved localized crushing at the anchor/concrete interface combined with a concrete cone detaching from the rest of the beam ahead of the anchor (Figure 6-62). In this failure mode, integrity of the beam was maintained by the steel reinforcement and CFRP side strips but generated sufficient movement at the anchor hole to cause anchor pull out (Figure 6-62).



(a)



(b)



(c)

Figure 6-62: Concrete specimen failure leading to anchor pullout

6.3.4.3 Test Results

In Table 6-20, the experimental results of the 12 tests conducted are summarized. The experimental results were used to evaluate the influence of parameters on strip strength and anchor strength. In Table 6-20:

P_{ult}	The ultimate applied load at failure.
P_{exp}	The expected beam load at failure which is calculated by equilibrium using the expected rupture stress for the CFRP strip provided by manufacturer ($\sigma_{exp} = 143$ ksi).
F_{ult}	The strip force at mid-span, which is calculated by equilibrium at ultimate load (P_{ult}).
σ_{ult}	The strip stress at mid-span which is evaluated at ultimate load = F_{ult}/A_{CFRP} in which A_{CFRP} is the cross-sectional area of the CFRP strip.
ϵ_{ult}	The mid-span strip strain in the fiber direction measured at P_{ult} taken from strain gauges. Both for mean and maximum

Table 6-20: Summary of experimental results for Series 4

Test #	Test ID	P_{ult}	P_{exp}	P_{ult} / P_{exp}	F_{ult}	σ_{ult}	Mean ϵ_{ult}	Max ϵ_{ult}	Failure Mode
1	S-5-1-S-6	14.1	12.1	1.17	16.7	165	0.0124	0.0129	Anchor Rupture
2	S-8-1-M-7	20.8	19.2	1.08	24.8	154	0.0095	0.0101	Strip Fracture
3	S-10-2-S-6	25.8	23.9	1.08	31.0	153	0.0089	0.0107	Strip Fracture
4	D-5-1-L-6	17.7	24.0	0.741	21.2	104	0.0075	0.0093	Delamination
5	S-10-1-M-9	24.4	24.0	1.02	29.1	144	0.0130	0.0141	Strip Fracture
6	D-10-2-L-6	39.6	47.4	0.836	47.8	118	0.0082	0.0112	Concrete
7	D-5-1-L-12	26.5	23.7	1.12	32.0	159	0.0103	0.0107	Strip Fracture
8	D-10-1-L-12	48.5	46.6	1.04	59.5	149	0.0105	0.0127	Strip Fracture
9	D-10-2-L-12	52.8	46.6	1.13	65.0	162	0.0101	0.0111	Strip Fracture
10	D-10-1-M-12	46.9	46.0	1.02	58.3	146	0.0106	0.0128	Concrete
11	D-10-1-M-12-c	39.0	46.0	0.849	48.3	120	0.0089	0.0107	Anchor Rupture
12	T-5-1-M-18	36.7	34.9	1.05	45.2	151	0.0105	0.0105	Strip Fracture

6.3.4.3.1 Size Effects

6.3.4.3.1.1 Effects of Strip Width

When comparing a 5-in. wide strip to a 10-in. wide strip, Table 6-21 clearly shows the 10-in. strips fractured at a much lower ultimate stress compared to the 5-in. strips. This trend also holds for multiple layers. However, when comparing a 10-in. strip with two anchors across the width, and a 5-in. strip with one anchor, the fracture stresses are much closer; this is because they have the same strip width per anchor. This trend is seen for two layers as well.

Table 6-21: Effect of strip width

Test #	Test ID	Layout			Stress (ksi)
		Number of layers	Width of strip	Number of anchors	
1	S-5-1-S-6	1	5	1	165
3	S-10-2-S-6		10	2	153
5	S-10-1-M-9		10	1	144
7	D-5-1-L-12	2	5	1	159
9	D-10-2-L-12		10	2	162
8	D-10-1-L-12		10	1	149

6.3.4.3.1.2 Effects of Number of Layers

Up to three layers of CFRP were tested and it was found that regardless of the number of layers, the strips could be developed to fracture. No significant trends could be observed with respect to the number of layers and strip stress at fracture when only the number of layers was considered.

6.3.4.3.1.3 Effects of Strip Width per Anchor

Both one and two anchors per strip width were investigated in this series. It was found that one anchor was able to fracture a strip having a width of 10-in. and a tensile force up to 60 kips (2 layers). These results therefore demonstrate the effectiveness of CFRP anchors for strips up to a tributary width of 10-in. While using one anchor was shown to be possible with wide strips, it also resulted in higher strains along the centerline of the strip compared to its edges. This implies that a single anchor does not distribute stresses as evenly for wide strips as for narrower ones. Figure 6-63 shows the placement of strain gauges at mid-span across the width of the strip.

When using one anchor to develop a 10-in. strip, the largest longitudinal strains were observed to occur consistently along the centerline of the strip after the strip began to debond (Figure 6-64). Both edge strain gauges (north and south) recorded significantly smaller strains than the centerline strain because the stress at the edge of strip is not as easily transferred to the anchor as the stresses in the middle of the strip with a nearly direct transfer to the anchor. In addition, debonding of the strip is usually initiated at the edge of the strip. By using two anchors over a 10-in. strip width instead of one, a much different strain profile was produced. Figure 6-65 shows how the centerline strain is no longer the largest, post debonding, when two anchors are used and that the strain variation at any given load is smaller for two anchors than for one anchor.

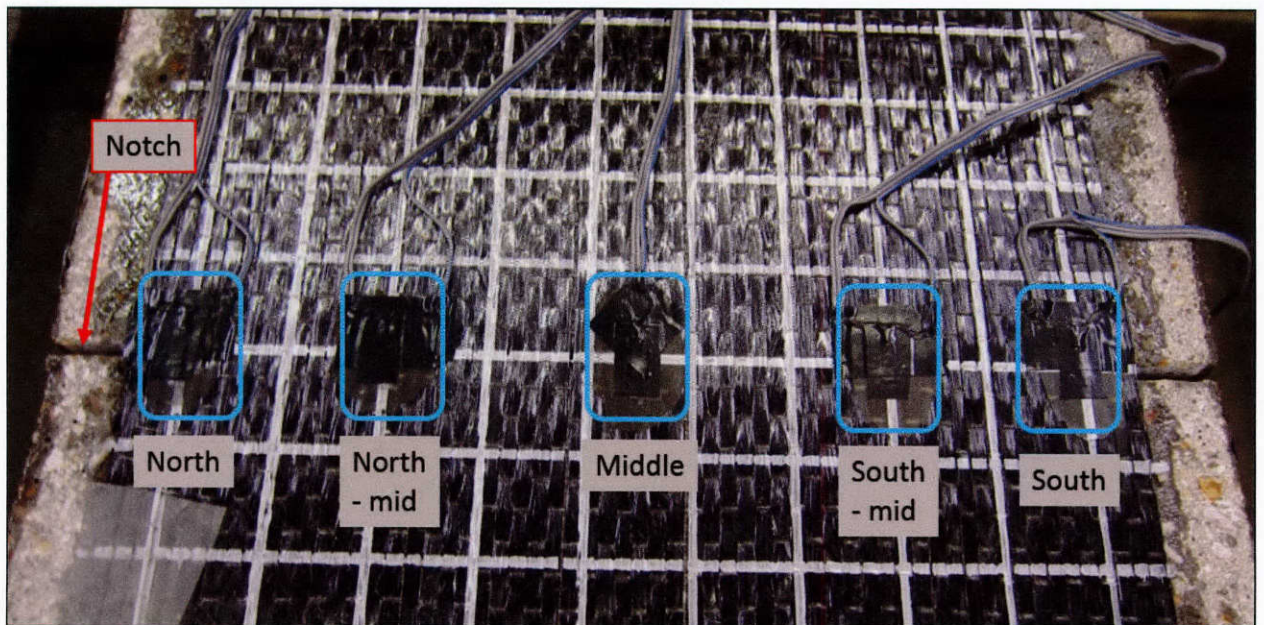


Figure 6-63: Placement of strain gauges in Series 4

Load-Strain D_1A_10W_12

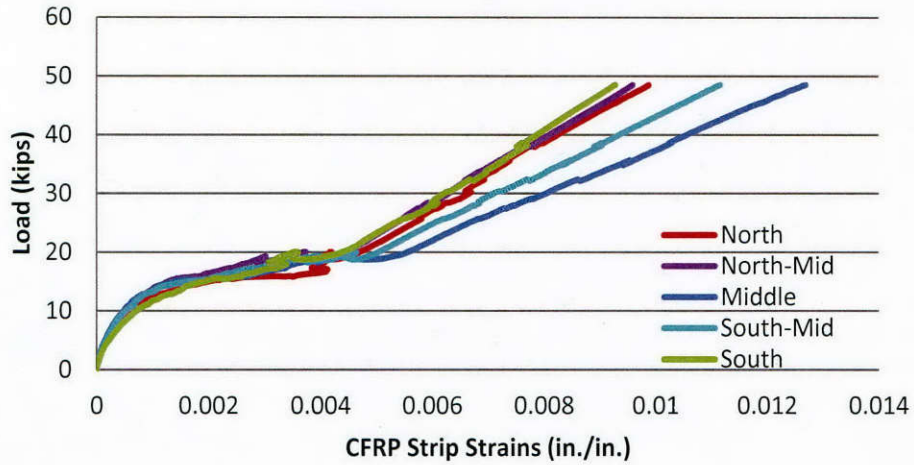


Figure 6-64: Strains for a 10-in. wide strip with one anchor

Load-Strain D_2A_10W_12

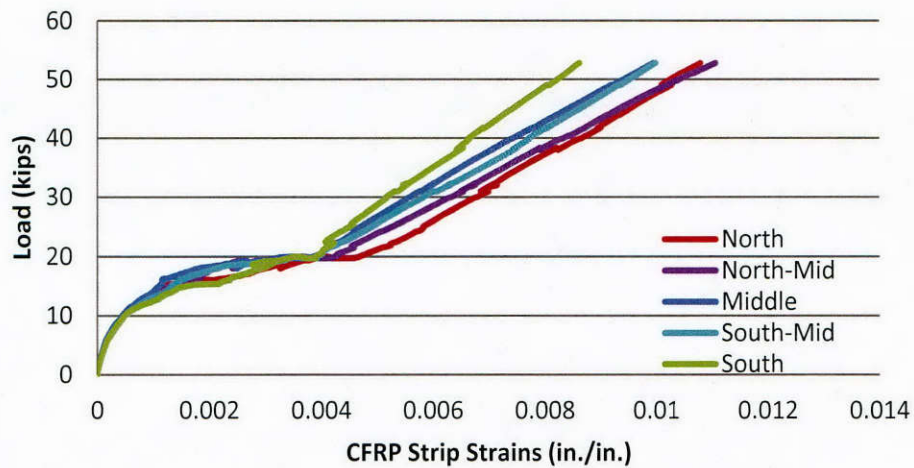


Figure 6-65: Strains for a 10-in. wide strip with two anchors

6.3.4.3.1.4 Effects of the Anchor Material Ratio

Anchor material ratios of 1.72, 2, and 2.8 were tested in this series. Because of the limited size of the test matrix, the effects of the anchor material ratio on strip strength could not be evaluated. Only one specimen in this series failed below its expected value by anchor rupture, indicating that a material ratio of 2.0 can adequately develop the strength of CFRP strips up to 10-in. wide and having two layers of material. The specimen that suffered anchor failure has a relatively small anchor-hole chamfer radius given the size of the anchor used. This failure and the chamfer radius are discussed in a subsequent section.

6.3.4.3.1.5 Size Effect Relations

To investigate the effect of using wider and thicker CFRP strips, or multiple layers, on the ultimate strip stress at fracture, a normalized strip area parameter was used. The parameter was calculated by dividing the CFRP strip laminate sectional area by the number of anchors used across the strip width and the anchor material ratio (Equation 6-10). The strip laminate area was obtained by multiplying the strip width by the number of layers and thickness of the CFRP strips.

$$\text{Normalized strip area parameter} = \frac{A_{CFRP}}{n_A * AMR} \quad \text{Equation 6-10}$$

Where:

A_{CFRP} : Sectional area of CFRP laminate, in².

n_A : Number of anchors across the strip width

AMR: Anchor material ratio

This parameter is plotted in Figure 6-66 versus the strip stress at ultimate load. A linear-regression trend line is superposed on the data points in Figure 6-66 and highlights a clear size effect for strip strength. The size effect observed in Series 1 are again found in Series 4. As a general trend, the smaller the normalized strip area parameter, the higher the fracture stress at ultimate load. The data points plotted in Figure 6-66 correspond to tests in Series 4 that failed by strip fracture except for one point that corresponds to an anchor rupture failure. The anchor rupture point is included in the figure because it falls above the trend line at a low strip area parameter, signifying that the trend would have only been accentuated if the anchor did not fail and the specimen experienced a higher failure load.

The observed trend in Figure 6-66 indicates that the larger the CFRP strip area developed per anchor, the lower the stress at fracture of that strip. Similarly, the smaller the anchor material area per strip area developed, the lower the stress at fracture of that strip. This size effect is attributed to the increased effectiveness of larger anchors in distributing strains more evenly across CFRP strips and reducing strain concentrations. This was demonstrated in Series 1 with optical measurement distributed strain measurements over the strip surface.

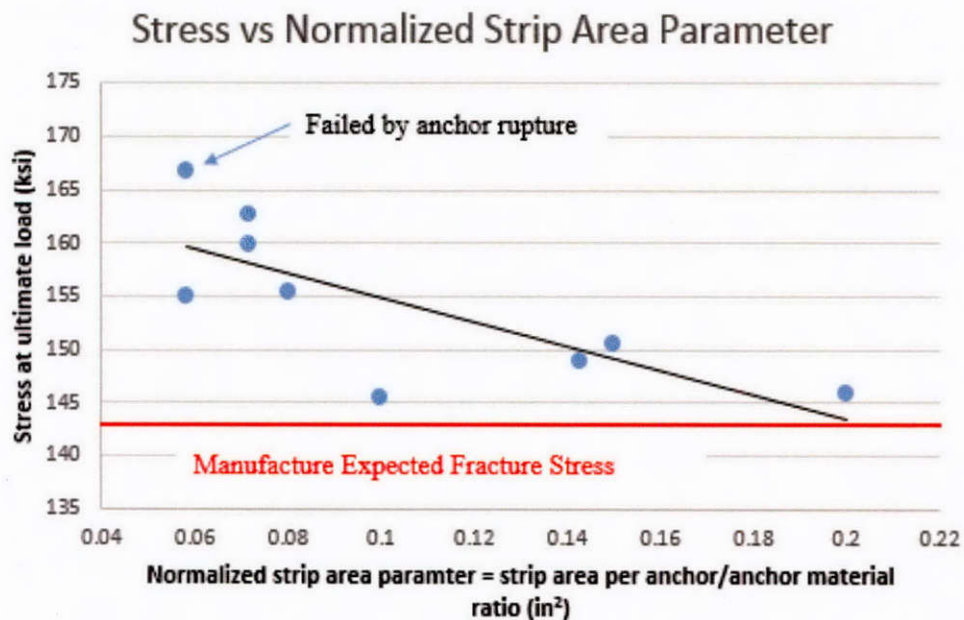


Figure 6-66: Comparison of failure stress versus normalized strip area parameter

Series 1 data corresponding to tests having a strip fracture mode are added to the data from Series 4 in Figure 6-67. With all the data points from Series 1 and 4, the overall trend remains of lower strip fracture stress with a larger strip area per anchor size.

A key observation in this plot is that no strip fracture stress was lower than the manufacturer's provided expected fracture stress of 143 ksi. However, the observed trend line in Figure 6-67 indicates a limit of about 0.2 in² on the normalized strip area parameter beyond which the stress at fracture of CFRP strips may become lower than the expected stress at fracture. This limit corresponds to a CFRP strip that is 0.04-in. thick, 10-in. wide, which is developed by a single anchor with an anchor material ratio of 2.0.

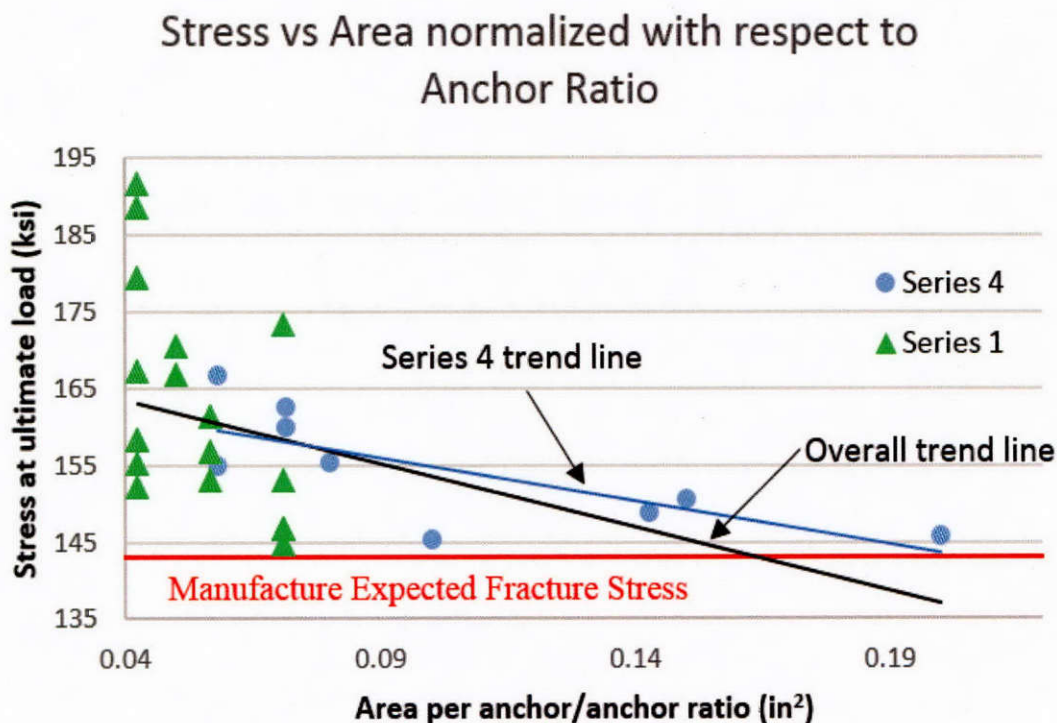


Figure 6-67: Comparison of failure stress for tests from Series 1 and 4

6.3.4.3.2 Anchor to Strip Overlap Length

The overlap length between the anchor and strip should be sufficient to ensure the bond stress generated by the load transfer between the strip and anchor does not exceed the manufacturer limit, which was 500 psi for the materials used in this study. In Series 1 to 3, only one layer of CFRP was used in the strips, which required an overlap length of 6-in. to avoid a delamination failure. For this series, this overlap length was changed in order to maintain an equivalent bond stress when varying the number of layers. The design bond stress of 500 psi was provided by the manufacturer and proven to work based on this series. Figure 6-68 plots the anchor/strip interface bond stress values at ultimate load for the tests of this series. Of the two specimens that had a higher designed bond stress, one failed in delamination, and the other in the concrete. A stress just over 700 psi was achieved before the specimen suffered a delamination failure between the anchors and the CFRP strip. It is important to note that no specimen failed by delamination below a bond stress of 700 psi. However, given the limited number of tests conducted in this series, the manufacturer provided 500 psi limit is deemed appropriate for designing the overlap length between anchors and strips for the material used. It is important to note that the design stress may be different for other manufactures; therefore 500 should not be assumed for all CFRP and epoxy materials, instead the design bond stress must be used according to manufacturer specifications.

Bond Stress at Ultimate Load

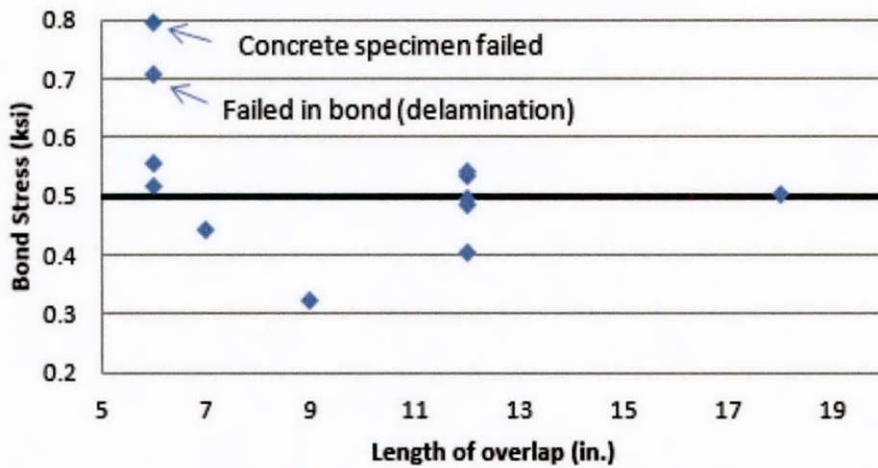


Figure 6-68: Bond stress between CFRP anchor and strip at ultimate load

6.3.4.3.3 Chamfer Radius of Anchor Hole

There are two directly comparable tests in Series 4 that compare chamfer radius. Both tests used one anchor to develop a 10-in. wide strip with two layers of materials. One specimen had a chamfer radius of 0.5-in. while the other specimen chamfer radius was taken as 1.4 times the anchor hole radius. The specimen with the smaller chamfer radius failed prematurely by anchor rupture at the chamfer. The specimen with the larger radius test failed in the concrete. However, the stress in the CFRP strip at failure was much larger than that of the specimen failing by anchor rupture and larger than the expected fracture stress.

6.3.4.4 Conclusions

This series confirmed the size effects seen in Series 1. The observed trend indicates that the larger the CFRP strip area developed per anchor, the lower the stress at fracture of that strip. Similarly, the smaller the anchor material area per strip area developed, the lower the stress at fracture of that strip. This size effect is attributed to the increased effectiveness of larger anchors in distributing strains more evenly across CFRP strips and reducing strain concentrations. This was demonstrated in Series 1 with optical measurement distributed strain measurements over the strip surface.

An individual CFRP anchor was shown to develop the expected strength of CFRP strips up to 10-in. wide, even when using two layers of material in the strip. However, using two anchors for a 10-in. strip width (or a 5-in. anchor tributary width) resulted in an improved strip stress distribution and a higher stresses at strip fracture.

CFRP anchors were shown to develop the expected strength of up to three layers of CFRP. However, the anchor to strip overlap length needed to be increased proportionally with number of layers to maintain an interface bond stress between anchors and strips below the manufacturer specified bond strength. The manufacturer provided bond stress was 500 psi for the material used. The design bond stress is likely different for other materials.

An anchor material ratio of 2 was shown to be sufficient in all cases where it was used, as long as the anchor hole chamfer radius was taken as 1.4 times the hole radius.

Chapter 7. Evaluation of Non-Destructive Test Procedures

7.1 OBJECTIVE

The objective of this task was to identify in-situ non-destructive evaluation methods suitable for assessing the quality of CFRP strip and anchor installation. Two non-destructive testing (NDT) methods, sounding and ultrasonic, were investigated in the laboratory.

7.2 DETECTION OF ARTIFICIALLY INSTALLED DEFECTS

7.2.1 CFRP Strip Installation and Defect Detection

In order to assess the applicability of the proposed NDT methods, three types of artificial defects were created on a 6-in. tall by 6-in. wide by 24-in. long concrete specimen (Figure 7-1). The three circular defects had the same 1.5-in. diameter. Each defect was created by applying a thin layer of lubricant oil, sand, or an air pocket formed by a plastic sheet. One layer of CFRP was then installed on the beam surface with the defects (Figure 7-2). These defects were intended to simulate possible defects seen during construction when concrete surfaces are contaminated by grease or debris. Air pockets are commonly seen in CFRP strip installations, and result in complete debonding between the CFRP strip and concrete.



Figure 7-1: Artificial defect fabrication

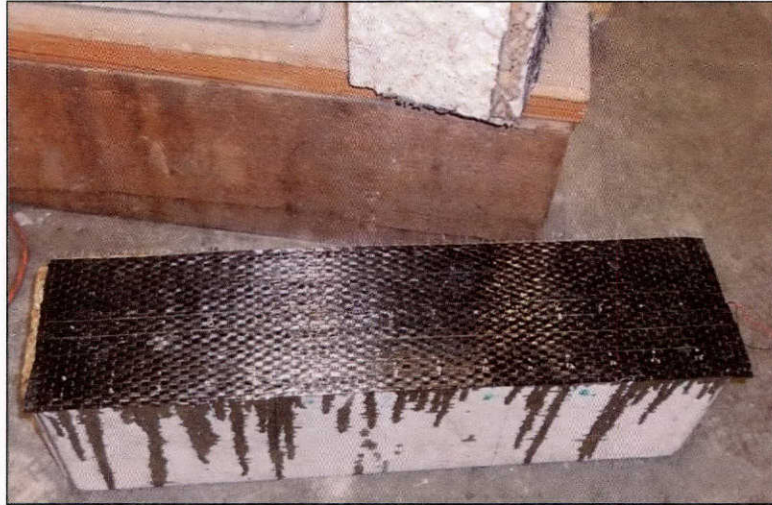


Figure 7-2: Specimen with artificial defects after CFRP installation

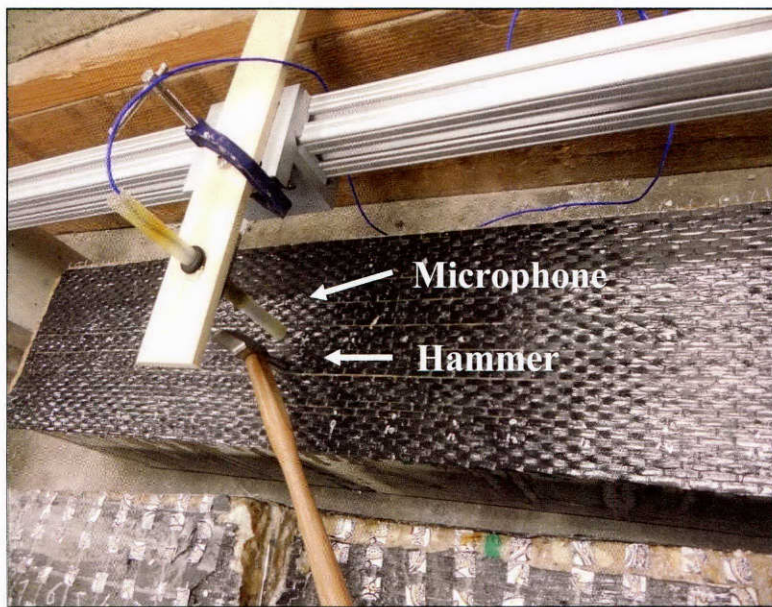


Figure 7-3: Sounding method test setup

The sounding method was used to detect the defects. A hammer (Figure 7-3) was used to impact the CFRP of the well-bonded, oily, sandy, and completely debonded areas. A microphone with a preamplifier attached to a signal conditioner was used to detect in-air signals. The microphone was 5mm above each measuring point. The microphone has a 6.3mm diameter and a flat sensitivity response of 3.16 mV/Pa over a broad frequency range (4Hz to 80kHz at ± 2 dB). The broad range frequency response and high sensitivity ensure detection of all frequency components of interest, which is the focus of this test. The output from the signal conditioner is digitized and captured by a digital oscilloscope and analyzed in the time and frequency domains. The sampling frequency was 1MHz and 8000 data points (8ms) were recorded at each measuring point.

Time domain signals obtained from different testing areas using the sounding method are shown in Figure 7-4. As seen in the figure, signals from the well-bonded, oily, and completely debonded surface area can be easily distinguished in the time domain. The signal from the well-bonded area has a large amplitude direct acoustic wave followed by a train of resonance waves, which lasts for over 6ms. The signal from the completely debonded area has a much higher

amplitude and longer ringing time compared to the signal from the well-bonded area because a flexural resonance vibration mode is formed in the debonded region. Thus, an air pocket is the easiest type of defect to identify. In the oily surface case, because of poor bonding between CFRP and concrete, energy could not penetrate into the concrete; therefore the sound energy was mainly caused by the direct impact force on the CFRP surface. This type of debonding does not cause the flexural resonance mode as in the air pocket case, because the oil between the CFRP and concrete dampens the vibration. The sandy surface produced signals similar to that of a well-bonded area, since the epoxy may have penetrated into the sand and formed a hardened mixture that could transmit mechanical waves as efficiently as the well-bonded area. Therefore, this type of defect could not be easily distinguished using the sounding method.

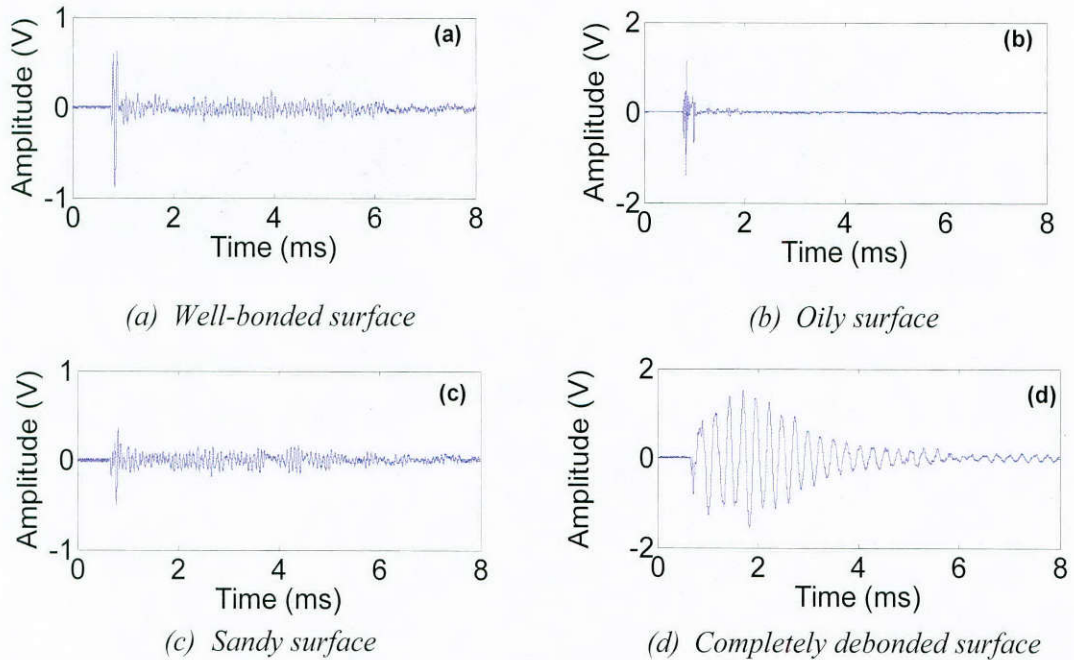


Figure 7-4: Time domain signals

Signals were further analyzed in the frequency domain using wavelet analysis. Results are shown in Figure 7-5. The signal from the completely debonded area has a dominant resonance frequency (3.9 kHz), which is significantly lower than the frequency of the signal from the well-bonded area (12.5 kHz). A different feature was found in the signal from the oily surface, as seen in Figure 7-5(b), where the wave energy is mainly focused in a much higher frequency range (from 35kHz to 50kHz) compared to that obtained from the well-bonded area. This is probably because the oil formed a weak bond between the concrete and CFRP surface and generated a considerably large nonlinear effect. Both the time and frequency domain features from the sandy surface signals are very similar to that of a well-bonded area. The sandy surface defect could not be easily distinguished through the wavelet analysis.

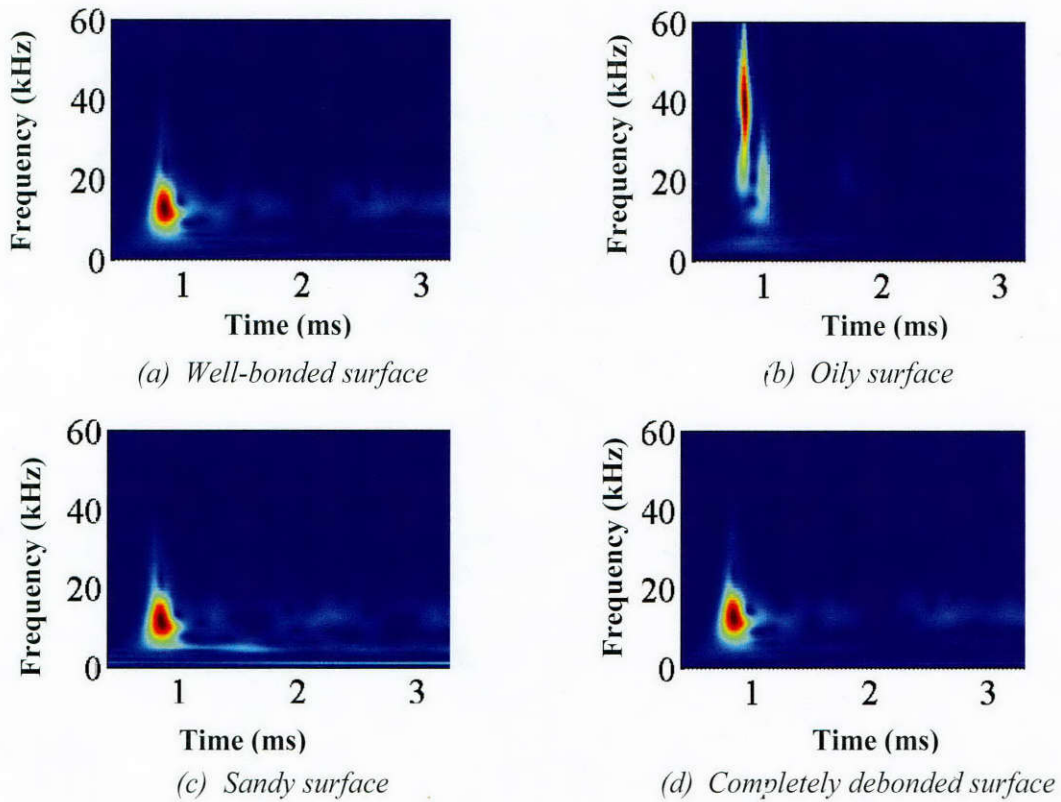


Figure 7-5: Wavelet of signals

7.2.2 CFRP Anchor Installation and Defect Detection

Different anchor conditions were installed on a concrete slab to check the feasibility of the sounding method for detecting defects in the CFRP anchor holes (Figure 7-6). Half of the surface of the slab was ground while the other had no surface preparation. Four anchor holes were drilled on the slab; each hole had the same diameter (5/16-in.) and depth (4-in.). Anchor groups #1 and #4 were installed to the full 4-in. depth. Foam inserts (2-in. long and 5/16-in. diameter) were inserted at the bottom of anchor holes #2 and #3 so that only 2 inches of the anchor could be installed into the hole. This type of defect was used to simulate the condition when the anchors were not installed to the designed depth. Other than the anchor defects, similar artificial debonding defects as in the previous section were utilized. The slab with artificial defects before and after the CFRP strip and anchor installation is shown in Figure 7-7 and Figure 7-8. The pulse velocity of the concrete slab was tested using the through transmission method and was found to be approximately 4300 m/s; this corresponds to an impact-echo frequency of 13.8 kHz.

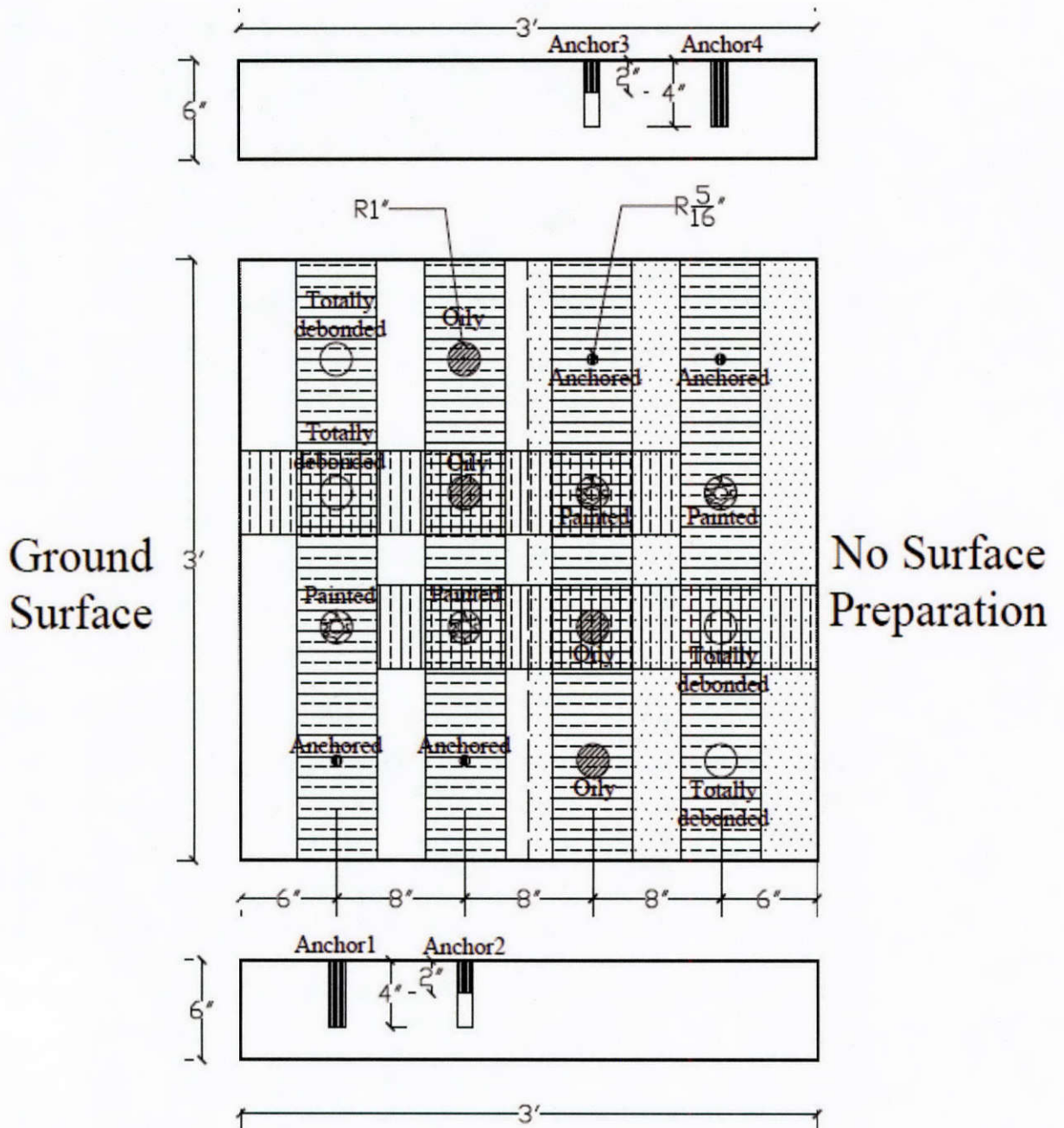


Figure 7-6: Schematic of the CFRP and anchor defects



Figure 7-7: Concrete slab before installation of CFRP strips and anchors

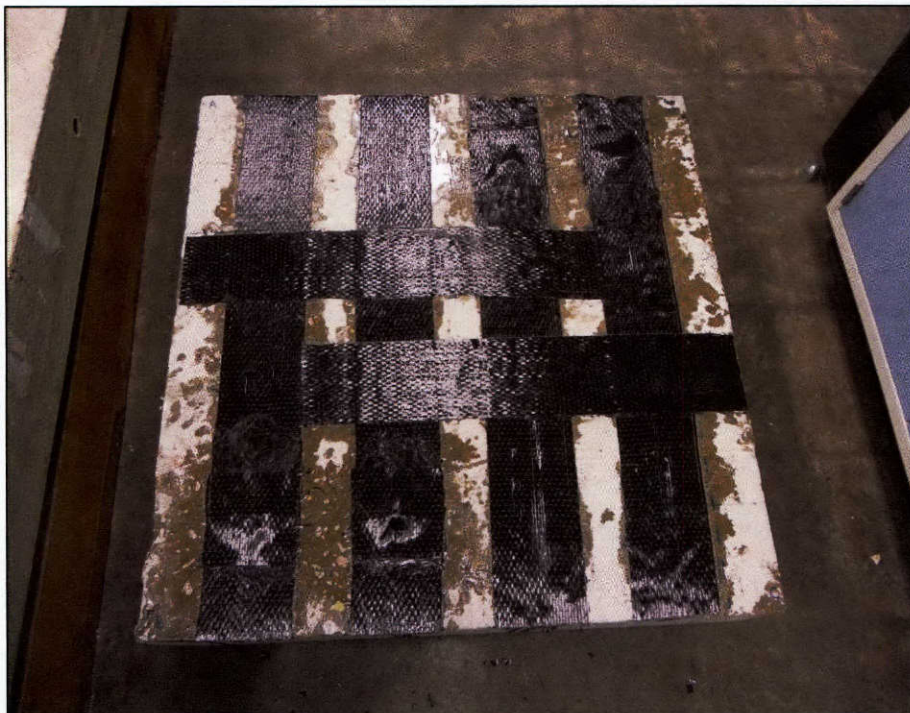


Figure 7-8: Concrete slab after installation of CFRP strips and anchors

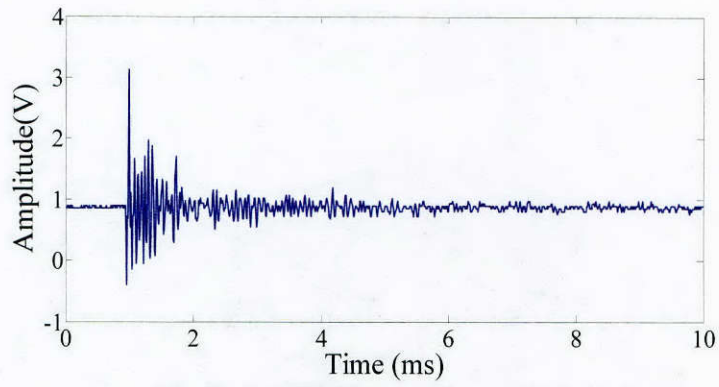


Figure 7-9: Anchor defect detection using the sounding method

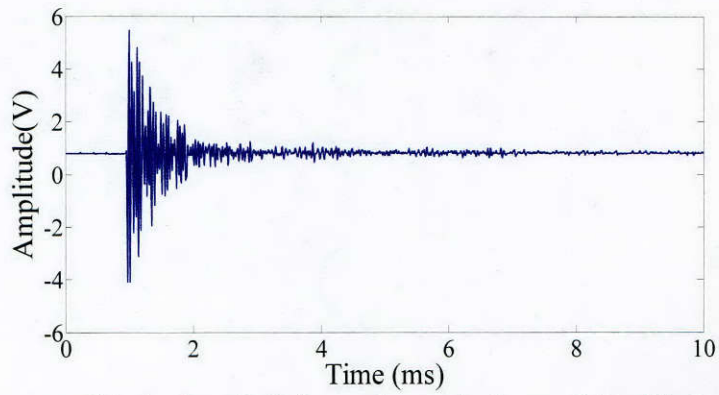
In the sounding test, a steel ball with a diameter of 7.5mm (Figure 7-9) was used to impact the top surface of the CFRP anchor. The same microphone and data acquisition system as that used in the CFRP strip tests were used. The sampling frequency was 100 kHz and 1000 data points were recorded at each measuring point.

Two example time domain signals obtained from anchor #1 and anchor #2 are shown in Figure 7-10. Although the signal from anchor #2 shows more high frequency components, there is no clear feature to distinguish the two time domain signals. A frequency analysis was then performed to transform the time domain signals to frequency domain (Figure 7-11). Different peak frequencies are shown in the frequency spectra. The signal from anchor #1 has a peak frequency at 13.9 kHz. Calculations show that this frequency corresponds to the impact-echo mode of the concrete slab in a solid region. This result indicates that the fully installed anchor was well-bonded with the concrete.

The frequency domain signal from anchor #2 shows a clear peak at 24 kHz, which indicates that a resonance mode may be formed by the defective anchor installation. It was also found that the resonance frequency signal of anchor #2 varies from impact to impact, thus multiple tests were performed at both anchor #1 and anchor #2 to check variations. In Figure 7-12, the variation of peak frequency measured at anchors #1 and #2 in multiple repeated tests is shown. The signals from anchor #1 had a very consistent peak frequency at 13.9 kHz in all tests, while the signals from anchor #2 show variation in the range of 22.5 kHz to 35.4 kHz. Despite these variations, the peak frequency obtained from anchor #2 is consistently higher than that of anchor #1. Therefore, the peak frequency may be used as a feature to detect anchor installation defects.

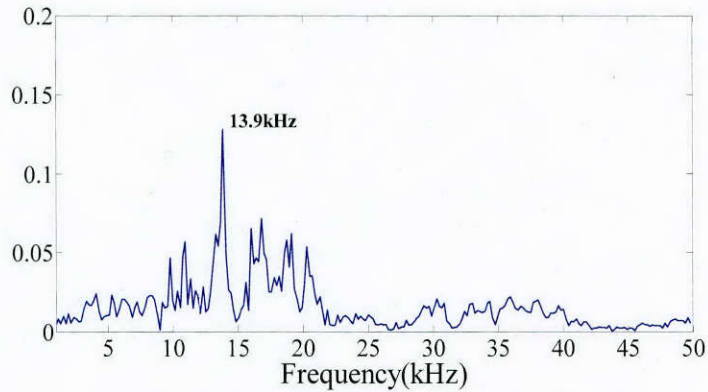


(a) Anchor #1 (4-in. anchor embedment)

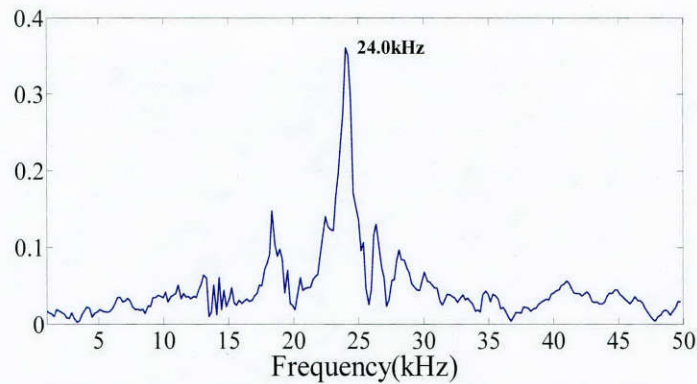


(b) Anchor #2 (2-in. anchor embedment, 2-in. filler)

Figure 7-10: Time domain signals for anchor #1 and anchor #2



(a) Anchor #1 (4-in. anchor embedment)



(b) Anchor #2 (2-in. anchor embedment, 2-in. filler)

Figure 7-11: Frequency domain signals for anchor #1 and anchor #2

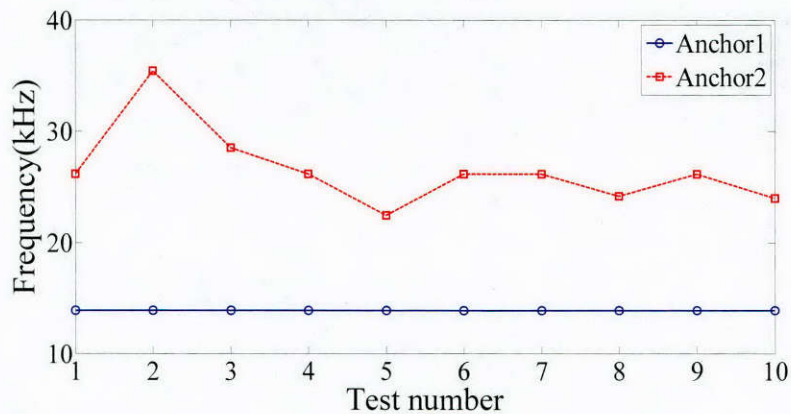


Figure 7-12: Frequency variation of signals obtained from anchor #1 and anchor #2

7.3 LOADING INDUCED DEBONDING DETECTION

In previous sections, NDT methods were studied on specimens with artificial defects. In this section, NDT tests were conducted to characterize load induced CFRP debonding on a standard beam specimen (6-in. by 6-in. by 24-in.) as described in Chapter 6. The debonding originated as load on the beam increased. The load was slowly increased during the test, up to failure of the specimen.

At failure, the partially debonded CFRP strip fractured. After failure, the specimen was sent to the NDT laboratory to perform further nondestructive tests to evaluate the debonding length between the CFRP strip and the concrete substrate.

7.3.1 Sounding Tests

Since the beam was loaded at the center, and the debonding develops approximately symmetrically, the sounding test was only conducted on the right half of the fractured beam. There were 15 measuring points equally spaced (3/4-in.) from the center notch towards the end of the specimen (see Figure 7-13), with measuring point #1 at 1/2-in. from the notch.

A steel ball with the diameter of 7.5mm was used to impact the CFRP surface from points #1 to #15, and the same microphone and test setup as in the previous tests were used. The sampling frequency was 1MHz and 10000 data points were recorded at each measuring point (10ms signal duration).

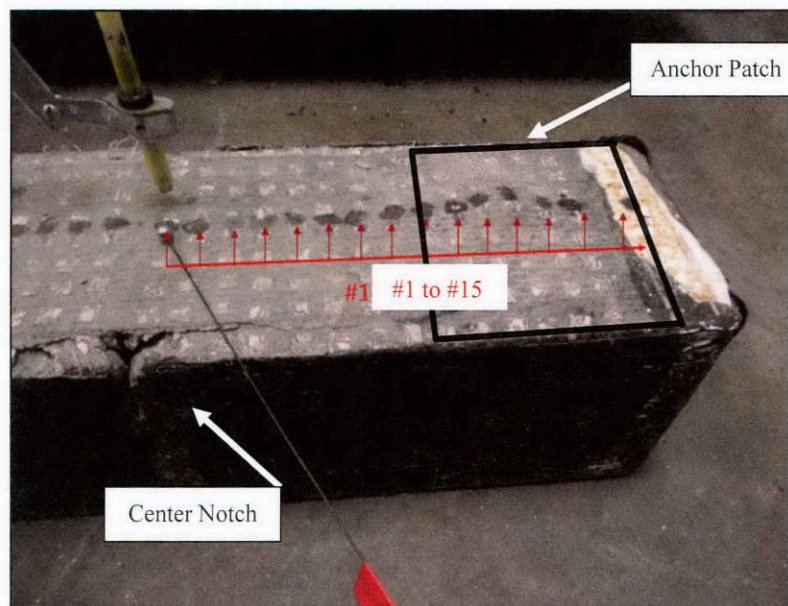
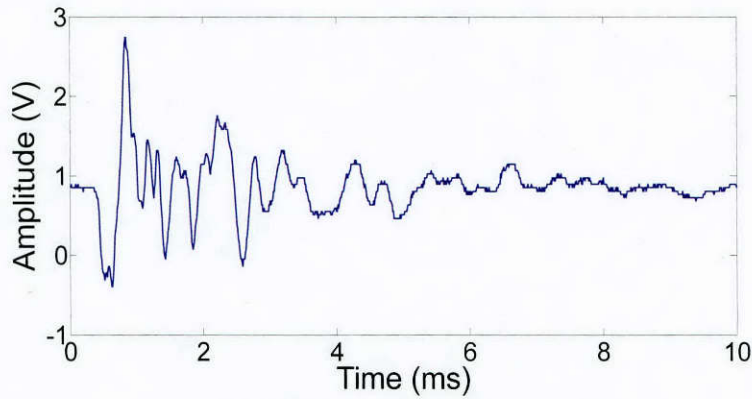
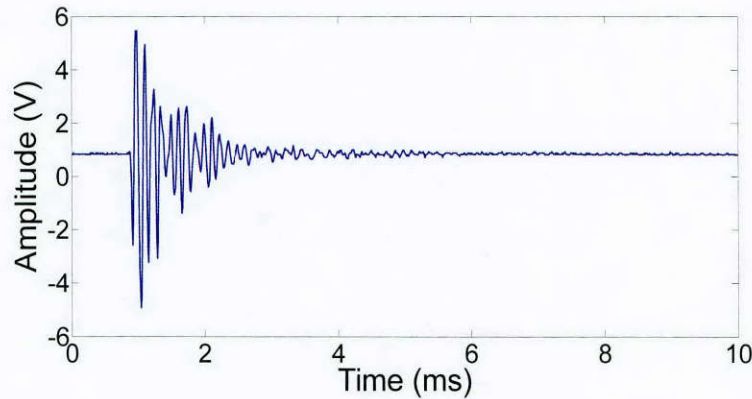


Figure 7-13: Load induced debonding detection using the sounding method

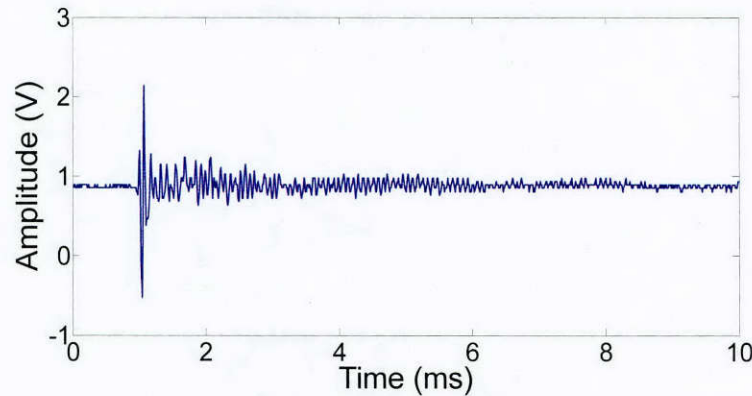
Figure 7-14 shows three example time domain signals, #1 (1/2-in. from the notch), #7 (5-in.) and #14 (10.25-in.). As seen in the figure, signals from these three measuring points have very different features. The signal from measuring point #1 has a very low frequency and long duration compared to the other two signals. The #7 signal shows a typical exponential decay with time, and the amplitude drops to the noise floor around 3ms. The #14 signal shows a high amplitude initial pulse followed by a long lasting ring signal, which is similar to the signals obtained from the well-bonded CFRP regions in previous sections.



(a) Point #1 (1/2-in. from notch)



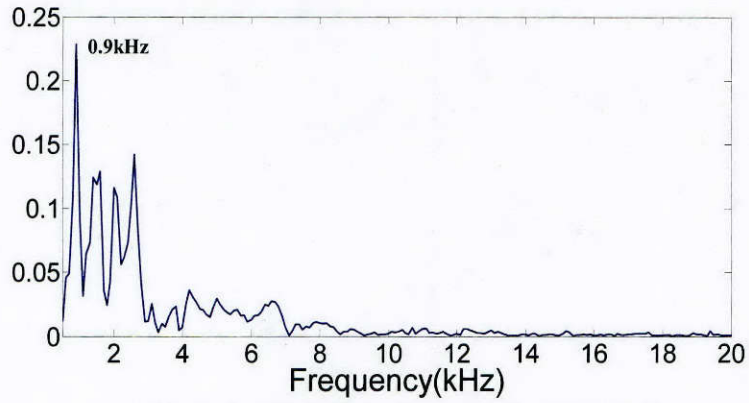
(b) Point #7 (5-in. from notch)



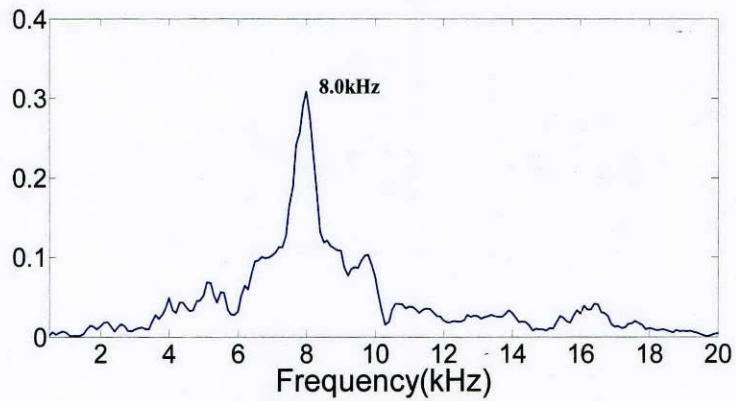
(c) Point #14 (10.25-in. from notch)

Figure 7-14: Time domain signals from measuring points

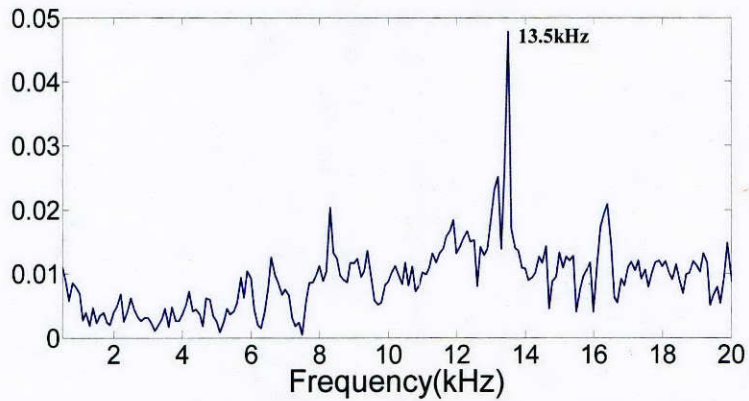
Signals obtained from these points were further analyzed in the frequency domain. As seen in Figure 7-15, the signal from point #1 has a very low peak frequency (0.9 kHz) and low frequency component (below 3 kHz), which indicates the CFRP strip has completely debonded from the concrete surface. The peak frequency signal from point #14 was 13.5 kHz, which corresponds to the impact-echo mode of the beam.



(a) Point #1 (1/2-in. from notch, debonded)



(b) Point #7 (5-in. from notch, debonded)



(c) Point #14 (10.25-in. from notch, well-bonded)

Figure 7-15: Frequency domain signals from measuring points

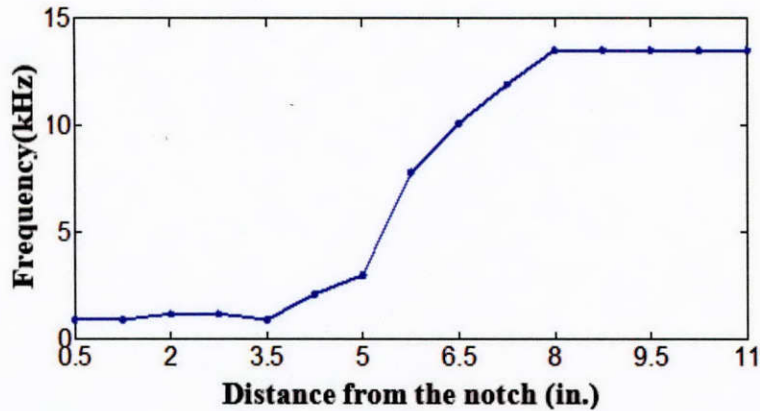


Figure 7-16: Changes in resonance frequencies along the length of the beam

In Figure 7-16, the peak frequencies along all measuring points from #1 to #15 are plotted. The curve shows a clear transition from low frequency to high frequency as the distance increased away from the center notch. As seen in the figure, the resonance frequencies for measuring points #1 to #7 (1/2-in. to 5-in. from the notch) are all below 5 kHz, while the resonant frequency starting from measuring point #11 (8-in. from the notch) is constant at 13.5kHz. Points #7 through #10 experienced a transition in the resonance frequencies. These points correspond to the boundary of the anchor patch, as shown in Figure 7-13. Based on the sounding test results, it can be estimated that the first 5-inches of the CFRP strip had completely debonded from the concrete substrate and portions of the anchor patch region (5-in. to 8-in.) had also partially debonded.

7.3.2 Ultrasonic Tests

Low cost PZT disks were used to generate and receive ultrasonic waves. A PZT actuator (source) was installed on the side surface of the beam while a PZT sensor scanned from measuring points #1 to #15 on the right half of the fractured beam (Figure 7-17). A 100 V, 500 kHz square wave pulse, drove the PZT source. The receiving sensor was connected to the pulser-receiver with a gain of 20dB. The amplified receiving signals were then digitized and 10000 data points were recorded and transferred to a computer. In each measurement, 200 signals were averaged and saved to improve the signal-to noise ratio.

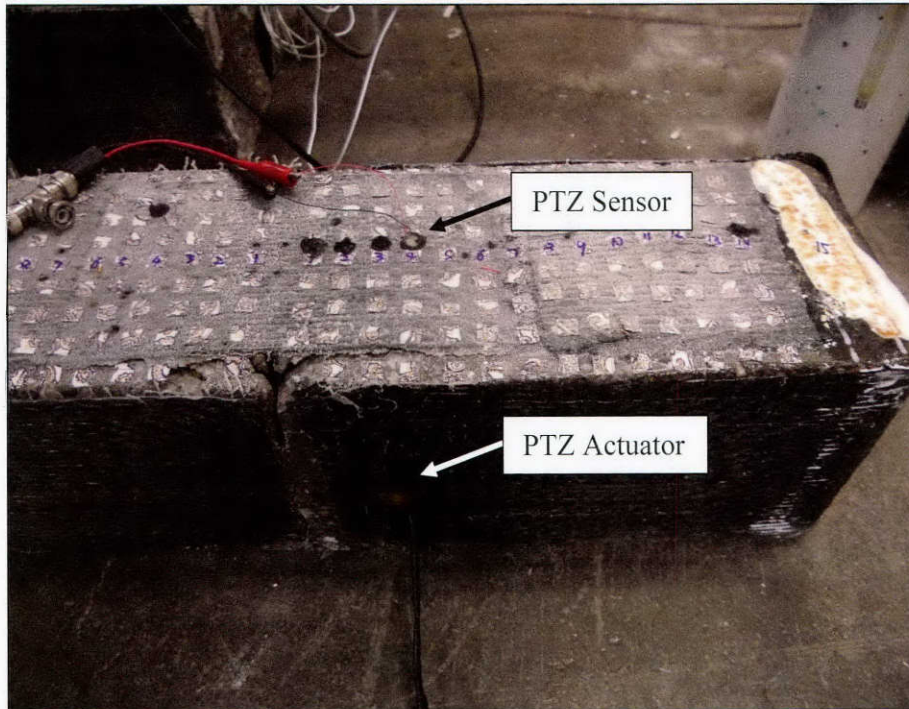


Figure 7-17: Load induced debonding detection using the ultrasonic method

Debonding of the CFRP strip significantly decreases the energy transmission between the sensors. The time domain signals from measuring points #1 to #15 are shown in Figure 7-18. It is clearly seen that before measuring point #7 (5-in. from the notch), the amplitudes of the signals are very low, which implies that from measuring points #1 to #7, the CFRP debonded.

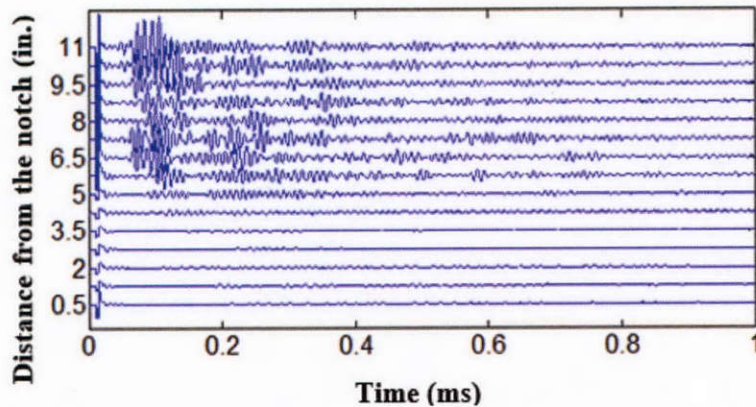


Figure 7-18: Time domain signals from the ultrasonic method

Figure 7-19 shows the signal amplitudes of different measuring points (normalized to the signal amplitude at point #15). The signal amplitudes of points #1 to #7 are less than 20% of the amplitude at measuring point #15. This large difference implies that energy transmission could be used as an index to evaluate debonding between the CFRP strips and concrete substrate.

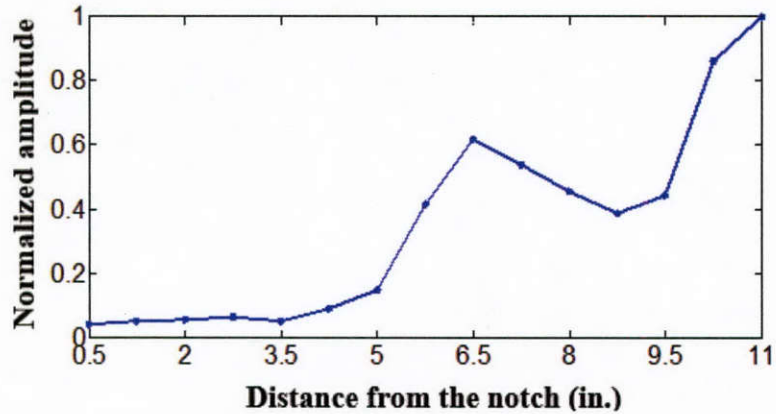


Figure 7-19: Normalized signal amplitude for ultrasonic method

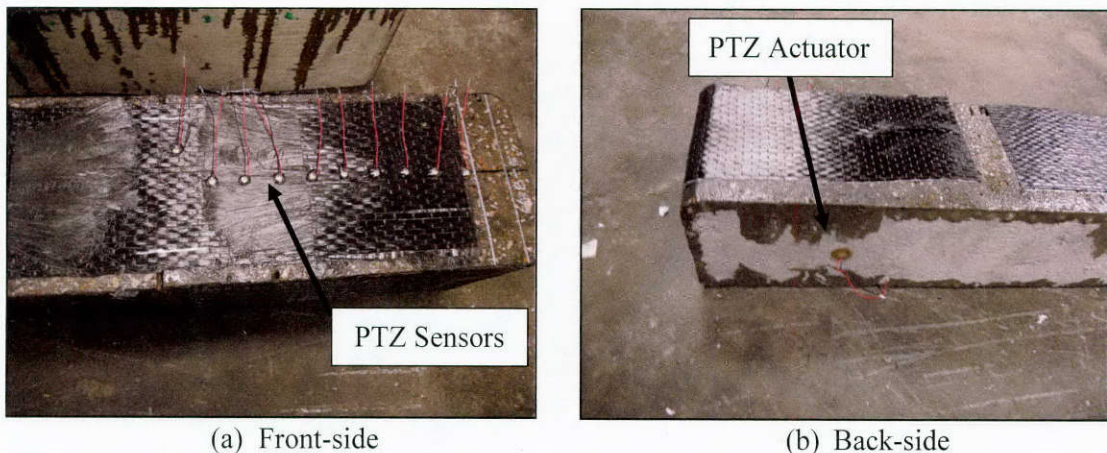
The nondestructive debonding test results were further compared with the strain measurement results from an optical measurement system. The results agree very well with the nondestructive test results, which implies that the sounding method and ultrasonic method could be used to detect debonding between the CFRP strips and concrete substrate.

7.4 IN-SITU DEBONDING MONITORING

In the previous two sections, the effectiveness of NDT methods for debonding detection was described. The feasibility of using NDT methods for real-time monitoring of CFRP debonding was also studied.

7.4.1 Standard Beam Debonding Monitoring

The loading test setup is the same as that shown in Chapter 6. The beam was loaded monotonically at 1-kip intervals. The beam was monitored up to 13-kips. After that, the beam was loaded continuously to failure. NDT data was acquired using the ultrasonic method during the loading intervals. A 100 V, 500 kHz square wave pulse generated from a pulser-receiver, drove the actuating source. The receiving sensor was connected to the pulser-receiver with a gain of 20dB. The amplified receiving signals were then digitized at a sampling rate of 10 MHz and 10000 data points were recorded and transferred to a computer. A 200-point average was used to improve the signal-to-noise ratio. An Agilent 34903 module switch was used to scan all receiving sensors in sequence.



(a) Front-side

(b) Back-side

Figure 7-20: Sensor arrangement on beam

Figure 7-21 shows the signals of sensor #9 obtained at loads of 0 and 13-kips, respectively. The initial parts of the two signals are almost identical, and they also have about the same peak amplitudes and first arrival times. This result implies that at 13-kip, the CFRP at sensor #9 is still well-bonded with the concrete substrate.

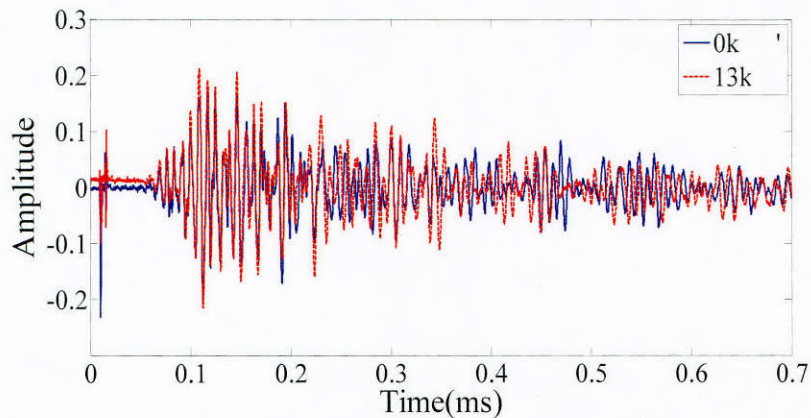


Figure 7-21: Signals of sensor #9

For comparison, signals from sensor #2 obtained at 0 and 13-kips of load are shown in Figure 7-22. It is clearly seen that the amplitude at 13-kips is considerably lower than when the beam was intact (i.e., no load). In addition, the first arrival time at 13-kips is also delayed. The plot implies that at 13-kips, the CFRP strip is completely debonded from the concrete substrate at the location of sensor #2.

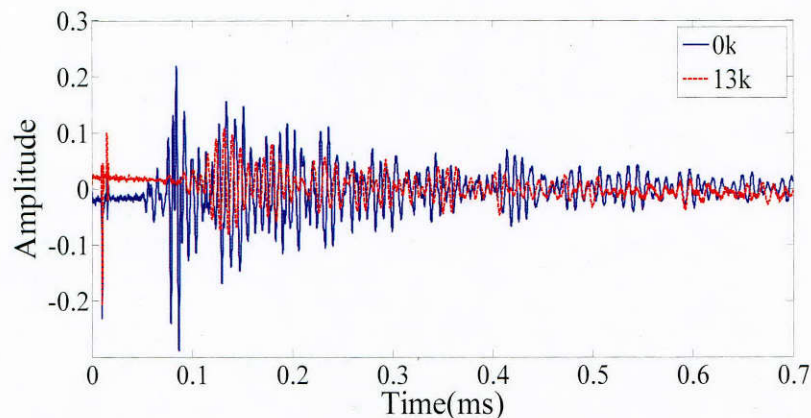


Figure 7-22: Signals of sensor #2

In Figure 7-23, the difference in the wave propagation path when debonding occurs between the CFRP and concrete is shown. Before debonding occurs, the wave could propagate directly through the concrete and CFRP bonding surface with high amplitude. When debonding occurs, the ultrasonic wave takes a longer wave path and loses more energy.

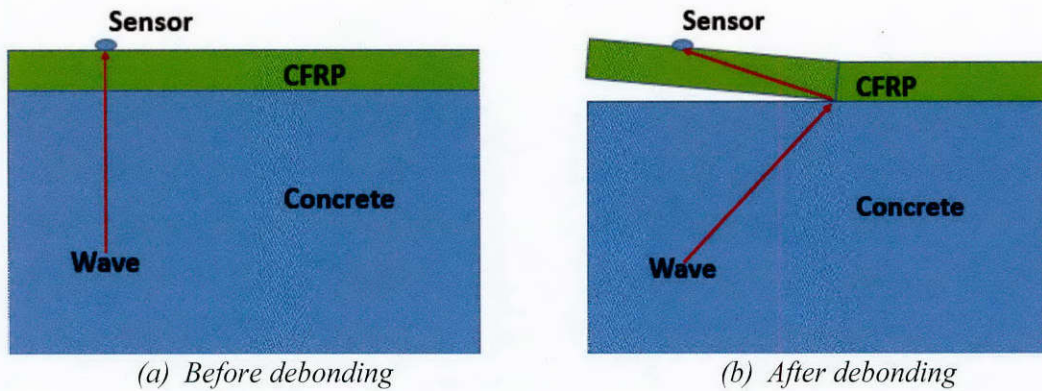


Figure 7-23: Wave propagation

In Figure 7-24, the signal amplitudes obtained during the loading process are shown. The amplitude of the signal obtained from sensor #1 first dropped at 8-kips, followed by an amplitude drop of the signal obtained from sensor #2 at 9-kips. Thus, debonding first occurred at sensor #1 at around 8-kips, and then propagated to sensor # 2 at 9-kips. The CFRP at sensor #9 and # 10 remained well-bonded during the entire loading process.

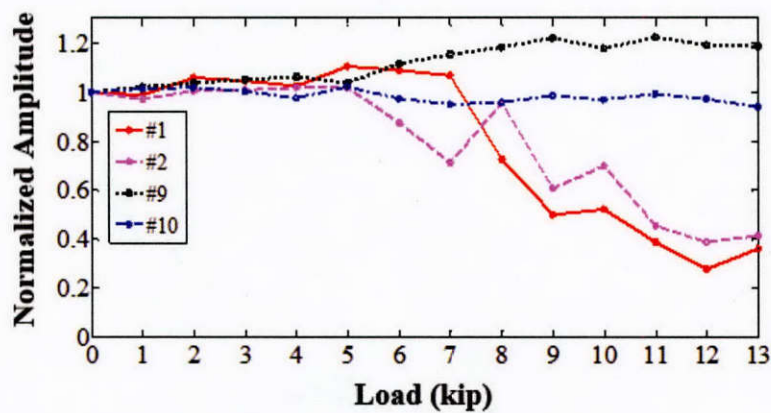


Figure 7-24: Debonding process of the beam

The CFRP debonding length at a load of 13-kips can be estimated in Figure 7-25. As seen in the figure, the amplitudes of sensors #1 to #4 at 13-kips are around 40% of the amplitude in the unloaded state. Though an amplitude increase was observed from sensors #4 to #6, the normalized amplitudes are still below one. Hence, that the length of CFRP strip from sensors #4 to #6 is likely partially debonded.

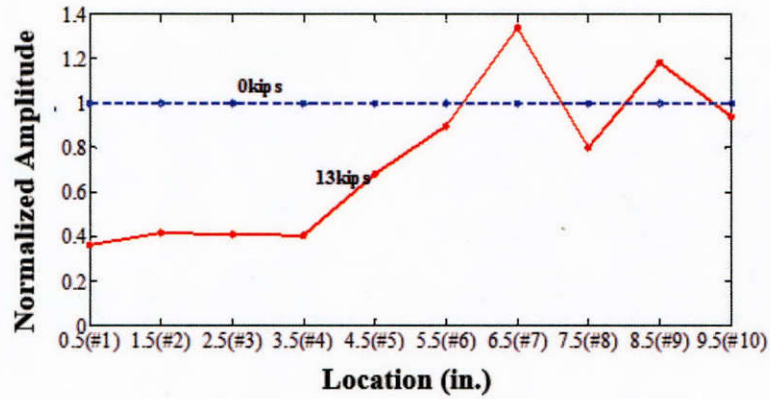


Figure 7-25: Evaluation of debonding length

7.4.2 Monitoring T-Beam Debonding

Nondestructive tests were performed on a T-beam (Figure 7-26) with a 14-in. web width. The cross-section of the T-beam is shown in Figure 7-27. Thirteen PZT disks were installed on the web of the T-beam along a straight line. One PZT disk, used as the actuator, was mounted 17-in. away from the end of the beam, 6 receiving PZT sensors were mounted on the concrete surface to monitor the crack initiation/development, and 6 receiving PZT sensors were mounted on the CFRP surface to monitor the initiation of CFRP debonding. The distance between two adjacent receiving PZT disks was 5-inches.

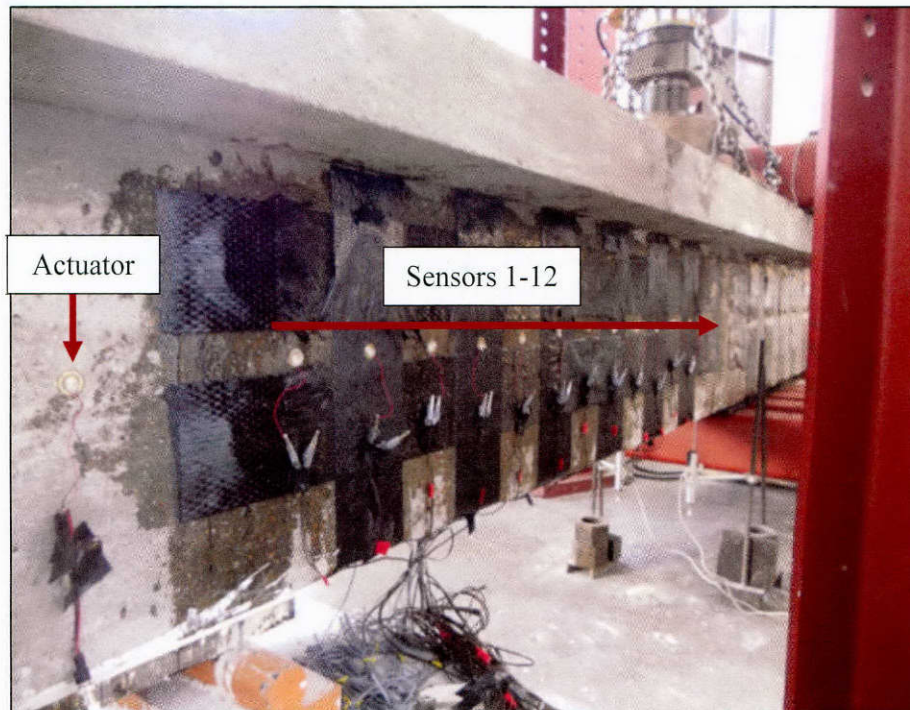


Figure 7-26: T-beam PZT sensor arrangement

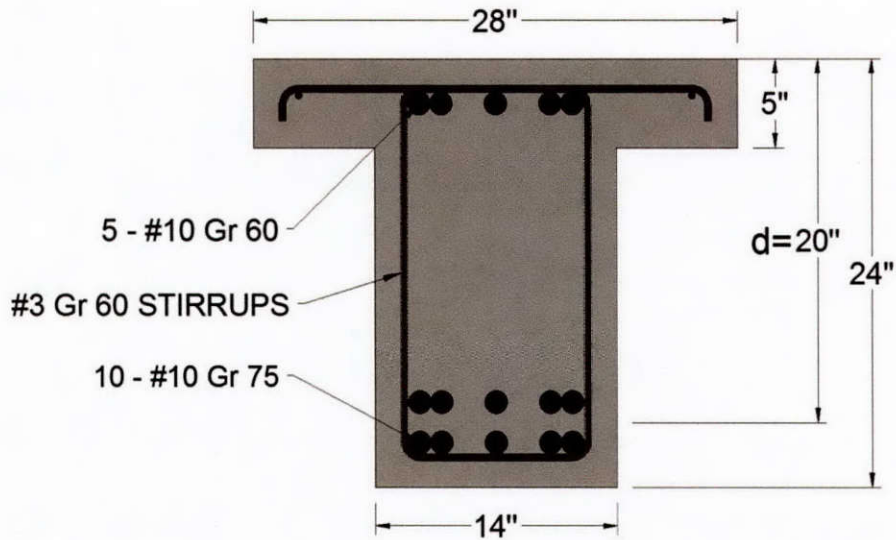


Figure 7-27: Cross-section of T-beam

The T-beam was loaded monotonically at 50-kip intervals of total load. The beam surface was observed visually and nondestructive test data was acquired after each loading interval up to 200-kips of total load. The T-beam was then loaded continuously to failure. The actuating sensor was driven by a 200 V, 100 kHz square wave pulse generated from a pulser-receiver, and the receiving sensors were connected to the pulser-receiver with a gain of 40dB. The amplified receiving signals were then digitized at a sampling rate of 10 MHz, and 10000 data points were recorded and transferred to a computer. An average of 200 signals were averaged and saved to improve the signal-to noise ratio.

Figure 7-28 shows the time domain signals of all sensors when the T-beam was not loaded. It was observed that the signal amplitude decreased the farther away the receiving sensor was from the actuating sensor. It was also noticed that the amplitude of the signals obtained on the CFRP surface were lower than those obtained on the adjacent concrete surface due to the attenuation induced by the CFRP.

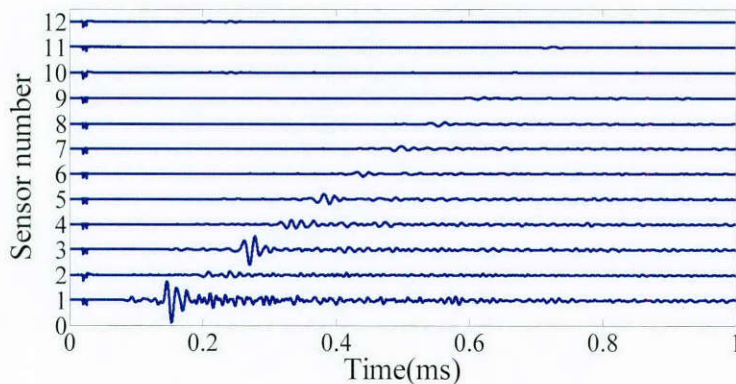


Figure 7-28: Time domain signals for the T-beam prior to loading

However, after normalizing the data with the peak amplitude of each signal, even the weakest signals could be clearly observed (Figure 7-29) and the surface wave propagation trend (see the red dotted line) could be easily detected. In this test, the measured surface wave speed of

the concrete was approximately 2238 m/s. It was noticed that the data from sensor #10 and # 12 were abnormal. Therefore, the data from these sensors could not be used.

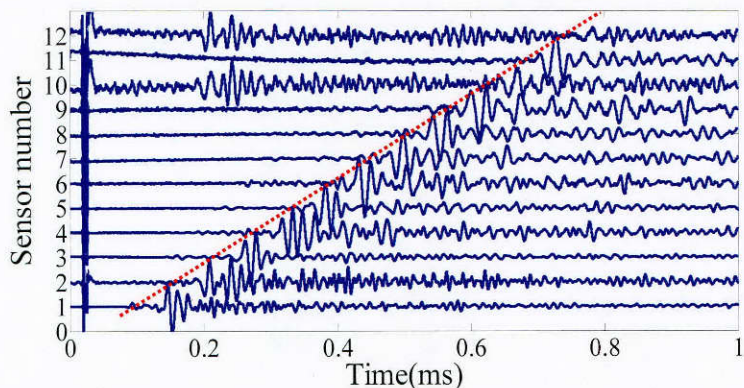


Figure 7-29: Normalized time domain signals for the T-beam prior to loading

Figure 7-30 shows the signal amplitudes from the T-beam in-situ debonding monitoring. As seen in the figure, the ultrasonic signal amplitudes show a clear drop between sensors #7 and #8 at 100-kips. At a load of 150-kips, a sharp drop between sensor #6 was observed, which corresponded to the growth of a shear crack and local CFRP debonding (Figure 7-31). The strain contour plot at 150-kips from an optical measurement system confirmed the ultrasonic test results.

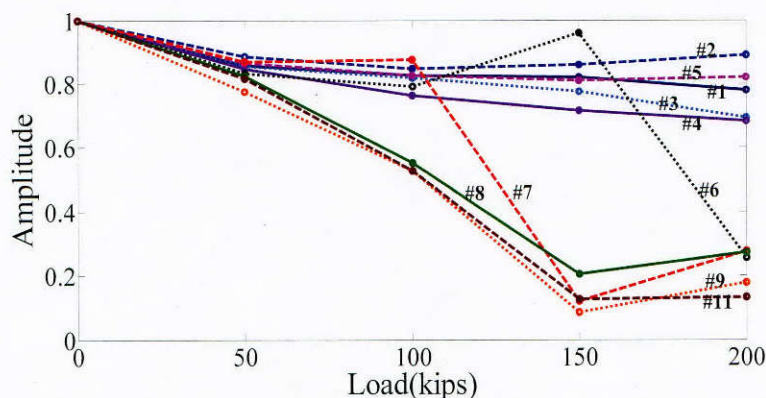


Figure 7-30: Changes in the normalized peak amplitude due to the applied load

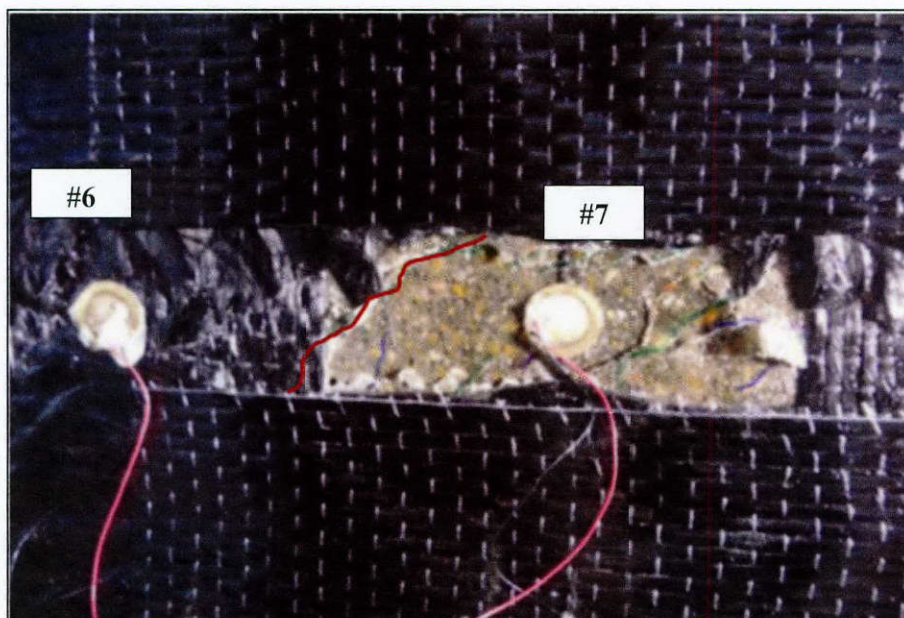


Figure 7-31: Shear crack formation at sensors #6 and #7

7.5 FINDINGS AND RECOMMENDATIONS

For artificial debonding defects between the CFRP strip and concrete, the sounding method detected the completely debonded and oily surfaces, while no distinguishable features were found from the signals of the sandy surface. Sounding signals obtained at properly installed CFRP anchors have the same feature as those obtained from well-bonded areas. When anchor holes were not completely filled, the spectrum of the sounding signal showed high frequency components. However, this feature could not quantitatively determine the anchor depth.

Both the sounding method and ultrasonic method located debonding between the CFRP strip and concrete substrate. The sounding method is easy to apply and more suitable for in-situ testing.

The ultrasonic method was used for monitoring debonding and cracking of a standard beam and a T-beam during loading. The ultrasonic method effectively detected the CFRP debonding process during loading. The ultrasonic method could detect crack initialization well before the cracks were visible.

Chapter 8. Design and Detailing Recommendations for CFRP Anchors

8.1 DESIGN APPROACH

Anchored CFRP strengthening systems consist of CFRP strips bonded to the surface of a concrete member where they are needed to resist tensile forces, and CFRP anchors that anchor the CFRP strips to the concrete section. The overall layout of the CFRP anchored system developed in this study is shown below in both plan and isometric views in Figure 8-1 and Figure 8-2 respectively.

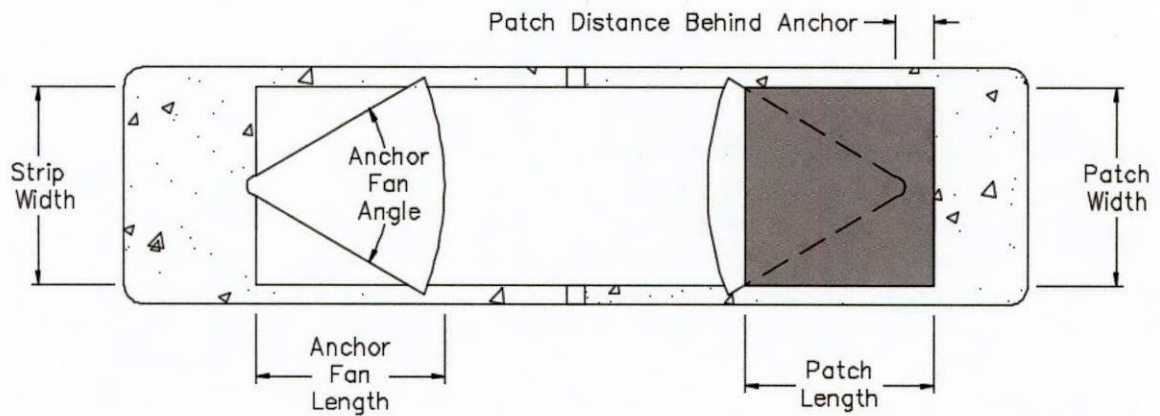


Figure 8-1: Plan view of anchor system; left: anchor prior to adding patches, right: patches over anchor

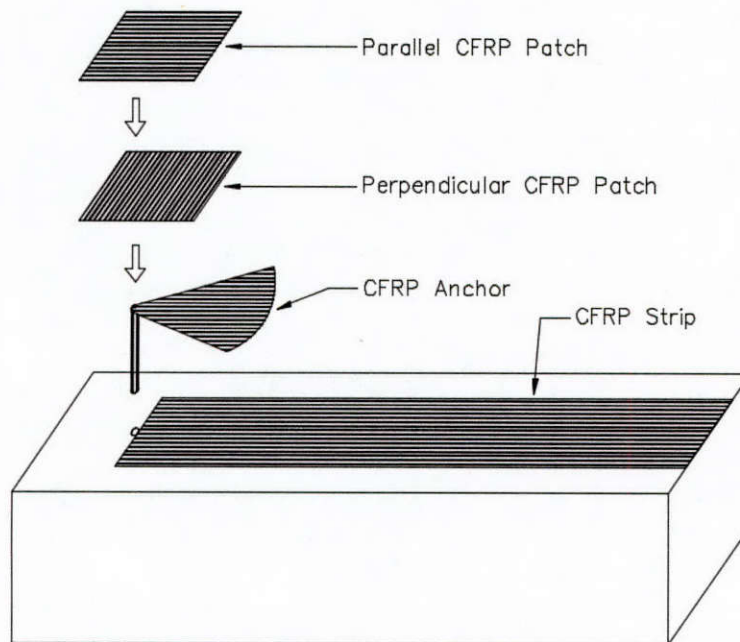


Figure 8-2: Isometric view of anchor system

CFRP strips are made of CFRP fibers embedded in an epoxy matrix to create a hardened laminate. CFRP strips are a brittle material having a modulus of elasticity that is less than half that

of reinforcing steel and an expected fracture stress in the range of 140 ksi. Due to the brittle nature of CFRP materials, they are highly sensitive to stress concentrations that can be generated from changes in direction (e.g., at bends), inadequate installation (e.g., when ripples are introduced in applications), or uneven distributions of stresses generated by the anchorage systems. For these reasons, only a fraction of the CFRP ultimate strain should be utilized in design. However, CFRP anchors should be designed such that the expected tensile strength of the CFRP strips can be developed to ensure that the strip fractures before the anchor ruptures.

CFRP anchors are designed based on the cross-sectional fiber area, or tensile strength, of the strip they are developing. Due to stress concentrations that occur at the anchor-hole edge where the anchor material is bent, a significantly larger cross-sectional area of CFRP fibers is required in the anchor compared with what is in the CFRP strip. In this study, this ratio of anchor to strip CFRP fiber area is recommended to be at least 2.0 to reliably achieve a strip fracture mode. This material ratio was matched to a specific anchor-hole geometry—especially the anchor-hole edge chamfer radius, to limit stress concentrations in the anchor material.

In the following sections, guidelines for designing CFRP anchors and their embedment holes are provided. These guidelines assume the strip and anchor materials are the same and have the same properties. The guidelines are only applicable to carbon fiber anchors since the limited tests performed in this study on glass fiber anchors did not produce acceptable performance. Further investigation of glass fiber anchors is needed to fully qualify their use. The anchor details developed in this study were shown to develop the full strength of CFRP strips even when the strips were fully debonded from the concrete surface. However, due to the beneficial effects of adequate bonding of strips to concrete, such as reducing stress concentrations in anchors and reducing crack widths in concrete members, it is recommended to always use adequately bonded strips in anchored CFRP systems.

8.2 DESIGN GUIDELINES

8.2.1 Notations and Definitions

AMR_D = design anchor material ratio = the ratio of anchor fiber material to that of the strip it is developing. This ratio is recommended to be at least equal to 2.0.

AMR_A = actual anchor material ratio = the ratio of anchor fiber material to that of the strip it is developing. This ratio is calculated after anchors have been chosen and is the true AMR for the specified anchors.

A_{Eqv} = anchor equivalent laminate cross-sectional area, in.²; this area is needed to determine the required fiber area in anchors as well as determine the diameter of the anchor hole.

d_{hole} = diameter of the anchor hole, in.

$f_{u,Exp}$ = manufacturer specified expected tensile stress at fracture of the CFRP laminate material, psi

LF_{anchor} = CFRP anchor fan length, in.

$LF_{anchor-min}$ = minimum permitted anchor fan length based on the specified design values for the inter-laminate bond stress capacity (σ_b), in.

n_a = number of manufactured anchor per anchor hole

n_A = number of anchors per strip width

n_l = number of laminate layers in the CFRP strip

R_c = anchor edge chamfer radius, in.

T_f = $(w_f n_l t_l f_{u,Exp})$ = strip tensile capacity based on the manufacturer specified expected tensile stress at fracture, lbs.

t_l = specified thickness of the laminate material used in the CFRP strip, in.

t_f	=	$(n_l t_l)$ = total thickness of the CFRP strip, in.
w_f	=	width of the CFRP strip, in.
$w_{f,A}$	=	the tributary width of strip developed per anchor, in.
$\gamma_{s,Sp}$	=	manufacturer specified fiber weight per surface area in the laminate material, oz/in. ²
$\gamma_{s,Exp}$	=	$1.25 \gamma_{s,Sp}$ = expected fiber weight per surface area in the laminate material, oz/in. ²
λ_s	=	weight of fibers in the strip per length, oz/in.
λ_A	=	specified weight of fibers in the anchor per length, oz/in.
λ_{A-Req}	=	required weight of fibers in the anchor per length, oz/in.
σ_b	=	specified design value for the inter-laminate bond stress capacity, psi.
θ_{anchor}	=	CFRP anchor fan angle, degrees (recommended not to exceed 60°)

8.2.2 Sizing CFRP Anchors

The cross-sectional area ($w_f n_l t_l$) of a CFRP strip can be determined based on the force it is required to resist in a particular strengthening project. The width of a CFRP strip (w_f) as well as the number of laminate layers (n_l) are determined according to the required strip tensile strength (T_f). Equation 8-1 can be rearranged to solve for either the width of strip or number of laminate layers required.

$$T_f = (w_f n_l t_l f_{u,Exp}) \quad \text{Equation 8-1}$$

Anchor design is based on the tributary strip width the anchor is engaging ($w_{f,A}$). For instance, in a 10 in. wide strip developed by two anchors, the anchors have the same tributary width as a single anchor developing a 5 in. strip. In both cases, the anchors will be designed to develop the strength of a 5 in. wide strip. The anchor tributary width is determined based on the desired number of anchors per strip.

$$w_{f,A} = w_f / n_A \quad \text{Equation 8-2}$$

In this study, CFRP anchors were found to effectively develop the strength of CFRP strips with tributary widths ranging from 3 to 10 in. Anchors were, however, more effective in developing narrower tributary widths, resulting in higher strip stresses at fracture. This size effect is attributed to anchors generating more even stress distributions in narrower strips, or conversely smaller stress concentrations in narrower strips. Selecting smaller anchor tributary widths is therefore recommended for improved performance. A balance should however be struck between improved performance and increasing the number of anchors and the associated increased construction time and cost. It is not recommended to use an anchor tributary width greater than 10 in.

The minimum required weight of anchor fibers per unit length ($\lambda_{m,A-Req}$) can then be evaluated. $\lambda_{m,A-Req}$ is equal to the weight per unit length of dry fiber in the strip width developed by the anchor multiplied by the design anchor material ratio (AMR_D). As discussed previously, an anchor material ratio of at least 2.0 is recommended.

$$\lambda_{A-Req} = AMR_D \times (w_{f,A} n_l \gamma_{s,Exp}) \quad \text{Equation 8-3}$$

Anchors having a specified fiber weight per unit length (λ_A) greater than (λ_{A-Req}) should be selected.

$$\lambda_A \geq \lambda_{A-Req} \quad \text{Equation 8-4}$$

Once the anchors are selected and provided fiber weight per unit length (λ_A) is known, the actual anchor material ratio can be calculated.

$$AMR_A = \frac{\lambda_A}{w_{f,A} n_l \gamma_{s,Exp}} \quad \text{Equation 8-5}$$

It is important to note that the required fiber weight of the anchor is based on the expected dry fiber weight per surface area of the laminate ($\gamma_{s,Exp}$). When weighting laminate fiber sheets, the expected fiber weight was found to be about 25% higher than the minimum fiber weight per surface area specified by the manufacturer ($\gamma_{s,Sp}$). Since the CFRP laminate fiber weights tend to run significantly higher than the minimum weight provided by the manufacturer ($\gamma_{s,Exp} = 1.25 \gamma_{s,Sp}$), the expected weight should be used in determining the fiber weight of the anchors so as not to under design the anchors.

The anchor equivalent laminate cross-sectional area is required for determining the anchor-hole diameter and can be evaluated as follows:

$$A_{Eqv} = AMR_A \times (w_{f,A} n_l t_l) \quad \text{Equation 8-6}$$

8.2.2.1 Anchor Fan Details

Anchor fan details are illustrated in Figure 8-3.

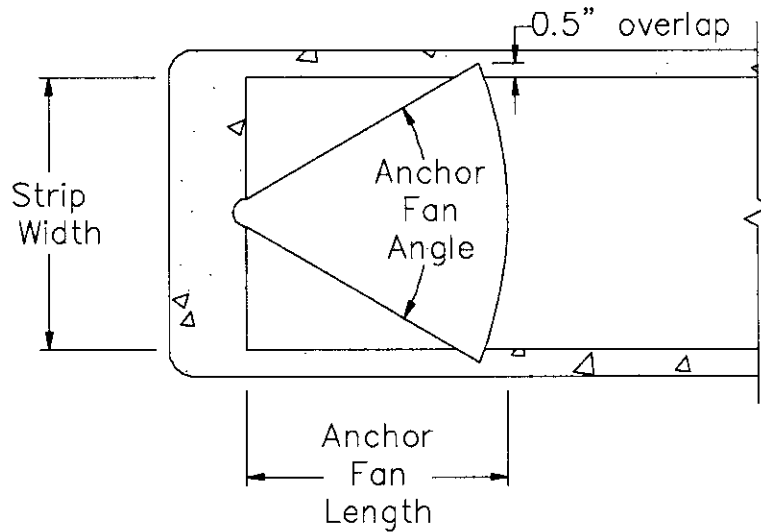


Figure 8-3: Anchor fan details

An effective anchor fan needs to extend 0.5 in. past the edges of the CFRP strip. In the case of multiple anchors per strip width, the anchor fans should overlap by at least 0.5 in. at their ends. This ensures that the entire width of the strip is engaged. The length of an anchor fan is directly related to the width it needs to span and the selected fan angle. The length of an anchor should also be sufficient to preclude an interlaminar bond failure between the anchor and the strip it is developing. The minimum anchor fan length should therefore be evaluated first based on the manufacturer specified interlaminar bond stress capacity (σ_b).

$$LF_{anchor-min} = \frac{T_f}{w_f \times \sigma_b} \quad \text{Equation 8-7}$$

Equation 8-7 assumes that the contact area between anchors and strip is a rectangle with length equal to fan length and width equal to strip width. This is primarily because the CFRP patches placed on top of the anchors contribute to transferring stresses.

Once the minimum anchor length is determined, the actual length of the anchor can be obtained by selecting a fan angle (θ_{anchor}) smaller or equal to 60° using the following relation:

$$LF_{anchor} = \frac{(w_f/2) + 0.5}{\tan\left(\frac{\theta_{anchor}}{2}\right)} \geq LF_{anchor-min} \quad \text{Equation 8-8}$$

In general, a smaller fan angle produces a more gradual transfer of force to the anchor. Kim (2011) recommended a fan angle less than 60° for effective transfer of tensile loads from CFRP strips. Results from this study further support that conclusion. Considering that the tensile load transfer from the outer fibers in a strip is less efficient as the angle between the CFRP strip fiber and the anchor-fan fibers increases, a maximum anchor-fan angle of 60° is recommended for anchor design.

8.2.3 Anchor Hole Details

Parameters for anchor hole details are illustrated in Figure 8-4.

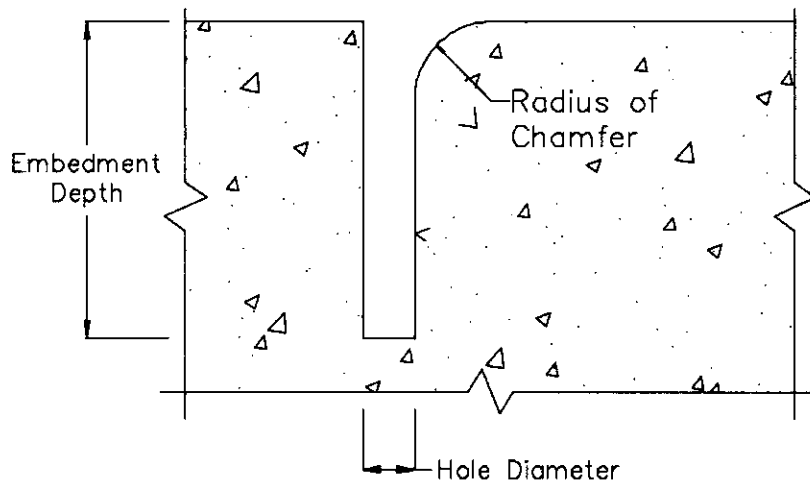


Figure 8-4: Anchor hole details

8.2.3.1 Diameter of Anchor Hole

An anchor hole area at least 1.4 times larger than the equivalent laminate area of CFRP anchors (A_{Eqv}) was previously recommended (Pham, 2009). This continues to be the recommendation and was supported throughout testing. While previous work and some work in this study tested relatively small anchors (developing a single layered 5 in. strip), tests conducted in this study on larger anchors developing a double layered 10 in. wide strip further demonstrated that the factor of 1.4 is applicable to larger anchors. To determine the required diameter of the anchor hole, Equation 8-9 can be used.

$$d_{hole} = \sqrt{\frac{4 \times 1.4 \times A_{Eqv}}{\pi}} \quad \text{Equation 8-9}$$

8.2.3.2 Hole Edge Chamfer Radius

To reduce stress concentrations at the edge of an anchor hole, the hole edge can be rounded. A chamfer radius of 0.5 in. as recommended by Pham (2009) was used effectively in all tests in this study where anchors having an anchor material ratio (AMR) not less than 2.0 developed strips with width not exceeding 5in. When larger anchors were tested (for a double layered 10 in. wide strip), however, the 0.5 in. chamfer radius was found to be inadequate. A relation for increasing the chamfer radius (R_c) with increasing anchor size or hole diameter was developed and presented below.

$$R_c = 1.4 d_{anchor} / 2 \geq 0.5 \text{ in.} \quad \text{Equation 8-10}$$

8.2.3.3 Embedment Depth

In TxDOT project 0-6306 it was recommended that a 6 in. anchor embedment depth be used. In this study, anchor embedment depths of 4 and 6 in. were successfully used. While the embedment depth was not found to be a significant factor affecting the strength of anchored CFRP systems, anchorage regions sustained higher levels of damage with 4 in. depths as compared to 6 in. depths. A 6 in. anchor embedment depth is therefore recommended. In cases where a 6 in. embedment depth is impractical, a depth as low as 4 in. may be used. In all cases, however, the anchors need to be embedded at least 2 in. into the concrete core of a reinforced concrete member.

8.2.4 Anchor Patch Geometry

The patches over the CFRP anchor are vital in the stress transfer from the strip to the anchor. Anchor patches should have the same width as the CFRP strip and the same length as the CFRP anchor. The patches should start 2 in. behind the anchor hole (patch distance behind anchor in Figure 4-1). This distance helps distribute stresses around the anchor hole and prevent premature anchor rupture and delamination between anchor and strip.

8.3 DESIGN EXAMPLE

The design of an anchored CFRP system is given next for a given strengthening scenario, which requires a factored strip strength (T_f) of 28,000 lbs. The material properties of the CFRP fibers and laminate are:

Laminate expected fracture stress: $f_{u,Exp} = 143,000$ psi

CFRP laminate thickness: $t_l = 0.02$ in.

Weight of dry fibers in the laminate per unit surface area $\gamma_{s,Sp} = 9.3$ oz/yd.²

$$\gamma_{s,Exp} = 1.25\gamma_{s,Sp} = 11.6 \frac{\text{oz}}{\text{yd.}^2} = 0.00897 \frac{\text{oz}}{\text{in.}^2}$$

1/2" CFRP anchor fiber weight per unit length, $\lambda_A = 0.08$ oz/in.

5/8" CFRP anchor fiber weight per unit length, $\lambda_A = 0.125$ oz/in.

In this design, one layer of CFRP and one anchor are selected. Other designs with a narrower multi-layered narrower strips or a multi-anchored wide strip can be performed following the same procedure outlined next.

1. The required width of the CFRP strip (w_f) can be determined using Equation 8-1.

$$28,000 \text{ lbs} = (w_f \times 1 \times 0.02" \times 143,000 \text{ lbs}) \quad \rightarrow \quad w_f = 9.8" \cong 10"$$

2. Only one anchor will be used to develop the entire strip ($n_A = 1$), Equation 8-2 can be used to determine the tributary anchor width.

$$w_{f,A} = 10''/1 \quad \rightarrow \quad w_{f,A} = 10''$$

3. Once the tributary width is established, Equation 8-3 can be used to determine the required dry fiber weight per anchor (λ_{A-Req}) assuming a design anchor material ratio (AMR_D) of 2.0.

$$\lambda_{A-Req} = 2 \times (10'' \times 1 \times 0.00897 \text{ oz}/in^2) \quad \rightarrow \quad \lambda_{A-Req} = 0.179 \text{ oz}/in$$

Since this weight is larger than either of the available 1/2" and 5/8" anchors, the choice is made to combine two 5/8" anchors to make a larger anchor having a dry fiber weight $\lambda_A = 0.25 \text{ oz}/in^2$, which is larger than λ_{A-Req} (Equation 8-5). Once the anchor is chosen, the actual anchor material ratio must be calculated.

$$AMR_A = \frac{0.25 \text{ oz}/in}{10'' \times 1 \times 0.00897 \text{ oz}/in^2} \quad \rightarrow \quad AMR_A = 2.8$$

4. The anchor equivalent laminate area is then calculated for use later in determining the required anchor hole diameter (Equation 8-6).

$$A_{Eqv} = 2.8 \times (10'' \times 1 \times 0.02'') \quad \rightarrow \quad A_{Eqv} = 0.56 \text{ in}^2$$

*It is important to note that nominal anchor diameters provided by the manufacturer (i.e., 1/2-in. and 5/8-in.) **should not** be used in calculating anchor area for prefabricated anchors. The nominal dimensions are not exact and will provide incorrect material ratios if used in design.

5. The anchor fan geometry is determined using Equation 8-7 and Equation 8-8.

$$LF_{anchor-min} = \frac{28000 \text{ lbs}}{10'' \times 500 \text{ psi}} \quad \rightarrow \quad LF_{anchor-min} = 5.6'' \cong 6''$$

$$LF_{anchor} = \frac{(10''/2) + 0.5''}{\tan\left(\frac{60^\circ}{2}\right)} \geq 6'' \quad \rightarrow \quad LF_{anchor} = 9.5'' \cong 10''$$

Assuming an anchor fan angle of 60° provides a sufficient anchor length to satisfy interlinear bond requirements. An anchor length of 10 in. is selected.

6. The diameter of the anchor hole is determined based on the equivalent anchor area and Equation 8-9.

$$d_{hole} = \sqrt{\frac{4 \times 1.4 \times 0.56 \text{ in}^2}{\pi}} \quad \rightarrow \quad d_{hole} = 0.999'' \cong 1.0''$$

Hole diameters should be rounded up to the nearest 16th of an inch

7. The chamfer radius at the hole edge is given by Equation 8-10.

$$R_c = 1.4 \times (1"/2) \geq 0.5" \quad \rightarrow \quad R_c = 0.7" \cong 0.75"$$

Round the chamfer radius up to the nearest eighth of an inch.

8. Embedment depth is chosen to be 6". Therefore the total anchor length needs to be 10"+6"= 16" (anchor fan length + embedment depth)
9. With all other parameters determined, the dimensions of the overlapping patches are determined to be 10 in. x 10 in. (overlap length x strip width). Two patches are needed, one with a principal fiber direction parallel to the CFRP strip and one with the principal fiber direction perpendicular to the strip, both having the same dimensions. Both patches are placed 2 in. behind the center of the anchor hole ("Patch distance behind anchor" in Figure 8-1).

Figure 8-5 shows the designed CFRP system details.

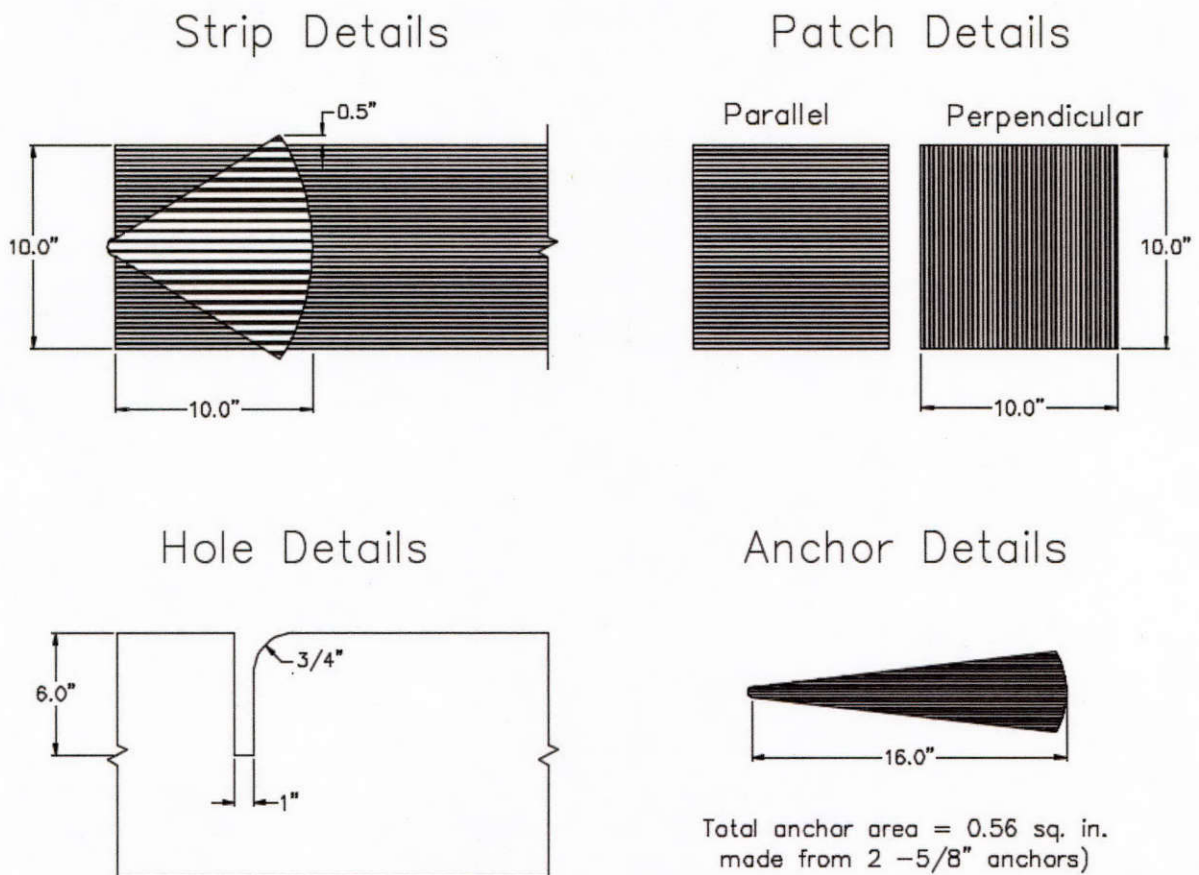


Figure 8-5: Example layout

Chapter 9. Design and Detailing Recommendations for CFRP Shear Strengthening

9.1 OBJECTIVE

In this chapter, a rational and unified design methodology for CFRP shear strengthening is presented. The methodology is supported by test data and is consistent with the 2014 AASHTO and ACI 440.2R-08 shear design procedures. Additionally, guidelines on CFRP detailing requirements are provided.

9.2 MATERIAL INTERACTION

Material interactions in shear behavior have often been ignored in search of simple design methodologies. However, ignoring significant material interactions can often lead to high variability between experimentally measured and predicted shear capacities. The following sections highlight the interactions that influenced the shear contributions of the concrete and transverse reinforcement, which helped reduce the variability between the measured and predicted shear capacities.

9.2.1 Concrete Contribution

ACI 440.2R-08 specifies a simple lower-bound shear stress capacity for concrete that is equal to two times the square root of the concrete compressive strength (in psi units). This value was empirically derived as the lower-bound shear stress at which the first inclined shear crack forms in plain concrete beams. Using vertical equilibrium, the lower-bound concrete shear stress is multiplied by the vertical shear area ($b_w d$) to determine the concrete shear contribution.

Implicit in the derivation of the concrete contribution is the assumption that the concrete shear stress does not increase after the shear crack has formed, which is inconsistent with the test results that were shown in the previous chapters. One reason for the discrepancy is due to the definition of the shear area. The concrete contribution is assumed to have a linear correlation with the vertical shear area. However, a stronger correlation was observed between the concrete contribution and the inclined shear area, as shown by Figure 9-1 which acts parallel to the shear crack plane (Figure 9-1(b)). Consequently, the inclined shear area is dependent on the inclined shear crack angle (θ) relative to the longitudinal axis of the member.

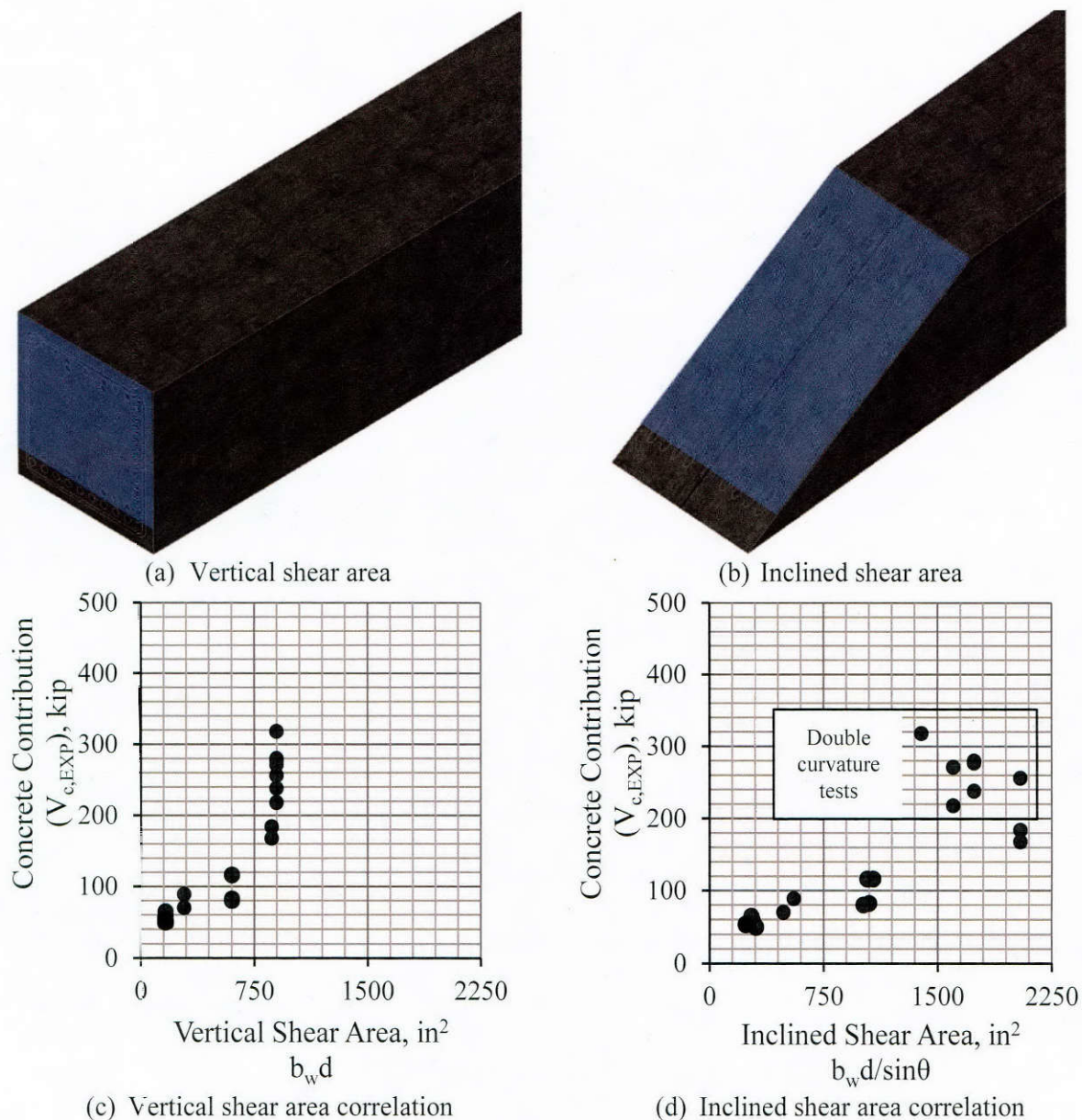


Figure 9-1: Comparison of the shear area definition

Through the investigation of the inclined shear area, the concrete contribution was also found to be affected by the loading conditions as illustrated by the highlighted double curvature tests shown in Figure 9-1 (d). Consequently, the single and double curvature pile cap girder control specimens were investigated to determine the influence the loading conditions had on the concrete contribution.

Recall that the only difference between the single and double curvature control specimens was the existence of a point of inflection in the middle of the double curvature specimens' constant shear span. Thus, the double curvature specimens had an effective span-to-depth ratio (M/V_d), measured between the points of peak and zero moment, that was half of its actual span-to-depth ratio (a_v/d). Consequently, the results show that as the effective span-to-depth ratio decreases, the concrete contribution increases. Therefore, a relationship between the effective span-to-depth ratio and the concrete contribution was developed.

A correlation between the concrete shear stress coefficient and the total vertical transverse reinforcement shear stress was observed as shown in Figure 9-2. The interaction between the two materials suggests that the transverse reinforcement provides a clamping force across the shear crack, which allows the concrete contribution to increase as the amount of transverse reinforcement increases.

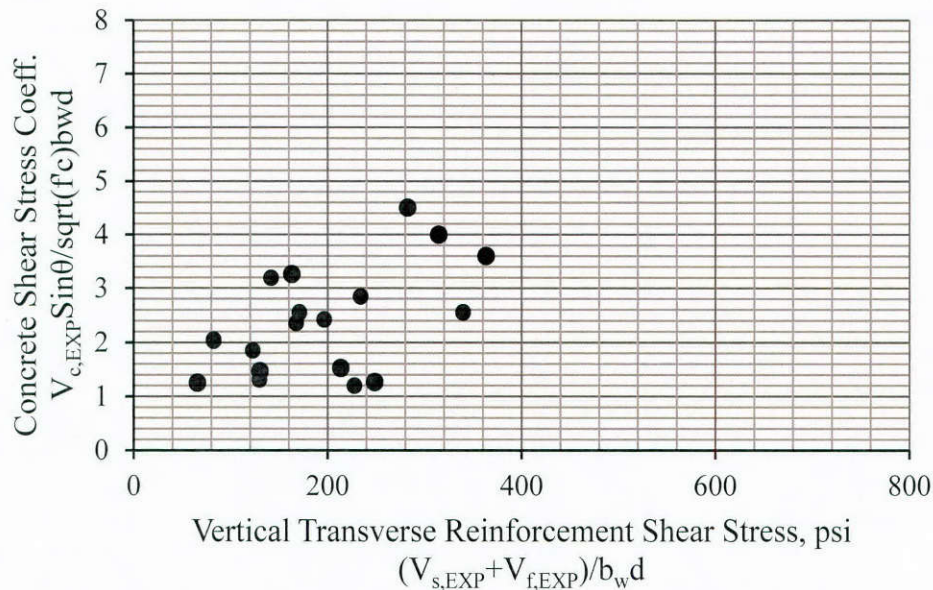


Figure 9-2: Correlation between the concrete shear stress coefficient and the transverse reinforcement

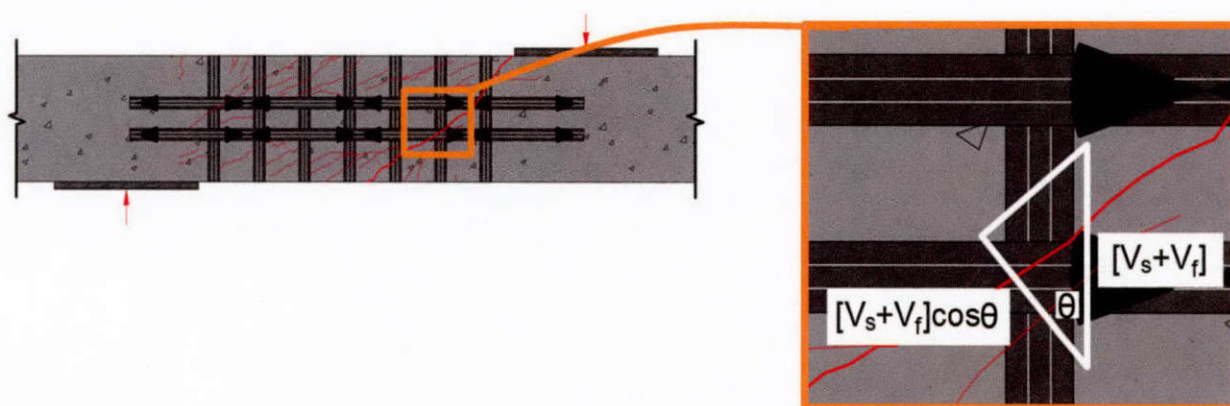


Figure 9-3: Clamping force perpendicular to the shear crack

The component of the vertically oriented transverse reinforcement that acts perpendicular to the shear crack is shown in Figure 9-3. The normal force provided by the vertical transverse reinforcement helps improve the concrete contribution through enhanced aggregate interlock. However, the fraction of the transverse reinforcement that helps increase the concrete contribution is dependent on the effective coefficient of friction of the aggregate interlock along the critical shear crack. The effective coefficient of friction was determined to be half based on an investigation of the collected tests results. However, more research will need to be conducted to determine if there is a range of effective coefficient of frictions. It is noteworthy that the horizontal CFRP

reinforcement should not be included in the evaluation of the clamping force at present due to a lack of experimental data.

In addition to providing information about the interaction between the concrete and transverse reinforcement, Figure 9-2 also indicated that the lower bound concrete shear stress coefficient should be changed from 2.0 to 1.25. The final form of the concrete shear contribution, shown in Equation 9-1, includes the effects of the inclined shear crack angle, the loading conditions, and the amount of vertical transverse reinforcement.

$$V_{c,mod} = \frac{1.25\sqrt{f'_c}b_wd}{\sin(\theta)} \left(\frac{1}{(M/Vd)^2} + 0.9 \right) + \frac{1}{2}(V_s + V_f) \cos(\theta) \text{ [in lb. units]} \quad \text{Equation 9-1}$$

Equation 9-1 represents the concrete contribution at the peak shear capacity as opposed to the typically assumed concrete contribution at the onset of the first inclined shear crack. The concrete contribution in Equation 9-1 assumes that the concrete has not crushed and that the aggregate interlock is maintained at the onset of the transverse reinforcement failure (i.e., steel reinforcement yielding and CFRP reinforcement fracturing). The aforementioned assumptions can be reasonably made by providing limits to the concrete contribution.

An upper-bound concrete contribution limit was determined based on the experimental data to prevent the concrete from crushing before the transverse steel reinforcement yielded and the CFRP reinforcement fractured. In several tests, the concrete shear stress coefficients reached a value of 5.0 without crushing the concrete. On the other hand, numerous 24-in. deep T-beams crushed the web concrete without fracturing the CFRP reinforcement at concrete shear stress coefficients above 5.5. From these findings, a reasonable upper bound value for the concrete shear stress coefficient can be taken as 5.0.

In special circumstances (i.e., members without transverse reinforcement, span-to-depth ratios above 3.0, and 39-deg. or greater shear crack angles), Equation 9-1 will result in concrete shear stress coefficients that are less than 2.0. However, the ACI 440.2R-08 design code states that the concrete shear stress coefficient need not be taken less than 2.0 if a minimum amount of transverse reinforcement is provided, which was supported by the experimental data. Hence, a lower-bound concrete shear stress coefficient equal to 2.0 is satisfactory.

The permissible range for the concrete contribution is shown in Equation 9-2, which assumes that a minimum amount of transverse reinforcement, consistent with ACI 318-14 or AASHTO (2014), is provided.

$$2\sqrt{f'_c}b_wd \leq V_c \leq 5\sqrt{f'_c}b_wd \text{ [in psi units]} \quad \text{Equation 9-2}$$

The loss of aggregate interlock at the peak shear capacity is mitigated by limiting the width of the shear crack relative to the maximum aggregate size as will be explained in Section 9.2.2.2.

9.2.2 Transverse Reinforcement Contribution

From previous research, it has been reported that there is an interaction between the steel stirrups and the externally bonded CFRP transverse reinforcement. Specifically, researchers have suggested that increasing the amount of transverse steel reinforcement adversely effects the shear contribution of the CFRP and vice-versa. Though, an interaction between the transverse steel and CFRP reinforcement does not appear to exist at the ultimate shear capacity for anchored CFRP layouts since the transverse steel reinforcement must yield prior to fracturing the CFRP strips.

However, the shear contribution of the transverse reinforcement is affected by the angle of the inclined shear crack. A shallow inclined shear crack angle (θ), relative to the longitudinal axis of the member, will engage more stirrups and anchored CFRP strips than a typically assumed 45-degree shear crack angle, which results in higher than expected shear capacity.

Typical reinforced concrete members are designed such that the flexural capacity of the member governs. In doing so, the longitudinal reinforcement is proportioned so that it will yield prior to crushing the compression zone. Low longitudinal reinforcement ratios tend to allow flexural cracks to form, which can turn into flexural-shear cracks if the member is experiencing high shear stresses (Figure 9-4).

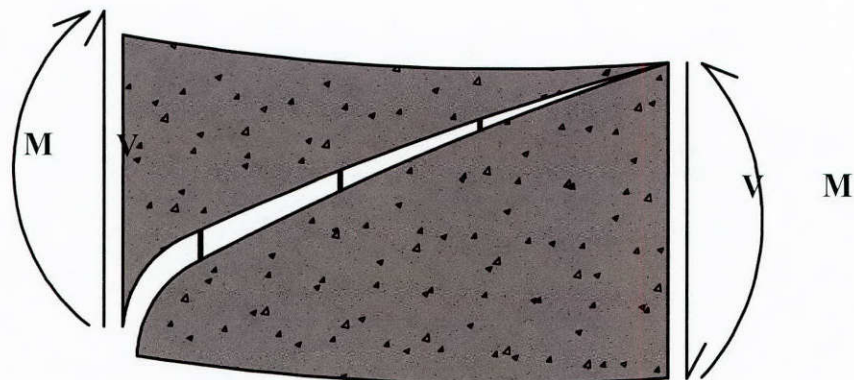


Figure 9-4: Flexural-shear crack

Based on the Modified Compression Field Theory (MCFT) (Vecchio and Collins, 1986), flexural-shear crack angles can be calculated for various transverse reinforcement ratios and horizontal strains (ϵ_x) as shown in Figure 9-5. The plot indicates that the shear crack angle is less influenced by the transverse reinforcement ratio compared to the horizontal strain. Therefore, the shear crack angles can be approximated by a linear equation that is only dependent on the horizontal strain. Compared to the results from the MCFT, Equation 9-3, developed for the simplified MCFT, conservatively overestimates the shear crack angles on average.

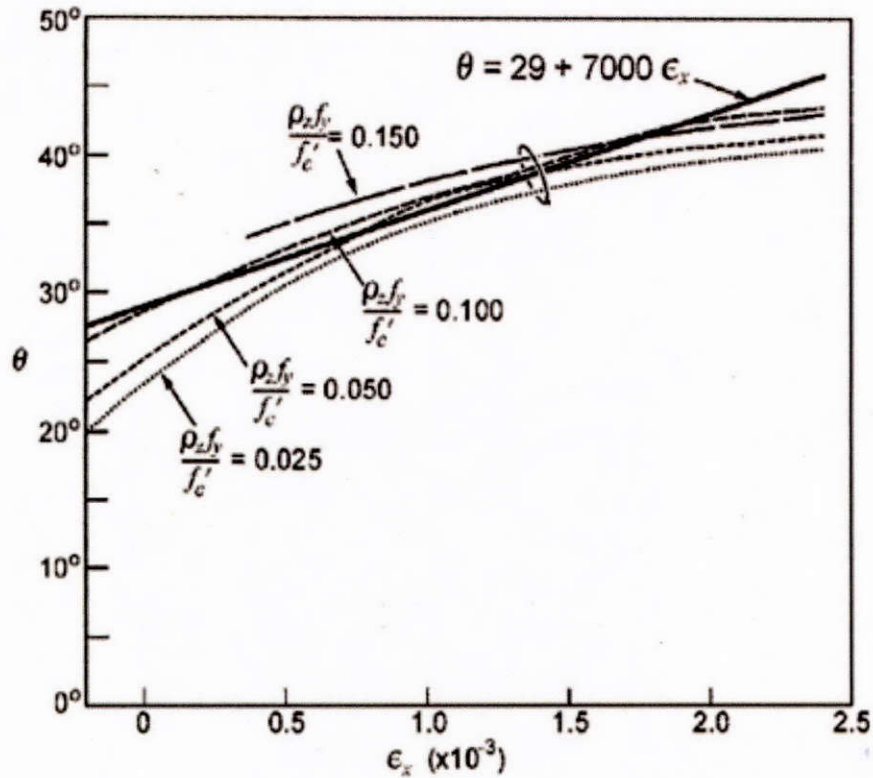


Figure 9-5: Evaluation of theta using the full and simplified MCFT (Bentz et al., 2006)

$$\theta = 29 + 7000\epsilon_x \quad \text{Equation 9-3}$$

For simplicity, the angle of a flexural-shear crack can be assumed to be constant over the height of a member based on the average horizontal strain that occurs near mid-depth of the member. The average horizontal strain can be approximated by halving the net longitudinal strain at the centroid of the longitudinal tension reinforcement as shown in Equation 9-4.

$$\epsilon_x = \epsilon_s / 2 \quad \text{Equation 9-4}$$

However, the constant shear crack angle will change along the length of the member since external forces cause a strain gradient to develop in the longitudinal tension reinforcement. Evaluating Equation 9-3 and Equation 9-4 at the location of the peak moment will result in the largest possible shear crack angle, which in turn reduces the shear capacity since the shear crack crosses less transverse reinforcement. Therefore, the shear crack angle can be evaluated at the location of the peak moment. Equation 9-5, an adaptation from AASHTO (2014), can be used in lieu of computing the flexural strain distribution to determine the strain at the centroid of the tension reinforcement. Note that the shear term (V), at the location of M , goes to zero when the peak moment in the span corresponds to the peak moment in the member.

$$\epsilon_s = \frac{\left(\frac{|M|}{0.9d} + |V_{@M}|\right)}{E_s A_s} \quad \text{Equation 9-5}$$

Knowing the average shear crack angle, the shear contribution of the transverse reinforcement can be multiplied by $\cot(\theta)$ to determine the number of steel stirrups and CFRP strips that cross the shear crack.

9.2.2.1 Evaluation of the Shear Crack Angle

The average shear crack angles from a number of specimens were measured using sketches of the experimental crack patterns as shown in Figure 9-6. The shear crack angles were then computed using Equation 9-3 and Equation 9-4 based on the estimated tensile longitudinal strains from Equation 9-5 in the peak moment regions. A comparison between the experimental and predicted shear crack angles is shown in Figure 9-7.

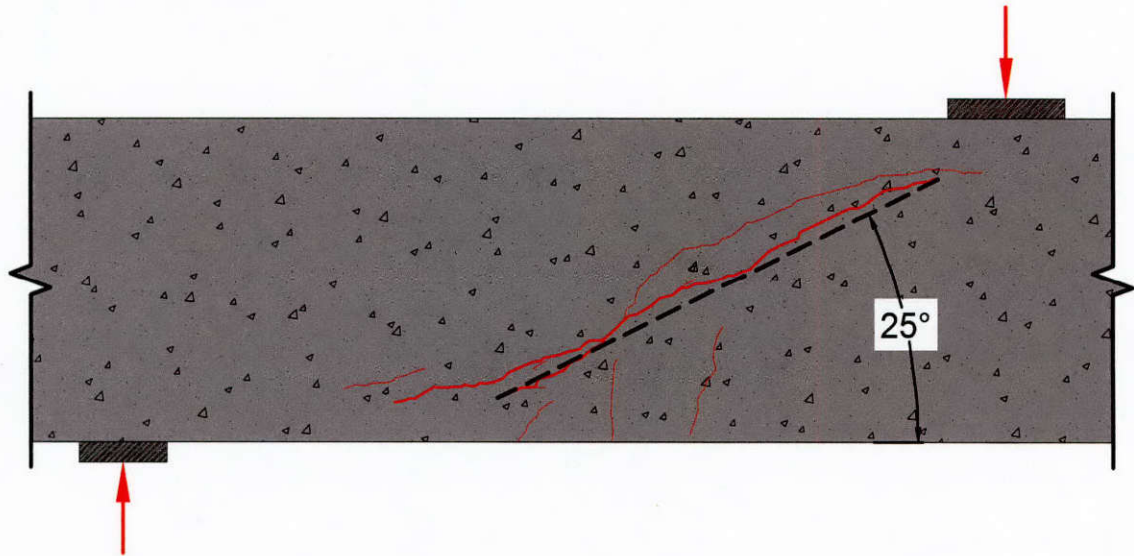


Figure 9-6: Experimental shear crack angle for S-U-VN-HN

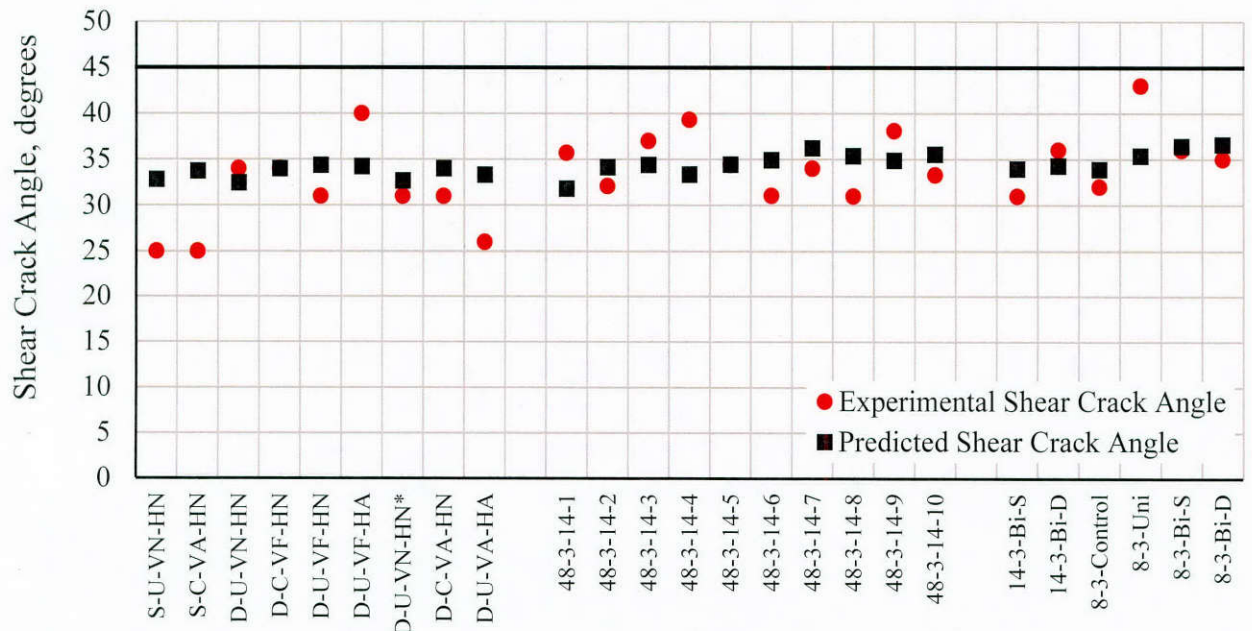


Figure 9-7: Comparison of shear crack angles

Based on Figure 9-7, there is good agreement between the experimental and predicted shear crack angles, thus validating the proposed method for calculating the shear crack angle. Notice that all of the experimental and predicted angles were less than the assumed 45-degrees indicating that the transverse reinforcement contributed more to the shear capacity than ACI 440.2R-08 would have allowed. However, the shallow shear crack angles are a result of the high longitudinal reinforcement ratios used in these specimens, which resulted in relatively low longitudinal strains at the onset of the shear failure.

9.2.2.2 Effective CFRP Fracture Strain

The minimum and average CFRP strains in the CFRP strips across the critical shear crack at the ultimate shear capacity of the member are shown in Figure 9-8. These CFRP strains were measured using the high-resolution optical measurement system.

ACI Committee 440 (2008) intended for the effective CFRP strain to be a lower bound of the average CFRP fracture strain. The effective CFRP fracture strain was also intended to prevent excessive shear crack widths, which could result in the loss of aggregate interlock prior to fracturing the CFRP strips. As a result, ACI Committee 440 (2008) recommended a maximum effective CFRP fracture strain of 0.004-in./in.

However, the test data in Figure 9-8 shows that the CFRP anchors enabled the CFRP strips to reach minimum CFRP strains near or in excess of the 0.004-in./in. limit imposed by ACI Committee (2008). In fact, the lower bound effective strain of the CFRP at failure can be taken as 60-percent of the CFRP laminate fracture strain (i.e., 0.006-in./in. for the CFRP used in this project). Note that in this project, the loss of aggregate interlock never preceded fracturing of the CFRP strips.

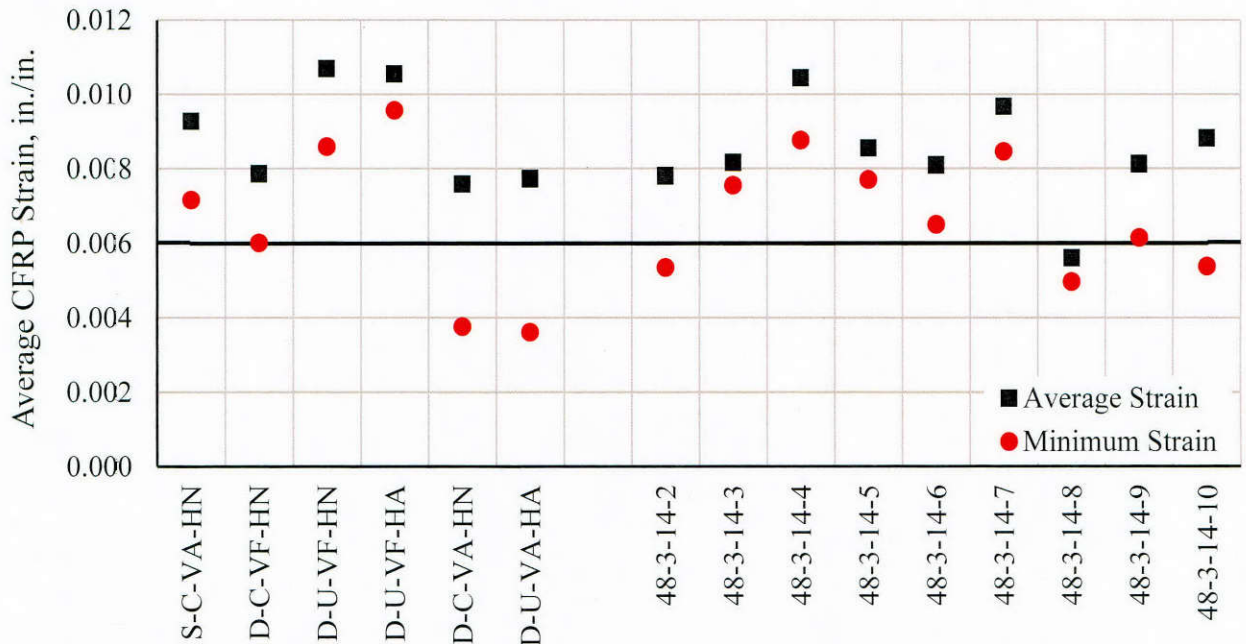


Figure 9-8: Minimum and average CFRP strains across the critical shear crack at failure

Notice that specimen 48-3-14-8 had an average CFRP fracture strain that was less than 60-percent of the CFRP fracture strain. The reduction in the average CFRP fracture strain was caused by the combined adverse effects of the double layer uni-directional layout and the 10-in. wide CFRP strips. Past studies have indicated that strength gains are not linearly proportional to the number of CFRP layers used. Moreover, wide CFRP strips have lower average CFRP fracture strains due to a non-uniform strain distribution along the strip's width. To mitigate these problems,

it is recommended to use single layer CFRP layouts with narrow CFRP strips, which helps provide adequate load distribution and redundancy.

Being able to reach the recommended effective CFRP fracture strain limit assumes that the concrete aggregate interlock is not lost prior to failing the transverse steel and CFRP reinforcement. Through an investigation of vertical displacement compatibility in which critical shear crack widths and maximum aggregate sizes were compared relative to CFRP strains, it was determined that using a 3/4-in. or greater maximum aggregate size will likely prevent the premature loss of aggregate interlock. Thus, the CFRP can satisfactorily achieve an effective CFRP fracture strain of 0.006 in./in.

9.3 SHEAR DESIGN EQUATIONS

The proposed shear design equations are intended to be used for strengthening members that have span-to-depth (a_v/d) ratios greater than 2.0 (i.e., sectional shear behavior). In members with span-to-depth ratios less than 2.0, the use of either uni- or bi-directional CFRP layouts was found to be ineffective in improving the shear capacity.

9.3.1 Strength Reduction Factors

Shear design guidelines are expected to have an adequate margin of reliability such that the expected shear capacity will be greater than the design, or factored, shear capacity. To achieve this level of reliability, a strength reduction factor of 0.75 is proposed and is consistent with ACI 440.2R-08.

Moreover, ACI 440.2R-08 utilizes an additional strength reduction factor (ψ_f) applied directly to the CFRP shear contribution to account for the relative reliability of each type of CFRP system. For instance, fully wrapped systems have a reduction factor of 0.95 whereas unanchored U-wrap and two-sided external applications have a reduction factor of 0.85. Based on the test data, the reliability and efficiency of fully wrapped and anchored CFRP systems were shown to be similar regardless whether the members were uncracked or pre-cracked. Consequently, the use of the ACI 440.2R-08 CFRP reduction factor was not considered since all of the tests had anchored or fully wrapped systems.

9.3.2 Proposed Shear Strengthening Design Guidelines

The proposed shear strengthening design guidelines are shown in Table 9.1 while the definition of the variables are shown in Table 9.2.

Table 9-1: Proposed shear strengthening design equations

Factored Shear Strength for Members with Span-to-Depth Ratios (a_v/d) ≥ 2.0:			
$\phi V_n = 0.75(V_c + V_s + V_f)$			<i>Equation 9-6</i>
Determination of the Critical Shear Crack Angle:			
$\varepsilon_s = \frac{(\frac{ M }{0.9d} - V_{@M})}{E_s A_s}$	<i>Equation 9-7</i>		
$\theta = 29 + 3500\varepsilon_s$	<i>Equation 9-8</i>	or use the observed inclined crack angle for $29^\circ \leq \theta \leq 50^\circ$	<i>Equation 9-9</i>
Concrete Contribution to Shear Capacity:			
$V_c = 1.25 \sqrt{f'_c} b_w d \left(\frac{1}{\sin(\theta)} \right) \left(\frac{1}{(M/Vd)^2} + 0.9 \right) + \frac{1}{2} (V_s + V_f) \cos(\theta)$		[Detailed]	<i>Equation 9-10</i>
or			
$V_c = 2 \sqrt{f'_c} b_w d$		[Simple]	<i>Equation 9-11</i>
Limit of Concrete Contribution:			
$2\sqrt{f'_c} b_w d \leq V_c \leq 5\sqrt{f'_c} b_w d$			<i>Equation 9-12</i>
Steel Contribution to Shear Capacity:			
$V_s = \frac{A_{vs} f_{yt} d (\sin \alpha_s + \cos \alpha_s)}{s} \cot(\theta)$			<i>Equation 9-13</i>
$= \frac{A_{vs} f_{yt} d}{s} \cot(\theta)$		for $\alpha_s = 90^\circ$	<i>Equation 9-14</i>
CFRP Contribution to Shear Capacity:			
$V_f = \frac{A_{vf} f_{fe} d_{fv} (\sin \alpha_f + \cos \alpha_f)}{s_f} \cot(\theta)$			<i>Equation 9-15</i>
$= \frac{A_{vf} f_{fe} d_{fv}}{s_f} \cot(\theta)$		for $\alpha_f = 90^\circ$	<i>Equation 9-16</i>
where $A_{vf} = 2nt_f w_f$ and $f_{fe} = 0.6\varepsilon_u E_f \leq 0.006E_f$		for $a \geq 3/4$ in.	
Upper Limit of Steel and CFRP Contributions:			
$[V_s + V_f] \leq 8\sqrt{f'_c} b_w d$			<i>Equation 9-17</i>

Note: For the materials used in the test program, the lower bound average CFRP strain at fracture was 0.006-in./in. For CFRP materials with a significantly different fracture strain (0.01-in./in.) or elastic modulus (13,900-ksi), the lower bound average strains should be verified.

Table 9-2: Variable notation

a	maximum aggregate size, in.
A_s	area of the longitudinal tension reinforcement, in. ²
a_v	shear span measured from the edge to edge of the loading and reaction plates, in.
A_{vf}	area of vertical CFRP transverse reinforcement within spacing s_f , in. ²
A_{vs}	area of steel transverse reinforcement within spacing s , in. ²
b_w	web width, in.
d	distance from the extreme compression fiber to the centroid of the longitudinal tension reinforcement, in.
d_{fv}	distance from the centroid of the anchor hole of vertical strips to the centroid of longitudinal tension reinforcement, or equal to d for fully wrapped systems, in.
E_f	tensile modulus of elasticity of CFRP based on ACI 440.2R-08 guidelines, psi
E_s	tensile modulus of elasticity of longitudinal steel reinforcement, psi
f_{fe}	effective stress in CFRP at failure, psi
f'_c	specified 28-day compressive strength of the concrete, psi
f_{yt}	specified yield strength of the transverse reinforcement, psi
M	peak factored design moment in the shear span being considered, lb.-in
n	number of CFRP plies
s	center-to-center spacing of the steel transverse reinforcement, in.
s_f	center-to-center spacing of the CFRP transverse reinforcement, in.
t_f	single ply laminate thickness of the CFRP reinforcement, in.
V	peak factored design shear force in the shear span being considered, lb.
V_c	concrete shear contribution, lb.
V_f	CFRP shear contribution, lb.
V_n	nominal shear strength, lb.
V_s	steel shear contribution, lb.
$V_{@M}$	factored design shear force where M is evaluated, lb.
w_f	width of the CFRP reinforcing plies, in.
α_f	angle of the CFRP transverse reinforcement relative to the longitudinal axis, deg.
α_s	angle of the steel transverse reinforcement relative to the longitudinal axis, deg.
ϵ_s	net longitudinal strain at the centroid of longitudinal tension reinforcement, in./in.
ϵ_u	CFRP fracture strain based on ACI 440.2R-08 guidelines, in./in.
ϕ	shear strength reduction factor, 0.75
θ	angle between the inclined critical crack and the tension chord of the member, deg.

The inclined shear crack angle (θ) can be calculated from the tensile strain at the centroid of the longitudinal reinforcement based on Equation 9-7 and Equation 9-8 in the peak moment region of the shear span or it can be taken as an observed shear crack angle. The inclined shear crack angle is limited based on AASHTO (2014) recommendations so that excessively small or large tensile strains will not produce unrealistic shear crack angles (Equation 9-9).

The concrete shear contribution (V_c) can be determined using the simple (Equation 9-11) or detailed (Equation 9-10) equation. However, the concrete shear contribution should be limited to prevent the concrete from crushing as indicated by Equation 9-12.

In typical designs, the steel stirrups and CFRP fibers will be oriented perpendicular ($\alpha=90$ -deg.) relative to the longitudinal axis of the member (Figure 9-9). Hence, the equations for the shear contributions of the steel stirrups and CFRP can be simplified by using $\alpha=90$ -deg. (Equation 9-14 and Equation 9-16).

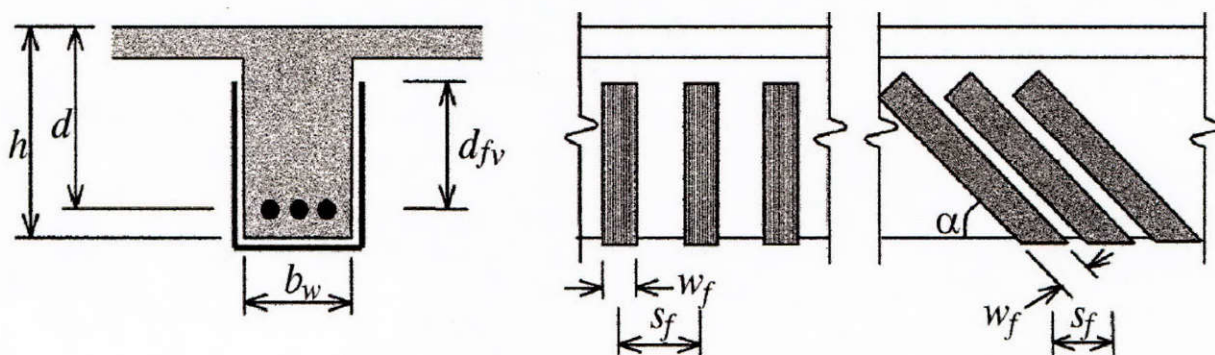


Figure 9-9: CFRP variables used for shear strength calculations (ACI Committee 440, 2008)

Figure 9-9 illustrates the variables used to calculate the CFRP shear contribution. Note that the effective depth of the CFRP strip (d_{fv}) is defined as the distance from the centroid of the anchor hole to the centroid of the longitudinal tension reinforcement for anchored systems, whereas the effective CFRP depth (d_f) is equal to the effective depth of the section (d) for fully wrapped systems.

The proposed shear design equations shown in Table 9-1 are not currently intended to account for the shear contribution provided by reinforcement that lies in the horizontal direction, parallel to the longitudinal reinforcement, due to insufficient experimental data. However, specimens with bi-directional CFRP layouts consistently reached higher loads at first diagonal cracking, smaller crack widths, and smaller member deformations at failure. Detailing requirements for bi-directional layouts are given in section 9.5.2 for cases where shear crack widths or member deformations need to be reduced.

Finally, the steel stirrup and CFRP reinforcement should be proportioned so that the combined shear stress is less than eight times the square root of the concrete compressive strength (in psi units). This requirement was also established to prevent the concrete from crushing before the steel yields and the CFRP fractures (Equation 9-17). Several tests in the program with large amounts of CFRP exhibited concrete crushing before any CFRP strips fractured.

9.4 EVALUATION OF THE DESIGN EQUATIONS

In this section, the proposed design equations are evaluated to provide a comparison between the simple and detailed concrete contribution equations. The detailed concrete contribution equation is then used to compare the experimental and predicted shear capacities. As a point of reference, an experimental-to-predicted ratio above 1.0 is desired.

9.4.1 Concrete Contribution Comparison

The concrete contribution can be predicted using either the simple (Equation 9-11) or detailed (Equation 9-10) equation. Recall that the total concrete contribution relation, shown in Equation 9-10, accounts for the concrete and transverse reinforcement interactions. Figure 9-10 shows the magnitude of the concrete contribution components based on the detailed equation, as well as the magnitude of the concrete contribution based on the simple equation.

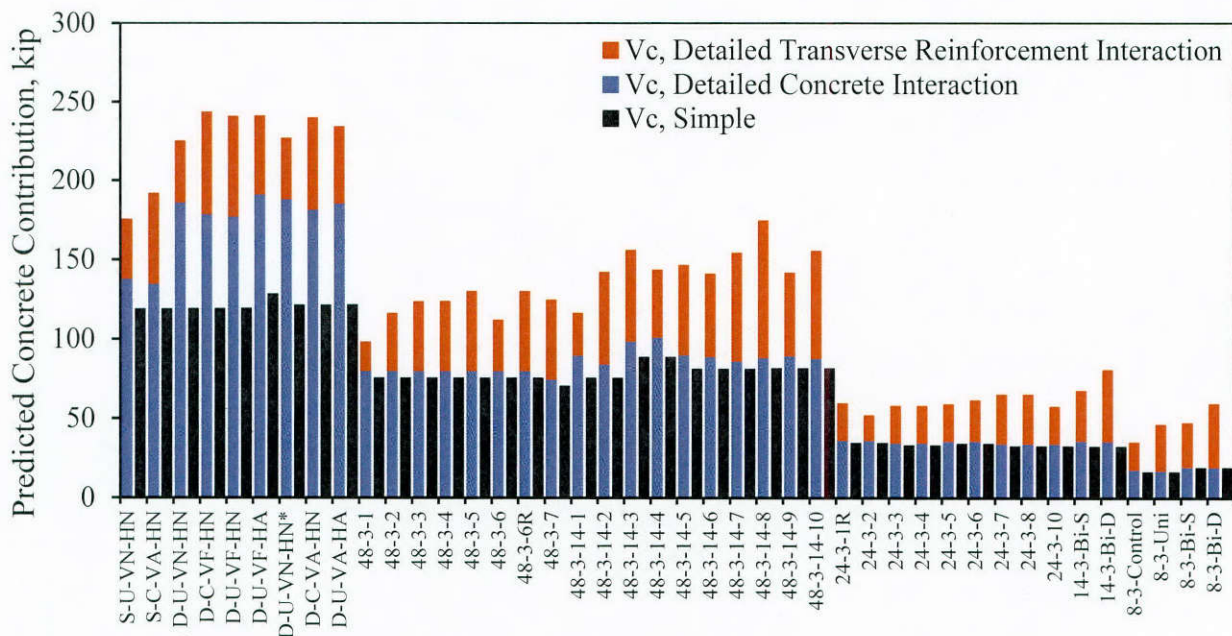


Figure 9-10: Comparison of the detailed and simple concrete contributions

While the simple concrete contribution equation can be evaluated more quickly, it can significantly underestimate the concrete contribution. An underestimation of the concrete contribution generally results in an underestimation of the nominal shear capacity. Consequently, for CFRP shear strengthening applications, more CFRP material would be required to bridge the gap between the shear demand and the shear capacity. Comparatively, the detailed equation provides predicted concrete contributions that are on average approximately equal to the experimentally measured concrete contributions.

9.4.2 Shear Capacity

The predicted shear capacity for each specimen was determined using the inclined shear crack angles from Figure 9-7, the detailed concrete contribution (Equation 9-10), the steel stirrup contribution (Equation 9-13), and the CFRP contribution (Equation 9-15). The experimentally measured shear capacities were then normalized relative to the predicted shear capacities as shown in Figure 9-11.

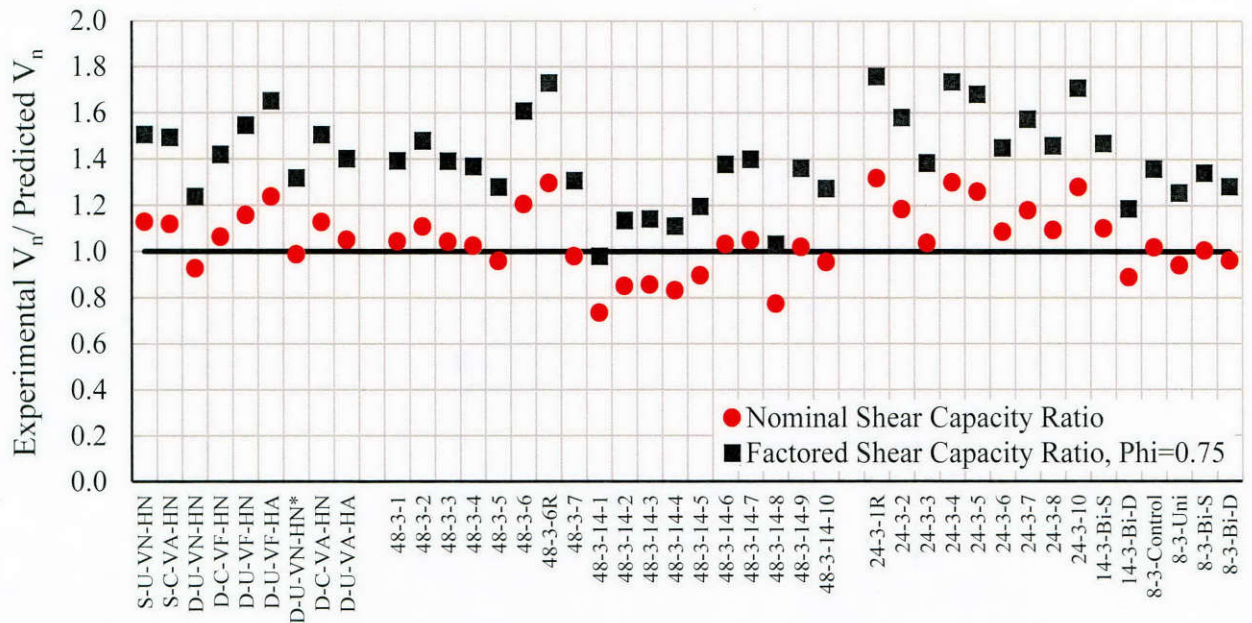


Figure 9-11: Comparison of the experimental-to-predicted shear capacity

The average ratio of the experimental-to-predicted nominal shear capacity was 1.05 with a standard deviation of 0.14. The nominal shear capacity ratios in Figure 9-11 indicate that unconservative shear capacities were predicted for a number of specimens, which is consistent with targeting the mean of the experimental values. However, once the strength reduction factor of 0.75 was applied, all of the predicted shear capacities were found to be less than the experimental shear capacities with the exception of specimen 48-3-14-1 (a control specimen), which had an experimental-to-predicted ratio of 0.98.

Using the detailed concrete contribution equation results in predicted shear capacities that are approximately equal to the experimentally measured shear capacities. Consequently, use of the detailed concrete contribution equation is recommended to help reduce the required amount of CFRP material. A comprehensive design example using both concrete contribution equations is presented in Appendix A. The design example illustrates the large amounts of CFRP material that are required when the simple concrete contribution equation is used.

9.5 DETAILING REQUIREMENTS FOR CFRP LAYOUTS

Properly detailing a CFRP layout is required to achieve the expected shear strength gains and shear crack width reductions. Figure 9-12 shows proper vertical CFRP spacing, horizontal-to-vertical CFRP reinforcement proportions, strip orientations, and anchor requirements.

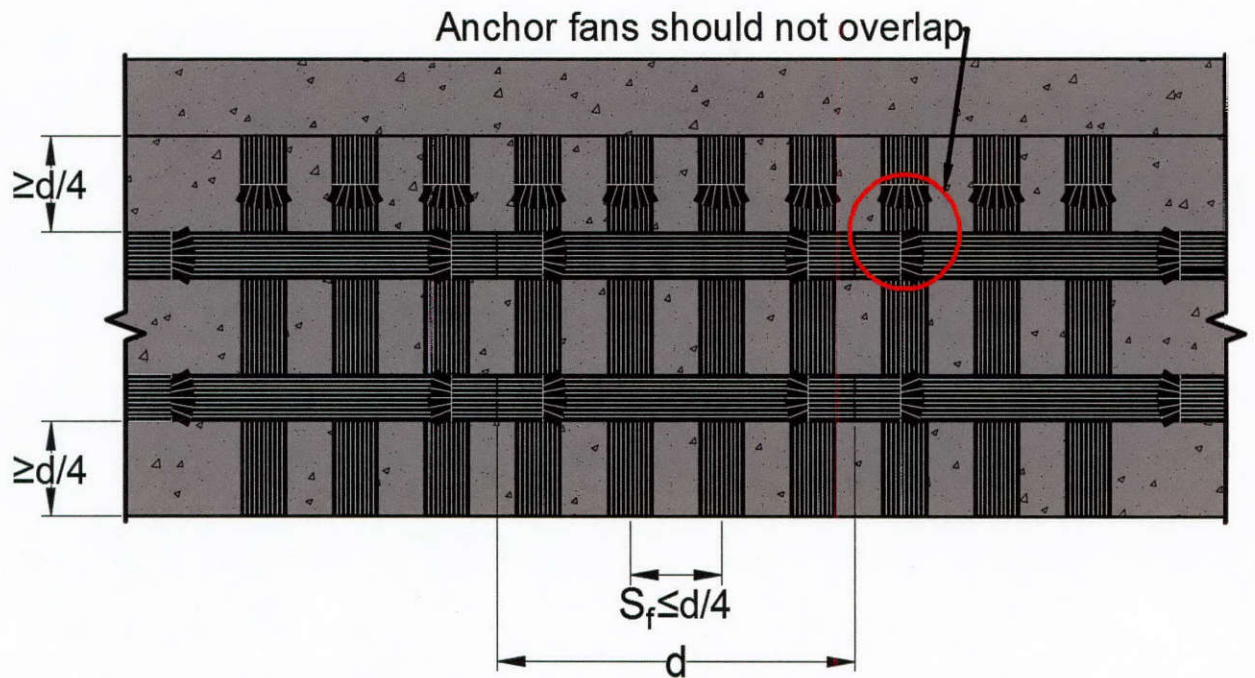


Figure 9-12: Detailing for a bi-directional CFRP layout

While the horizontally applied CFRP strips were not found to influence the CFRP shear contribution, they did provide higher loads at first diagonal cracking, smaller crack widths, and smaller member deformations at failure. Therefore, detailing requirements for bi-directional layouts are provided for cases where shear crack widths or member deformations need to be reduced.

9.5.1 Spacing Requirements

The center-to-center spacing of the vertical CFRP strips (S_f) should not exceed $d/4$ in the critical shear span. Exceeding this requirement caused steep shear cracks to form between the CFRP strips in some tests, thus reducing the shear capacity of the member. The majority of the members in the experimental program had a clear distance between the vertical strips equal to the width of the CFRP strip (w_f).

The clear distance between the nearest horizontal CFRP strip and the top or bottom of the web should not be less than $d/4$. In doing so, the horizontal strips will be placed in the middle portion of the web. By placing the strips in the middle portion of the web depth, the strips should control the shear crack widths without significantly increasing the flexural capacity of the member.

9.5.2 Use of Bi-directional CFRP Layouts

When crack control or reduced member deformations are desired, horizontal CFRP strips may be added. In those cases, the area of CFRP in the horizontal direction (A_{hf}) should be greater than or equal to half the vertical CFRP area (A_{vf}) that crosses the critical shear crack (Equation 9-18). In a typical design, the vertical CFRP strips would be designed for the required shear resistance. The horizontal strips would then be designed to reduce shear crack widths. Since the right hand portion of Equation 9-18 is known, the designer would only need to decide on the horizontal strip width (typically equal to the vertical width, w_f) to be able to calculate the number of horizontal strips required on each face of the web (N_h).

$$N_h A_{hf} \geq \frac{1}{2} \frac{A_{vf} d_{fv}}{s_f} \cot(\theta) \quad \text{Equation 9-18}$$

9.5.3 Strip Orientation

The proposed design equations imply that the shear contribution of the CFRP can be optimized if the strips are oriented perpendicular to the shear crack. However, shear crack angles change along the height of a web making the optimization not as ideal as expected. In some cases, the CFRP shear contribution can be overestimated. Therefore, it is recommended that the CFRP strips remain perpendicular and parallel to the longitudinal axis of the member. Such orientations also simplify installation of the strips. Moreover, note that the panel tests (Chapter 2) showed that bi-directional layouts were effective at controlling the shear crack widths regardless of the shear crack angle.

9.5.4 Anchor Requirements

CFRP anchors on the vertical strips should be placed as high on the web as possible while remaining below the longitudinal reinforcement (i.e., maximizing d_{fv}). The anchors should be drilled through the concrete clear cover and into the core of the member to prevent the possibility of pullout failures.

Intermediate anchors in the horizontal strips should be spaced not greater than d away from each other to minimize shear crack widths.

While the performance of the CFRP anchors were not shown to be affected by cracks, it is prudent to avoid placing anchors in regions of members being strengthened where significant cracks indicative of shear distress are already present. In such cases, it may be possible to relocate the strip to avoid anchor placement in the cracks. Moreover, CFRP anchor fans on the horizontal and vertical strips should not overlap (Figure 9-12) nor should the horizontal CFRP strips be anchored in high moment regions in order to avoid the development of detrimental stress concentrations.

Chapter 10. Quality Control of FRP Design, Installation, and Materials

10.1 OVERVIEW

Externally applied fiber reinforced polymers (FRP) are highly effective in retrofit and repair of concrete structures. However, FRP materials are extremely sensitive to the quality of their installation owing to their brittle nature. Errors or imperfections in installation can lead to stress concentrations and premature fracture of FRP materials. In addition, inadequate anchorage of FRP materials to concrete members will certainly curtail their strength. It is therefore essential to achieve proper anchorage and installation of FRP materials to realize the strength and serviceability benefits evaluated in their design. In this chapter, a simple test procedure is outlined for qualifying the installation and effectiveness of FRP strengthening systems anchored using FRP anchors. The procedure involves strengthening small-scale concrete beams and testing them in a three-point loading rig as is commonly done in modulus of rupture tests.

Since FRP materials have been introduced relatively recently, their properties are rapidly evolving. There is also no consensus as to how properties for these materials should be reported. The quality control test outlined in this chapter provides an efficient and simple means by which to qualify FRP materials for strengthening or repair applications, or to derive the FRP material properties needed in design.

10.2 TEST SPECIMEN AND PROCEDURE

The test procedure involves constructing small-scale concrete beam specimens, strengthening them using an anchored FRP system, and loading them to failure under a three-point load setup. Details of a strengthened test specimen are provided in Figure 10-1, Figure 10-2, and Figure 10-3, while Figure 10-4 illustrates the three-point loading scheme. The beam does not contain any steel reinforcement but is reinforced on the sides using U-wrapped FRP strips having the same properties as the tension strip being tested.

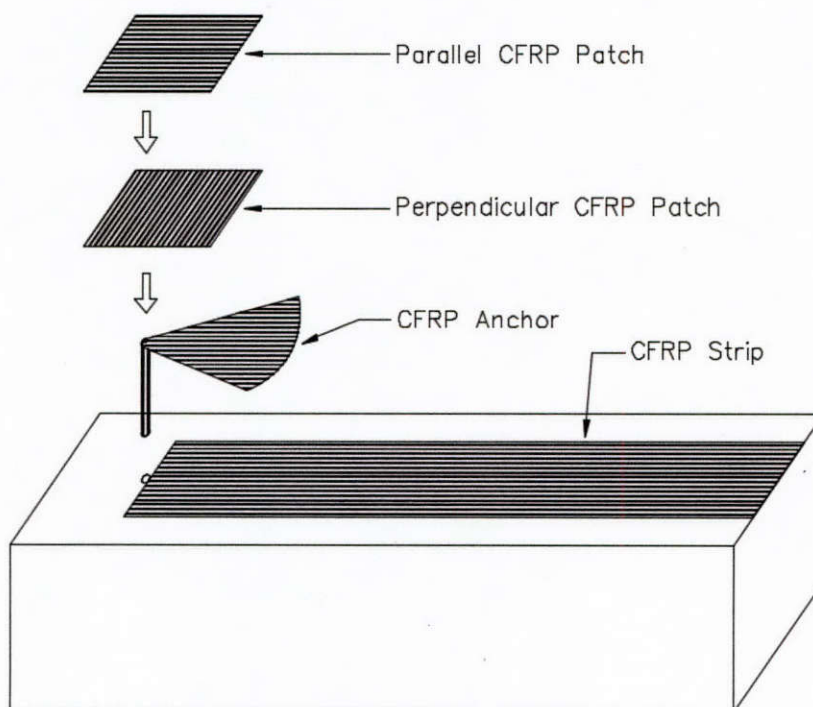
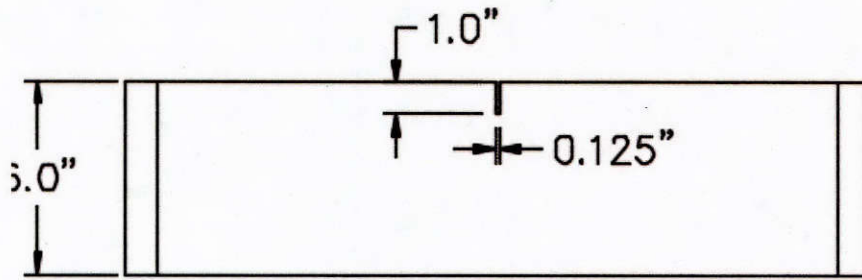
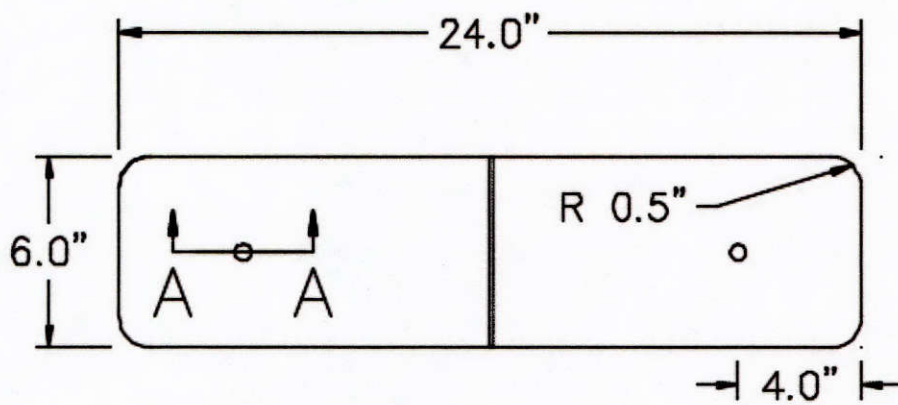


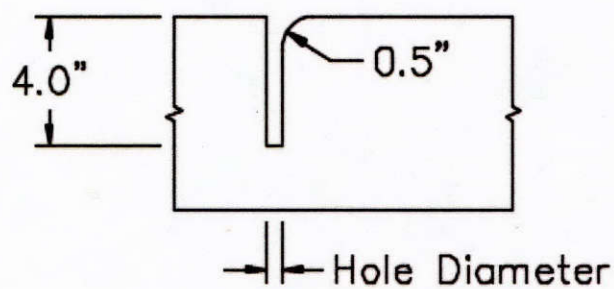
Figure 10-1: Isometric view of specimen



Elevation View

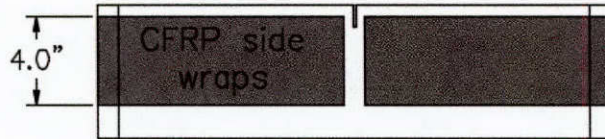


Plan View

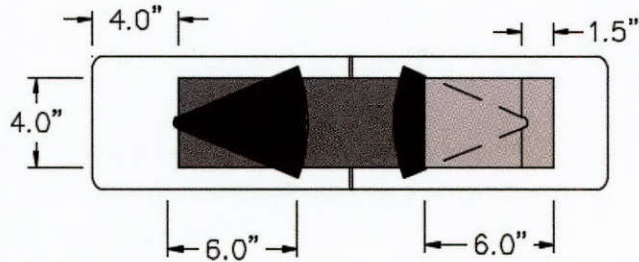


Section A-A

Figure 10-2: Test specimen details

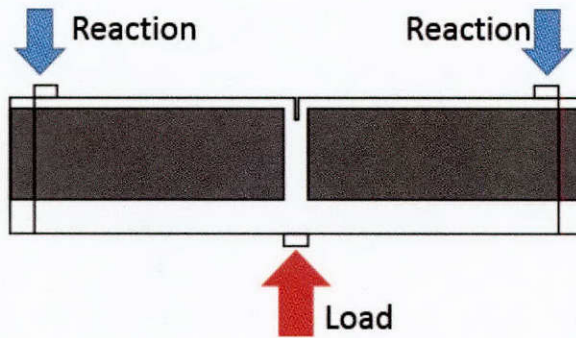


Elevation View

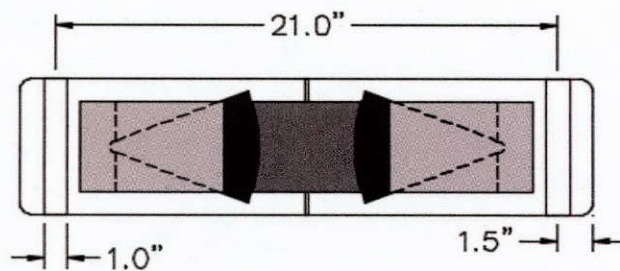


Plan View

Figure 10-3: FRP detailed layout, right side shows patch layout



Elevation View



Plan View

Figure 10-4: Test setup

The adjacent-to-strip anchor detail is recommended for use in the quantity control tests (section 6.2.3.3). This anchor detail is easier to install than the through-strip anchor detail where anchors need to be inserted through the strips they develop (section 6.2.3.3). This anchor hole diameter should be sized according to the design recommendation in section 8.2.3.1.

10.2.1 Test Boundaries

The beam design can only test FRP strips having a tensile strength not exceeding 15 kips. Higher strip strengths will increase the likelihood of a beam concrete failure. A 15 kip strip strength translates to a maximum applied load on the beam of 16.3 kips.

It is recommended to use a tension strip width of 4 in. In cases where other widths are needed, such as to test thicker stronger materials, strip width should not be taken smaller than 3 in. nor larger than 5 in.

The strength per unit width of the strip (related to strip thickness) should also be limited to avoid delamination failures between the anchors and the strip they develop. The anchor fan and patch dimensions shown in Figure 10-3 correspond to a bond stress capacity between the strip and anchors of 500 psi. Section 8.2.2.1 of this document provides a detailed explanation on how to evaluate the bond forces between anchors and strips. If higher bond forces need to be transferred, the anchor fan and patch lengths should be increased based on guidelines of Section 8.2.2.1.

10.2.2 Concrete Specimen Details

The concrete specimen consists of a modified ASTM C293 beam that is typically used for modulus of rupture tests. The prismatic beam is (6-in. x 6-in. x 24-in.) and modified from the standard modulus of rupture beams by introducing a notch at mid-span and rounding the side edges (Figure 10-2). This beam geometry was chosen for several reasons: 1) the beam is small enough to be maneuvered by two people without the use of lifting equipment; 2) the beam is large enough to allow testing of a practical range of FRP systems and materials; and 3) the beam has readily available forms and test setups as it is widely used for standard modulus of rupture tests. The notch at mid-span and edge rounding could either be performed on the specimen after casting or by adding inserts into the standard modulus of rupture beam forms (Figure 10-5). The test beam is not required to have steel reinforcement.

Concrete compressive strength was not found to have a major impact on the ultimate strength of the CFRP strengthening system developed in this study. Higher concrete strength did however reduce the likelihood of the test specimen having a concrete failure mode. It is therefore recommended that a concrete compressive strength not lower than 5 ksi be used for the test specimen. The concrete strength should be the same for tests in the same series.

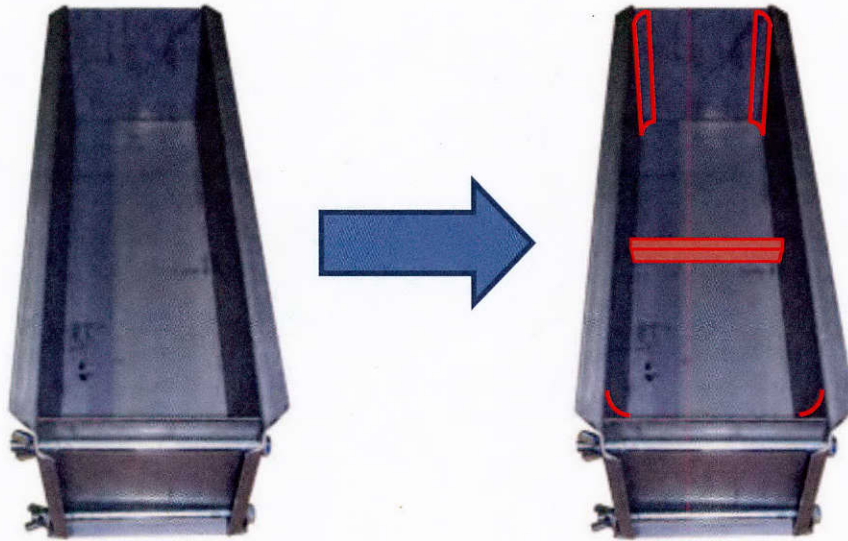


Figure 10-5: Formwork modifications

10.2.3 Concrete Specimen Preparation

Once the concrete is cast and cured, the surfaces of the beam that will receive CFRP strips must be ground to remove laitance and ensure adequate bond between the CFRP and concrete substrate. The anchor holes should then be drilled and the hole-edge chamfer radius rounded to the correct dimensions (Figure 10-2). If form inserts were not used, a 1 in. saw cut should be made at mid-span of the tension surface (Figure 10-2) and the side edges of the beam should be rounded through grinding to the dimensions shown in Figure 10-2. After all concrete work is complete, the entire beam should be cleaned from all dust and dirt, including the inside of the anchor holes.

10.2.4 FRP Installation

A detailed description of the FRP installation procedure can be found in Section 6.2.2 of this document. The following is a brief summary of that procedure. Epoxy should be mixed according to the manufacturer's instructions. The FRP strips, the surfaces of the beam where the strips will be placed, and the anchor holes should be saturated with epoxy. The FRP strips should then be placed on the concrete surfaces and using putty knives smoothed out to remove excess epoxy and any air bubbles under the strips. Next, the FRP anchors should be saturated, placed in the anchor holes, and fanned over the tension strip while making sure the anchors stay fully embedded in the holes. Once again, putty knives can be used to remove air bubbles and excess epoxy. The anchor FRP patches can then be saturated and placed one at a time over the anchor in the location shown in Figure 10-3. The fibers of the first patch should be perpendicular and those of the second patch parallel to the fibers of the main FRP strip. After the first patch is placed and air bubbles removed, its top surface should be saturated before applying the second and final patch over it. It is recommended that patches be placed 1.5-in. behind the center of the anchor hole due to limited space on the face of the beam and need for reaction plates. This is different from the 2-in. spacing recommended in section 8.2.4. It is essential to ensure that the strips, patches, and anchors are taut and in full contact with the concrete surfaces or underlying FRP. This process should be completed within the epoxy working time, which is provided by the manufacturer as a function of ambient temperature.

10.2.5 Testing

The concrete should be allowed to reach the desired strength and the FRP laminates should be fully cured according to manufacturer specifications before load testing can be performed.

10.2.5.1 Test Setup

The test setup involves applying a point load at mid-span of the strengthened beam specimen and providing two reaction points at locations shown in Figure 10-4. Several test setups can be used to achieve the desired loading. A self-reacting system comprised of a steel beam, threaded rods, a loading ram, a load cell, and a spherical head can be used (Figure 10-6). In this test setup, rollers and pins are not required at the reaction points since the longitudinal expansion and rotation of the beam during testing are accommodated by the laterally flexible threaded rods. Alternatively, a uniaxial testing machine can be used with rollers and pins as shown in Figure 10-7. If using a fixed reaction base, a roller must be present at least at one reaction to avoid introducing axial stresses in the beam. Pins should also be present at both reaction points to allow free beam rotation. Standard modulus of rupture test setups can also be used provided they have sufficient capacity to fail the strengthened beams (Figure 10-8). In all cases, it is essential to adequately center the loading point in the longitudinal and transverse directions to avoid skewing beam moments or introducing torsion in the specimen. Care should also be exercised in placing the reaction points.

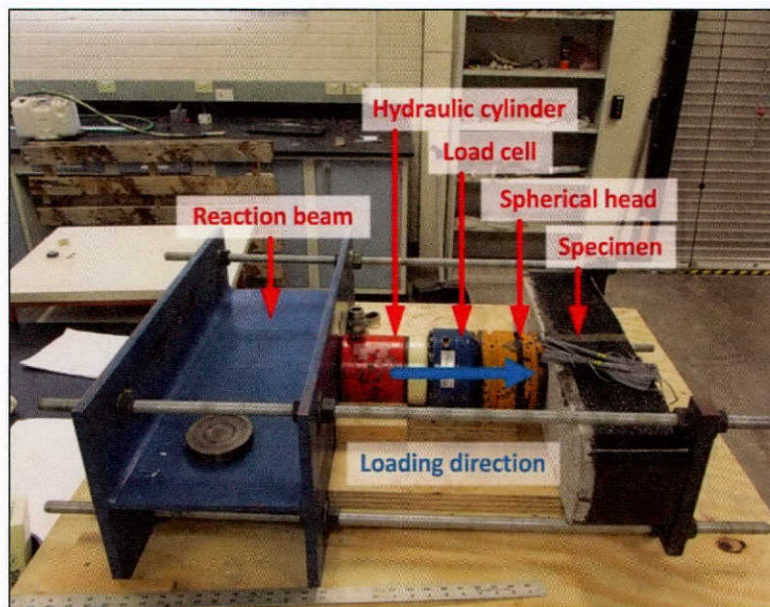


Figure 10-6: Self-reacting test setup

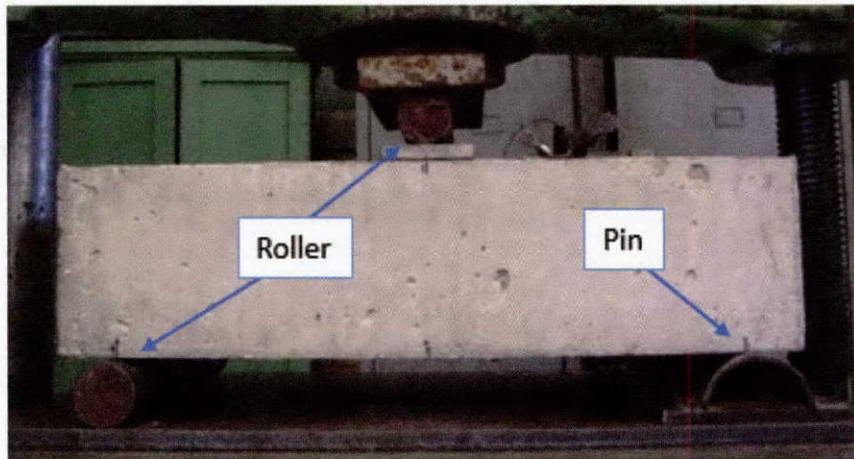


Figure 10-7: Boundary conditions

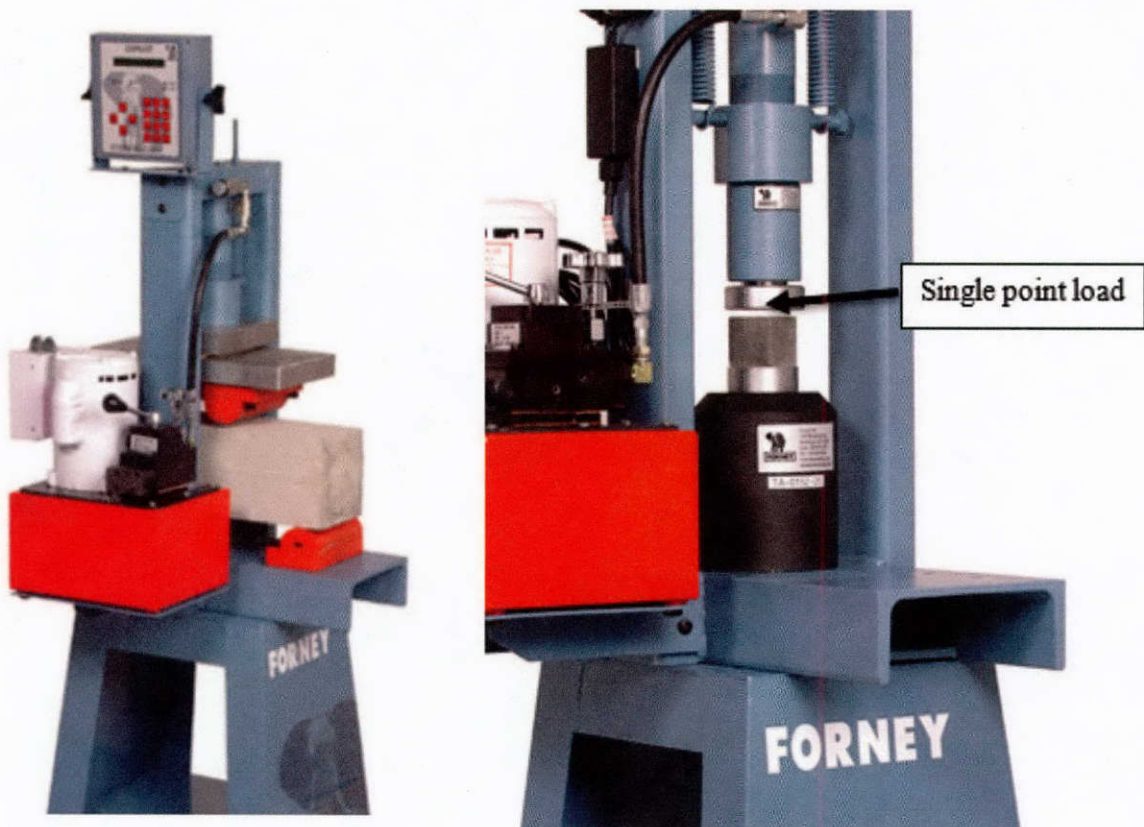


Figure 10-8: Commercial modulus of rupture test setup

10.2.5.2 Loading Protocol and Rate

The point load should be applied at a moderate rate of about 1 kip per 10 seconds. The loading should be increased monotonically up to failure.

10.2.5.3 Instrumentation

A load cell should be placed under the applied load to monitor the load through the test. Load cell readings are needed to calculate the stress in the tension FRP strip at failure. A procedure for calculating strip stresses from load data is provided in Section 6.2.4.2.1 of this document.

Depending on the application and data needed, FRP strain gauges can be applied at mid-span of the tension strip to monitor strains. A minimum of two gauges should be used. Strain readings could then be used in conjunction with stress measures to estimate the laminate material modulus of elasticity. Kim, 2014, describes in more detail how this can be done.

10.3 INTERPRETATION OF RESULTS

Tests can be interpreted through two performance measures: failure modes and stresses in the tension strip at failure. Four main failure modes can be expected:

- 1) Concrete failure: while the beam design was developed to preclude failures in the concrete, such failures may still occur and tests failing in the concrete should be discarded.
- 2) Delamination between anchors and strips: if the bond stress at failure between the anchors and the strips was lower than the manufacturer specified bond capacity, the epoxy used in the installation can be assumed to be deficient. If at delamination, the bond stress was higher than the bond capacity and the strip stress was less than the specified fracture stress, then the anchor and patch overlap length on the strip may have been miscalculated and should be re-evaluated.
- 3) Anchor rupture: anchor rupture can occur from: 1) inadequate anchor design with too little FRP material; 2) inadequate hole preparation, typically due to an improper hole-edge chamfer; and 3) installation error in which significant voids are introduced around the anchors and patches.
- 4) Strip fracture: strip fracture is the target failure mode for a properly designed and installed FRP system. The stress in the strip at fracture can be compared with the manufacturer provided design value or used to determine the design value for a new material based on recommendations in ACI 440.2R-8.

10.4 APPLICATIONS

10.4.1 Material and Design Qualification

10.4.1.1 Evaluating the Performance of New FRP Materials

When quantifying the material properties of FRP materials using the outlined test procedure, the effective stress in the CFRP strip at fracture can be evaluated using load-cell data and equilibrium as discussed in Section 6.2.4.2.1. If strain gauges are affixed on the FRP strip at mid-span, the modulus of elasticity of the FRP laminate can be approximated by dividing the stress by the gauge strain readings. ACI 440.2-R08 provides recommendations on the number of tests to conduct and the procedure to derive design stress and strain capacities from material testing.

10.4.1.2 Evaluating the Performance of New Designs

The test procedure can also be used to explore alternate anchor and patch geometries, different installation sequences, as well as mixing materials within the same system.

10.4.2 Pre-qualifying an Installer for Anchored FRP Systems

The test procedure can be used to pre-qualify installers of anchored FRP systems by requiring them to complete a series of successful installations for the FRP system or systems under consideration.

10.4.3 Evaluating Field Material and Installation Quality

Field conditions are often different from the idealized conditions present in a laboratory setting. The quality-control test procedure can be used to verify the quality of field installation and materials. Several small beams could be made available on site and strengthened using the same epoxy and FRP materials used in the project. These beams could then be tested to ensure the materials were adequately prepared and installed. It is advised in this scenario to prepare test specimens for every batch of epoxy used on the site. This test is akin to concrete cylinder tests conducted for every batch of concrete used in a project.

References

- AASHTO (2014), AASHTO LRFD Bridge Design Specifications, 7th edition, Washington, DC, USA.
- ACI Committee 318 (2014). Building Code Requirements for Structural Concrete (ACI 318-14), American Concrete Institute, Farmington Hills, Michigan, USA
- ACI Committee 440 (2008). Guide for the Design and Construction of Externally Bonded FRP Systems for Strengthening Concrete Structures (ACI 440.2R-08), American Concrete Institute, Farmington Hills, Michigan, USA
- Adhikary, B. B., Mutsuyoshi, H., & Ashraf, M. (2004). Shear strengthening of reinforced concrete beams using fiber-reinforced polymer sheets with bonded anchorage. *Aci Structural Journal*, 101(5).
- Alotaibi, N. K. (2014). *Shear strengthening of reinforced concrete beams with bi-directional carbon fiber reinforced polymer (CFRP) strips and CFRP anchors* Department of Civil, Environmental and Architectural Engineering. Austin, Texas, The University of Texas at Austin. Master Thesis.
- ASTM International, (2007), “Standard Test Method for Flexural Strength of Concrete Using Simple Beam With Center-Point Loading, (C293-07),” ASTM International, West Conshohocken, PA, USA, 3 pp.
- ASTM International, (2007), “Standard Test Method for Tensile Properties of Polymer Matrix Composite Materials, (D3039),” ASTM International, West Conshohocken, PA, USA, 13 pp.
- Bentz, E. C., Vecchio, F. J., & Collins, M. P. (2006). Simplified modified compression field theory for calculating shear strength of reinforced concrete elements. *Aci Structural Journal*, 103(4).
- Bousselham, A., & Chaallal, O. (2006). Behavior of reinforced concrete T-beams strengthened in shear with carbon fiber-reinforced polymer - An experimental study. *Aci Structural Journal*, 103(3), 339-347.
- Chen, J. F., & Teng, J. G. (2003). Shear capacity of FRP-strengthened RC beams: FRP debonding. *Construction and Building Materials*, 17(1), 27-41.
- Garcia, J.; Sun, W.; Kim, C.; Ghannoum, W. M.; and Jirsa, J. O., (2014) “Procedures for the Installation and Quality Control of Anchored CFRP Sheets for Shear Strengthening of Concrete Bridge Girders,” Report 5-6306-01-1, Center for Transportation Research (CTR), Austin, TX, 52 pp.
- Huaco, G. (2009). Quality Control Test for Carbon Fiber Reinforced Polymer (CFRP) Anchors for Rehabilitation. Department of Civil, Environmental and Architectural Engineering. Austin, Texas, The University of Texas at Austin. Master Thesis.
- Khalifa, A., & Nanni, A. (2000). Improving shear capacity of existing RC T-section beams using CFRP composites. *Cement & Concrete Composites*, 22(3), 165-174.

- Khalifa, A., Tumialan, G., Nanni, A., & Belarbi, A. (1999). Shear strengthening of continuous reinforced concrete beams using externally bonded carbon fiber reinforced polymer sheets. *ACI Special Publication*, 188.
- Kim, C. (2014). "Performance of Concrete Panels Strengthened using Carbon Fiber Reinforced Polymers (CFRP)". Department of Civil, Environmental and, Architectural Engineering. Austin, Texas, The University of Texas at Austin. Ph.D Dissertation.
- Kim, Insung (2008). Use of CFRP to Provide Continuity in Existing Reinforced Concrete Members Subjected to Extreme Loads. Department of Civil, Environmental and Architectural Engineering. Austin, Texas, The University of Texas at Austin. Ph.D Dissertation.
- Kim, I., Jirsa, J. O., & Bayrak, O. (2011). Use of carbon fiber-reinforced polymer anchors to repair and strengthen lap splices of reinforced concrete columns. *Aci Structural Journal*, 108(5).
- Kim, Y. G. (2011). "Shear Behavior of Reinforced Concrete T-Beams Strengthened with Carbon Fiber Reinforced Polymer (CFRP) Sheets and CFRP Anchors. Department of Civil, Environmental and Architectural Engineering." Austin, Texas, The University of Texas at Austin. Ph.D Dissertation.
- Kim, Y.; Quinn, K. T.; Satrom, C. N.; Garcia, J.; Sun, W.; Ghannoum, W. M.; and Jirsa, J. O., (2012) "Shear Strengthening of Large Reinforced and Prestressed Concrete Elements Using Carbon Fiber Reinforced Polymer (CFRP) Sheets and CFRP Anchors," Report 0-6306-1, Center for Transportation Research (CTR), Austin, TX, 296 pp.
- Orton, S. L. (2007). "Development of a CFRP System to Provide Continuity in Existing Reinforced Concrete Structures Vulnerable to Progressive Collapse". Department of Civil, Environmental and, Architectural Engineering. Austin, Texas, The University of Texas at Austin. Ph.D Dissertation.
- Orton, S., Jirsa, J. O., & Bayrak, O. (2009). Carbon fiber-reinforced polymer for continuity in existing reinforced concrete buildings vulnerable to collapse. *Aci Structural Journal*, 106(5).
- Orton, S. L., Jirsa, J. O., & Bayrak, O. (2008). Design Considerations of Carbon Fiber Anchors. *Journal of Composites for Construction*, 12(6), 608-616.
- Pellegrino, C., & Modena, C. (2006). Fiber-reinforced polymer shear strengthening of reinforced concrete beams: Experimental study and analytical modeling. *Aci Structural Journal*, 103(5), 720-728.
- Pham, L. T. (2009). "Development of a Quality Control Test for Carbon Fiber Reinforced Polymer Anchors". Department of Civil, Environmental and Architectural Engineering. Austin, Texas, The University of Texas at Austin. Master Thesis.
- Sokoli, D., Shekarchi, W., Buenrostro, E., Ghannoum, W.M., (2014). "Advancing behavioral understanding and damage evaluation of concrete members using high-resolution digital image correlation data". *Earthquakes and Structures* 7(5): 609-626.

- Sun, W. (2014). "Behavior of Carbon Fiber Reinforced Polymer (CFRP) Anchors Strengthening Reinforced Concrete Structures". Department of Civil, Environmental and, Architectural Engineering. Austin, Texas, The University of Texas at Austin. Ph.D Dissertation.
- Sun, W., & Ghannoum, W. (2015). Modeling of anchored CFRP strips bonded to concrete. *Construction and Building Materials*, 85, 144-156.
- Triantafillou, T. C. (1998). Shear strengthening of reinforced concrete beams using epoxy-bonded FRP composites. *Aci Structural Journal*, 95(2), 107-115.
- Vecchio, F. J., & Collins, M. P. (1986). *The modified compression-field theory for reinforced concrete elements subjected to shear*. Paper presented at the ACI Journal Proceedings.
- Wang, H. (2013). "Test of Glass Fiber Reinforced Polymer (GFRP) Anchors". Department of Civil, Environmental and Architectural Engineering. Austin, Texas, The University of Texas at Austin. Master Thesis.
- Zhang, Z. C., & Hsu, C. T. T. (2005). Shear strengthening of reinforced concrete beams using carbon-fiber-reinforced polymer laminates. *Journal of Composites for Construction*, 9(2), 158-169.

Appendix A: Design Example using the Proposed Design Guidelines

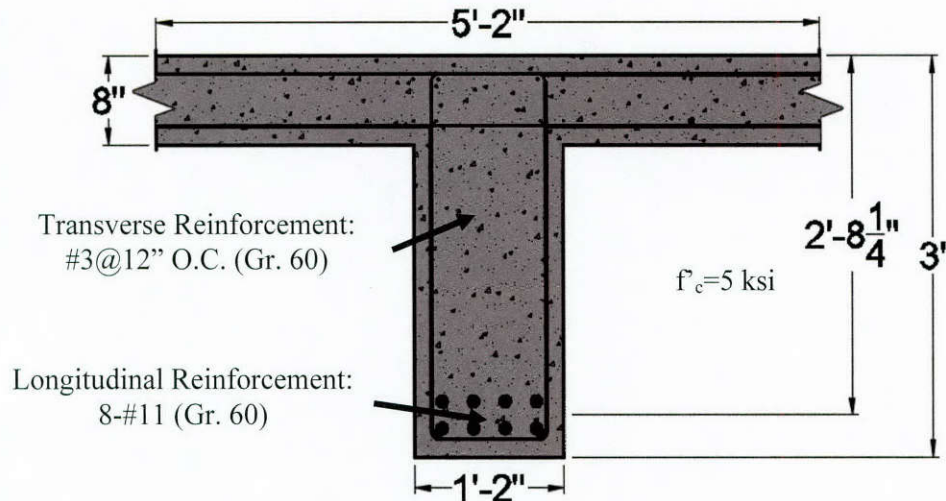


Figure A-1: Cross-section of the T-beam example

Design Problem:

A simply supported T-beam with a 48-foot span length was originally designed to resist a distributed load of 3.5-kips/foot. The load demand has subsequently increased to 7-kips/foot. While the moment capacity is sufficient, the shear capacity is inadequate. Anchored uni- and bi-directional CFRP layouts will be designed to strengthen the member in shear. Assume that the maximum aggregate size is greater than or equal to $\frac{3}{4}$ -in.

The required load demands are shown below:

$$M = 2,016 \text{ k-ft.} = 24,192 \text{ k-in. (i.e., peak moment)}$$

$$V = 168 \text{ kip (i.e., peak shear)}$$

$$V_{u@d \text{ from support}} = 149 \text{ kip (i.e., the critical section)}$$

Solution 1: Layouts using the Detailed Concrete Contribution

The following solution illustrates the design and detailing of uni- and bi-directional CFRP layouts using the proposed design guidelines with the detailed concrete contribution equation (Equation 9-10).

Uni-directional Layout (Vertical Strips):

1. Determine the strain in the longitudinal reinforcement at the peak moment region (ϵ_s).

$$\epsilon_s = \frac{\left(\frac{|M|}{0.9d} + V_{@M}\right)}{E_s A_s} = \frac{\left(\frac{|24,192|}{(0.9)32.25} + 0\right)}{29,000 (8 * 1.56)} = 0.0023 \text{ in./in.}$$

2. Determine the shear crack angle (θ).

$$\theta = 29 + 3500\epsilon_s = 29 + 3500(0.0023) = 37^\circ$$

$$29^{\circ} \leq \theta = 37^{\circ} \leq 50^{\circ}$$

3. Determine the steel shear contribution (V_s).

$$V_s = \frac{A_{vs}f_{yt}d}{s} \cot(\theta) = \frac{0.22(60)(32.25)}{12} \cot(37) = 47.1 \text{ kip}$$

4. Solve for the required CFRP contribution ($V_{f,req}$) using a closed form solution of the design guidelines.

$$V_{f,req} = \frac{\frac{V_u@d}{\phi} - \frac{1.25\sqrt{f'_c}b_wd}{\sin(\theta)} \left(\frac{1}{(M/Vd)^2} + 0.9 \right) - V_s \left[1 + \frac{\cos(\theta)}{2} \right]}{\left[1 + \frac{\cos(\theta)}{2} \right]}$$

$$\begin{aligned} V_{f,req} &= \frac{\frac{149}{0.75} - \frac{1.25\sqrt{5000}(14)(32.25)}{\sin(37)} \left(\frac{1}{\left(\frac{24,192}{(168)(32.25)} \right)^2} + 0.9 \right) - 47.1 \left[1 + \frac{\cos(37)}{2} \right]}{\left[1 + \frac{\cos(37)}{2} \right]} \\ &= \frac{198.67 - \frac{1.25\sqrt{5000}(14)(32.25)}{\sin(37)} \left(\frac{1}{\left(\frac{24,192}{(168)(32.25)} \right)^2} + 0.9 \right) - 47.1 \left[1 + \frac{\cos(37)}{2} \right]}{\left[1 + \frac{\cos(37)}{2} \right]} \end{aligned}$$

$$V_{f,req} = 49.8 \text{ kips}$$

5. Calculate the CFRP contribution (V_f)

CFRP properties:

$$E_f = 13,900 \text{ ksi}$$

$$t_f = 0.02 \text{ in.}$$

$$\epsilon_u = 0.01 \text{ in./in.}$$

$$\text{Assume the } d_{fv} = h - h_f - 1.5'' = 36'' - 8'' - 1.5'' = 26.5 \text{ in.}$$

$$\text{Assume the center-to-center spacing of the strips is } 8 \text{ in. } \leq d/4$$

Try one layer (ply) of 4 in. wide vertical CFRP strips

$$A_{vf} = 2nt_fw_f = 2(1)(0.02)(4) = 0.16 \text{ in.}^2$$

$$f_{fe} = 0.6\epsilon_u E_f = 0.6(0.01)(13900) = 83.4 \text{ ksi} \leq 0.006E_f$$

$$V_f = \frac{A_{vf}f_{fe}d_{fv}}{s_f} \cot(\theta) = \frac{0.16(83.4)(26.5)}{8} \cot(37) = 58.7 \text{ kip} > V_{f,req}$$

6. Check the transverse reinforcement contribution limit.

$$(V_s + V_f) = 47.1 + 58.7 = 105.8 \text{ kip} \leq 8\sqrt{f'_c}b_wd = 255.4 \text{ kip}$$

7. Determine the concrete contribution (V_c).

$$V_c = 1.25 \sqrt{f'_c} b_w d \left(\frac{1}{\sin(\theta)} \right) \left(\frac{1}{(M/Vd)^2} + 0.9 \right) + \frac{1}{2} (V_s + V_f) \cos(\theta)$$

$$V_c = \frac{1.25}{1,000} \sqrt{5000} (14) (32.25) \left(\frac{1}{\left(\frac{24,192}{(168)(32.25)} \right)^2} + 0.9 \right) + \frac{1}{2} (47.1 + 58.7) \cos(37)$$

$$V_c = 105.3 \text{ kip}$$

$$2\sqrt{f'_c} b_w d = 63.9 \text{ kip} \leq V_c = 105.3 \text{ kip} \leq 5\sqrt{f'_c} b_w d = 159.6 \text{ kip}$$

8. Check that the shear capacity is greater than the shear demand.

$$\begin{aligned} \phi V_n &= 0.75(V_c + V_s + V_f) = 0.75(105.3 + 47.1 + 58.7) = 158.3 \text{ kip} > V_{u@d} \\ &= 149 \text{ kip} \end{aligned}$$

Utilize 4 in. wide vertical CFRP strips spaced 8 in. on center starting within $d/2$ from the support and extending beyond 10-feet from the support where the existing shear capacity is sufficient.

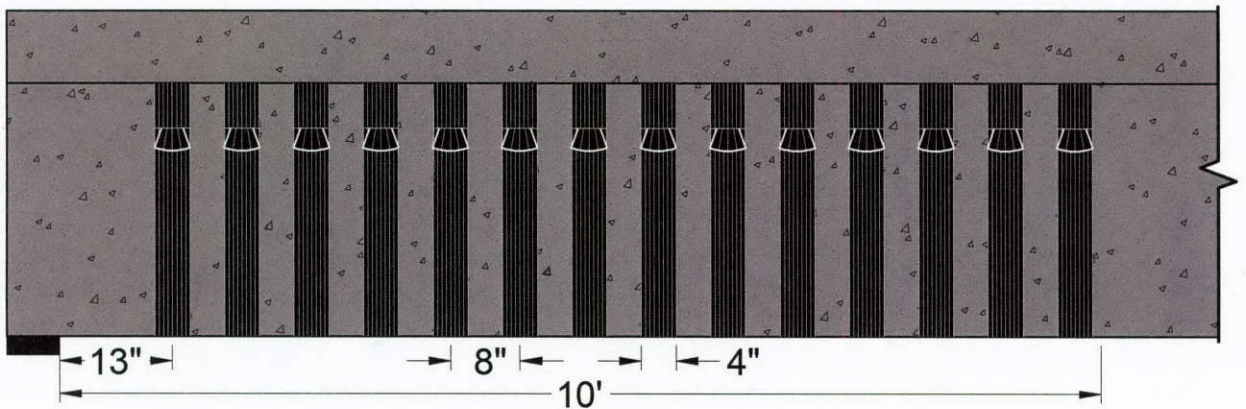


Figure A-2: Designed uni-directional layout using the detailed concrete contribution

Bi-directional Layout (Vertical and Horizontal Strips):

A bi-directional layout can be utilized to maximize the cracking shear load and/or minimize shear crack widths.

1. Determine the required area of CFRP in the horizontal direction (A_{hf}).

$$N_h A_{hf} \geq \frac{1}{2} \frac{A_{vf} d_{fv}}{s_f} \cot(\theta) = \frac{1}{2} \frac{0.16(26.5)}{8} \cot(37) = 0.35 \text{ in.}^2$$

Try using two horizontal CFRP strips within an area that is greater than $d/4$ away from the edge of the web region.

$$A_{hf} \geq 0.175 \text{ in.}^2$$

$$A_{hf,provided} = 2nt_f w_f = 2(1)(0.02)(5) = 0.2 \text{ in.}^2$$

Use two 5 in. wide horizontal CFRP strips spaced at 7 in. on center

- Determine the spacing of intermediate anchors (d_{fh}).

$$d_{fh} = 32 \text{ in.} \leq d = 32.25 \text{ in.}$$

Utilize two 5 in. wide horizontal CFRP strips spaced 7 in. on center with three intermediate anchors every 32 inches on each side of the web. The horizontal CFRP strips are placed $d/4$ away from the edge of the web region.

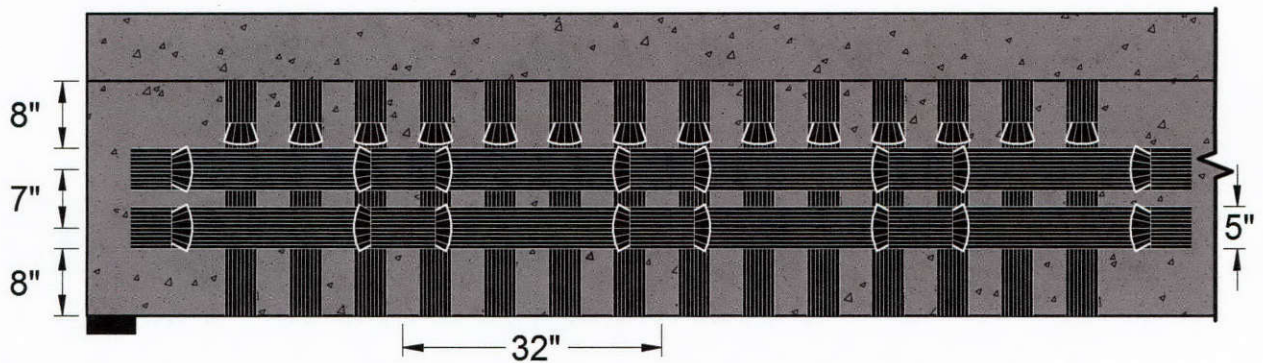


Figure A-3: Designed bi-directional layout using the detailed concrete contribution

Anchor Design:

The design and detailing recommendations for CFRP anchors can be found in Chapter 8. As mentioned in Chapter 8, the anchor design guidelines assume the strip and anchor materials are the same and have the same properties. Moreover, the guidelines are only applicable to carbon fiber anchors.

- Determine tributary widths of the CFRP anchor in the vertical and horizontal directions ($w_{f,a}$).

$$w_{f,A} = \frac{w_f}{n_A}$$

Vertical: Use a single anchor per strip

$$w_{f,A} = \frac{w_f}{n_A} = \frac{4}{1} = 4 \text{ in.}$$

Horizontal: Use a single anchor per strip

$$w_{f,A} = \frac{w_f}{n_A} = \frac{5}{1} = 5 \text{ in.}$$

Specify a single anchor design based on the largest tributary width (i.e., horizontal strips).

- Determine the required weight of anchor fibers per unit length (γ_{A-req}).

$AMR_D = 2.0$ (or greater is recommended)

$$\gamma_{s,sp} = 0.00717 \frac{OZ}{in.^2} \text{ (fiber specific)}$$

$$\gamma_{s,EXP} = 1.25(\gamma_{s,sp}) = 0.00897 \frac{OZ}{in.^2}$$

$$\gamma_{A-req} = AMR_D(w_{f,A})(n)(\gamma_{s,EXP}) = 2.0(5)(1)(0.00897) = 0.0897 \frac{OZ}{in.}$$

- Select a CFRP anchor based on the anchor's fiber weight per unit length (λ_A).

$$\gamma_A \geq \gamma_{A-req}$$

Utilize a CFRP anchor that has at least 0.09 OZ of fibers per inch of length.

$$\text{Say } \gamma_A = 0.125 \frac{OZ}{in.}$$

Note that the intermediate anchors on the horizontal strips need to be twice as larger as the anchors on the boundary of the CFRP layout since the anchors need to be splayed in opposing directions over the strip.

- Determine the actual anchor material ratio (AMR_A).

$$AMR_A = \frac{\gamma_A}{(w_{f,A})(n)(\gamma_{s,EXP})} = \frac{0.125}{(5)(1)(0.00897)} = 2.8 \geq 2.0$$

- Determined the equivalent cross-sectional area of the CFRP anchor (A_{EQV}).

$$A_{EQV} = AMR_A(w_{f,A})(n)(t_f) = 2.8(5)(1)(0.02) = 0.28 \text{ in.}^2$$

- Determine the overlap length of the CFRP anchor fan (LF_{anchor}).

$$\sigma_b = 500 \text{ psi} = 0.5 \text{ ksi}$$

$$\theta_{anchor} = 60 \text{ deg.}$$

$$T_f = (w_f)(n)(t_f)(f_{u,EXP}) = 5(1)(0.02)(143) = 14.3 \text{ kip}$$

$$LF_{anchor-min} = \frac{T_f}{w_f \sigma_b} = \frac{14.3}{5(0.5)} = 5.7 \text{ in.}$$

$$LF_{anchor} = \frac{\frac{w_f}{2} + 0.5}{\tan\left(\frac{\theta_{anchor}}{2}\right)} \geq LF_{anchor-min}$$

$$LF_{anchor} = \frac{\frac{w_f}{2} + 0.5}{\tan\left(\frac{\theta_{anchor}}{2}\right)} = \frac{\frac{5}{2} + 0.5}{\tan\left(\frac{60}{2}\right)} = 5.2 \text{ in.}$$

Say $LF_{anchor} = 6 \text{ in.} \geq LF_{anchor-min}$

Utilize a 6 in. CFRP anchor embedment depth. Thus, a 12 in. long CFRP anchor is required.

7. Determine anchor hole diameter (d_{hole}) and hole edge chamfer radius (R_c).

$$d_{hole} = \sqrt{\frac{4(1.4)(A_{EQV})}{\pi}}$$

$$R_c = \frac{1.4d_{hole}}{2} \geq 0.5 \text{ in.}$$

Recall that the intermediate anchors require twice the anchor size as the boundary anchors.

Vertical and Horizontal Boundary Anchors:

$$d_{hole} = \sqrt{\frac{4(1.4)(A_{EQV})}{\pi}} = \sqrt{\frac{4(1.4)(0.28)}{\pi}} = 0.7 \text{ in. say } 0.75 \text{ in.}$$

$$R_c = \frac{1.4d_{hole}}{2} = \frac{1.4(0.75)}{2} = 0.53 \text{ in. say } 0.5 \text{ in.} \geq 0.5 \text{ in.}$$

Horizontal Intermediate Anchors:

$$d_{hole} = \sqrt{\frac{4(1.4)(A_{EQV})}{\pi}} = \sqrt{\frac{4(1.4)(0.56)}{\pi}} = 1.0 \text{ in.}$$

$$R_c = \frac{1.4d_{hole}}{2} = \frac{1.4(1.0)}{2} = 0.7 \text{ in. say } 0.75 \text{ in.} \geq 0.5 \text{ in.}$$

8. Summary of CFRP anchor detailing.

Vertical Boundary Anchor:

$$\gamma_A = 0.125 \frac{OZ}{in.}$$

12 in. long CFRP anchor that has a 6 in. embedment depth

$$d_{hole} = 0.75 \text{ in.}$$

$$R_c = 0.5 \text{ in.}$$

Patch Size: 4 in. by 5 in.

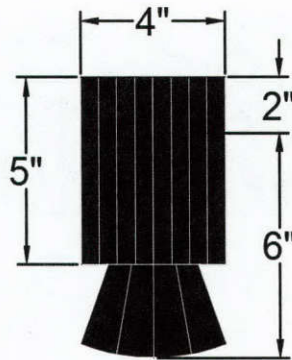


Figure A-4: Vertical boundary anchor

Horizontal Boundary Anchor:

$$\gamma_A = 0.125 \frac{OZ}{in.}$$

12 in. long CFRP anchor that has a 6 in. embedment depth

$$d_{hole} = 0.75 in.$$

$$R_c = 0.5 in.$$

Patch Size: 5 in. by 5 in.

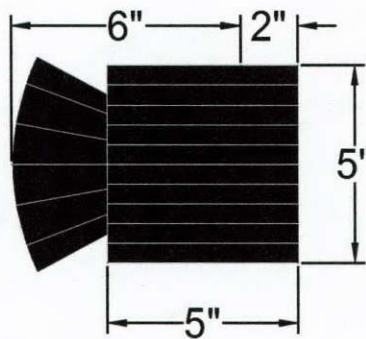


Figure A-5: Horizontal boundary anchor

Horizontal Intermediate Anchors:

$$\gamma_A = 0.25 \frac{OZ}{in.}$$

12 in. long CFRP anchor that has a 6 in. embedment depth

$$d_{hole} = 1.0 in.$$

$$R_c = 0.75 in.$$

Patch Size: 5 in. by 8 in.

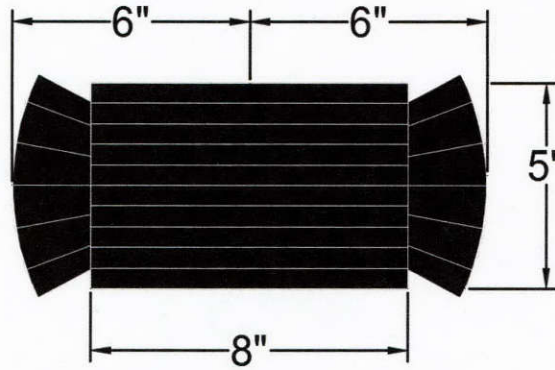


Figure A-6: Horizontal intermediate anchor

Solution 2: Layouts using the Simple Concrete Contribution

The following solution illustrates the design and detailing of uni- and bi-directional CFRP layouts using the proposed design guidelines with the simple concrete contribution equation (Equation 9-11).

Uni-directional Layout (Vertical Strips):

1. Determine the strain in the longitudinal reinforcement at the peak moment region (ϵ_s).

$$\epsilon_s = \frac{\left(\frac{|M|}{0.9d} + V_{@M}\right)}{E_s A_s} = \frac{\left(\frac{|24,192|}{(0.9)32.25} + 0\right)}{29,000 (8 * 1.56)} = 0.0023 \text{ in./in.}$$

2. Determine the shear crack angle (θ).

$$\theta = 29 + 3500\epsilon_s = 29 + 3500(0.0023) = 37^\circ$$

$$29^\circ \leq \theta = 37^\circ \leq 50^\circ$$

3. Determine the steel shear contribution (V_s).

$$V_s = \frac{A_{vs} f_{yt} d}{s} \cot(\theta) = \frac{0.22(60)(32.25)}{12} \cot(37) = 47.1 \text{ kip}$$

4. Determine the concrete contribution (V_c).

$$V_c = 2\sqrt{f'_c} b_w d = \frac{2}{1000} \sqrt{5000}(14)(32.25) = 63.9 \text{ kip}$$

5. Solve for the required CFRP contribution ($V_{f,req}$)

$$V_{f,req} = \frac{V_{u@d}}{\phi} - V_c - V_s = \frac{149}{0.75} - 63.9 - 47.1 = 87.7 \text{ kip}$$

6. Calculate the CFRP contribution (V_f)

CFRP properties:

$$E_f = 13,900 \text{ ksi}$$

$$t_f = 0.02 \text{ in.}$$

$$\epsilon_u = 0.01 \text{ in./in.}$$

Assume the $d_{fv} = h - h_f - 1.5'' = 36'' - 8'' - 1.5'' = 26.5$ in.

Assume the center-to-center spacing of the strips is 8 in. $\leq d/4$

Try one layers (ply) of 6 in. wide vertical CFRP strips

$$A_{vf} = 2nt_f w_f = 2(1)(0.02)(6) = 0.24 \text{ in.}^2$$

$$f_{fe} = 0.6\varepsilon_u E_f = 0.6(0.01)(13900) = 83.4 \text{ ksi} \leq 0.006E_f$$

$$V_f = \frac{A_{vf} f_{fe} d_{fv}}{s_f} \cot(\theta) = \frac{0.24(83.4)(26.5)}{8} \cot(37) = 88 \text{ kip} > V_{f,req}$$

7. Check the transverse reinforcement contribution limit.

$$(V_s + V_f) = 47.1 + 88 = 135.1 \text{ kip} \leq 8 \sqrt{f'_c} b_w d = 255.4 \text{ kip}$$

8. Check that the shear capacity is greater than the shear demand.

$$\begin{aligned} \phi V_n &= 0.75(V_c + V_s + V_f) = 0.75(63.9 + 47.1 + 88) = 149.3 \text{ kip} > V_{u@d} \\ &= 149 \text{ kip} \end{aligned}$$

Utilize 6 in. wide vertical CFRP strips spaced 8 in. on center starting within $d/2$ from the support and extending beyond 10-feet from the support where the existing shear capacity is sufficient.

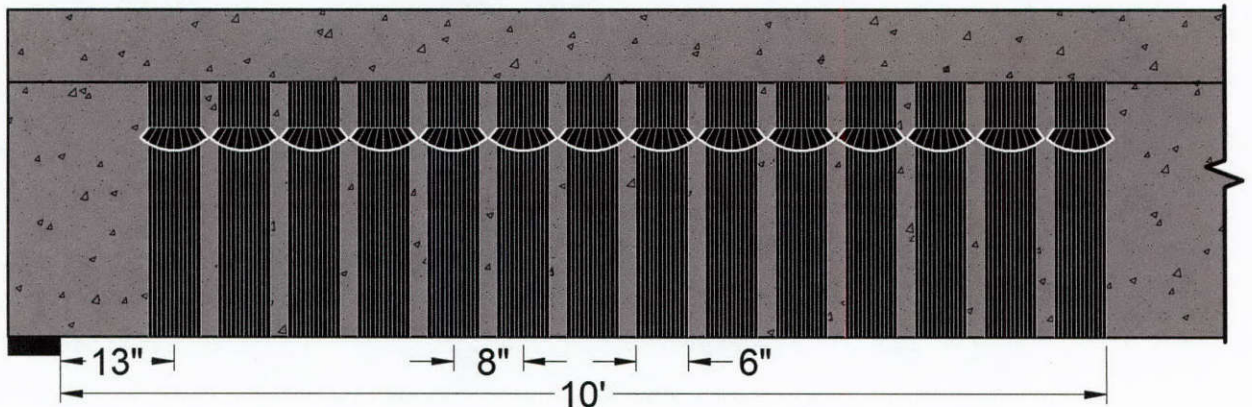


Figure A-7: Designed uni-directional layout using the simple concrete contribution

Bi-directional Layout (Vertical and Horizontal Strips):

A bi-directional layout can be utilized to maximize the cracking shear load and/or minimize shear crack widths.

1. Determine the required area of CFRP in the horizontal direction (A_{hf}).

$$N_h A_{hf} \geq \frac{1}{2} \frac{A_{vf} d_{fv}}{s_f} \cot(\theta) = \frac{1}{2} \frac{0.24(26.5)}{8} \cot(37) = 0.53 \text{ in.}^2$$

Try using two double layer horizontal CFRP strips within an area that is greater than $d/4$ away from the edge of the web region.

$$A_{hf} \geq 0.265 \text{ in.}^2$$

$$A_{hf,provided} = 2nt_f w_f = 2(2)(0.02)(4) = 0.32 \text{ in.}^2$$

Use two double layer 4 in. wide horizontal CFRP strips spaced at 7 in. on center

- Determine the spacing of intermediate anchors (d_{fh}).

$$d_{fh} = 32 \text{ in.} \leq d = 32.25 \text{ in.}$$

Utilize two double layer 4 in. wide horizontal CFRP strips spaced 7 in. on center with three intermediate anchors every 32 inches on each side of the web. The horizontal CFRP strips are placed $d/4$ away from the edge of the web region.

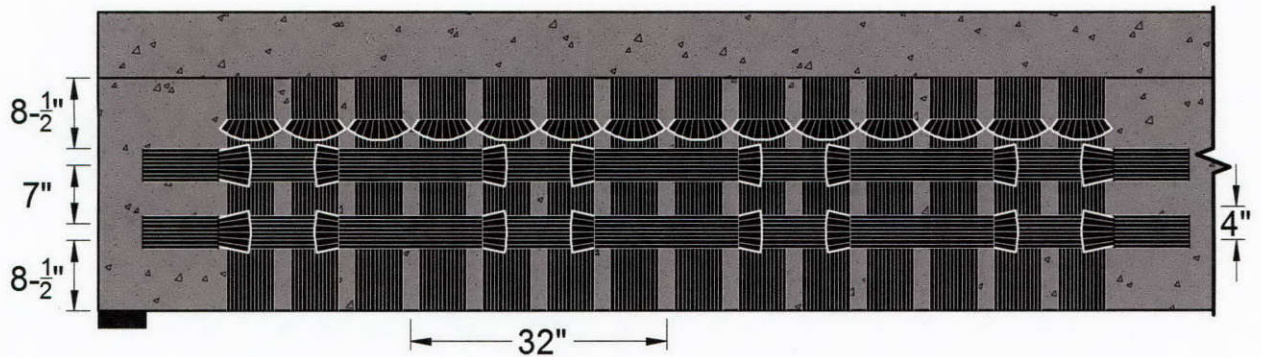


Figure A-8: Designed bi-directional layout using the simple concrete contribution

Anchor Design:

The design and detailing recommendations for CFRP anchors can be found in Chapter 8. As mentioned in Chapter 8, the anchor design guidelines assume the strip and anchor materials are the same and have the same properties. Moreover, the guidelines are only applicable to carbon fiber anchors.

- Determine tributary widths of the CFRP anchor in the vertical and horizontal directions ($w_{f,a}$).

$$w_{f,A} = \frac{w_f}{n_A}$$

Vertical: Use a single anchor per strip

$$w_{f,A} = \frac{w_f}{n_A} = \frac{6}{1} = 6 \text{ in.}$$

Horizontal: Use a single anchor per strip

$$w_{f,A} = \frac{w_f}{n_A} = \frac{4}{1} = 4 \text{ in.}$$

Two anchor designs are required since the vertical strip use one ply while the horizontal strips use two plies of CFRP strips.

- Determine the required weight of anchor fibers per unit length (γ_{A-req}).

$AMR_D = 2.0$ (or greater is recommended)

$$\gamma_{s,sp} = 0.00717 \frac{OZ}{in.^2} \text{ (Fiber Specific)}$$

$$\gamma_{s,EXP} = 1.25(\gamma_{s,sp}) = 0.00897 \frac{OZ}{in.^2}$$

Vertical:

$$\gamma_{A-req} = AMR_D(w_{f,A})(n)(\gamma_{s,EXP}) = 2.0(6)(1)(0.00897) = 0.11 \frac{OZ}{in.}$$

Horizontal:

$$\gamma_{A-req} = AMR_D(w_{f,A})(n)(\gamma_{s,EXP}) = 2.0(4)(2)(0.00897) = 0.144 \frac{OZ}{in.}$$

- Select a CFRP anchor based on the anchor's fiber weight per unit length (λ_A).

$$\gamma_A \geq \gamma_{A-req}$$

Vertical:

Utilize a CFRP anchor that has at least 0.11 OZ of fibers per inch of length.

$$\text{Say } \gamma_A = 0.125 \frac{OZ}{in.}$$

Horizontal:

Utilize a CFRP anchor that has at least 0.144 OZ of fibers per inch of length.

$$\text{Say } \gamma_A = 0.15 \frac{OZ}{in.}$$

Note that the intermediate anchors on the horizontal strips need to be twice as larger as the anchors on the boundary of the CFRP layout since the anchors need to be played in opposing directions over the strip.

- Determine the actual anchor material ratio (AMR_A).

$$AMR_A = \frac{\gamma_A}{(w_{f,A})(n)(\gamma_{s,EXP})} \geq 2.0$$

Vertical:

$$AMR_A = \frac{\gamma_A}{(w_{f,A})(n)(\gamma_{s,EXP})} = \frac{0.125}{(6)(1)(0.00897)} = 2.3 \geq 2.0$$

Horizontal:

$$AMR_A = \frac{\gamma_A}{(w_{f,A})(n)(\gamma_{s,EXP})} = \frac{0.15}{(4)(2)(0.00897)} = 2.1 \geq 2.0$$

5. Determined the equivalent cross-sectional area of the CFRP anchor (A_{EQV}).

$$A_{EQV} = AMR_A(w_{f,A})(n)(t_f)$$

Vertical:

$$A_{EQV} = AMR_A(w_{f,A})(n)(t_f) = 2.3(6)(1)(0.02) = 0.28 \text{ in.}^2$$

Horizontal:

$$A_{EQV} = AMR_A(w_{f,A})(n)(t_f) = 2.1(4)(2)(0.02) = 0.34 \text{ in.}^2$$

6. Determine the overlap length of the CFRP anchor fan (LF_{anchor}).

$$\sigma_b = 500 \text{ psi} = 0.5 \text{ ksi}$$

$$\theta_{anchor} = 60 \text{ deg.}$$

$$T_f = (w_f)(n)(t_f)(f_{u,EXP})$$

$$LF_{anchor-min} = \frac{T_f}{w_f \sigma_b}$$

$$LF_{anchor} = \frac{\frac{w_f}{2} + 0.5}{\tan\left(\frac{\theta_{anchor}}{2}\right)} \geq LF_{anchor-min}$$

Vertical:

$$T_f = (w_f)(n)(t_f)(f_{u,EXP}) = 6(1)(0.02)(143) = 17.2 \text{ kip}$$

$$LF_{anchor-min} = \frac{T_f}{w_f \sigma_b} = \frac{17.2}{6(0.5)} = 5.7 \text{ in.}$$

$$LF_{anchor} = \frac{\frac{w_f}{2} + 0.5}{\tan\left(\frac{\theta_{anchor}}{2}\right)} = \frac{\frac{6}{2} + 0.5}{\tan\left(\frac{60}{2}\right)} = 6.1 \text{ in.}$$

$$\text{Say } LF_{anchor} = 6 \text{ in.} \geq LF_{anchor-min}$$

Utilize a 6 in. CFRP anchor embedment depth. Thus, a 12 in. long CFRP anchor is required

Horizontal:

$$T_f = (w_f)(n)(t_f)(f_{u,EXP}) = 4(2)(0.02)(143) = 22.9 \text{ kip}$$

$$LF_{anchor-min} = \frac{T_f}{w_f \sigma_b} = \frac{22.9}{4(0.5)} = 11.5 \text{ in.}$$

$$LF_{anchor} = \frac{\frac{w_f}{2} + 0.5}{\tan\left(\frac{\theta_{anchor}}{2}\right)} = \frac{\frac{4}{2} + 0.5}{\tan\left(\frac{60}{2}\right)} = 4.3 \text{ in.}$$

$$\text{Say } LF_{anchor} = 12 \text{ in.} \geq LF_{anchor-min}$$

Utilize a 6 in. CFRP anchor embedment depth. Thus, an 18 in. long CFRP anchor is required.

7. Determine anchor hole diameter (d_{hole}) and hole edge chamfer radius (R_c).

$$d_{hole} = \sqrt{\frac{4(1.4)(A_{EQV})}{\pi}}$$

$$R_c = \frac{1.4d_{hole}}{2} \geq 0.5 \text{ in.}$$

Recall that the intermediate anchors require twice the anchor size as the boundary anchors.

Vertical Boundary Anchors:

$$d_{hole} = \sqrt{\frac{4(1.4)(A_{EQV})}{\pi}} = \sqrt{\frac{4(1.4)(0.28)}{\pi}} = 0.7 \text{ in. say } 0.75 \text{ in.}$$

$$R_c = \frac{1.4d_{hole}}{2} = \frac{1.4(0.75)}{2} = 0.53 \text{ in. say } 0.5 \text{ in.} \geq 0.5 \text{ in.}$$

Horizontal Boundary Anchors:

$$d_{hole} = \sqrt{\frac{4(1.4)(A_{EQV})}{\pi}} = \sqrt{\frac{4(1.4)(0.34)}{\pi}} = 0.78 \text{ in. say } 0.875 \text{ in.}$$

$$R_c = \frac{1.4d_{hole}}{2} = \frac{1.4(0.875)}{2} = 0.6125 \text{ in. say } 0.625 \text{ in.} \geq 0.5 \text{ in.}$$

Horizontal Intermediate Anchors:

$$d_{hole} = \sqrt{\frac{4(1.4)(A_{EQV})}{\pi}} = \sqrt{\frac{4(1.4)(0.68)}{\pi}} = 1.1 \text{ in. say } 1.125 \text{ in.}$$

$$R_c = \frac{1.4d_{hole}}{2} = \frac{1.4(1.125)}{2} = 0.79 \text{ in. say } 0.875 \text{ in.} \geq 0.5 \text{ in.}$$

8. Summary of CFRP anchor detailing.

Vertical Boundary Anchor:

$$\gamma_A = 0.125 \frac{OZ}{in.}$$

12 in. long CFRP anchor that has a 6 in. embedment depth

$$d_{hole} = 0.75 \text{ in.}$$

$$R_c = 0.5 \text{ in.}$$

Patch Size: 6 in. by 5 in.

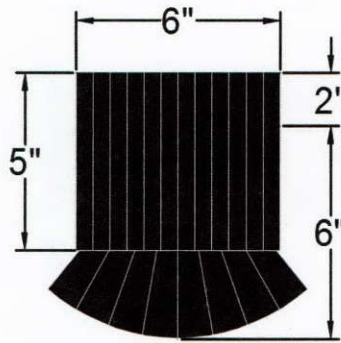


Figure A-9: Vertical boundary anchor

Horizontal Boundary Anchor:

$$\gamma_A = 0.15 \frac{OZ}{in.}$$

18 in. long CFRP anchor that has a 6 in. embedment depth

$$d_{hole} = 0.875 \text{ in.}$$

$$R_c = 0.6125 \text{ in.}$$

Patch Size: 4 in. by 9.5 in.

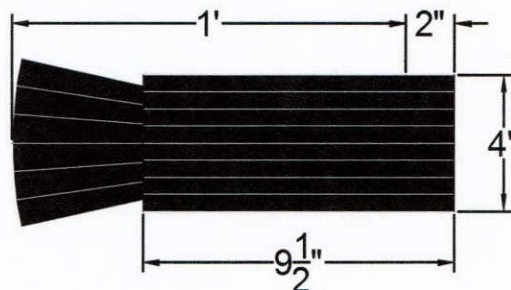


Figure A-10: Horizontal boundary anchor

Horizontal Intermediate Anchors:

$$\gamma_A = 0.3 \frac{OZ}{in.}$$

18 in. long CFRP anchor that has a 6 in. embedment depth

$$d_{hole} = 1.125 in.$$

$$R_c = 0.875 in.$$

Patch Size: 4 in. by 18 in.

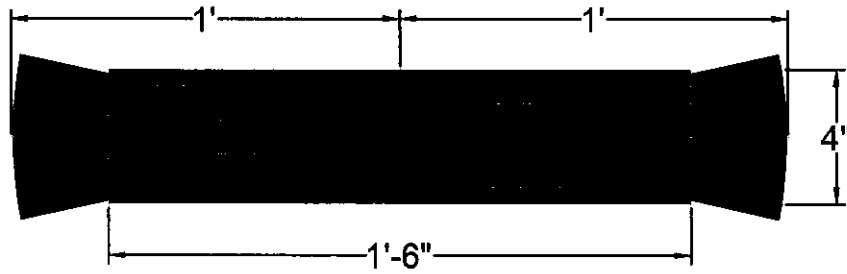


Figure A-11: Horizontal intermediate anchor

Center for Transportation Research

The University of Texas at Austin
1616 Guadalupe Street, Suite 4.202
Austin, TX 78701

Phone: (512) 232-3100
To order reports: (512) 232-3126 (CTR Library)
E-mail: ctrlib@austin.utexas.edu
Web site: ctr.utexas.edu
CTR Library Web site: ctr.utexas.edu/library/

